

THE CHEMICAL STRUCTURE AND THERMAL MODIFICATION OF LOW RANK COALS

Masakatsu Nomura, Takeshi Muratani, Satoru Murata, Shigeru Maeda,* and Akira O-ki*
Department of Applied Chemistry, Faculty of Engineering, Osaka University,
2-1 Yamada-oka, Suita, Osaka 565, Japan

*Department of Applied Chemistry, Faculty of Engineering, Kagoshima University
1-21-40 Ko-rimoto, Kagoshima 890, Japan

Keywords: Chemical structure, Low rank coal, Thermal modification

ABSTRACT

For two brown coals, Australian Yallourn and Indonesian South Banko coals, measurements of SPE/MAS ^{13}C NMR spectra, OH group analysis according to acetylation and silylation, Curie-point pyrolysis, and analysis of CO_2H groups were conducted. Based on these results, plausible chemical structural units of above brown coals were proposed and submitted to CAMD calculation to understand the interactive forces of units. On the other hand, these brown coals were found to show the higher reactivities when modified in the presence of water at around 350°C . The enhancement of these reactivities was examined by supposing what kinds of reaction take place based on the unit chemical structures proposed here and the interactive forces of these units.

INTRODUCTION

In 1987, Hüttinger *et al.* had proposed molecular structure of a typical Rheinische brown coal based on elemental analysis, pyrolysis experiments, and extrapolation of literature data and successfully explained the pyrolysis and hydrolysis data of brown coals [1]. In 1992, Hatcher *et al.* [2] and Nomura *et al.* [3] proposed chemical structural units of subbituminous coal and bituminous coal by applying solid state NMR data in the combination with conventional data such as from pyrolysis and quantification of functional groups, respectively. Nomura *et al.* pointed out the importance of the following subjects concerning the elucidation of chemical structure of coals: (1) more precise and quantitative evaluation of chemical bonds connecting aromatic rings; (2) search for analysis of constituents without accompanying coke formation; (3) reliable evaluation of real molecular weight of extracts; (4) research on qualitative and quantitative evaluation of non-bonding interactions in coal organic matrix; (5) study on the quantitiveness of CP/MAS ^{13}C NMR spectroscopy. These mean that, around 1992, these subjects remain uncertain. As for subject (1), Stock *et al.* proposed RuO_4 oxidation method as the means to evaluate aliphatic substituents on aromatic rings [4]. In this RuO_4 oxidation, aliphatic portion connecting aromatic rings could be converted to aliphatic dicarboxylic acid derivatives; This experiments showed that there were many different kinds of aliphatic dicarboxylic acids even though their amounts are so small. [5] However, the presence and amount of methylene bridge could not be detected and quantified by this method because resulting malonic acid is unstable under the reaction conditions. Solid state ^{13}C NMR is still powerful means, suggesting the distribution of different kinds of carbon contained in coal organic matrix. At present time, SPE/MAS ^{13}C NMR spectra are believed to be more quantitative than CP/MAS ^{13}C NMR spectra [6]. The advantage of using ^{13}C NMR spectral data for the evaluation of unit chemical structure is that the spectra can reflect the whole coal. As for subject (2) and (3) there has been no rapid progress since 1992. As for subject (4), much attention are paid to non-bonding interactions in coal organic matrix, however, there is few method to evaluate them in the quantitative way. Authors are now thinking that non-bonding interaction might be very important to consider the reaction taking place at the early stage of heating process. In that sense, the unit chemical structures proposed here and their non-bonding interactions based on CAMD study give us the meaningful clues to understand the reactivities of brown coal at the early stage of liquefaction and thermally modified brown coal.

EXPERIMENTAL SECTION

Coal samples. Two brown coals, Australian Yallourn and Indonesian South Banko coals (YL and SB), were employed in this study, which were provided by the courtesy of Nippon Brown Coal Liquefaction Co. Ltd. These were ground under 200 mesh and dried at 40°C in vacuo before use. Elemental analysis of these two coals are listed in Table 1.

Consecutive extraction and acetylation of THF-insoluble materials. A dried and pulverized coal samples (5 g) was put in a Soxhlet thimble, then being set in the apparatus. Extraction with tetrahydrofuran (THF) was conducted for one day. The resulting residue (THF-insoluble materials) was submitted to acetylation by refluxing in a solvent mixture of acetic anhydride-pyridine, then the acetylated samples being extracted again with THF. These procedures were repeated for three times (scheme of this extraction is shown in Figure 1). The resulting products were submitted to structural analysis according to GPC.

Solid state ^{13}C NMR measurement. CP/MAS and SPE/MAS ^{13}C NMR spectra were recorded on a Chemmagentic CMX-300 with MAS method (10 kHz). For the measurement, about 150 mg of coal were packed in a vessel (5 mm diameter x 8 mm long). The experimental conditions employed were as follows; 200 s pulse delay, 45° pulse width, and ca. 400 scan number. Deconvolution of the spectra was conducted on an Apple Macintosh computer with a commercial NMR data processing software, MacAlice (ver 2.0, JEOL Datum). The resulting spectra were divided into twelve Gaussian curves. For two brown coals, Yallourn and South Banko coals, SPE/MAS (Figure 2) and CP/MAS gave following *fa* values, 0.77 and 0.66, and 0.60 and 0.54, respectively.

Diffuse reflectance FT/IR (DR/FT/IR) measurement. Dried sample (50 mg) and KBr (450 mg) were mixed and ground by using an agate mortar. The resulting mixture was further

dried at 90 °C for 10 h in vacuo. FT/IR spectrum of the sample was recorded on a JEOL JIR-AQS20M with diffuse reflectance method (128 scans). Data acquisition and analysis were also carried out on the computer equipped with the spectrometer.

Gel permeation chromatography. Analysis by gel permeation chromatography (GPC) was conducted by using a Shimadzu LC-10AS liquid chromatographic system with a Shodex KF-80M GPC column (30 cm, stationary phase: polystyrene gel) and a Shimadzu SPD-10A ultraviolet detector ($\lambda=270$ nm). An extract (6.3 mg) was dissolved in 10 mL of DMF, 20 μ L of which was injected to the LC system, when either DMF or lithium bromide-containing DMF was used as eluant. Calibration of retention time-molecular weight relationships was conducted by using 14 kinds of standard polystyrene samples and benzene.

Quantitative analysis of OH groups. (1) Acetylation Method: According to the method reported by Blom *et al.* [7], analysis of OH groups was conducted. (2) Silylation method: According to the Friedman's method [8], we conducted silylation of coal. The details are referred in his paper.

Quantitative analysis of CO₂H groups. These analysis were conducted by ion exchange with sodium acetate [9] and ion exchange with sodium bicarbonate.

Computer simulation. Computer simulation was conducted on an Apple Power Macintosh personal computer by using a commercial CAMD (computer-aided molecular design) software, CAChe (CAChe Scientific, Inc., Version 3.7). At first, the structure proposed in this study was input to a computer, then, molecular mechanics (MM) calculation being conducted till root-mean-square error becomes less than 0.1 kcal/mol. Then, molecular dynamics (MD) calculation was carried out for 10 ps to avoid local minimum structure. From this calculation, intermediary conformers were output every 0.1 ps. Consequently, 100 conformers could be obtained, among which five lowest energy conformers were selected and submitted to MM calculation. At last, we selected the conformer having the lowest energy and defined it as the most reliable conformer.

RESULTS AND DISCUSSION

Construction of unit chemical structures of coals. As we cited already in the experimental section, SPE/MAS ¹³C NMR spectra were found to give higher *fa* value than CP/MAS ¹³C NMR spectra. From the carbon distribution based on ¹³C NMR, we found that α -methylene is more abundant in SB coal compared with YL coal, this indicating that SB coal is rich in methylene, polymethylene and more alkyl groups substituted on aromatic rings.

In brown coal, due to the presence of a lot of hydroxyl groups, hydrogen bonding interaction should be more significant, especially in constructing three dimensionally complicated structure. First of all, we extracted two brown coals by THF under refluxing conditions. In order to obtain much more amount of coal extract, we conducted consecutive extraction of residue after acetylation. As we pointed out the importance of molecular weight information of coal, we submitted these extracts to GPC where we found the following interesting phenomena: the use of LiBr-containing DMF as eluant, seems to be able to dissociate extracts due to breakage of hydrogen bonding. This experiments informed us of the molecular weight of the extract being around from 4000 to 6000 with the maximum peaks. Based on these findings, we firstly assumed average molecular weight of brown coals around 5000. Basing on elemental analysis and above molecular weight, following molecules are proposed for each coal; YL C₂₇₆H₂₃₅N₂O₆₇ and SB C₂₉₇H₂₇₀N₄SO₆₇. From *fa* values based on SPE/MAS ¹³C NMR spectra, numbers of aromatic carbons in each unit are decided to be 215 for YL and 196 for SB. As for the constituents of aromatics in coal, Curie-point pyrolysis data (at 670 °C for 3 s) were referred to. As for the aliphatic portion, we have to conduct RuO₄ oxidation even if at present time it is not quantitative, however, in this study we consulted the NMR data, which can give the distribution of different carbons in coal. By referring to the data on oxygen-containing groups, we tentatively proposed following numbers of each group in unit structure: YL -OH 31, -CO₂H 12, -CO₂Ar 6, -O- 38; SB -OH 28, -CO₂H 7, -CO₂Ar 4, -O- 29. Table 1 is the comparison of calculated values of models and observed values of original coals. These two models are submitted to computer simulation (Figure 3).

Computer simulation. Computer simulation of model structures was carried out using molecular mechanics and molecular dynamics in order to obtain the most stable conformation. Each energy term for the coal structural model for brown coals is listed in Table 2. As for potential energy, YL model was found to show a higher negative value than that of SB model, indicating that YL coal is more stable than SB coal. It is interesting to note that non-covalent bonding energy is higher negative value than covalent bonding energy in both models. Higher negative non-covalent bonding energy with YL model is indicating that hydrogen bonding is prevailing in this coal. We conducted liquefaction of two brown coals here and found that SB coal showed higher reactivity than YL coal (higher hexane soluble portion). At the early stage of liquefaction, OH groups are believed to play important roles in the reactivity. If we consider that YL coal, due to its high contribution of intermolecular hydrogen bonding, tends to conduct condensation reaction to a great extent, the resulting lower yield of lighter fraction could be explained in a reasonable way. In Japan, low rank coal is now processed around 350 °C in the presence of water using an 8.4t/day pilot plant, the resultant coals showing good reactivities. The reactivity of modified coal could be rationalized in this context. We are now conducting the measurements of FT/IR, swelling index and SEM observation of these modified brown coals to examine their properties.

REFERENCES

- 1) Hüttinger, K. J.; Michenfelder, A. W. *Fuel* 1987, 66, 1164.
- 2) Hatcher, P. G.; Faulon, J.-L.; Wenzel, K. A.; Cody, G. D. *Energy Fuels* 1992, 6, 813.
- 3) Nomura, M.; Matsubayashi, K.; Ida, T.; Murata, S. *Fuel Process. Technol.* 1992, 31, 169.
- 4) Stock, L. M.; Tse, K. T. *Fuel* 1983, 62, 974.
- 5) Murata, S.; Uesaka, K.; Inoue, H.; Nomura, M. *Energy Fuels* 1994, 8, 1379.
- 6) Franz, J. A.; Garcia, R.; Linehan, J. C.; Love, G. D.; Snape, C. E. *Energy Fuels* 1992, 6, 598.
- 7) Blom, L.; Edelhausen, L.; van Krevelen, D. W. *Fuel* 1957, 36, 135.
- 8) Friedman, S.; Kaufman, M. L.; Steiner, W. A.; Wender, I. *Fuel* 1961, 40, 33.
- 9) Funasaka, W. ed. *Nenryo Bunseki Siken-hou*, Nankodo, 1968, p.75.

Table 1. Comparison of calculated values of model and observed values of original coal with two brown coals

Yalloum coal						South Banko coal					
Ultimate analysis (wt%, daf)						Ultimate analysis (wt%, daf)					
C	H	N	S	O		C	H	N	S	O	
67.1	4.7	0.6	0	27.6		70.7	5.8	1.1	0.7	21.7	
(66.9)	(4.7)	(0.5)	(0.3)	(27.6)		(71.3)	(5.4)	(1.2)	(0.5)	(21.6)	
Oxygen-containing functional groups (wt%, daf)						Oxygen-containing functional groups (wt%, daf)					
-OH	10.37	(10.46)				-OH	9.32	(9.44)			
-COOH	10.60	(11.02)				-COOH	6.39	(5.94)			
Carbon aromaticity, fa						Carbon aromaticity, fa					
0.78 (0.77)						0.69 (0.66)					

Table 2. Each energy term for the coal structural model for brown coals

Energy term	YL	SB
total	-732.977	-604.096
Covalent bonding	-227.871	-158.460
stretch	11.432	11.972
angle	129.207	154.672
stretch bend	0.188	0.355
dihedral	-370.588	-326.310
improp torsion	1.888	0.850
Non-covalent bonding	-505.106	-445.636
electrostatics	-69.811	-42.020
van der waals	33.205	-14.801
hydrogen bond	-468.500	-388.815

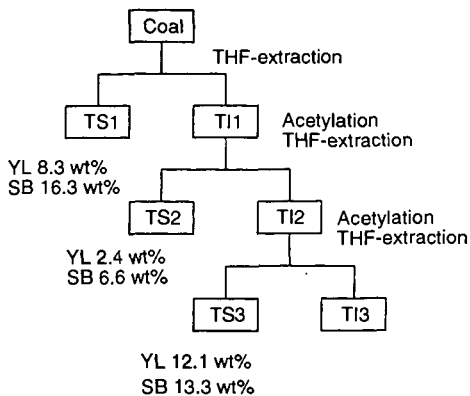


Figure 1. Procedure for consecutive extraction of two brown coals.

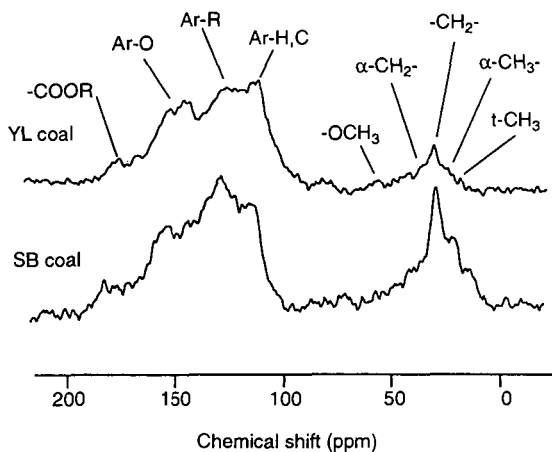


Figure 2. SPE/MAS ^{13}C NMR of two brown coals

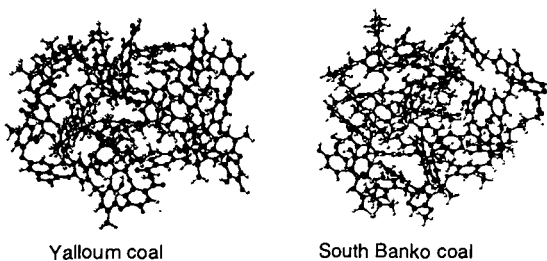


Figure 3. 3D skeeth for the model structures proposed

THE ROLE OF ETHER OXYGEN AND CARBON DOUBLE BONDS AS LINKAGES DURING THE DISSOLUTION OF KEROGENS WITH PERCHLORIC ACID

Chris W. McGowan, Kenneth J. Oestreich, Gloria Elayne Hood
Department of Chemistry, Tennessee Technological University, Cookeville, TN 38501

Deborah J. Davidson,
Chemical Technology Division, Oak Ridge National Laboratory, Oak Ridge, TN 37831

and Richard Markuszewski
Institute of Gas Technology, 1700 S. Mount Prospect Road, Des Plaines, IL 60018

Keywords: Kerogen Structure, Perchloric Acid, Coal, Oil Shale

INTRODUCTION

In 1966, Fester and Robinson (1) reported that 53.5 percent of the oxygen in the kerogen of Green River oil shale was present in ether functional groups. Fester and Robinson had measured the amount of carboxyl, ester, amide, carbonyl and hydroxyl oxygen with a series of chemical analyses. Ether oxygen was determined by measuring the difference between the sum of the amounts of each of the above functional groups and the total oxygen present. The idea that ether oxygen was a "linkage" between kerogen units was further supported by McGowan et. al. (2) in 1985. In that work, a kerogen concentrate of Green River oil shale was oxidized with solutions of perchloric acid having various concentrations and subsequent boiling points. The kerogen concentrate dissolved at boiling points between 160°C and 170°C. The dissolution range of the kerogen concentrate was compared to the dissolution ranges for a series of model compounds. The compounds (and linkages tested) were polyethylene (carbon-carbon single bonds), graphite (aromatic carbon bonds), nylon (amide bonds) and polyethylene oxide (ether bonds). Polyesters, which readily hydrolyze and dissolve in cold perchloric, were not tested. Polyethylene required a boiling point of 202°C before dissolution occurred (the polymer caught on fire inside the reaction vessel). Boiling, concentrated perchloric at 202°C did not dissolve graphite to any appreciable extent. Nylon also resisted dissolution but a portion was dissolved at 202°C. Both the dissolution ranges and infrared spectra supported the conclusion that ether oxygen was being attacked during the dissolution of the kerogen concentrate from Green River oil shale.

Several additional kerogens have also been reacted with perchloric acid. These include a kerogen concentrate from Chattanooga Shale (3); and two bituminous coals, an Illinois #6 coal and a Charming Creek coal from New Zealand (4). The kerogen concentrate from Chattanooga Shale and the Illinois #6 coal dissolved in boiling point ranges similar to the kerogen of Green River oil shale. However the Charming Creek coal dissolved between 180°C and 190°C. Since the dissolution range for the Charming Creek coal fell outside the range of that for ether oxygen, several additional model compounds were tested. In this paper, the results for the dissolution of three new model compounds and two new kerogens is reported. The new model compounds are poly-m-phenoxyene (aromatic ether bonds), polybutadiene and a polybutadiene with 20 percent styrene copolymer (carbon double bonds). The new kerogens were a Mequinenza lignite from Spain and an Elizabethtown anthracite from Pennsylvania.

When cold or dilute, perchloric acid is a non-oxidizing acid. When hot and concentrated, perchloric acid is powerful oxidizing agent. The apparent reduction potential rises slowly as the concentration and subsequent boiling point increases. The apparent potential rises from 0.8 V at a boiling point of 130°C to 2.0 V at 203°C, the boiling point of the concentrated acid (5).

EXPERIMENTAL

The poly-m-phenoxyene and the polybutadiene-styrene copolymer were obtained from Dr. Vernon Allen of the Department of Chemistry at Tennessee Technological University. The polybutadiene was a Taktene 220 sample obtained from Ms. Pat Kolda at the Bayer Plant in Orange, TX. The Mequinenza coal was obtained by the Ames Laboratory at Iowa State University and was originally supplied by Dr. Sabino Moinelo at the Instituto Nacional del Carbon in Spain. The Elizabethtown coal was supplied by Dr. John Riley of the Department of Chemistry at Western Kentucky University. The ultimate analysis of the Mequinenza coal was determined by Analytical Services at Ames Lab and that of the Elizabethtown coal by the Materials Characterization Center at Western Kentucky. The results appear in Table 1. For comparison purposes, the ultimate analyses for the Illinois #6 and Charming Creek coals as determined at Ames Lab also appear in Table 1.

Table 1. Ultimate Analysis of Coal Samples (on a dry basis)

coal (rank)	carbon	hydrogen	nitrogen	oxygen	sulfur
Elizabethville (anthracite)	83.7	2.30	1.10	0.57	0.74
Charming Creek (bitum.)	79.0	5.32	0.95	9.26	5.44
Illinois#6 (bituminous)	62.2	4.13	1.60	15.5	3.45
Mequinenza (lignite)	53.7	3.94	0.85	9.55	9.93

Safety Note

All reactions were performed under total reflux, in a perchloric acid hood and behind an explosion shield. Generally 1-g samples were reacted at low boiling points and 0.1-g samples at 203°C. An explosion occurred when a 0.2 g sample of the polybutadiene was reacted with concentrated perchloric acid having a boiling point of 203°C. A stopper in the side-arm of the reaction flask was shattered and glass was embedded in the plastic explosion shield. When the sample size was reduced to 0.1 g, no explosion occurred.

Procedure

All reactions were performed in a modified Bethge Apparatus designed to maintain a constant boiling solution. The apparatus has been described by McGowan and Diehl (6). A perchloric acid solution was added to the Bethge Apparatus and the boiling point was adjusted to the desired value. Approximately 50 mL of solution remained. After cooling, a weighed 1.0-g or 0.1-g sample of the model compound or coal was added. The reaction vessel was heated for 1.5 hrs. After cooling, the reaction mixture was filtered. The residue was dried and weighed, and the amount of undissolved material was determined.

RESULTS AND DISCUSSION

The results for the dissolution of the Mequinenza lignite and the Elizabethville anthracite appear in Fig. 1. The lignite sample dissolved between 160°C and 170°C. This dissolution was almost identical to that of the kerogen of Green River oil shale and Illinois #6 coal. The hypothesis that ether linkages were being attacked in this coal was consistent with the high oxygen content and low rank of this coal. The anthracite sample appeared to have two dissolution ranges. One from 170°C to 180°C and a second from 190°C to 203°C. The first range was similar to the dissolution of the kerogen of Chattanooga Shale and was within the range of the dissolution of ethers. The second range was consistent with the dissolution polyethylene and, as presented below, with polybutadiene. The results for the dissolution of poly-m-phenoxylyene, polybutadiene and the polybutadiene-styrene copolymer appear in Fig. 2. Poly-m-phenoxylyene gained weight at all boiling points up to 190°C. The infrared spectra of the undissolved material indicated that the polymer had been extensively chlorinated. This chlorination process had been previously observed for other aromatic compounds (7). The polymer was almost completely dissolved at 203°C. The polybutadiene-styrene copolymer displayed a spike in the percent undissolved material at a boiling point of 185°C before dissolving at 190°C. The infrared spectra of the residue from the 185°C reaction also indicated extensive chlorination of the polymer. Although the polybutadiene-styrene copolymer may be a better model compound to represent the kerogen of a coal, it was decided that a polymer containing a double bond without aromatic rings should also be investigated. Polybutadiene displayed a smaller spike in the amount of undissolved material at a boiling point of 190°C. The sample was partially dissolved at 195°C and completely dissolved at 203°C. There was a kinetic problem with the dissolution of the polybutadiene. Even though the polymer was cut up into small particles, they would coalesce into large particles when heated with the perchloric acid solutions; thereby decreasing the surface area of the polymer. When a 1.0-g sample of the polymer was reacted at 195°C, the percent undissolved material was 125 percent. When a 0.1-g sample was reacted at 196°C, the percent undissolved material was 68 percent. Even with this problem, the dissolution of polybutadiene was similar to the dissolution of polyethylene and the second dissolution range of the Elizabethville coal. These results showed that the presence of aromatic rings in a polybutadiene polymer resulted in the double bonds being more susceptible to oxidation by perchloric acid. This could result from just the presence of the rings or could be enhanced by the chlorination of the rings. Since the presence of aromatic rings in the kerogens of coals is highly probable and if double bonds in the kerogen were being attacked, then the dissolution of the kerogen should be similar to the dissolution of the polybutadiene-styrene copolymer.

As the molar ratio of oxygen to carbon decreased, the range of boiling points of perchloric acid solutions, over which dissolution occurred, increased. This is shown in Table 2. The obvious implication would be that as the oxygen content dropped, the available ether linkages that could be attacked would also drop. Each increase in the dissolution range was accompanied by an order of magnitude decrease in the oxygen to carbon ratio.

Table 2. Molar O/C Ratios and Dissolution Ranges for Coal Samples

coal	molar O/C	Dissolution Range (b.p HClO ₄)
Elizabethville	0.0051	190°C to 203°C (2nd)
Charming Creek	0.088	180°C to 190°C
Illinois #6	0.19	160°C to 170°C
Mequinzenza	0.14	160°C to 170°C

CONCLUSIONS

The results of this study indicated that kerogens which contain a large amount of oxygen were dissolved by boiling perchloric acid solutions when ether oxygen was attacked. However, as the oxygen content of the kerogens decreased other bonds had to be attacked in order to dissolve the kerogen. For the kerogens in this study, the Illinois #6 coal, the Mequinzenza coal and the Green River oil shale were dissolved when aliphatic ether oxygen was attacked. The Charming Creek coal dissolved when carbon double bonds were attacked. The Chattanooga Shale and the first dissolution range for the Elizabethville coal were probably the result of the attack on aliphatic ethers, although the possibility of an aromatic-aliphatic ether has not been eliminated. The second dissolution range for the Elizabethville coal was probably due to the oxidation of carbon single bonds although the oxidation of carbon double bonds was a possibility.

LITERATURE CITED

1. Fester, J.I. and W.E. Robinson, *Adv. Chem. Ser.* (55), 22, 1966.
2. McGowan, C.W., R.C. Pearce and H. Diehl, *Fuel Process. Technol.*, 10, 195, 1985.
3. Stanton, B.J., R.M. Morris and C.W. McGowan, *Fuel Process. Technol.*, 29, 85, 1991.
4. McGowan, C.W. and R. Markuszewski, *Fuel Process. Technol.*, 17, 29, 1987.
5. Smith, G.F., *Analyst*, 80, 16, 1955.
6. McGowan, C.W. and H. Diehl, *Fuel Process. Technol.*, 10, 169, 1985.
7. McGowan, C.W., K. Q. Cates and R. Markuszewski, *Prepr. Pap. -Am. Chem. Soc., Div. Fuel Chem.*, 33, 225, 1988.

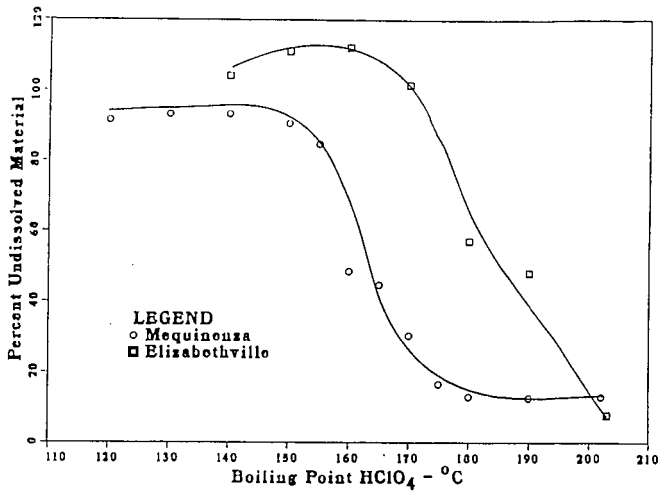


Figure 1. Dissolution Curves for the Mequinensa and Elizabethtown Coals

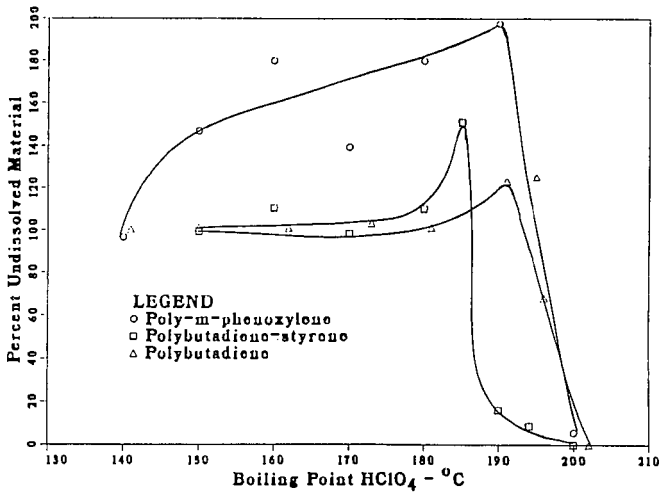


Figure 2. Dissolution Curves for the Model Polymers

SOLUBILIZATION OF AN AUSTRALIAN BROWN COAL OXIDIZED WITH HYDROGEN PEROXIDE IN CONVENTIONALLY USED SOLVENTS AT ROOM TEMPERATURE

Kazuhiro MAE, Taisuke MAKI, Jun ARAKI, and Kouichi MIURA
Department of Chemical Engineering, Kyoto University, Sakyo-ku, Kyoto 606-01, Japan

Key words: Extraction of brown coal, Liquid Oxidation of coal, Methanol based binary solvents

INTRODUCTION

It is very important to develop effective methods for utilizing low rank coals such as brown coal and lignite, which are most abundant fossil resources. One of the inherent drawbacks for utilizing the coal lies in the difficulty of handling such as transportation and storage. To overcome the drawback, several methods for fluidifying the coal have been proposed. Preparation of coal-water mixture (CWM) is one of such methods, but low rank coals are not suitable for CWM preparation, because they have lots of hydrophilic functional groups such as -COOH and -OH. Liquefaction is another means to fluidify the low rank coals, but it is a technology of the next generation. Therefore, it would be very profitable if some practical methods which are suitable to fluidify low rank coals are developed. The authors have focused on the extraction of low rank coals in conventionally used solvents as one of such methods.

Extraction and swelling of coals by various solvents have been performed for decades as a means to examine the coal structure, but only the coals of a certain rank could be extracted by 70 wt% or so with a special solvent.¹ The extraction yield of low rank coals has been less than 10 wt% even in a highly polar solvents.¹⁻⁴ To increase the extraction yield of lower rank coals, several pretreatments of coals were performed.^{5,6} However, the treatments under severe conditions and/or in highly polar solvents are required to extract the low rank coal to a large extent. On the other hand, several researchers^{7,8} found that the coal was largely swollen with alcohol based binary solvents. We have recently found that an Australian brown coal oxidized by H₂O₂ for 2 h at 60°C was extracted at room temperature by 84 wt% in a mixed solvent of methanol and 1-methylnaphthalene.⁹

In this paper we performed the extraction of low rank coals modified by several oxidation methods in several combinations of low molecule alcohol and non-polar solvent systems to examine the validity of the proposed method. Then, the extraction mechanism of coal in the mixed solvents of methanol and non-polar solvents was discussed from the viewpoint of the change in coal structure and solvent properties.

EXPERIMENTAL

Oxidation of coal

Three kinds of coals, an Australian brown coal (Morwell, MW), a Canadian brown coal (Highvale, HV), and a Japanese sub-bituminous coal (Taiheiyō, TC) were used as raw coals. The coals were ground into fine particles of less than 74 μm, and dried in vacuo at 110°C for 24 h before use. The oxidation of the coals was performed as follows: 2 g of coal particles were mixed with 20 ml of 30% aqueous hydrogen peroxide (HPO) in a flask. After treating the mixture for 2 h in a water bath kept at a constant temperature of 25 °C or 60 °C, an excess of cold water was added to the flask to terminate the oxidation. The oxidized coals were filtrated and evacuated at 60 °C for 24 h. To examine the effect of the oxidation method, MW coal was also oxidized in an air stream at 250 °C (AO) using a thermogravimetric analyzer until no weight change was detected. The oxidized coals were abbreviated to (oxidation method)(treatment temperature).(treatment time(h)) such as HPO60.2 and AO250.2, etc.

Extraction of oxidized coals

The raw coals and the oxidized coals were extracted at 25°C by alcohol based binary solvents of m-xylene (m-X), 1-methylnaphthalene (1MN), 2-methylnaphthalene (2MN), benzene (B), and tetralin (Tet), phenol (Ph) and tetrahydrofuran (THF). Methanol (MeOH), ethanol (EtOH), 1-propanol (PrOH) and 2-methyl-1-propanol (2M1P) were used as the alcohols. The extraction was performed as follows: 200mg of the oxidized coal were mixed with 6 ml of solvent and were kept for 4h at 25 °C under the irradiation of an ultrasonic wave. After centrifuging the mixture and removing the extract, 6 ml of fresh solvent were added to the residue and the mixture was treated for 3 h at 25 °C under the irradiation of the ultrasonic wave. This centrifugation-extraction cycle was repeated three times. The residue was then washed with an excess of methanol and evacuated for 24 h at 60 °C. The extraction yield was calculated from the weight difference between the oxidized coal and the residue, and was represented on the basis of dry oxidized coal.

Characterization of the oxidized coal and their extracts

The change in coal properties through the oxidation was examined from the ultimate analysis, ¹³C-n.m.r., TG-MS, and F.T.i.r. measurements. The extracts were dissolved by

DMF, then they were served to molecular weight distribution measurement using the GPC technique.

RESULTS AND DISCUSSION

Changes in coal properties through oxidation

The oxidation pretreatment was performed to change the coal into more extractable structure. However, the oxidation inevitably causes the loss of coal itself. Therefore, the degree of the oxidation must be optimized by taking into account both the extraction yield and the loss of coal. Then, the changes in the solid yield and the loss of coal through the oxidation were examined first. Table 1 lists the carbon conversions of the coals to solid, CO_2 , and water soluble organics through the oxidation. The ultimate analyses, and the atomic H/C and O/C values for the oxidized coals are also listed. When MW coal was oxidized by air for 4 h at 250°C (AO250.4), the carbon conversion to CO_2 was 0.20, indicating that 20% of carbon is lost through the oxidation. On the other hand, when MW coal was oxidized by H_2O_2 for 2 h at 60°C (HPO60.2), the carbon conversion to CO_2 was 0.04 and the carbon conversion to the water-soluble organics was 0.17. Since the water soluble organics can be recovered and utilized,¹⁰ the loss of coal was judged to be only 4% for HPO60.2 prepared from MW. This was also the case for HPO60.2 prepared from HV. These results indicate that the H_2O_2 pretreatment is superior to the air oxidation pretreatment from the viewpoint of minimizing the carbon loss through the pretreatment.

Then, the changes in coal properties through the H_2O_2 oxidation were examined in more detail from several analyses for MW coal. Both the H/C and O/C values of the solid increased through the oxidation for HPO25.4 and HPO60.2 as listed in Table 1. We have shown that both hydrogen and oxygen are introduced into the coal, mainly as the form of OH groups, through the H_2O_2 oxidation in a previous paper.¹⁰ This is peculiar to the H_2O_2 oxidation. Comparing the F.T.i.r. spectra between the oxidized coals and the raw coal, the amount of carboxyl groups was found to increase by the oxidation. Table 2 gives the carbon distributions estimated by the ^{13}C -n.m.r. for the raw coal and the HPO60.2. The amounts of COOH, O-aliphatic (including R-OH), and aliphatic carbon increased, on the contrary, the f_{a} value and the amounts of Ar-OH (including Ar-O-Ar), substituted and protonated carbons decreased through the H_2O_2 oxidation. From the above results, it was judged that the H_2O_2 oxidation decomposed a part of the covalent bondings such as Ar-OH, Ar-O-Ar, and substituted carbon, then produced -COOH, C-O-C and R-OH in the coal.

Extraction of oxidized coal by methanol and 1-methylnaphthalene mixtures

The solvent extraction of lower rank coals is believed to be affected by non-covalent interactions such as hydrogen bonding as well as the solubilization ability of the solvent.¹¹ The HPO60.2 prepared from MW coal was supposed to be enriched with the hydrogen bonding sites because of the increase in the oxygen functional groups. Therefore, the solvent suitable to extract the HPO60.2 must have the potential for breaking the hydrogen bonding in addition to the potential for dissolving the coal.

Methanol is known not to dissolve but swell coal to a large extent. On the other hand, two aromatic ring compounds such as naphthalene, naphthalene derivatives, etc., which are recovered from the coal conversion process, are judged to be solvents suitable to dissolve the coal, judging from the solubility parameter. This suggests that the extraction of the HPO60.2 is expected to be enhanced by using mixed solvents of methanol and aromatic compounds.

Figure 1 shows the extraction yields of the raw coal and the oxidized coals in a mixed solvent of methanol and 1-methylnaphthalene (1MN/MeOH). The abscissa in Fig.1 represents the volume fraction of methanol (f_v) in the mixed solvent. The extraction yield of the raw coal was 10 wt% at most at around $f_v=0.6$, and the extraction yield of HPO25.4 was slightly larger than that of the raw coal. The HPO60.2 was extracted little in pure methanol or pure 1MN, but was extracted to a large extent in the mixed solvent of $f_v=0.2$ to 0.9. At $f_v=0.56$ the extraction yield reached up to 84 wt% on the oxidized coal basis, which is comparable to the extraction yield in DMF. The value of 84 wt% on the oxidized coal basis corresponds to 66 wt% on the raw coal basis for HPO60.2. Even this value of the extraction yield is much larger than the values reported by now. If we add the water soluble organic acids recovered during the pretreatment to the extraction yield, the extraction yield reaches more than 80 wt% on the raw coal basis. The molecular weight distribution (number basis) of the 1MN/MeOH ($f_v=0.56$) extract of HPO60.2 ranged from 240 to 10000, and the average molecular weight was found to be 837.

Extraction of the oxidized coal by several mixtures of small molecule alcohols and solvents

Next, we examined the effect of the solvent type on the extraction of HPO60.2 prepared from MW. Figure 2 shows the extraction yields at 25°C in the mixed solvents of 1MN and several small molecule alcohols. The extraction yields in 1MN/EtOH, 1MN/PrOH were also as high as the extraction yields in 1MN/MeOH, but the maximum yield in 1MN/2M1P was

only 42 wt%. Since 2M1P has the largest molecule size of the alcohols tested, its penetration into the coal matrix would be retarded. Figure 3 shows the extraction yields of the HPO60.2 at 25 °C in the mixed solvents of MeOH and aromatic compounds. In 2MN/MeOH the HPO60.2 was also extracted to a large extent at $f_v=0.3$ to 0.9, and reached up to 80 wt% at $f_v=0.56$. However, in Xy/MeOH the HPO60.2 was extracted by only 33 wt% at maximum at $f_v=0.76$. This small extraction yield is probably due to less solubilization potential of m-xylene. On the other hand, the extraction yields of the HPO60.2 in the mixed solvents of methanol and THF or PhOH reached up to almost 80 wt% at $f_v=0.36$ in both binary solvents. The f_v value corresponding to the maximum extraction yield for these binary solvents was smaller than that in the mixed solvents of methanol and non-polar solvents.

Effect of coal type on the extractability of the oxidized coal

The H₂O₂ oxidation pretreatment was very effective to increase the solvent extraction yield for Morwell coal. To examine the effect of the H₂O₂ oxidation pretreatment for other coals, we extracted several coals oxidized by H₂O₂ for 2 h at 60 °C. Figure 4 compares the extraction yields of the oxidized coals in DMSO and 1MN/MeOH. The HPO60.2 prepared from MW coal was extracted more than 80 wt% in both DMSO and 1MN/MeOH as described above. For the HPO60.2 prepared from HV brown coal, the yield of DMSO-extract reached 82wt%, but the yield of 1MN/MeOH-extract was 48 wt%. For the HPO60.2 prepared from TC subbituminous coal, the extraction yields in 1MN/MeOH and DMSO were 30 wt% and 37wt%, respectively. The small extraction yield of TC coal was presumed to be due to a small extent of the oxidation. The solid yield through the H₂O₂ oxidation was 0.94 for TC as shown in Table 1. So, we oxidized the TC coal by H₂O₂ for 24h at 40 °C (HPO40.24) to increase the extent of oxidation. The solid yield through the oxidation was 80 wt%, whose value was almost same as that of HPO60.2 prepared from MW. The extraction yield of the HPO40.24 in DMSO increased up to 55 wt%, but not so large as that for the brown coals. These results suggest that the extraction yield of the coal oxidized by H₂O₂ in 1MN/MeOH is strongly dependent on coal type, and that the proposed method is more effective for lower rank coals.

Role of the binary solvent mixture on the extraction of the oxidized coal

The secondary interaction of brown coal is mainly due to hydrogen bonding and ionic force as reported by Nishioka.¹² Green et al.⁸ showed that the swelling ratio of coal increased in N-N-dimethylaniline and methanol mixture, and concluded that methanol could interact with the specific sites of the coal surface and break the hydrogen bonding. Lucht et al.¹³ and Suuberg et al.¹⁴ also claimed that methanol having a small molecule easily penetrated and swelled the coal to interact with the specific site of coal. Table 3 lists several properties of methanol, ethanol, DMF, DMSO, and pyridine. The values of relative dielectric constant for methanol and ethanol are as large as those for DMF and DMSO. The values of the hydrogen bond index summarized by van Krevelen¹⁵ and Guttman's ΔH for methanol and ethanol are larger than those for DMF, respectively. In addition methanol molecule is small and easy to penetrate into coal matrix as stated above. These discussion suggests that methanol well has a potential to break hydrogen bonding in coal.

Then the extraction mechanism of HPO60.2 prepared from MW in methanol based binary solvents was presumed as follows: Methanol disrupts the hydrogen bonding in the HPO60.2 and interacts with functional groups at first, then the penetration of aromatic compounds such as 1MN is enhanced. Since the aromatic compounds have the potential to solubilize the coal molecule interacting with methanol, the HPO60.2 could be extracted to a large extent. Then the solubilization of the methanol adducted coal may be regarded as the solubilization of the bituminous coal.

The regular solution theory may not be applied to the extraction of low rank coal,¹¹ but it seemed to be applicable to the extraction of the HPO60.2 in methanol based binary solvents, judging from the above discussion. Following the regular solution theory, the extraction yield is maximized when the solubility parameters of both coal and solvent are close together.¹⁵ Since the oxidized coal is adducted with methanol through its functional groups, the coal molecule would be enveloped by methanol molecules. Then, the solubility parameter of the HPO60.2 was calculated by taking into account the contribution of methanol adducted in terms of the following equation:¹⁶

$$\delta(\text{coal}) = \frac{7.0+63.5f_a+63.5(\text{H/C})+106(\text{O/C})+51.8(\text{N+S/C})}{-10.9+12f_a+13.9(\text{H/C})+5.5(\text{O/C})-2.8((\text{N+S/C}))} \quad (1)$$

Figure 5 shows the change in the solubility parameter of HPO60.2, $\delta(\text{HPO60.2})$, against the amount of methanol adducted. The $\delta(\text{HPO60.2})$ value decreased with the increase of the amount of methanol adducted. If it is assumed that methanol adducts with carboxyl groups first and then ArOH with of HPO60.2, the $\delta(\text{HPO60.2})$ decreased from 13.1 to 11.5 first, and finally to 10.8 (cal/cm³)^{0.5} with the increase of the amount of methanol adducted.

The solubility parameter of the mixed solvent, δ , was calculated by¹⁶

$$\delta^2 = \delta_d^2 + \delta_h^2 + \delta_p^2 \quad (2)$$

where δ_d , δ_h , and δ_p represent the solubility parameters deriving from dispersion forces, hydrogen bondings, and polar forces, respectively. The values of δ_d , δ_h , and δ_p are calculated from the values of pure solvents by

$$\delta_i^2 = x_1 \cdot \delta_{i1}^2 + (1 - x_1) \cdot \delta_{i2}^2 \quad (\delta_i: i = d, h, p) \quad (3)$$

where x_1 is the mole fraction of alcohol, and δ_{i1} and δ_{i2} are the solubility parameters of alcohol and nonpolar solvent, respectively.

Figure 6 shows the extraction yield of HPO60.2 at 25°C against the solubility parameter of the solvent calculated by eqs.(2) and (3). The $\delta(\text{HPO60.2})$ value was assumed to change from 13.1 to 10.8 (cal/cm³)^{0.5} with the increase of the amount of methanol adducted as stated above. The extraction yield and the solubility parameter of the solvent correlated very well and the extraction yield reached a maximum at $\delta \approx 11.5$ (cal/cm³)^{0.5}. The value of 11.5 (cal/cm³)^{0.5} corresponded to the $\delta(\text{HPO60.2})$ value calculated by assuming that methanol adducted with all carboxyl groups of HPO60.2. Thus the regular solution theory seemed to be applicable to the extraction of HPO60.2 with the alcohol based mixed solvent.

This supports the extraction mechanism mentioned above: Methanol and/or ethanol penetrate into the coal matrix easily, break the hydrogen bonding or ionic interaction in coal, and interact with the oxygen functional groups tightly. This facilitates the penetration of the binary solvent of non-polar solvent and alcohol. The macromolecules enveloped with alcohol will be easily extracted by the mixed solvent having strong solubilization potential. This may be speculative because the extraction behavior is also affected by the phase separation equilibrium among coal, binary solvent and extracts. We will examine the extraction behavior in more detail in future work. However, it is noteworthy that the regular solution theory hold unexpectedly for the extraction of the oxidized coal with alcohol based mixed solvents.

CONCLUSION

A new method was developed for extracting a great deal of brown coal at room temperature in conventionally used solvents. When an Australian brown coal, Morwell, was preoxidized with H₂O₂ for 2 h at 60 °C, the covalent bondings were partly decomposed and many carboxyl groups and C-O-C groups were formed. The oxidized coal was extracted in several alcohol based binary solvents. The maximum extraction yields of the oxidized coal surprisingly reached more than 80 wt% in the binary solvents of methanol/1-methylnaphthalene, ethanol/1-methylnaphthalene, methanol/2-methylnaphthalene, and methanol/phenol at an suitable alcohol fraction. The average molecular weight (number basis) of the extract was 837. The proposed extraction method will be useful to develop a new coal conversion method as well as to facilitate the transportation of coal.

ACKNOWLEDGMENT

The authors give sincere thanks to Drs. Tadashi Yoshida and Hideaki Sasaki of Hokkaido National Industrial Research Institute for the ¹³C-n.m.r. measurement of our samples. This work was financially supported by NEDO International Joint Research (Coal and Wastes as Oil Alternative Energy and Chemicals) .

REFERENCES

1. Iino, M.; Takanohashi, T.; Ohsuga, H.; Toda, K.; *Fuel*, **1988**, *67*, 1639-1645.
2. Pugmire, R.J.; Solum, M.S.; Bai, S.; Fletcher, T.H.; Woods, S.; Grant, D.M., *Prepr. ACS Fuel Div.* vol 38, No.2, **1993** 647-654.
3. Marzec, A.; Juzwa, M.; Betej, K.; Subkowiak M.; *Fuel Process. Techn.*, **1979**, *2*, 35-44.
4. Morgan, D.L.; *Prepr. ACS Fuel Div.* vol 37, No.4, **1992** 1996-2001.
5. Nishioka, M.; *Fuel*, **70**, **1991** 1413-1419.
6. Winans, R.E.; McBeth, R.L.; Hunt, J.E.; *Prepr. ACS Fuel Div.* vol 38, No.2, **1993** 561-564.
7. Hombach, H.-P.; *Fuel*, **1980**, *59*, 465-470.
8. Green, T.K.; Larsen J.W., *Fuel*, **1984**, *63*, 1538-1543.
9. Miura, K.; Mae, K.; Maki, T.; Araki, J., *Chemistry Letters*, **1995** 909-910.
10. Miura, K.; Mae, K.; Okutsu, H.; Mizutani, N., *Energy & Fuel* in press.
11. Larsen, J.W.; Schawver, S., *Energy & Fuels*, **1990**, *4*, 74-77.
12. Nishioka, M., *Fuel*, **1993**, *72*, 1719-1724.
13. Lucht, L.M.; Peppas, N.A., *Erdol und Kohle erdgas*, **1987**, *40*, 483-485.
14. Suabarg, E.M.; Otake, Y.; Lanngrner, M.J.; Leung, K.T.; Milosavljevic, I., *Energy & Fuels*, **1994**, *8*, 1247-1262.
15. van Krevelen, D.W., *"Coal" 2nd edn*, Elsevier Scientific: New York, **1981**
16. Painter, P.C.; Graf, J.; Coleman, M.M., *Energy & Fuels*, **1990**, *4*, 379-384.

Table 1 Carbon conversions through the oxidation and ultimate analysis of oxidized coals.

Sample	Carbon conversion through oxidation			Ultimate analysis of the oxidized coal [wt%, daf]					mol ratio	
	solid	CO ₂	water soluble % organics	C	H	N	O(diff)	O/C[-]	H/C[-]	
MW Raw	1.00	-	-	64.0	4.7	0.7	30.6	0.359	0.881	
HPO25.4	0.96	0.02	0.02	61.6	4.6	0.6	33.2	0.404	0.896	
HPO60.2	0.79	0.04	0.17	60.1	4.9	0.7	34.3	0.428	0.978	
AO250.4	0.80	0.20	0	68.4	3.8	1.0	26.8	0.294	0.666	
HV Raw	1.00	-	-	67.0	4.3	1.0	27.7	0.310	0.770	
HPO60.2	0.70	0.08	0.22	63.0	4.3	1.0	31.7	0.377	0.919	
TC Raw	1.00	-	-	72.4	5.6	1.4	20.6	0.213	0.928	
HPO60.2	0.94	0.02	0.04	71.3	5.9	1.5	21.3	0.224	0.993	
HPO40.24	0.80	0.07	0.13	71.2	7.3	1.1	20.4	0.208	1.199	

Table 2 Carbon distributions of Morwell coal and the H₂O₂ oxidized coal determined by ¹³C-n.m.r.

sample	Raw	HPO60.2
Aromatic carbon		
H-C=O, =C=O	1.81	3.83
COOH	5.90	8.54
Ar-OH	9.01	6.93
Substitute	12.66	9.32
Protocate	34.09	24.55
Aliphatic carbon		
C-O-C	0.94	6.01
O-Methyl	1.63	3.69
Aliphatic	27.22	28.40
Methyl	6.73	8.73
total	36.53	46.83
Structural parameter	f _a [-]	0.63 0.53
M ₀ [kg/kmol]	156.4	196.8

Table 3 Comparison of the solvent properties between alcohol and polar solvents

Solvent	Methanol	Ethanol	DMF	DMSO	Py	1MN	Xy
Relative dielectric constant	32.6	24.3	36.7	46.7	12.3	-	-
Guttman ΔH (=DN*AN/100)	7.8	7.4	5.7	5.8	4.5	-	-
Hydrogen bond index	8.9	8.9	6.4	-	8.7	-	-
Solubility Parameter							
δ (cal/cm ³) ^{0.5}	14.6	13.0	12.2	13.1	10.7	10.4	8.4
δ _d (cal/cm ³) ^{0.5}	7.6	7.7	8.5	9.2	9.3	10.4	8.3
δ _p (cal/cm ³) ^{0.5}	10.9	9.6	5.5	5.0	2.9	0.0	0.5
δ _a (cal/cm ³) ^{0.5}	6.1	4.3	6.7	8.0	4.3	0.2	0.5

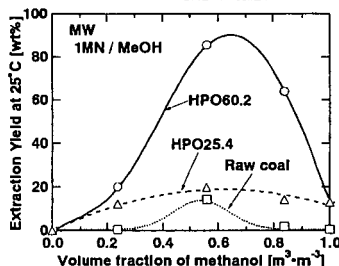


Figure 1 Extraction yield of the raw coal and H₂O₂ oxidized coal prepared from Morwell coal measured at 25°C in methanol and 1-metylnaphthalene mixture.

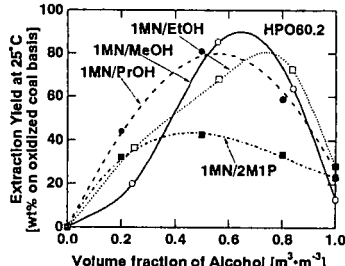


Figure 2 Extraction yield of the HPO60.2 prepared from Morwell coal measured at 25°C in the mixed solvents of several alcohols and 1-metylnaphthalene.

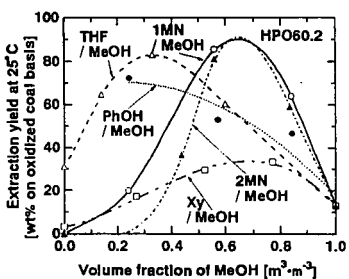


Figure 3 Extraction yield of the HPO60.2 prepared from Morwell coal measured at 25°C in various methanol based binary solvents.

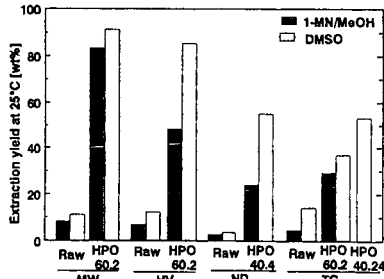


Figure 4 Effect of coal type on the extraction yield of the H₂O₂ oxidized coal.

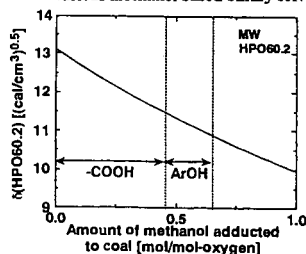


Figure 5 Change in the solubility parameter of HPO60.2 adducted with methanol.

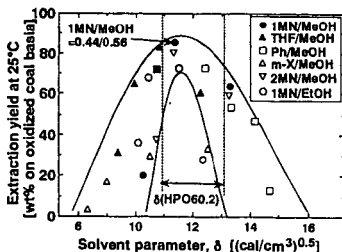


Figure 6 Relationship between the extraction yield of HPO60.2 prepared from Morwell coal and the solubility parameter of the solvent.

LINKAGES BETWEEN AROMATIC STRUCTURES IN THE ARGONNE PREMIUM COAL SAMPLES

Randall E. Winans and Nancy A. Tomczyk
Chemistry Division
Argonne National Laboratory
Argonne, IL 60439

Keywords: Argonne coals, structure lengths, mass spectrometry

ABSTRACT

The objective of this study is to elucidate the nature of the important linkages between aromatic clusters and variations of these links with coal rank. From studies using methods such as NMR and mass spectrometry, we have considerable information on the size and types of aromatic clusters in the Argonne coals. In this study, extracts, model polymers, extracted coals, and modified coals are examined by temperature resolved high resolution mass spectrometry. There is evidence that strong bond cleavage may be very important for volatile release in pyrolysis of higher rank coals.

INTRODUCTION

There is significant general information on the size and nature of the aromatic structures in coals, especially the Argonne Premium Coal Samples. A battery of methods have been used yielding global information by NMR,¹ XANES,^{2,3,4} XPS,⁵ and TGFTIR,^{6,7} and more specific class and size distribution by FIMS,⁸ HRMS,^{9,10} and LDMS.¹¹ The nature and distribution of the linkages between these clusters is less well defined but are obviously important in any thermal process. A large number of studies have been done on the pyrolysis of the Argonne coals, for example: modified Rock-Eval pyrolysis,¹² pyrolysis MS,^{8,12} and TGFTIR.^{6,7} It has been assumed that ethylene linkages are important in coals and that they are reactive. However, there is no direct evidence that this is the case.

EXPERIMENTAL

A complete description of the Argonne Premium Coal Samples is available via internet at: <http://www.anl.gov/PCS/pcshome.html> and has been published.¹³ Important analytical data on the coals and pyridine extracts¹¹ are shown in Table 1. Nitrogen values are fairly constant between 1.3-1.7 N/100 carbons.

Desorption high resolution mass spectra are taken on a 3-sector MS-50 either in electron impact or chemical ionization mode. Samples are heated from 200 to 700 °C at 200 °C/min on a probe directly in the source. The chemical ionization gas used was iso-butane. A Diels-Alder adduct of maleic anhydride and perdeuteroanthracene is used as an internal standard. Precise mass measurements are averaged from scans over the entire temperature range. Formulae are assigned and the data sorted via a procedure developed in this program. Only formulae that fit within ± 3.5 millimass units are considered.

Table A-1. Selected Analysis and Yields for the Argonne Premium Coal Samples.

Sample #	Name	%C	H	S	Per 100 Carbons			Pyridine Solubles Yield (w%)
					O			
					<i>a</i>	<i>b</i>	<i>c</i>	
8	Beulah-Zap	74.1	80	0.4	21	31	7.7	18
2	Wyodak-Anderson	76.0	86	0.2	18	22	7.3	29
3	Illinois #6	80.7	77	1.2	13	10	5.0	29
6	Blind Canyon	81.3	86	0.2	11	12	7.4	25
4	Pittsburgh	85.0	77	0.4	8	9	6.0	24
7	Lewiston-Stockton	85.5	76	0.3	9	10	6.7	17
1	Upper Freeport	88.1	66	0.3	7	8	6.4	28
5	Pocahontas #3	91.8	59	0.2	2	4	3.7	3

a - Coal

b - Extract

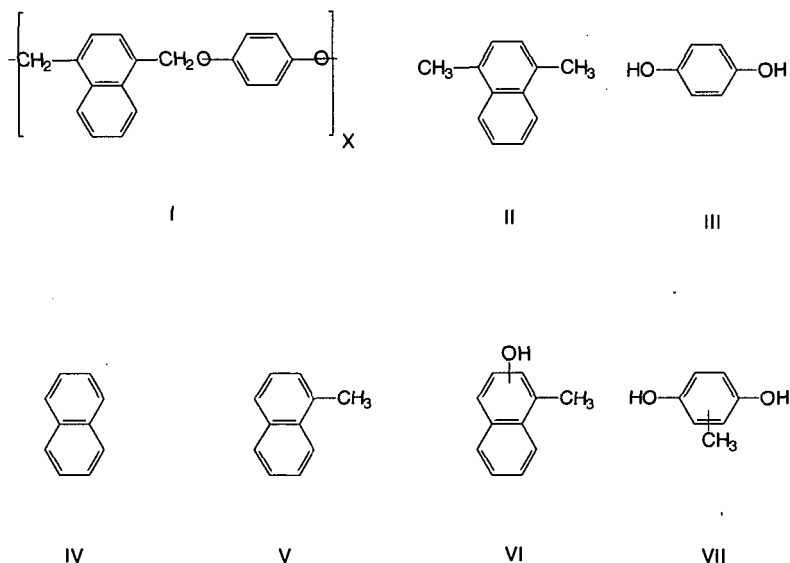
c - Furans and Ethers

High resolution mass spectrometry data can be sorted by both heteroatom content and by hydrogen deficiency which is also termed double bond equivalents and is related to z-number. From hydrogen deficiency, the size of aromatic clusters can be estimated.

RESULTS AND DISCUSSION

In absolute numbers of oxygens per 100 carbon atoms determined by HRMS, the furans plus ethers are relatively constant compared to the total oxygen in the extracts as is shown in Table 1. This would suggest that the influence of these types of structures are relatively important and constant across all ranks for vitrinite rich coals.

Because of these results, we decided to reinvestigate the reactivity of a model polymer with ether links. DCIMS results were examined since ions observed are the result of thermal fragmentation and not fragmentation in the source of the spectrometer. From the mass spectra recorded as a function of temperature a series of products were observed and are shown in Scheme 1 along with the polymer (I).¹⁴



Scheme 1

Strong bond cleavages occur at higher temperatures which would yield naphthalene (IV) and methyl naphthalene, and especially with the rearranged polymer resulting in VI and VII. For example, the naphthalene yield, which only can be formed from cleavage of strong bonds, is maximum at 500 °C. In contrast, dihydroxybenzene ($m/z = 110$) and dimethylnaphthalene peak at 300 °C. In Figure 1a, the temperature profile for dihydroxybenzene is compared between the polymer and the Illinois coal (APCS 3) extract. The coal yields below 400 °C are very small and maximize between 400-500 °C which would suggest that the bonding is not via oxygen-methylene linkages as is the case for the polymer. Ring methylated dihydrobenzene (VII) results from rearrangement of the polymer followed by cleavage. It is probably represented in the second peak for $m/z = 124$ at ~475 °C (see Figure 1b). The Illinois bituminous coal has a maximum at this temperature and several at even higher temperatures. While the low rank subbituminous coal is very broad and has a maximum at even a higher temperature; this broad type of distribution was also observed for phenol in lignite pyrolysis.¹² The oxygen functionality is likely to be undergoing some secondary reactions prior to release from the macromolecular matrix.

Burnham, et al.¹² using PyMS noticed greater high temperature tails for small unsubstituted aromatics compared to corresponding methyl derivatives for the higher rank coals. They suggested that this may be due to increased breaking of Ar-Ar bonds. We observed in the high rank coals that

larger aromatics are released in greater quantities at high temperature compared to lower temperature while substituted aromatics tend to be more abundant at lower temperature. In Figure 1c, we observed this effect for pyrene/fluoranthene ($m/z=202$) compared to C_2 -pyrene ($m/z=230$) for the Pocahontas extract. In the lower rank Pittsburgh seam coal (Figure 1d), the unsubstituted pyrene which can only be released by strong bond breaking, is still more abundant at high temperatures, but in addition, the alkylated aromatic is also released at higher temperatures.

CONCLUSIONS

The evidence suggests the strong bond breaking in pyrolysis is significant in higher rank coals and could play a role in the lower rank coal pyrolysis. We are examining methods to better quantitate the extent of these types of cleavages in coal pyrolysis.

ACKNOWLEDGMENTS

This work was performed under the auspices of the Office of Basic Energy Sciences, Division of Chemical Sciences, U.S. Department of Energy, under contract number W-31-109-ENG-38.

REFERENCES

1. T. H. Fletcher, S. Bai, R. J. Pugmire, M. S. Solum, S. Wood, and D. M. Grant, *Energy Fuels* **7**, 734 (1993).
2. G. N. George, M. L. Gorbaty, S. R. Kelemen, and M. Sansone, *Energy Fuels* **5**, 93 (1991).
3. G. P. Huffman, S. Mitra, F. E. Huggins, N. Shah, S. Vaidya, and F. Lu, *Energy Fuels* **5**, 574 (1991).
4. S. Mitra-Kirtley, O. C. Mullins, J. Branthaver, J. Van Elp, and S. P. Cramer, *Prepr., Div. Fuel Chem., ACS* **38**, 756 (1993).
5. S. R. Kelemen, M. L. Gorbaty, and P. J. Kwiatek, *Energy Fuels* **8**, 896 (1994).
6. R. Bassilakis, Y. Zhao, P. R. Solomon, and M. A. Serio, *Energy Fuels* **7**, 710 (1993).
7. P. R. Solomon, M. A. Serio, R. M. Carangelo, and R. Bassilakis, *Energy Fuels* **4**, 319 (1990).
8. N. Simmleit, H.-R. Schulten, Y. Yan, and H. L. C. Meuzelaar, "Thermochemical Analysis of U.S. Argonne Premium Coal Samples by Time-Resolved Pyrolysis FIMS," in *Advances in Coal Spectroscopy*, H. L. C. Meuzelaar (ed.), Plenum Press, New York, 1992, 295.
9. R. E. Winans, Y. Kim, J. E. Hunt, and R. L. McBeth, *Proceedings, 1995 International Conference on Coal Science, Oviedo, Spain (1995)*, 87.
10. R. E. Winans, "Mass Spectrometric Studies of Coals and Coal Macerals," in *Advances in Coal Spectroscopy*, H. L. C. Meuzelaar (ed.), Plenum Press, New York, 1992, 255.
11. J. E. Hunt and R. E. Winans, *Proceedings, 1995 International Conference on Coal Science, Oviedo, Spain (1995)*, 319.
12. A. K. Burnham, M. S. Oh, and R. W. Crawford, *Energy Fuels* **3**, 42 (1989).
13. K. S. Vorres, *Energy Fuels* **4**, 420 (1990).
14. T. G. Squires, B. F. Smith, R. E. Winans, R. G. Scott, and R. Hayatsu, *Proceedings, 1983 International Conference on Coal Science, Pittsburgh, PA (1983)*, 292.

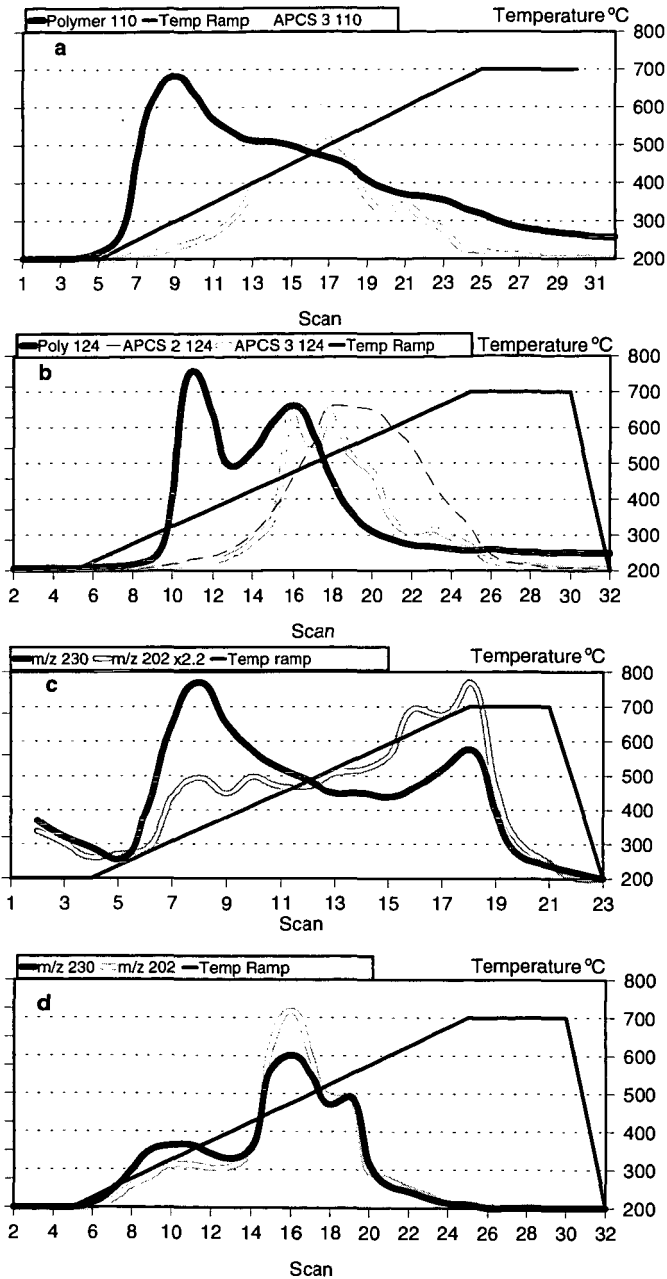


Figure 1. Individual ion pyrograms from DCIMS for (a) Pocahontas (APCS 5) pyridine extract; (b) Pocahontas whole coal; (c) Pittsburgh (APCS 4) pyridine extract; and (d) $m/z = 124$, for the polymer (I), Wyodak-Anderson subbituminous coal (APCS 2) pyridine extract, and Illinois No. 6 (APCS 3) pyridine extract.

A Question Concerning Coal Structure and/or Reactivity. The Reaction of Maleic Anhydride with Pittsburgh No. 8 Coal

John W. Larsen, James E. Roberts, Deanna Metka Quay
Chemistry Department
Lehigh University
Bethlehem, Pennsylvania 18015

ABSTRACT. Maleic anhydride reacts readily with coals under Diels-Alder conditions and the coals gain 10% or more in mass. This reaction has been carried out using ^{13}C labeled maleic anhydride and Pittsburgh No. 8 coal. The results are consistent with the occurrence of the Diels-Alder reaction. There is evidence against the occurrence of all other conceivable (to us) reactions. The amount of maleic anhydride incorporated is inconsistent with all published coal structures. Either coal structures are seriously in error by omitting a significant population of reactive diene structures or coal reactivity is strongly enhanced by mechanisms not understood.

INTRODUCTION. Several groups have studied the reaction of maleic anhydride and coals and, with one exception, concluded a Diels-Alder reaction was responsible for the mass increase.¹⁻⁵ This conclusion immediately leads to a significant dilemma. The maleic anhydride uptake observed by all workers is too large to be consistent with a Diels-Alder reaction between maleic anhydride and current published coal structures. The amount of incorporation is much higher than would be predicted by the number of reactive diene structures thought to be present. Such reactive structures in coals are primarily anthracene and higher acenes. β -naphthol undergoes a Diels-Alder reaction, but only under forcing conditions much more vigorous than those used with coal.⁶ There are two possible explanations for the large maleic anhydride incorporation. One is that the coal structures are in error and contain more reactive dienes than suspected. This is a reasonable conclusion because such reactive dienes are unlikely to survive any of the degradation conditions so far used to probe coal structure and would be spectroscopically indistinguishable from the aromatics. Another possible explanation is that functional groups, for example naphthalenes, might be reactive in coals under conditions much milder than in other situations. Stated another way, coals are showing strongly enhanced reactivity. Either of these explanations raises fundamental questions about the chemistry and structure of coals and it is this which makes the study of the maleic anhydride-coal reaction important. Reported here is a thorough re-examination of this reaction.

EXPERIMENTAL METHODS. Argonne samples of Pittsburgh No. 8 coal were reacted with maleic anhydride in chlorobenzene. The coal was dried by distilling off some of the chlorobenzene-water azeotrope. Work-up followed the procedure used by Nishioka.⁵ Samples of maleic anhydride independently labeled at both carbonyl and vinyl carbons were used. Solid state NMR spectra of the coals were obtained using a General Electric GN300 solid state NMR spectrometer operating at 75.4MHz for carbon using a Doty Scientific, Inc. 7 mm or 5 mm probe and a radio frequency feedback control circuit. The spectrometer was operated with radio frequency field strengths of 50 to 63 kHz for carbon and protons while acquiring 1 K of complex data points with a dwell time of 15 μs , a receiver gate time of 15 μs , and a filter delay of 15.75 μs . The times for the recycle delays were selected after the proton and carbon spin lattice relaxation times T_1 , of 0.23-0.27 s for protons and 0.2-9.8 s for carbons were determined. Relaxation delays of 2 s for cross polarization experiments, and 60 s for Bloch decay experiments were employed. The data were processed using a baseline correction, exponential multiplication equivalent to 100Hz line broadening and one zero-fill followed by Fourier transformation. The spectra were phased using an auto phase function followed by linear baseline adjustment and another auto phase so that only minor adjustments were required. Samples were examined under magic angle spinning and high power proton decoupling. Sapphire rotors with Kel-F[®] end caps were used to minimize ^{13}C background. Bloch decay single pulse experiments were used for most of the coal spectra. A cross polarization ^{13}C - ^{13}C double quantum filter pulse sequence was also utilized.¹¹

RESULTS. Figure 1 shows solid state ^{13}C Bloch decay NMR spectra for a physical mixture of Pittsburgh No. 8 coal and maleic anhydride and Pittsburgh No. 8 coal after reactions with a mixture of 50% ^{13}C maleic anhydride labeled in the 2 and 3 (vinyl) positions or in the 1 and 4 (carbonyl) positions.

RESULTS AND DISCUSSION. The NMR spectra show that the vinyl carbons have become sp^3 hybridized carbons in the adduct and that the carbonyl carbons remain unaltered. That the carbonyl carbons have not shifted confirms earlier reports that ester formation has not occurred and rules out Nishioka's assertion that a charge transfer interaction was responsible for maleic anhydride incorporation.^{1,2,5} If charge transfer was responsible for the upfield shift of the vinyl carbons, then a large upfield shift of the carbonyl carbons must also occur due to the presence of the transferred electron in the maleic anhydride LUMO. The conversion of the vinyl carbons from sp^2 to sp^3 is consistent with the occurrence of a Diels-Alder reaction. A ^{13}C - ^{13}C double quantum experiment confirms the double bond is converted to a single bond.

There are several other reactions which might also convert the vinyl carbons to sp^3 . An ene reaction would do this, but there is no precedent in the literature for an ene reaction between maleic anhydride and either phenols or alkyl aromatics. Maleic anhydride can be homo polymerized only with difficulty and it has been demonstrated that the unshared electrons in coals are remarkably inefficient at inducing polymerizations; vitrinite radicals are not capable of initiating the polymerization of vinyl pyridine.^{7,8} The radical addition of maleic anhydride to benzylic positions is a known reaction, but adding radical initiators or using peroxide containing air-oxidized coals did not give any increase in maleic anhydride incorporation ruling out this pathway.^{7,9} Michael addition to phenols or thiols is possible.¹⁰ This reaction does not occur with phenols in coals, but does occur with coal thiol groups. The amount of thiol sulphur in this coal is much too small to explain the observed maleic anhydride incorporation.

It is clear that maleic anhydride is adding to the coals via a reaction involving the carbon-carbon double bond. The most reasonable candidate for this reaction remains the Diels-Alder. We are left with the puzzle with which we began, although this puzzle is now based on firmer ground. Either there are under characterized reactive diene structures in coals or the maleic anhydride reaction with coals is somehow enhanced. In one investigation of this latter possibility, we attempted to catalyze the Diels-Alder reaction between maleic anhydride and naphthalene by carrying it out in the presence of added coal. The added coal had no effect. It is clear from these results that major features of coal structure and/or reactivity are still not understood.

ACKNOWLEDGMENT: We are grateful to the U. S. Department of Energy for partial support of this research.

REFERENCES

1. Duty, R. C.; Liu, H. F. *Fuel* **1980**, *54*, 546-550.
2. Larsen, J. W.; Lee, D. *Fuel* **1983**, *62*, 1351-1354.
3. Quinga, E. M. Y.; Larsen, J. W. *Energy Fuels* **1987**, *1*, 300-304.
4. Zher 'akova, G.; Kochkan'an, R. *Fuel* **1990**, *69*, 898-901.
5. Nishioka, M. *Energy Fuels* **1991**, *5*, 523-525.
6. Wariyar, N. S. *Proc. Indian Acad. Sci.* **1956**, *43A*, 231-236.
7. Trivedi, B. C.; Colbertson, B. M. *Maleic Anhydride* Plenum Press: New York 1982.
8. Flowers, R. A. II; Gebhard, L. A.; Larsen, J. W.; Silbernagel, B. G. *ENERGY FUELS* **1989**, *3*, 762-764.
9. Bickford, W. G.; Fisher, G. S.; Dollean, F. G.; Swift, C. G. *J. Amer. Oil. Chem. Soc.* **1948**, 251-254.
10. Zcenty, F. G.; Vinegard, B. D.; Schlepplik, A. A. *J. Org. Chem.* **1962**, *27*, 3140-3146.
11. Bax, A.; Freeman, R.; Kempself, S. *J. Am. Chem. Soc.* **1980**, *102*, 4849-4851. Menger, E. M.; Vega, S.; Griffin R. G. *J. Am. Chem. Soc.* **1989**, *108*, 2215-2218.

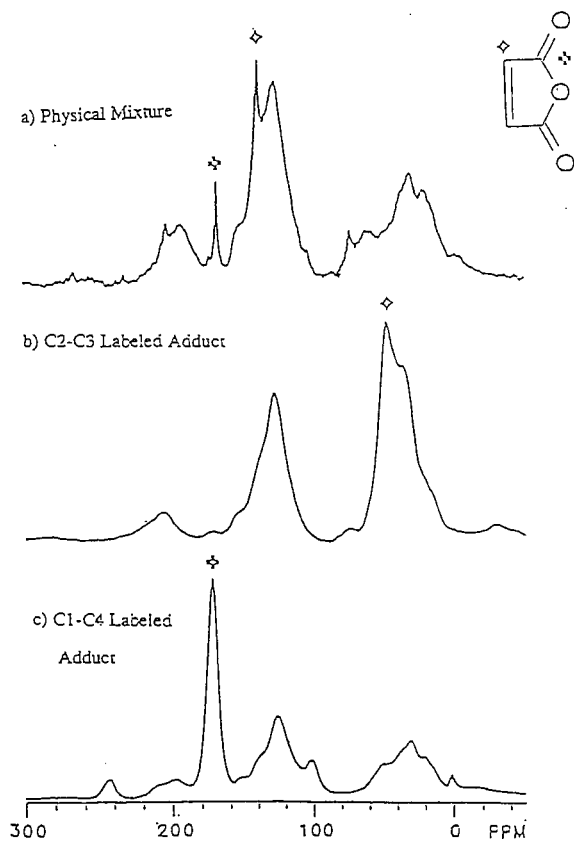


Figure 1. Solid State ^{13}C NMR spectra for a) a physical mixture of Pittsburgh 8 coal and maleic anhydride and Pittsburgh No. 8 coal reacted with b) $^{13}\text{C}_2$ $^{13}\text{C}_3$ and c) $^{13}\text{C}_1$ $^{13}\text{C}_4$ labeled maleic anhydride for 10 days in chlorobenzene at 110°C , then Soxhlet extracted with methanol for 3 days and dried.

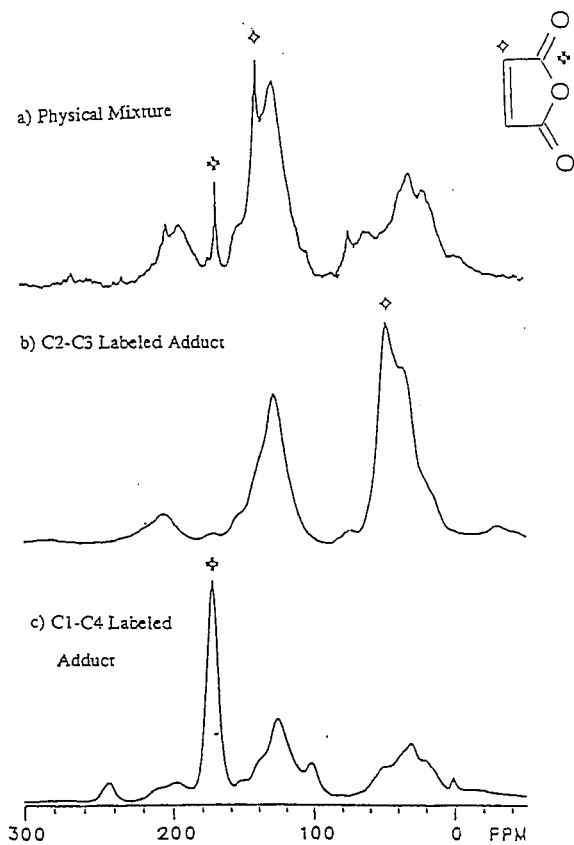


Figure 1. Solid State ^{13}C NMR spectra for a) a physical mixture of Pittsburgh 8 coal and maleic anhydride and Pittsburgh No. 8 coal reacted with b) $^{13}\text{C}_2$ $^{13}\text{C}_3$ and c) $^{13}\text{C}_1$ $^{13}\text{C}_4$ labeled maleic anhydride for 10 days in chlorobenzene at 110°C , then Soxhlet extracted with methanol for 3 days and dried.

HEAT TREATMENT OF COALS IN VARIOUS SOLVENTS AT TEMPERATURES AS LOW AS 175 - 300°C

Masashi Iino, Jianli Shen, Satoshi Ashida, Chunqi Li, and Toshimasa Takanohashi
Institute for Chemical Reaction Science, Tohoku University
Katahira, Aoba-ku, Sendai 980-77, JAPAN

KEYWORDS: Heat treatment, dissolution reaction, solvent effect

INTRODUCTION

Neavel (1) reported that more than 90% of a high-volatile bituminous coal became soluble in pyridine by coal liquefaction less than 5 min. at 400°C in tetralin. We are interested in the dissolution mechanism at this initial stage of coal liquefaction, since this stage seems to be a key step to control liquefaction yield and product selectivity. So, heat treatments of coals were carried out at temperatures as low as 175-300°C in various solvents which have different hydrogen donatability (2,3).

We are also interested in the mechanism of retrogressive reactions which concurrently occur with dissolution reactions in coal liquefaction. Although the details of retrogressive reactions are still obscure, hydrogen donation to coal fragments is essential for their suppression. Especially radicals formed during the initial stage of coal liquefaction must be stabilized to suppress efficiently the retrogressive reactions which could result in the formation of refractory, high-molecular weight substances. We have used carbon disulfide- N-methyl-2-pyrrolidinone (CS₂-NMP) mixed solvent (1:1 by volume) as an extraction solvent for the heat treated coals. The CS₂-NMP mixed solvent has been found to give high extraction yields (40-65wt%, daf) at room temperature for many bituminous coals (4). We also found that the extracts obtained with the mixed solvent include a considerable amount of the very heavy component which is not soluble in THF or pyridine, but soluble in the mixed solvent, i.e., heavier extract fraction than preasphaltene. (5).

In the previous study (2,3) the heat treatments of several bituminous coals such as Upper Freeport and Illinois No. 6 coals were carried out in solvents of different hydrogen-donatability under N₂ atmosphere. In tetralin retrogressive reaction was observed at 175-250°C and dissolution proceeded at 300-350°C. While in dihydroanthracene (DHA) or hexahydroanthracene (HHA), which have higher hydrogen-donatability than tetralin, the coals used underwent dissolution reactions even at low temperatures such as 175-250°C. The quantity of hydrogen transferred from the solvents to coals, which was estimated from dehydrogenation of the solvents such as anthracene from DHA, was found to be well correlated with the extent of the dissolution reactions occurred. However, recent study on the heat treatment of coals in NMP, which seems to have little hydrogen-donatability from its chemical structure, showed that for some coals NMP gave higher dissolution yields than HHA, the strongest hydrogen donor among the solvents we used.

In this study the heat treatments of coals in NMP at 175-300°C were carried out and the dissolution mechanism in NMP will be discussed, compared with that in HHA.

EXPERIMENTAL

The coals used in this study are shown in Table 1. NMP and HHA were used as a solvent for heat treatment of coals.

Heat treatment of the coal was performed in 50ml magnetically stirred autoclave at 175, 250, and 300°C, respectively. 1g of the coal and 5g of the solvent were charged into the autoclave, which was pressurized with nitrogen to 5.0 MPa at room temperature. After the heat treatment, the coal was fractionated into the CS₂-NMP mixed solvent-insoluble fraction (MI) and -soluble fraction (MS), and then MS further into tetrahydrofuran (THF) -insoluble, the mixed solvent soluble fraction (TIMS) and THF-soluble fraction (TS), with the mixed solvent and THF at room temperature under ultrasonic irradiation, as shown in Figure 1. The quantity of MI and TIMS was determined after drying overnight in vacuum at 80°C and that of TS was calculated by difference, i. e., 100-MI-TIMS. The dissolution yield was defined here as the sum of TIMS and TS.

RESULTS AND DISCUSSION

Heat treatment of coals in NMP and HHA

Figure 2 shows the fraction distribution after the heat treatment of Upper Freeport coal in NMP and HHA at 175°C, 250°C, and 300°C, together with the fraction distribution before the heat treatment, i. e., for the raw coal, which was obtained from the extraction of the raw coal with the CS₂-NMP mixed solvent and the fractionation of the extract obtained. At 175°C NMP gave higher dissolution yield (TIMS + TS) than HHA and little effect of temperature on the dissolution yield and fraction distribution was observed in NMP, unlike the case with HHA, suggesting different dissolution mechanisms for NMP and HHA. Figure 3 shows the result for Zao Zhuang coal and the similar tendency was obtained as Upper Freeport coal. Figure 4, 5 and 6 show the results for Pittsburgh No. 8, Illinois No. 6 and Beulah-Zap coals, respectively. The heat treatments of Pittsburgh No. 8 and Illinois No. 6 coals gave nearly 80% of the dissolution yields at 300°C, higher than those in HHA. Figure 7 shows the plot of net dissolution yields for the heat treatment of the coals in NMP and HHA at 300°C versus C% of the coals. The net dissolution yields here are the dissolution yield corrected for the yield for the raw coal, i. e., $(\text{TIMS} + \text{TS})_{300^\circ\text{C}} - (\text{TIMS} + \text{TS})_{\text{raw coal}}$. Figure 7 shows that for the low rank coals NMP gave higher net dissolution yields than HHA. Figure 8 shows radical concentrations of the raw Zao Zhuang coal and after the heat treatment for 1h at 300°C in HHA (a) and NMP (b). This clearly shows that in HHA the radical concentrations decrease as the increase of the heat treatment temperature, but in NMP the reverse tendency was obtained. As described in INTRODUCTION, hydrogen transfer from HHA to the coals was observed and it was well correlated with the dissolution yields. However, in the heat treatment in NMP no dehydrogenated derivatives of NMP was detected, indicating no hydrogen transfer from NMP to the coals.

Dissolution Mechanism in NMP and HHA

It is clear from the results described above that the dissolution reactions in NMP and HHA proceed through different mechanisms. In HHA coal radicals, which formed by the scission of very weak covalent bonds at 175-300°C and/or indigenous radicals activated by heat at these temperatures, may be responsible for the dissolution. These radicals are stabilized by the hydrogen donation from HHA and the dissolution reactions proceed. When the heat treatment was carried out in tetralin at 175 and 250°C, which is a much poorer hydrogen donor than HHA and hardly donate hydrogen to the radicals at these low temperatures, retrogressive reactions such as the addition to aromatic rings and coupling reactions occur.

The dissolution mechanism in NMP is not clear, though it is sure that hydrogen transfer from NMP to the coals does not occur. NMP is a polar solvent and a better solvent for coal extraction than pyridine, especially for low-rank coals which have many polar groups. One tentative explanation is that NMP dissolves much of coal molecules and radicals at 175-300°C and prevent retrogressive reactions which would occur in a non-polar solvent. Ionic reactions is also conceivable in NMP, though we have no evidence for it now.

Finally, it should be noted that the results above described were obtained by the use of the CS₂-NMP mixed solvent as an extraction solvent for the reaction mixture. If THF is used as a starting extraction solvent instead of the mixed solvent, we can only see small change of TS in the heat treatments carried out here.

CONCLUSIONS

Heat treatments of 7 coals were carried out in HHA which is a strong hydrogen donor, and in NMP which is a strong extraction solvent for coals, at temperatures as low as 175-300°C. HHA and NMP gave high dissolution yields for high- and low-rank coals, respectively. Hydrogen donation from HHA to coal radicals and high solubility for coal molecules and radicals are suggested to be responsible for these dissolutions.

REFERENCES

1. Nieve, R. C. *Fuel*, **1976**, *55*, 237-242.
2. Shen, J., Takanohashi, T., and Iino, M. *Energy Fuels*, **1992**, *6*, 854-858.
3. Shen, J., and Iino, M. *Energy Fuels*, **1994**, *8*, 978-983.
4. Iino, M., Takanohashi, T., Osuga, H., and Toda, K. *Fuel*, **1988**, *67*, 1639-1647.
5. Iino, M., Takanohashi, T., Obara, S., Tsueta, H., and Sanokawa, Y. *Fuel*, **1989**, *68*, 1588-1593.

Table 1 Ultimate and ash analyses of coals

Coal	Ultimate analysis (wt%,daf ^b)					Ash (wt%,db ^c)
	C	H	N	S	O ^a	
Pocahontas No.3 (PC)	89.7	4.5	1.1	0.7	4.0	4.8
Zao Zhuang (ZZ)	86.9	5.1	1.5	1.6	4.9	7.4
Upper Freeport (UF)	86.2	5.1	1.9	2.2	4.6	13.1
Pittsburgh No.8 (PB)	82.6	5.5	2.1	2.4	7.4	8.7
Illinois No.6 (IL)	76.9	5.5	1.9	5.6	10.1	10.4
Wyoming (Wy)	75.1	5.5	1.1	0.4	17.9	5.2
Beulah-Zap (BZ)	71.6	4.8	1.0	0.9	21.7	9.6

^a By difference

^b Dry ash free basis

^c Dry basis

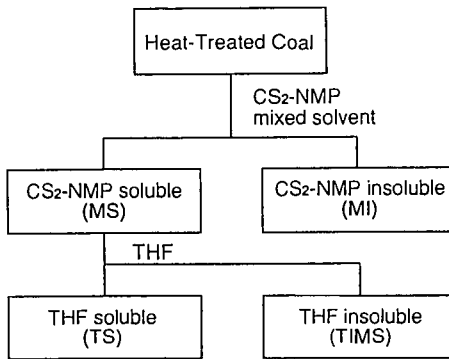


Figure 1 Extraction and fractionation procedures for the heat treated coals

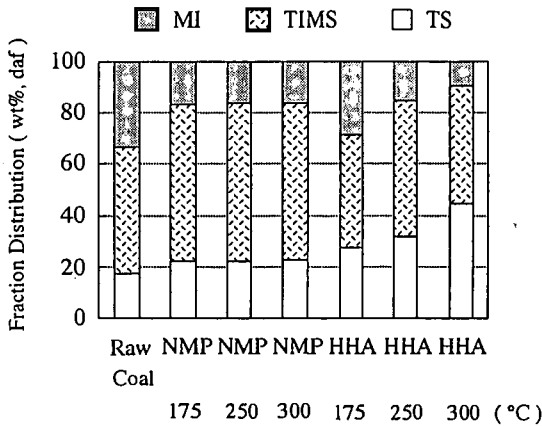


Figure 2 Fraction distribution after the heat treatment of Upper Freeport coal at 175-300°C in NMP and HHA for 1h, together with that for the raw coal.

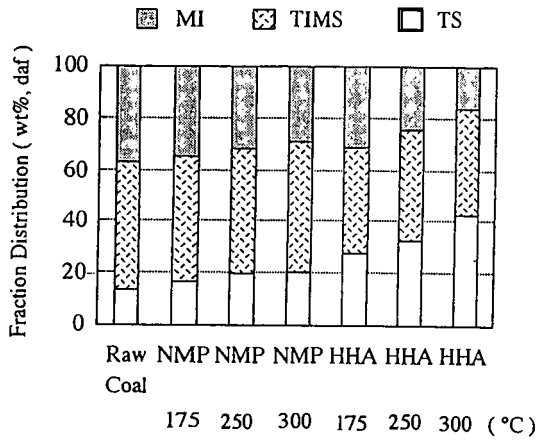


Figure 3 Fraction distribution after the heat treatment of Zao Zhuang coal at 175-300°C in NMP and HHA for 1h, together with that for the raw coal.

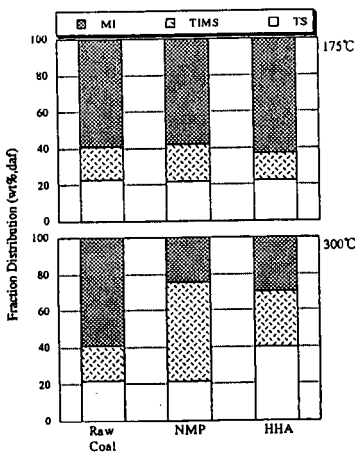


Figure 4 Fraction distribution after the heat treatment of Pittsburgh No. 8 coal at 175 and 300°C in NMP and HHA for 1h, together with that for the raw coal.

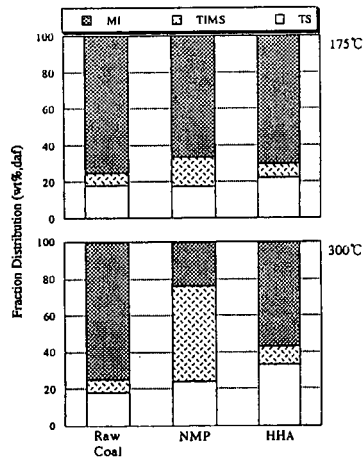


Figure 5 Fraction distribution after the heat treatment of Illinois No. 6 coal at 175 and 300°C in NMP and HHA for 1h, together with that for the raw coal.

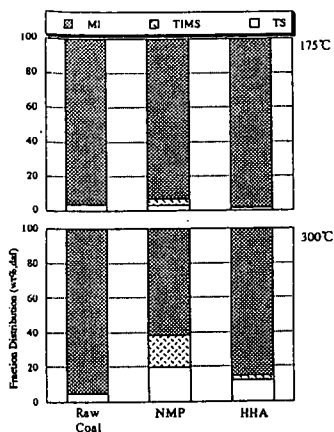


Figure 6 Fraction distribution after the heat treatment of Beulah-Zap coal at 175 and 300°C in NMP and HHA for 1h, together with that for the raw coal.

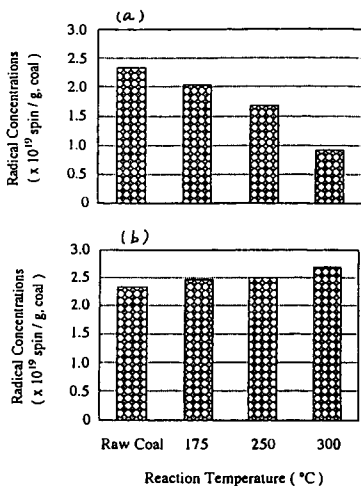


Figure 8 Radical concentrations of the raw Zao Zhuang coal and after the heat treatment for 1h at 300°C in HHA (a) and NMP (b).

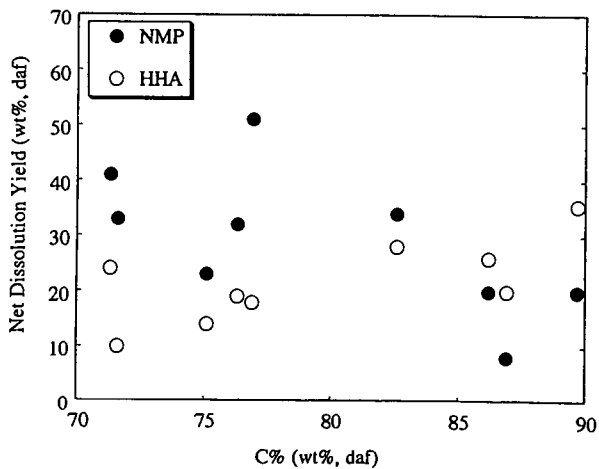


Figure 7 Plot of net dissolution yields for the heat treatment of the coals in NMP (●) and HHA (○) for 1h at 300°C versus C% of the coals.

PREDICTING ^{13}C NMR MEASUREMENTS OF CHEMICAL STRUCTURE OF COAL BASED ON ELEMENTAL COMPOSITION AND VOLATILE MATTER CONTENT

D. Genetti and T. H. Fletcher

Department of Chemical Engineering, Brigham Young University, Provo, Utah 84602

Keywords: coal structure, ^{13}C NMR

INTRODUCTION

Devolatilization models based on quantitative measurements of chemical structure, such as available through ^{13}C NMR analysis, have been successful in predicting tar volatiles yields as a function of heating rate, temperature, pressure, and coal type.¹ However, due to limited resources, ^{13}C NMR structural parameters have only been obtained for about 35 coals at the present time. Industrial interest in coal devolatilization has led to several attempts to correlate structural parameters affecting devolatilization as a function of the ultimate analysis of coals. Serio, et al.² used a triangular (i.e., linear) interpolation technique to estimate the input parameters for the FG-DVC devolatilization model.³ Niksa and Kerstein⁴ also developed a procedure that estimates the coal structural parameters based on simple linear correlations of ultimate analysis.^{5,6}

An extensive statistical analysis to determine the validity of linear correlations of ^{13}C NMR structural parameters based on ultimate analysis; preliminary results of this analysis were presented by Genetti and coworkers.⁷ A database including elemental composition, the ASTM volatile matter content, and ^{13}C NMR structural parameters for 30 coals of widely varying rank and composition was used in the analysis. The database was closely examined using the SPSS[®] statistical computer package. Using SPSS[®], a correlation matrix was calculated between all of the chemical structural parameters obtained from the NMR analysis. From the correlation matrix, the strength of relationships between the individual elements and the derived parameters were easily determined. The parameters were also examined for relationships among themselves. Multi-variate linear regression was then performed to derive equations that predict each of the parameters as a function of the elemental composition and volatile matter content. The r^2 value was then determined for each correlation.

The r^2 value is the coefficient of determination which determines the relative strength of correlation ($r^2=1$ is a perfect correlation). In this analysis the r^2 values ranged from 0.17 for $\sigma+1$ to 0.59 for M_8 ($r^2=0.49$ for P_0 and $r^2=0.38$ for MW_{cl}). The low r^2 values indicate a only weak linear correlation between the ^{13}C NMR structural parameters and the ultimate analysis. However, even when r^2 is zero, a strong non-linear correlation is possible. As a result of this study, it was determined that correlations based on linear regressions of ultimate analysis are unsuitable for predicting ^{13}C NMR structural parameters with reasonable accuracy. The purpose of this investigation is to develop non-linear correlations that predict the chemical structure parameters generally measured by ^{13}C NMR and required for the CPD devolatilization model:¹ (i) the average molecular weight per side chain (M_8); (ii) the average molecular weight per aromatic cluster (MW_{cl}); (iii) the ratio of bridges to total attachments (P_0); and (iv) the total attachments per cluster ($\sigma+1$).

CORRELATION OF M_8 , MW_{cl} , P_0 , AND $\sigma+1$

The database collected for 30 coals of varying rank used by Genetti, et al.⁷ is shown in Table 1. The database includes the elemental composition, the volatile matter content, and the measured values of the four chemical structural parameters derived from ^{13}C NMR analysis that are required in the CPD model.

Coals 1-7 are Argonne premium coals, 8-16 are coals used at Sandia National Laboratories, data for 17-18 came directly from Advanced Fuel Research, and coals 19-30 are coals from the Penn State coal sample bank. The volatile matter content data for the Penn State coals were taken directly from the Penn State coal sample database. Ultimate analysis on the Penn State coals was performed independently by Western Analytical and Huffman Laboratories and the average values are listed in Table 1. It is apparent that a diverse range of coals were used in this investigation.

Each ^{13}C NMR parameter was plotted against the different elemental constituents and the volatile matter content in order to determine relative dependence on each variables. This made it possible to see visually and quantitatively any possible correlation patterns. A non-linear (e.g., polynomial) correlation was then made for each of these plots, and the r^2 value was calculated to determine the strength of correlation. For example, it was determined that the value of M_8 depends significantly on the relative contents of carbon, hydrogen, oxygen, and volatile matter. Once it was determined that M_8 was dependent on carbon, hydrogen, oxygen, and volatile matter content, the best fit equations from the four plots were added together. Once the form of the equation was determined, coefficients were determined by minimization of the sum square error between the measured value and the predicted value of M_8 . Any obvious outlying points were removed. Only the DECS-13 coal was a consistent outlier for the M_8 correlation. The following is the equation resulting from the final optimization ($r^2=0.87$).

$$M_8 = c_1 + c_2 x_C + c_3 10^{4.2H} + c_4 x_O + c_5 x_O^2 + c_7 VM + c_8 VM^2 \quad (1)$$

where C, H, O, and VM represent the mass percent carbon, hydrogen, oxygen, and ASTM volatile content on a *daf* basis, and the c_i are empirical coefficients. This procedure was repeated for $\sigma+1$, P_0 , and MW_{cl} . A modified cubic correlation was also determined ($r^2 = 0.88$), but this correlation gave unrealistic values of MW_{cl} and $\sigma+1$ for low rank coals ($\%O > 25\%$) and high rank coals (VM

< 10%). For example, values of MW_{cl} for low rank coals were less than 100 daltons; the lowest NMR measurement for any coal was ~200 daltons. These unrealistic values seemed to be the result of extrapolations of the cubic curve fit beyond the original data set. Quadratic-type correlations did not give such poor extrapolations, and hence are shown here. Correlations for MW_{cl} , P_0 , and $\sigma+1$ were made with the following form:

$$y = c_1 + c_2C + c_3C^2 + c_4H + c_5H^2 + c_6O + c_7O^2 + c_8N + c_9N^2 + c_{10}S + c_{11}S^2 + c_{12}VM + c_{13}VM^2 \quad (2)$$

Coefficients for the quadratic fits are shown in Table 2. Coals with dry ash free carbon contents exceeding 95% (i.e., anthracites) were removed from the correlation. Thus, this model is only useful for coals with up to 95% C (daf). Additional ^{13}C NMR data are needed for coals with high carbon contents before a reliable correlation can be made for these coals.

It is anticipated that elemental composition may correlate with the coal structure parameters for many coals. However, it is recognized that often it is the exception to the rule that causes problems, and hence the need for additional ^{13}C NMR data, especially for "problem" coals. Therefore, these types of correlations should be used as a representation of the average of a database of coals and will fail occasionally for unique coals. Also, note that no cross correlations were used in Eqs. 1 or 2; this may be a subject of future work.

To determine the accuracy of the models, the measured values were plotted against the predicted values for each of the four structural parameters and the r^2 values were determined. The following r^2 values were determined: for M_5 , $r^2=0.87$; for MW_{cl} , $r^2=0.53$; for P_0 , $r^2=0.71$; for $\sigma+1$, $r^2=0.73$ (see Table 2). The outlier coals for each correlation are listed and were omitted from the r^2 calculation.

CORRELATION FOR C_0

The CPD model requires an estimation for the number of stable bridges existing in the parent coal or that are formed early in the pyrolysis process for low rank coals. This parameter has generally been used for low volatile bituminous coals to represent bi-aryl linkages and for lignites to represent early crosslinking. In the past, this has been a tuning parameter for these types of coals, and had to be changed as a function of heating rate, since crosslinking occurs at different rates as a function of heating rate. Based on the research performed below, a rough correlation for C_0 was developed for high heating rate applications. For low rank coals, oxygen content in the parent coal was used, since this correlates well with early crosslinking. For high rank coals, carbon content was used, since this may correlate well with the bi-aryl linkages. The correlation for C_0 becomes:

$$C_0 = \max\{(0.0177 \%C - 1.4542), 0.0\} + \max\{(0.0143 \%O - 0.1136), 0.0\} \quad (3)$$

Equation 5 was used below for all CPD model predictions that used the correlated chemical structure parameters. It is hoped that additional research on bi-aryl linkages and the chemistry behind early crosslinking in low rank coals will eliminate the need for such empiricism.

CPD MODEL PREDICTIONS

Five coals for which ^{13}C NMR and devolatilization data are available were tested in the CPD model. Volatiles yields were taken from the FFB experiments reported by Fleicher and Hardesty.⁸ Ultimate analysis and volatile matter data were used in the correlations to estimate the ^{13}C NMR parameters required as input for the CPD model. The CPD model was then used to predict tar and total mass release. The CPD model predictions made using the correlation were then compared against the measured experimental yields as well as versus yields predicted using the actual ^{13}C NMR measurements (from Table 1). Figure 1 compares the measured values and the predicted values of mass release for the five coals tested. It can be seen that the use of the structural parameters from the correlation gives predictions of total mass release that are as good or better than the use of the actual NMR data. This may be due to the fact that the correlation tends to smooth the NMR data.

Seventeen coals reported by Xu and Tomita⁹ were also used to test the reliability of this correlation. Table 3 lists these coals with their ultimate analysis and the four ^{13}C NMR parameters estimated by the correlation. It appears by looking at the estimated ^{13}C NMR values that the correlation works quite well overall; all estimated values are within expected ranges. Table 4 lists the predicted and measured values of mass and tar release for the 17 coals. Figure 2 shows the predicted and measured mass release vs. %C in the parent coal for the data from Xu and Tomita.⁹ The predicted mass release compares relatively well to the measured mass release for most of the coals tested. The correlation coefficient between the predicted and measured total volatiles yield was 0.89. The predictions of tar yield are lower than measured experimentally, especially for the low rank coals. The exact cause for this discrepancy is not known. In the Xu and Tomita experiment; the mass of char and the concentrations of major light gases are measured, and the tar yield is obtained by difference. This may lead to errors if light gases are present that are not measured, or if some fragmentation occurs. The tar yields reported by Xu and Tomita for low rank coals seem to be much higher than reported elsewhere in the literature.

The CPD model currently subtracts 7 daltons from the value of M_5 in order to account for some methyl (-CH₃) groups attached permanently to the aromatic cluster. However, since M_5 for the Hongay coal was 6 daltons, a minimum corrected value of 1 dalton was used in all CPD calculations. It may be necessary to develop a separate correlation for coals with carbon contents greater than 90% daf.

CONCLUSIONS

The non-linear correlation of ^{13}C NMR measurements with ultimate analysis and volatile matter content is a promising approach to obtain data to model devolatilization behavior where ^{13}C NMR data are not available. The correlation, combined with the CPD model, works very well in predicting total volatiles yield for low to high rank coals. Coals of very high rank (>95 %C) were not included in this correlation due to drastically different structure and lack of sufficient data. Flat flame burner devolatilization tests are planned on a number of these coals to obtain provide additional volatile yield data.

REFERENCES

1. Fletcher, T. H., A. R. Kerstein, R. J. Pugmire, and M. D. Grant, *Energy and Fuels*, **6**, 414-431 (1992)
2. Serio, M. A., P. R. Solomon, and Y. Zhao, 25th Symposium (International) on Combustion, 553-560 (1994).
3. Solomon, P. R., D. G. Hamblen, R. M. Carangelo, M. A. Serio, and G. V. Deshpande, *Energy and Fuels*, **2**, 405-422 (1988).
4. Niksa, S. and A. R. Kerstein, *Energy and Fuels*, **5**, 647-665 (1991).
5. Niksa, S. and A. R. Kerstein, *Energy and Fuels*, **5**, 673-683 (1991).
6. Niksa, S. and A. R. Kerstein, *Energy and Fuels*, **8**, 659-670 (1994).
7. Genetti, D. B., T. H. Fletcher, and R. J. Pugmire, "Predicting ^{13}C NMR Measurements Based on Coal Elemental Composition," in *Coal Science*, edited by J. A. Pajares and J. M. D. Tascón, **1**, 331-334, Elsevier, New York (1995).
8. Fletcher, T. H. and D. R. Hardesty, "Compilation of Sandia Coal Devolatilization Data: Milestone Report," for DOE/PETC under contract FWP 0709, Sandia Report No. SAND92-8209, available NTIS (May, 1992).
9. Xu, W.-C. and A. Tomita, *Fuel*, **66**, 627-631 (1987).

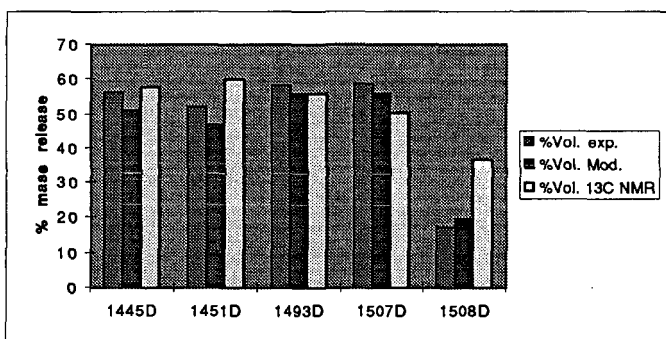


Figure 1. Comparison of total mass release with measured total volatile yields in a flat flame burner (Fletcher and Hardesty⁸).

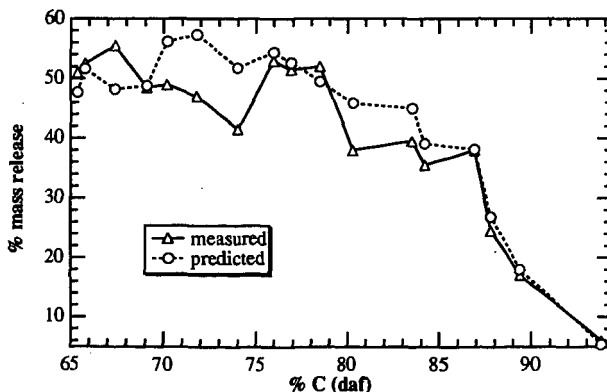


Figure 2. Predicted and measured mass release vs. %C in the parent coal for the data from Xu and Tomita.⁹

Table 1
Coal Data Set Used for Development of Empirical Correlations

#	COAL SAMPLE	C	H	O	N	S	VM	$\sigma+1$	P_o	MW _{cl}	M _s
1	NORTH DAKOTA	72.94	4.83	20.34	1.15	0.70	49.78	4.10	0.64	269	40
2	WYODAK	75.01	5.35	18.02	1.12	0.47	49.03	5.60	0.55	408	42
3	BLIND CANYON	80.69	5.76	11.58	1.57	0.37	48.11	5.10	0.49	366	36
4	ILLINOIS #6	77.67	5.00	13.51	1.37	2.38	47.39	5.00	0.63	322	27
5	PITTSBURGH #8	83.20	5.32	8.83	1.64	0.89	41.67	4.70	0.64	330	28
6	STOCKTON	82.58	5.25	9.83	1.56	0.65	37.64	4.80	0.69	272	20
7	UPPER FREEPORT	85.50	4.70	7.51	1.55	0.74	31.62	5.30	0.67	312	17
8	POCAHONTAS	91.05	4.44	2.47	1.33	0.50	19.53	4.40	0.74	307	13
9	PSOC 1443	72.34	5.21	20.11	1.35	0.94	78.67	4.80	0.59	297	36
10	PSOC 1488	76.00	5.23	17.27	0.94	0.53	44.22	4.70	0.54	310	37
11	PSOC 1468	95.36	1.38	1.86	0.84	0.53	3.92	4.70	0.89	656	12
12	PSOC 1445D	75.60	5.26	17.33	1.32	0.49	48.17	5.00	0.48	384	45
13	PSOC 1451D	84.23	5.54	7.56	1.65	1.01	38.69	4.80	0.48	329	33
14	PSOC 1493D	74.12	4.96	13.18	1.45	6.29	43.37	5.50	0.52	402	39
15	PSOC 1507D	66.56	4.26	25.16	1.12	2.89	49.59	4.40	0.59	392	58
16	PSOC 1508D	88.83	4.37	5.14	1.06	0.60	17.18	4.20	0.70	285	18
17	GOUDEY A	87.90	3.77	4.65	1.31	2.37	36.94	4.80	0.64	284	21
18	GOUDEY B	88.49	4.94	1.40	3.42	1.75	19.27	5.00	0.65	295	19
19	DECS-1	71.62	7.11	18.84	1.33	1.10	56.52	5.80	0.42	505	55
20	DECS-7	73.67	6.04	18.22	1.08	1.00	48.11	5.10	0.55	381	43
21	DECS-11	67.81	6.85	23.66	0.91	0.76	62.01	4.60	0.68	329	42
22	DECS-13	87.03	5.19	5.48	1.65	0.65	26.08	4.50	0.72	483	72
23	DECS-18	80.15	6.04	7.44	1.62	4.75	46.93	5.30	0.48	370	35
24	DECS-20	85.16	5.81	6.49	1.52	1.01	39.70	4.70	0.64	247	21
25	DECS-21	93.61	2.77	2.90	0.17	0.56	5.08	3.80	1.00	216	13
26	DECS-27	76.73	6.14	15.03	1.32	0.79	41.50	5.20	0.55	361	34
27	PSOC-1515	89.23	4.13	4.95	0.90	0.78	11.92	6.00	1.00	231	4
28	PSOC-1516	87.34	4.92	4.12	1.37	2.24	20.83	4.50	0.35	354	21
29	PSOC-1520	69.55	6.45	21.70	0.91	1.39	62.47	3.70	0.64	282	46
30	PSOC-1521	89.96	4.67	2.79	1.70	0.88	22.11	4.40	0.69	225	14

$\sigma+1$: Attachments per cluster

MW: Average molecular weight per cluster

P_o : Intact bridges

M_s: Average molecular weight per side chain

VM: ASTM volatile matter (daf)

Table 2
Coefficients for Quadratic Correlation of ¹³C NMR data

	M _s	MW	P_o	$\sigma+1$
C ₁	161	-587.73	-0.39	-2.2
C ₂	-1.76	22.32	-4.0E-03	0.32
C ₃	5.28E7	-0.17	2.0E-04	-2.6E-03
C ₄	-2.37	90.31	-5.4E-02	-2.1
C ₅	-1.27	-8.40	5.3E-03	0.19
C ₆	3.42E-2	-0.52	5.9E-03	0.10
C ₇	8.76E-1	0.04	6.3E-04	-4.5E-03
C ₈	-9.04E-3	1.28	5.5E-03	1.321
C ₉		-0.01	2.5E-04	-0.20
C ₁₀		-5.67	0	0
C ₁₁		2.49	0	0
C ₁₂		0.37	-1.8E-05	-1.2E-02
C ₁₃		-0.02	1.1E-06	3.9E-05
r ²	0.87	0.535	0.71	0.73
Outliers	DECS-13	PSOC-1468	PSOC 1516	PSOC-1515
	PSOC-1468		DECS 1	PSOC-1468
			PSOC-1515	

Table 3
17 Coals Tested by Xu and Tomita⁹.

	Cdaf	Hdaf	Odaf	Ndaf	Sdaf	VMdaf	σ+1	P_o	MW	M₆
Yallourn	65.40	4.90	28.80	0.6	0.3	53.93	3.33	0.75	362	59.3
Rhein Braun	65.80	5.50	27.60	0.8	0.3	56.46	3.67	0.71	358	57.5
Morwell	67.40	5.00	26.80	0.5	0.3	52.54	3.52	0.71	362	54.7
Velva	69.10	4.80	23.90	1.4	0.6	52.34	4.77	0.64	356	50.3
Soyakoishi	70.20	5.20	22.40	1.8	0.2	46.42	5.18	0.62	366	48.0
South Baulah	71.80	4.70	19.20	1.4	2.9	44.70	5.25	0.55	364	44.6
Colowyo	74.00	5.00	18.60	1.9	0.4	38.75	5.56	0.59	363	40.0
Taiheiyō	76.00	6.50	16.00	1.2	0.3	56.02	5.19	0.57	318	37.1
Millmerran	76.90	6.60	15.40	0.5	0.6	54.80	4.54	0.58	313	35.8
Wandoan	78.50	5.80	14.40	0.9	0.4	49.76	4.69	0.59	327	33.5
Hunter Valley	80.30	5.00	12.20	2	0.4	37.18	5.55	0.59	337	30.0
Liddell	83.50	5.40	8.40	2.1	0.6	37.58	5.30	0.60	318	26.6
Newvale	84.20	5.00	8.90	1.4	0.5	34.18	4.87	0.63	316	24.3
Yubari Shinko	86.90	5.60	5.20	1.9	0.3	40.51	4.73	0.66	293	23.7
Vicary Creek	87.80	4.70	4.90	2.1	0.4	24.74	4.97	0.68	298	17.8
Keystone	89.40	4.40	3.10	2.2	0.8	16.83	4.91	0.71	284	12.8
Hongay	93.70	3.30	1.30	1.2	0.8	7.66	4.66	0.85	207	5.3

Table 4
Predicted and Measured Mass Release and Predicted Tar Yield
(data from Xu and Tomita⁹)

COAL	% mass release (daf)		% tar release (daf)	
	pred.	meas.	pred.	meas.
Yallourn	48	51	14	20
Rhein Braun	52	53	14	22
Morwell	48	56	15	26
Velva	49	49	17	18
Soyakoishi	56	49	9	21
South Baulah	57	47	14	17
Colowyo	52	42	10	19
Taiheiyō	54	53	16	30
Millmerran	53	52	22	30
Wandoan	50	52	21	28
Hunter Valley	46	38	15	22
Liddell	45	40	19	22
Newvale	39	36	19	19
Yubari Shinko	38	38	17	22
Vicary Creek	27	25	12	12
Keystone	18	17	10	8
Hongay	5	6	4	3

A SIMPLIFIED METHOD TO DETERMINE $f(E)$ AND k_0 IN THE
DISTRIBUTED ACTIVATION ENERGY MODEL FOR COAL PYROLYSIS

Kouichi Miura and Taisuke Maki
Department of Chemical Engineering, Kyoto University
Kyoto 606-01, Japan

Keywords: Coal pyrolysis, Distributed activation energy model, Argonne premium coal

INTRODUCTION

To analyze complex reactions such as pyrolysis of fossil fuels, thermal regeneration reaction of activated carbon *etc.*, the so called distributed activation energy model (DAEM) has been widely utilized. The model has been applied to represent the change in overall conversion¹⁻³ and/or the change in the yield of a given component⁴⁻⁶ during the coal pyrolysis. The model is represented as follows when it is applied to represent the change in total volatiles.

$$1 - V/V^* = \int_0^{\infty} \exp(-k_0 \int_0^t e^{-E/RT} dt) f(E) dE \quad (1)$$

where V is the total volatiles evolved by time t , V^* is the effective volatile content of the coal, $f(E)$ is a distribution curve of the activation energy to represent the differences in the activation energies of many first-order irreversible reactions, and k_0 is the frequency factor corresponding to the E value. The distribution curve $f(E)$ is defined to satisfy

$$\int_0^{\infty} f(E) dE = 1 \quad (2)$$

The focus of the analysis is the estimation of k_0 and $f(E)$. The distribution curve $f(E)$ is generally assumed by a Gaussian distribution with mean activation energy E_0 and standard deviation σ . On the other hand, the frequency factor k_0 is assumed to be a constant in general for all reactions to avoid the complexity of the analysis.

Since k_0 and $f(E)$ are interrelated as clarified by several investigators^{7,8}, k_0 is assigned on some basis first, and $f(E)$, namely E_0 and σ , is determined to fit experimental data. Therefore, eq 1 becomes just a correlation equation when we can not determine k_0 on some sound basis. Even the assumption of a constant k_0 value may not be valid when $f(E)$ spreads over wide range of E values. Furthermore, the assignment of the Gaussian distribution to $f(E)$ does not always reflect real situations.

Recently one of the authors has presented a simple method to estimate both $f(E)$ and k_0 from three sets of experiments performed at different heating profiles without assuming any functional forms for $f(E)$ and k_0 ⁹. The procedure to estimate $f(E)$ and k_0 is summarized below:

1. Measure V/V^* vs. T relationships at three different heating rates at least.
2. Calculate nominal rates $\bar{k} = dV/dt/(V^*-V)$ at several but same V/V^* values at the different heating rates, then make Arrhenius plots of \bar{k} at the same V/V^* values.
3. Determine activation energies from the Arrhenius plots at different levels of V/V^* , then plot V/V^* against the activation energy E .
4. Differentiating V/V^* by E gives $f(E)$, because the following relation holds approximately:

$$V/V^* = 1 - \int_{E_a}^{\infty} f(E) dE = \int_0^{E_a} f(E) dE \quad (3)$$

5. Calculate k_0 corresponding to each E_s value at all the heating rates using

$$0.545aE_s/k_0RT^2 = e^{-E_s/RT} \quad (4)$$

then employ the averaged k_0 value as a true k_0 value.

No *a priori* assumption is required for the functional forms of $f(E)$ and $k_0(E)$. In other

words we can determine k_0 and E at any levels of V/V^* .

In this paper the method was applied to estimate $f(E)$ and k_0 for the pyrolysis of 19 coals including the Argonne premium coals. It was found that $f(E)$ was significantly dependent on coal rank. However, the k_0 vs. E relationships were found to be classified into three groups depending on coal rank. Using the three k_0 vs. E relationships, we presented to estimate $f(E)$ from a single experimental run performed under a constant heating rate.

EXPERIMENTAL

Table 1 lists the ultimate analyses for the 19 coals used in this work. The weight change accompanying the pyrolysis of coal was measured by use of a sensitive thermobalance (Shimadzu TG-50) under three different heating rates (α) of 5, 10, and 20 K/min in a nitrogen atmosphere. The measured weight-time relationships were converted to the relationships of V/V^* vs. T . Pyrolysis using a Curie point pyrolyzer (Japan Anal. Ind. JHP-2S) was also performed for several coals. The coal particles were heated at 3000 K/s to 280, 386, 485, or 578 °C and kept for 10 s at the temperature. The change in V/V^* was calculated from the total weight change of the coal particles.

RESULTS AND DISCUSSION

$f(E)$ curves and k_0 vs. E relationships estimated by the proposed method for 19 coals

Figure 1 shows the relationships of V/V^* vs. T measured at $\alpha = 20$ K/min. The temperature at which the reaction starts and the shape of the curves are significantly different among the coals.

The relationships between V/V^* vs. E can be obtained through the procedures 1 to 3 mentioned above and are shown for the Argonne premium coals in the figure above and for the other coals in the figure below in Figure 2. Differentiating the curves graphically by E , $f(E)$ curves for the coals could be obtained as shown in Figure 3. The shape of the curves are significantly different among the coals: the peaks appear at $E=220-280$ kJ/mol, and the activation energy E spreads from 150 to 400 kJ/mol. These results clearly show that $f(E)$ can not be represented by a single Gaussian distribution. For the Argonne premium coals, the peak position shifted to higher E values with the increase of coal rank. This is well expected because the higher rank coals are decomposed at higher temperatures as shown in Fig. 1. For the other coals, the order of peak position does not always follow the order of coal rank as shown in Fig. 3b. This is probably because the coals were collected from various countries.

Figure 4 shows the k_0 vs. E relationships estimated for all the coals. Interestingly, the relationships were little dependent on coal types except three low rank coals, SY, MW, and BD. The difference in k_0 was only the order of 10^2 at maximum at a same E without the lower rank coals. This means that the coal pyrolysis consists of similar reactions having almost same rates for these coals. Only the proportions of the reactions are judged to be different among the coals, which is represented by the difference of $f(E)$ curves. The k_0 value increased from the order of 10^{10} to the order of 10^{25} s⁻¹ while E increases from 150 to 400 kJ/mol. The following compensation effect approximately held between the k_0 values and E for all the coals.

$$k_0 = \alpha e^{\beta E} \quad (\alpha, \beta; \text{constants}) \quad (5)$$

It is obvious that k_0 can not be assumed as constants for the pyrolysis of these coals.

Figure 5 compares the experimental TG curves and the curves calculated using $f(E)$ and k_0 estimated for MW coal. Not only the curves ($\alpha = 5, 10, \text{ and } 20$ K/min) utilized for obtaining $f(E)$ and k_0 but the data obtained at $\alpha=3000$ K/s showed good agreement with the calculated curves. This clearly indicates the validity of the presented method.

Figure 6 shows the $f(E)$ curves obtained by Burnham et al.¹⁰ for the Argonne premium coals by the conventional method. The peak position of $f(E)$ is not in the order of the coal rank: the peak position of the lowest rank coal, ND coal, is at $E=260$ kJ/mol, whereas the peak position of the highest rank coal, POC coal, is at $E=220$ kJ/mol. This would be because the k_0 value assigned to ND coal is larger than that assigned to POC coal. In the conventional method the $f(E)$ curve is dependent on the value of k_0 assigned as stated above. Therefore, we must be careful in interpreting the meaning of the activation energy when we resort to the conventional method.

A method to determine $f(E)$ from a single experiment

Figure 4 shows that the k_0 vs. E relationships are little affected by the coal type. This means

that the k_0 vs. E relationships may be represented by several relationships. Then the k_0 vs. E relationships in Fig. 4 were examined in more detail, and they were found to be grouped into three relationships depending on the coal rank as shown in Figs. 7a to 7c, where the relationships were approximated by eq 5.

Once we can know the k_0 vs. E relationship, we can obtain the relationship between E vs. T by using eq 4 for a selected heating rate α . Then $f(E)$ can be estimated from a single TG curve obtained at the heating rate. The procedure is given as follows:

- (1) Measure V/V^* vs. T relationship at a heating rate α .
- (2) Calculate the E vs. T relationship using eq 4 by choosing the k_0 vs. E relationship corresponding to the coal rank from three correlating equations.
- (3) Convert the V/V^* vs. T relationship into V/V^* vs. E relationship using the k_0 vs. E relationship obtained in (2).
- (4) Differentiate the V/V^* vs. E relationship by E gives $f(E)$.

Although the procedure is rather simple, the procedure (2) requires trial and error calculation. Then, the E vs. T relationships for $\alpha = 20\text{K/min}$ were calculated, and shown in Figure 8. Measuring the V/V^* vs. T relationship at $\alpha = 20\text{K/min}$ and using Fig. 8, one can obtain $f(E)$ curve straightforwardly.

Figure 9 compares the $f(E)$ curves estimated by the simple method using the V/V^* vs. T relationship measured at $\alpha = 20\text{K/min}$ and those estimated by the original method for several coals. The $f(E)$ curves estimated using the simple method are rather smooth and the peak intensities are smaller than those estimated using the original method. However, the E values at the peak positions obtained by the two methods are almost same. The V/V^* vs. T relationships were well reproduced using the $f(E)$ curves estimated by the simple method. One of the difficulties in applying the original method was to obtain E at smaller V/V^* region ($V/V^* < 0.1$) and at higher V/V^* region ($V/V^* > 0.1$). This was because the V/V^* vs. T curves obtained under three different heating rates become so close. Using the simple method, we can the procedure to obtain E . This largely facilitates the estimation of $f(E)$. Since the $f(E)$ curves estimated by the simple method are rather close to those obtained by the original method, the simple method is well utilized to estimate $f(E)$ curve.

CONCLUSION

The new method presented by the authors for estimating both the distribution curve $f(E)$ and the frequency factor $k_0(E)$ in the distributed activation energy model (DAEM) was applied to the analysis of pyrolysis reaction of 19 coals. It was found that the $f(E)$ curve spreads over 150 to 400 kJ/mol and that the frequency factor k_0 increases from 10^{12} to 10^{26} s^{-1} with the increase of E . The assumption of a constant k_0 value could not be employed for these coal. The validity of the proposed method was clarified through these works. Furthermore, a simple method was presented for estimating $f(E)$ from a single experiment. The $f(E)$ curves estimated by the simple method are rather close to those obtained by the original method, indicating the validity of the simple method. Using the simple method, we can estimate $f(E)$ easily and straightforwardly.

REFERENCES

1. Pitt, G.J., *Fuel*, **1962**, *41*, 267-274.
2. Suuberg, E.M.; Peters, W.A.; Howard, J.B., *Ind. Eng. Chem. Process Des. Dev.*, **1978**, *17*, 37-46.
3. Reynolds, J.G.; Burnham, A.K., *Energy & Fuels*, **1993**, *7*, 610-619.
4. Solomon, P.R.; Hamblen, D.G.; Carangelo, R.M.; Serio, M.A.; Deshpande, G.V., *Energy Fuels*, **1988**, *2*, 405-422.
5. Grant, D.M.; Pugmire, R.J.; Fletcher, T.H.; Kerstein, A.R., *Energy Fuels*, **1989**, *3*, 175-186.
6. Niksa, S.; Kerstein, A.R., *Energy Fuels*, **1991**, *5*, 647-665.
7. Anthony, D.B.; Howard, J.B., *AIChE J.*, **1976**, *22*, 625-656.
8. Du, Z.; Sarofim, A.F.; Longwell, J.P., *Energy & Fuels*, **1990**, *4*, 296-302.
9. Miura, K., *Energy Fuels*, **1995**, *9*, 302-307.
10. Burnham, A.K.; Oh, M. S.; Crawford, R. W., *Energy & Fuels*, **1989**, *3*, 42-55.

Table 1. Ultimate analyses of the coals used

Coal	Ultimate analysis (wt% d.a.f.)			
	C	H	N	O(diff.)
Beulah-Zap (ND)	72.9	4.8	1.2	20.1
Wyodak (WY)	75.0	5.4	1.1	18.5
Illinois#6 (IL)	77.6	5.0	1.4	16.0
BlindCanyon (UT)	80.6	5.8	1.6	12.0
Lewinston-Stockton (ST)	82.5	5.3	1.6	10.6
Pittsburg#8 (PITT)	83.2	5.3	1.6	9.9
UpperFreeport (UF)	85.5	4.7	1.6	8.2
Pocahontas (POC)	91.0	4.4	1.3	3.5
Soya (SY)	66.1	5.2	1.5	27.2
Morwell (MW)	67.1	4.9	0.6	27.4
Baiduri (BD)	72.3	4.7	1.4	21.6
Onbilin(OB)	78.3	5.6	1.7	14.4
Taiheiyu(TC)	78.7	6.2	1.2	13.9
Ebeneza(EN)	81.2	6.1	1.6	11.1
Tiger Head(TH)	82.3	5.6	1.8	10.3
Taung(TT)	82.7	4.7	1.1	11.5
Ensuyotshon(ET)	82.8	5.6	1.5	10.1
Blair Athol (BA)	82.9	4.7	1.8	10.6
Newlands(NL)	85.9	4.9	1.7	7.5

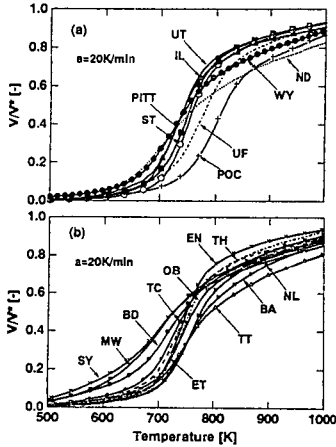


Figure 1. V/V^* vs. T relationships measured at $a=20K/min$ for 19 coals.

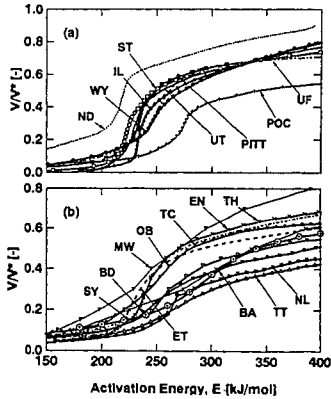


Figure 2. V/V^* vs. E relationships estimated by the proposed method.

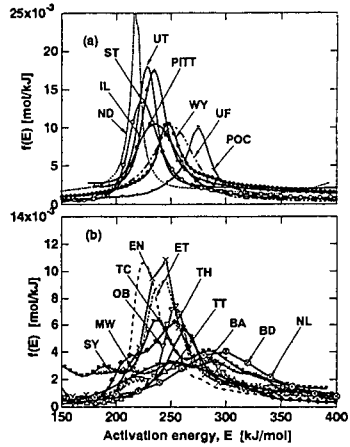


Figure 3. $f(E)$ curves estimated by the proposed method.

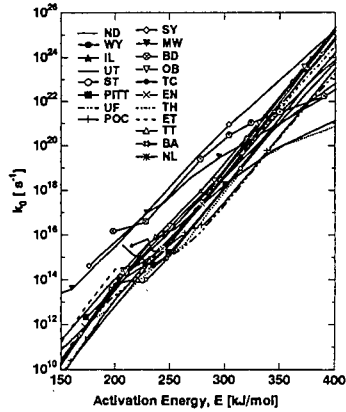


Figure 4. k_0 vs. E relationships estimated by the proposed method.

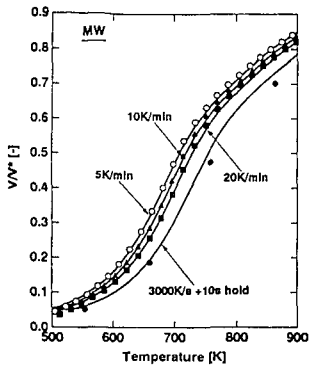


Figure 5. Comparison between the experimental V/V^* vs. T curves and calculated ones using $f(E)$ and k_0 estimated.

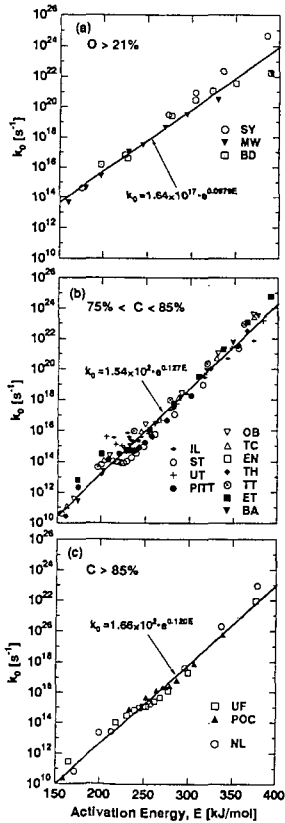


Figure 7. k_0 vs. E relationships approximated for three groups of coal rank.

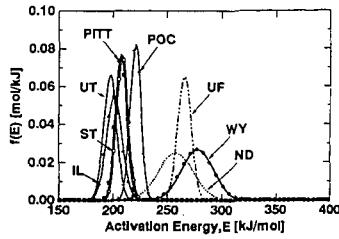


Figure 6. $f(E)$ curves for the Argonne coals estimated by Burnham et al. using the conventional method.

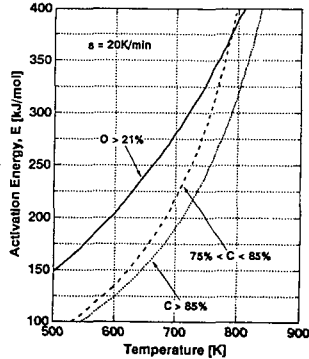


Figure 8. E vs. T relationships for $a = 20$ K/min for three groups of coal rank.

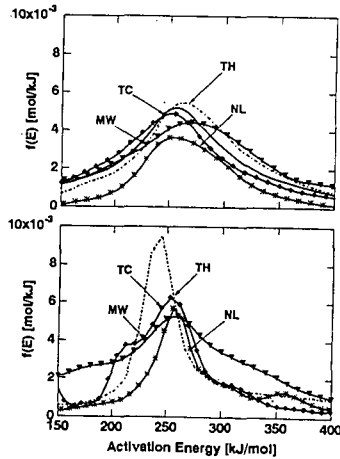


Figure 9. Comparison of the $f(E)$ curves estimated by the simple method (above) and those estimated by the original method (below).

PORPHYRIN- AND METALLOPORPHYRIN-DERIVED CARBONS AS MODELS FOR COAL CHARs

Jenny M. Jones, Jonathon Agnew, James Kennedy and Ben Watts
Department of Fuel and Energy, University of Leeds, Leeds, U.K., LS2 9JT

Keywords: Coal, porphyrins, NO_x, catalysis.

INTRODUCTION

Factors which govern the release of fuel-nitrogen as NO_x (rather than N₂) during coal combustion are of interest because of the environmental implications. Coal is a complex material which can be considered to be composed of large polymeric, molecules comprising aliphatic cross-linked polyaromatic structural units which contain many heteroatom types and functionalities. Within this polymeric matrix smaller molecules are dispersed, together with mineral particles, metal salts etc. Model coals derived from carbonisation of organic precursors offer an approach for examining the role of some of these variables (nitrogen-functionality, oxygen content, metal type, environment and content etc.) on NO_x formation during combustion. In principle, such models are easier to characterise, compared to coal, with regards to their chemical and physical properties.

The nitrogen in coal is virtually exclusively organic and typical nitrogen contents are in the range 0.7-2.1 wt%. The chemical form of the nitrogen is mainly pyrrolic and pyridinic, with smaller amounts of quaternary nitrogen within the aromatic units. Lower rank coals may possess other functional groups such as amines. As a consequence model coals derived from carbazole, acridine, or ammonia-treated carbons etc. have been studied for their combustion behaviour.¹⁻⁵

One source of this nitrogen in coal is derived from porphyrin and other plant protein structures which are degraded via different routes during coal diagenesis. These types of systems have been identified in coals as well as coal extracts.^{6,7} Such systems are of interest because of their ability to chelate metals, in particular vanadium and iron. Nitrogen chelates and chelated metal species are expected to have very different nitrogen release behaviour during combustion, compared to free pyrrolic or pyridinic systems because: (i) the nitrogen:carbon ratio is unusually high in the porphyrin chelate; (ii) the nitrogen atoms are in close spatial proximity within the chelate; (iii) there exists intimate contact between the chelated metal and the nitrogen atoms.

In the present study, model coals derived from porphyrin and metalloporphyrin chelates have been characterised for their chemical and physical properties with particular emphasis on their behaviour during pyrolysis and combustion. To the authors' knowledge such types of systems have not been studied previously.

EXPERIMENTAL

The model carbons were prepared by atmospheric pressure co-carbonisation of a 10:1 by weight acenaphthylene and the porphyrin (or metalloporphyrin) mixture under an argon atmosphere. The heating rate was 1 K/min and initially the carbons were heat-treated at 873 K for 1 h. Carbons treated at higher temperatures were heated again in argon at 4 K/min to the desired temperature and held for 1 h. Surface areas were measured by the BET method using a Quantachrom Quantasorb QS-13 surface area analyser. Pyrolysis studies at 1273 K were performed using a Chemical Data Systems, Inc., 190 Pyroprobe pyrolysis system interfaced to a Perkin-Elmer 8700 capillary GC, with FID and NPD detectors. Combustion studies were performed in a Shimadzu TGA-50H thermogravimetric analyser (15 K/min heating rates) in air, or in 20% O₂/Ar using a Stanton Redcroft STA 1500 thermogravimetric analyser coupled to a VG Quadrupole mass spectrometer by means of a heated capillary sampling probe. Further details are described elsewhere.¹

RESULTS AND DISCUSSION

The elemental analyses of the model coals are given in Table 1, together with surface areas, where available. The surface areas of the carbons were, in general, quite low which may be expected for the anisotropic acenaphthylene derived carbons, due to small pore sizes. The N:V ratio in the carbon prepared from pure tetraphenyl porphine (CTTPV) is much larger than that in the precursor suggesting that much of this metal is no longer chelated, and may be present as the oxide. In contrast, the N:M ratio for the 873K heat-treated Fe- and Co-containing co-carbonised carbons are essentially unchanged compared with the corresponding metalloporphyrin precursors, which may indicate that the chelate is intact, to some extent.

The evolved gas profiles during the temperature programmed combustion (TPC) of the tetraphenyl porphine starting material are given in Figure 1. The main fuel-N product is N_2 , and relatively large amounts of NO, HCN and other cyano species were detected. The cyano species are seen to be evolved during the onset of combustion, while the majority of fuel-N is evolved as N_2 towards the latter stages of combustion. This type of behaviour is often seen for coals and coal chars, where nitrogen is retained in the char until its eventual release at high levels of burnout.

The evolved gas profiles during TPC of the carbonised tetraphenylporphyrin and carbonised vanadyl porphyrin are given in Figures 2 and 3 respectively and Table 2 quantifies the differences in the fuel nitrogen conversions. Comparison of Figures 1 and 2 show that the structural changes which occur during carbonisation have profound effects on the fuel-N released. In particular, the HCN gas evolution profile is quite different, and far more N_2 is evolved after carbonisation. This N_2 is evolved at almost the same temperature as observed during the TPC of the pure tetraphenylporphine precursor, suggesting structural similarities. The evolution of N_2 during combustion may be indicative of N atoms in the carbon structure which are close spatially. Alternatively mobile C(N) surface species may participate. The presence of the metal (Figure 3, and Table 2) also has a marked effect on the fuel-N conversions. This may be the result of a catalytic effect of vanadium on the reduction of NO to N_2 . The catalytic effects of the metal on combustion is illustrated dramatically when comparisons of Figures 2 and 3 are made. Catalysis was seen to occur for the combustion of all the co-carbonised carbons, and a compensation effect on the rates was apparent, as shown in Figure 4.

During pyrolysis of the co-carbonised samples, the major products observed were hydrogen cyanide and acetonitrile. The presence of the metal decreased the amount of both these species which may be indicative of the persistence of M-N interactions in the carbons.

CONCLUSIONS

Carbons derived from porphyrin and metalloporphyrin precursors can be used to investigate the influence of such moieties on the conversion of fuel-nitrogen in coals. The presence of metals catalyses the combustion and appears to lower the amount of fuel-N converted to HCN in the volatiles, and increase the fuel-N to N_2 conversions. It is unclear, at the present time, as to whether chelated or unchelated metals are responsible for this.

REFERENCES

1. Jones, J. M., Harding, A. W., Brown, S. D., and Thomas, K. M. *Carbon* 1995, **33**, 833.
2. Grant, K. A., Zhu, Q., and Thomas, K. M. *Carbon* 1994, **32**, 883
3. Wang, W. and Thomas, K. M., *Fuel* 1993, **72**, 293.
4. Jones, J. M., and Thomas, K. M. *Carbon* 1995, **33**, 1129.
5. Thomas, K. M., Grant, K., and Tate, K. *Fuel* 1993, **72**, 941.
6. Bonnett, R., Burke, P.J., Dewey, C.R., Fairbrother, A.E., and Major, H.J.; *Fuel*, 1991, **70**, 1227;
7. Haenel, M.W.; *Fuel*, 1992, **71**, 1211.

ACKNOWLEDGEMENT

The TG-MS data was obtained in the Northern Carbon Research Laboratories, Department of Chemistry, University of Newcastle upon Tyne, U.K.

TABLE 1: Properties of the model carbons

sample i.d.†	HTT (K) ‡	wt% C	wt% H	wt% N	wt% O*	wt% metal	surface area (m ² /g)
CTPP-873	873	83.1	2.4	8.8	5.7	-	nm
CTPPV-873	873	52.1	1.4	5.5	13.5	27.5	nm
ACE-TPP-873	873	94.1	2.1	0.5	3.3	-	5
ACE-TPP-V-873	873	93.1	1.7	1.6	0.9	2.7	5
ACE-TPP-Fe-873	873	92.1	1.8	1.6	3.0	1.5	5
ACE-TPP-Co-873	873	89.6	1.7	1.8	5.0	1.9	3
ACE-TPP-Cu-873	873	89.5	1.8	1.6	5.0	2.1	3
ACE-PC-873	873	92.2	2.1	0.8	4.9	-	2
ACE-PC-V-873	873	88.6	1.8	2.8	3.2	3.6	11
ACE-TPP-1073	1073	97.4	0.9	0.6	1.1	-	2
ACE-TPP-V-1073	1073	93.2	1.0	1.5	1.4	2.9	6
ACE-TPP-Fe-1073	1073	96.2	0.3	0.7	1.2	1.6	149
ACE-TPP-Co-1073	1073	94.6	0.3	0.7	2.2	2.2	57
ACE-TPP-Cu-1073	1073	94.5	0.7	1.5	1.2	2.1	3
ACE-TPP-1273	1273	95.9	0.3	0.5	3.3	-	3
ACE-TPP-V-1273	1273	95.2	0.3	1.1	0.5	2.9	2

†ace - acenaphthylene; tpp - tetraphenylporphyrin (free base or chelated to denoted metal); nm: not measured. *By difference. ‡HTT: Heat treatment temperature.

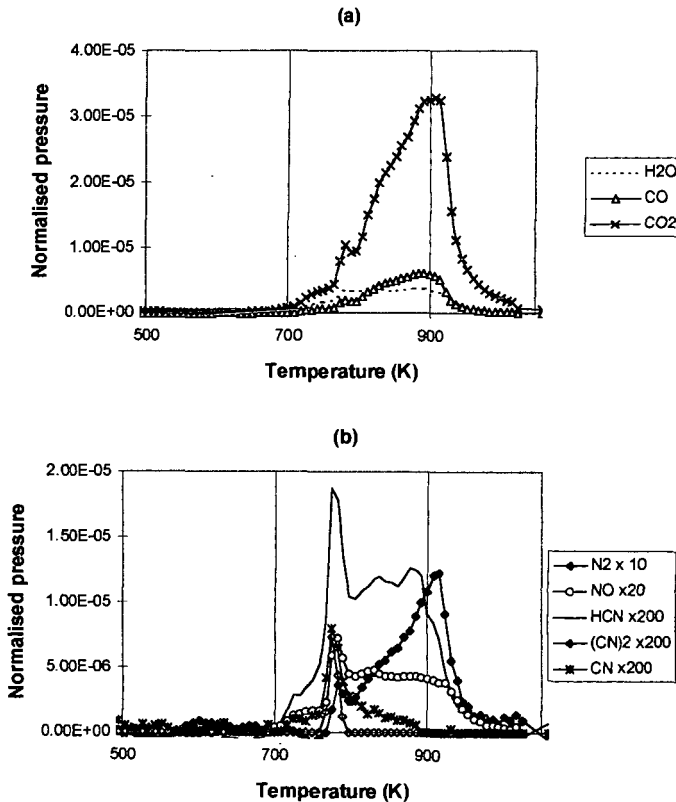


FIGURE 1: Gas evolution profiles during the temperature programmed combustion of tetraphenylporphine in 20% O₂/Ar (a) major products, (b) fuel nitrogen products.

TABLE 2: Product distribution ratios during temperature programmed combustion.

Product Ratio	TPP	CTPP-873	CTPPV-873
CO/CO ₂	0.173	0.713	0.235
NO/N	0.090	0.213	0.033
HCN/N	0.021	0.0005	0.041
N ₂ /N	0.452	0.807	0.822
C ₂ N ₂ /N	0.002	-	-
CN/N	0.004	-	-
Total N/fuel N	0.569	1.0205	0.896

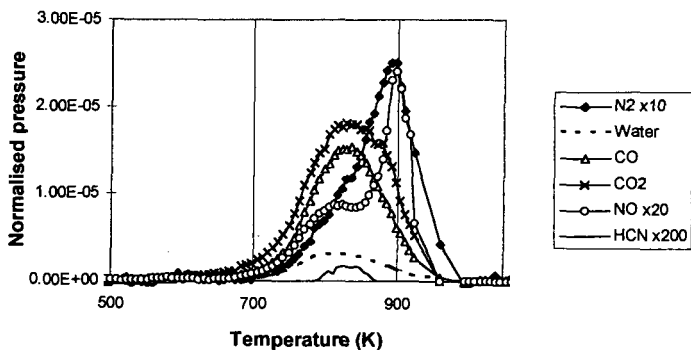


FIGURE 2: Gas Evolution profiles during the temperature programmed combustion of CTPP-873 in 20% O₂/Ar

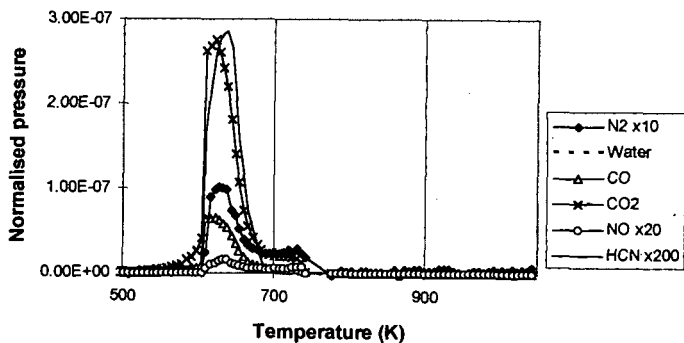


FIGURE 3: Gas Evolution profiles during the temperature programmed combustion of CTPPV-873 in 20% O₂/Ar

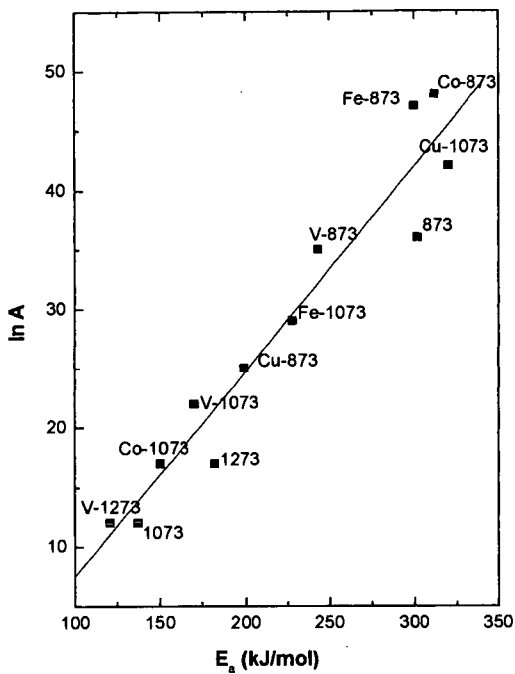


FIGURE 4: Compensation effect for metal-free and metal containing carbons. The ACE-TPP prefix has been dropped from the sample designation.

A NEW METHOD TO ESTIMATE HYDROGEN BONDINGS IN COAL BY UTILIZING FTIR AND DSC

Kouichi MIURA, Kazuhiro MAE, and Fumi-aki MOROZUMI

Department of Chemical Engineering, Kyoto University, Kyoto 606-01 JAPAN

Key words: Strength distribution of hydrogen bonding in coal, Wavenumber shift of O-H stretching vibration, Enthalpies of hydrogen bonding

INTRODUCTION

Several attempts have been made to estimate the change in the macromolecular network of coal using DSC and F.T.i.r. techniques. Lucht et al.,¹ Mackinnon et al.,² and Yûn et al.³ examined the glass transition of coal by the DSC measurement. Mackinnon et al.² observed the 2nd order phase glass transition at around 110 °C during the heating of various coals. They speculated that the 2nd order phase glass transition at low temperature was caused by the change in hydrogen bondings, although the direct evidence was not shown. We also demonstrated that a part of hydrogen bondings in coal are released between 100 and 200 °C from in-situ F.T.i.r. analysis.⁴ Painter et al.⁵ examined in detail the hydrogen bondings in coal using F.T.i.r., and classified the hydrogen bondings into 5 types.

In liquid phase, on the other hand, hydrogen-bonded adduct formation reactions between the OH functional groups of phenols and various bases have been examined in detail. The reaction is represented by



where Ph-OH \cdots B represents the hydrogen-bonded adduct, and ΔH is the enthalpy change of the reaction. When the hydrogen bonding is formed, the wavenumber of the O-H stretching vibration shifts to a low wavenumber and generates heat ($\Delta\text{H} < 0$). The enthalpy change, ΔH , and the OH wavenumber shift, $\Delta\nu_{\text{OH}}$, were measured for various phenol-base combinations, and a linear relation was found to hold between ΔH and $\Delta\nu_{\text{OH}}$ by many investigators.⁶⁻⁹ The relation obtained by Drago et al.⁶, for example, is given by

$$-\Delta\text{H} = 0.067 \Delta\nu_{\text{OH}} + 2.64 \quad [\text{kJ/mol}] \quad (2)$$

The values of $-\Delta\text{H}$ was interpreted as the energy related to hydrogen bonding Ph-OH \cdots B by many investigators.¹⁰⁻¹³ However, Drago et al. thought that ΔH consists of two contributions: the change in the phenol O-H bond energy, δD_{OH} , and the bond dissociation energy of hydrogen bond formed, D_{HB} , as

$$\Delta\text{H} = \delta D_{\text{OH}} - D_{\text{HB}} \quad (3)$$

They thought that D_{HB} is an index better than ΔH for the strength of the hydrogen bond. Then a relationship between δD_{OH} and $\Delta\nu_{\text{OH}}$ as well as a relationship between D_{HB} and $\Delta\nu_{\text{OH}}$ are required. They approximated the stretching of the hydrogen-bonded OH by the anharmonicity stretching of free OH, and related δD_{OH} with $\Delta\nu_{\text{OH}}$ as follows:

$$\delta D_{\text{OH}} = (hcN/4x_e) \delta\nu_{\text{OH}} = D_{\text{OHf}} (\delta\nu_{\text{OH}}/\nu_e) = 0.131\Delta\nu_{\text{OH}} \quad (4)$$

where h is Planck's constant, c is the speed of light, D_{OHf} is the bond dissociation energy of free O-H in kJ/mol and ν_e is the wavenumber of harmonic vibration of the free OH in cm^{-1} , and x_e is the anharmonicity constant for the oscillator.

From eqs.(2) and (4) D_{HB} was assumed to be represented by

$$D_{\text{HB}} = k \delta D_{\text{OH}} + \text{const.} \quad (5)$$

Substituting eq.(4) into Eq.(5), the following equation is obtained.

$$D_{\text{HB}} = k_1 \Delta\nu_{\text{OH}} + k_2 \quad (k_1, k_2: \text{const.}) \quad (6)$$

If the constants k_1 and k_2 can be determined, the relationship between D_{HB} and $\Delta\nu_{\text{OH}}$ is obtained. In liquid phase the following equation has been established for the $D_{\text{HB}}\text{-}\Delta\nu_{\text{OH}}$ relationship⁶:

$$-D_{\text{HB}} = 0.198 \Delta\nu_{\text{OH}} + 2.64 \quad [\text{kJ/mol}] \quad (7)$$

In this paper an equation relating the bond dissociation energy of the hydrogen bonding, D_{HB} , and $\Delta\nu_{\text{OH}}$ for coal was derived by extending the method of Drago et al. Then the strength distribution of hydrogen bondings in coal was estimated using the equation. Finally, the change in the hydrogen bondings through the heating of coal was examined.

EXPERIMENTAL

Sample preparation

A Japanese sub-bituminous coal, Taiheiyô (TC, C; 74.5%, H; 6.0%, N; 1.3%, S; 0.2%, O; 18.0% daf), was used as a raw coal. The coal was ground into fine particles of less than 74 μm , and dried in vacuo at 70 °C for 24 h before use. Irreversibly swollen coals (VDC) were prepared as follows: the coal particles were mixed with tetralin in a mass ratio of 1 to 0.6 in a stainless steel tube, and they were pressurized up to 1 MPa by nitrogen. The tube was immersed in a sand bath which was kept at a constant temperature at 150 or 220 °C and kept there for 1 h to prepare the swollen coal. Then, the swollen coal was evacuated at 70 °C for 24 h to remove completely the solvent retained. Even after removing the solvent the coal was still swollen to some extent. Then the coal was abbreviated to

VDC (vacuum dried coal). The VDCs prepared from the coals swollen at 150 and 220 °C were abbreviated to VDC(150°C) and VDC(220°C), respectively. The VDC(220°C) was further cooled to -100 °C using liquid nitrogen to prepare the sample in which some hydrogen bondings were restored. This sample was abbreviated to VDC(-100°C). The chars were prepared by pyrolyzing the coal at 5 K / min up to several temperatures to examine the change in hydrogen bondings during the pyrolysis.

F.T.i.r. and Calorimetric Measurement

The F.T.i.r. spectra of the raw coal, the VDCs and the pyrolysis chars were measured by the KBr method using a F.T.i.r. spectrometer (Shimadzu, FTIR 4300). The DSC profiles and the TG curves of the raw coal and the VDCs were measured under a constant heating rate of 5 K / min by use of a differential scanning calorimeter (Shimadzu, DSC 50) and a thermobalance (Shimadzu, TGA 50), respectively.

RESULTS AND DISCUSSION

Comparison of F.T.i.r. spectra between the raw coal and VDCs

The F.T.i.r. spectra were measured for all the samples. The spectrum of the O-H stretching vibration related to hydrogen bonding appears between 2600 and 3600 cm^{-1} ,⁵ so the base line was drawn between these wavenumbers by a usual method.^{14,15} Two sharp peaks at around 2800 cm^{-1} are due to aliphatic C-H vibrations, these peaks were eliminated following Solomon's method,¹⁶ then the absorption peak related to hydrogen bondings was 3000 to 3600 cm^{-1} for TC coal. The spectra obtained after the treatment are shown by the dotted lines in Figure 1. Comparing the spectra, the intensity of peak at 3630 cm^{-1} , which is assigned as the free OH, is almost same for all the samples, indicating that free OH groups are not produced through the solvent swelling and the heat treatment. Many peaks are involved between 3000 and 3600 cm^{-1} in the spectrum. Painter et al. showed that absorption bands of five hydrogen-bonded OH groups are involved in the spectrum: OH- π bonds (3516 cm^{-1}), self-associated OH groups (3400 cm^{-1}), OH-ether hydrogen bonds (3300 cm^{-1}), tightly bound cyclic hydrogen bonds (3200 cm^{-1}) and OH-N hydrogen bonds (2800-3100 cm^{-1}).⁵ Following these assignments, each spectrum was fitted by five Lorentz-Gaussian distributions as shown by the solid lines in Fig.1. The OH wave number shift, $\Delta\nu_{\text{OH}}$, for each hydrogen bonding is exactly estimated from the five peaks for the raw coal. The intensity of peak at around 3300 cm^{-1} was the strongest for the raw coal. As compared with the spectrum of the raw coal, the intensity of peak at around 3300 cm^{-1} decreased, and the intensities of peaks at around 3400 cm^{-1} and 3520 cm^{-1} increased for VDC(220°C). The intensities of peaks at around 3400 cm^{-1} and 3520 cm^{-1} decreased, and the intensity of peak at around 3300 cm^{-1} increased for VDC(-100°C). The intensities of peaks at around 3130 and 3040 cm^{-1} were almost same for all the samples. These results clearly show that the strong hydrogen bond and free OH were not affected by the solvent swelling and the heat treatment. Only the ether-OH, the self-associated OH groups, and the OH- π bonds were released or restored through the treatments.

Then we can visualize the change in the hydrogen bonding in coal as shown in Figure 2. When the coal is heated to as high as 200 °C or so, relatively weak hydrogen bonds such as OH-ether bond are released, but strong hydrogen bonds assigned at low wavenumber do not change. As a result the movement of the macromolecule of coal is restricted, then the OH in the hydrogen bonds released can not become free OH. It will form another weak hydrogen bonds.

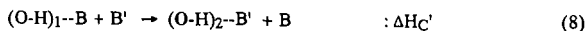
Figure 3 shows the DSC profiles measured for the raw TC and the VDCs. Thermogravimetric (TG) curves were measured under the same conditions. Distinct differences were found among the DSC profiles at the temperature region of 100 to 300 °C, whereas no difference was found among the TG curves of the four samples. The DSC profile of the raw coal showed the largest endothermicity of the three samples: the endothermic rate started to increase at around 100 °C, reached a maximum at ca. 250 °C, decreased to reach a minimum at 300 °C or so, and finally increased rapidly with the further increase of temperature. On the other hand, the endothermic rate of VDC(220°C) whose swelling ratio was largest was almost constant up to 200 °C, then started to increase, and finally almost coincided with that of the raw coal. The endothermic rate of VDC(150°C) which was slightly swollen lay between the endothermic rates of the raw coal and VDC(220°C). The DSC profile of VDC(-100°C) was close to that of VDC(150°C) up to 200 °C, but over 200 °C it was closer to that of the raw coal. The difference between the DSC profiles of the raw coal and the VDCs is judged to arise from the differences in the hydrogen bondings among the samples. The difference of the enthalpy levels between the raw coal and the VDC at 25 °C, ΔH_C , is obtained by heating both samples up to 220 °C where both enthalpy levels are considered to be same as shown in Fig.4. The enthalpy ΔH_C could be related to the difference of the strength of hydrogen bondings between the samples.

Estimation of the hydrogen bondings in coal using F.T.i.r. and DSC

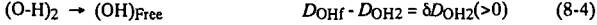
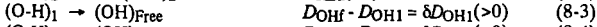
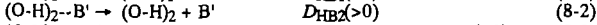
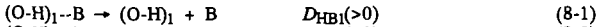
a) Formulation of equation relating D_{HB} and $\Delta\nu_{\text{OH}}$ in coal

The equation developed by Drago et al.⁶ for relating D_{HB} and $\Delta\nu_{\text{OH}}$ may not be applied to analyze the hydrogen bonding in coal, because it was obtained in liquid phase and coal contains several types of hydrogen bondings. However, the equation relating δD_{OH} and $\Delta\nu_{\text{OH}}$, eq.(4), was assumed to hold for the hydrogen-bonded OH in coal, because it is for intramolecular movement. Then the concept developed by Drago et al.⁶ was extended to formulate the equation relating D_{HB} and $\Delta\nu_{\text{OH}}$ using the experimental data, ΔH_C and $\Delta\nu_i$, obtained above.

First, we consider the change of a hydrogen bond, (O-H)₁-B, into another hydrogen bond, (O-H)₂-B', as a chemical reaction.



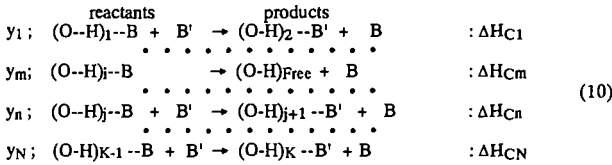
where B and B' represent electron donor atoms or molecules. The enthalpy change through the reaction, $\Delta H_C'$, is positive when the hydrogen bond becomes weaker through the reaction and vice versa. If we assume that $\Delta H_C' > 0$, the OH wavenumber shift decreases from $\Delta \nu_{OH1}$ to $\Delta \nu_{OH2}$, and the O-H bond dissociation energy increases from D_{OH1} to D_{OH2} as shown in Fig.5. The above reaction was apparently divided into the following reactions:



where $(O-H)_i$ represents the hydrogen-bonded OH groups, $(OH)_{Free}$ represents the free OH, D_{HBi} is the bond dissociation energy of hydrogen bond defined by Drago et al.,⁶ and δD_{OHi} ($i = 1, 2$) is the difference between the dissociation energy of the free O-H bond, D_{OHf} , and that of hydrogen bonded O-H, D_{OHi} . Since eq.(8-1) - eq.(8-2) + eq.(8-3) - eq.(8-4) makes eq.(8), $\Delta H_C'$ is represented by

$$\Delta H_C' = (D_{HB1} - D_{HB2}) - (\delta D_{OH1} - \delta D_{OH2}) \quad (9)$$

Next, eq.(8) was extended to all the reactions of the hydrogen bondings in coal as follows:



where all the possible reactions are taken into account in the N reactions, y_n is the contribution of each reaction defined so as to satisfy $\sum y_n = 1$, and the electron donors, B and B', for different reactions are not always same. The sum of $(O-H)_k$ and free OH, N_{OH} [mol/kg], is the total amount of OH groups in coal. The enthalpy change for each reaction, ΔH_{Cn} , is represented in the same manner as eq.(9). Then, summing up the reactions in eq.(10), the difference in the enthalpy between the products (p), and the reactants (r), ΔH_C [kJ/kg-coal], is represented by

$$\begin{aligned} \Delta H_C &= N_{OH} \sum y_n \Delta H_{Cn} \\ &= N_{OH} [\{ \sum (\sum y_n)_r D_{HBi} \}_r - \{ \sum (\sum y_n)_p D_{HBi} \}_p] \\ &\quad - N_{OH} [\{ \sum (\sum y_n)_r \delta D_{OHi} \}_r - \{ \sum (\sum y_n)_p \delta D_{OHi} \}_p] \end{aligned} \quad (11)$$

where y_n is set equal to 0 when i-th species is not involved in the n-th reaction. Then the term $(\sum y_n)_r$ is equal to the fraction of hydrogen-bonded $(O-H)_i$ of the all OH, and it was represented by f_i . The terms $\sum (\sum y_n)_r D_{HBi}$ and $\sum (\sum y_n)_r \delta D_{OHi}$, therefore, correspond to the average values of D_{HB} and δD_{OH} , respectively. They were represented by \bar{D}_{HB} and $\bar{\delta D}_{OH}$, respectively. By using the representation eq.(9) is rewritten as

$$(\bar{D}_{HB})_r - (\bar{D}_{HB})_p = \Delta H_C / N_{OH} + [(\bar{\delta D}_{OH})_r - (\bar{\delta D}_{OH})_p] \quad (12)$$

By inserting eqs.(4) and (6) into δD_{OHi} and D_{HBi} in eq.(11), eq.(13) is rewritten as

$$k_1 \{ (\bar{\delta \nu_{OH}})_r - (\bar{\delta \nu_{OH}})_p \} = \Delta H_C / N_{OH} + 0.131 \{ (\bar{\delta \nu_{OH}})_r - (\bar{\delta \nu_{OH}})_p \} \quad (13)$$

where

$$\bar{\delta \nu_{OH}} = \sum (\sum y_n)_r \Delta \nu_{OHi} = \sum f_i \Delta \nu_{OHi} \quad (14)$$

Thus a general equation relating ΔH_C and $\Delta \nu_{OHi}$ was formulated. When the raw coal and one of the VDCs are chosen as the reactants and the products in eq.(13), respectively, ΔH_C was measured by DSC, and $\Delta \nu_{OHi}$ ($i = 1 \sim 5$) were measured by F.T.i.r. for both the raw coal and the VDC as stated above. The value of N_{OH} could be determined from ¹³C-n.m.r. Then, knowing f_i , the k_1 value in eq.(13) can be determined. The value of f_i can be determined from the F.T.i.r. spectra if the relative sensitivities of the five peaks are known. Since the sensitivities are not known now, they were assumed to be same as a first approximation. Then the relations between D_{HB} , ΔH and $\Delta \nu_{OH}$ could be obtained as

$$D_{HB} = 0.20 \Delta \nu_{OH} \quad (15)$$

$$\Delta H = 0.069 \Delta \nu_{OH} \quad (16)$$

Figure 6 compares the D_{HB} - $\Delta \nu_{OH}$ and ΔH - $\Delta \nu_{OH}$ relationships obtained here (eqs.(15) and (16)) with those obtained by Drago et al. in liquid phase (eqs.(7) and (2)). The experimental data in liquid phase obtained by several researchers⁸⁻⁹ are also shown. Eqs.(16) and (2) were very close, and they correlate the experimental data very well. Eqs.(15) and (7) also almost coincided. This shows that same D_{HB} - $\Delta \nu_{OH}$ and ΔH - $\Delta \nu_{OH}$ relationships hold in liquid phase and solid phase, and that eq.(15) is valid to estimate the hydrogen bondings in coal.

(b) Estimation of the strength distribution of hydrogen bonding in coal

Once eq.(15) is found to be valid, the strength distribution of hydrogen bond in coal is straightforwardly estimated. The hydrogen bondings in coal were represented by 5 types, and they were approximated by Gauss-Lorentz functions as stated earlier. The amount of OH corresponding

to each hydrogen bonding, n [mol/mol], is calculated from the intensity of each peak, and D_{HB} corresponding to the peak is calculated from $\Delta\nu_{OH}$ using eq.(15). Then, plotting the n values against D_{HB} , we can obtain the strength distribution of hydrogen bonding. The values of D_{OH} and δD_{OH} are also obtained using eqs.(3), (15) and (16).

Figure 7 shows the strength distributions of hydrogen bondings in the raw TC coal and the VDCs. The values of D_{HB} , D_{OH} , and ΔH at maximum n value were 68.0, 42.0 and 23.8 kJ/mol-OH, respectively, for the raw coal. The value of 23.8 kJ/mol-OH for ΔH is reasonable, judging from the values reported.¹⁰⁻¹³ The strength distribution for VDC(220°C) shows that the hydrogen bondings of D_{HB} = 68.0 and 90.0 kJ/mol-OH decreased, but the hydrogen bondings of D_{HB} = 22.8 and 42.0 kJ/mol-OH increased through swelling.

(c) Change in the strength distribution of hydrogen bonding during the pyrolysis

The change in the strength distribution of hydrogen bonding during the pyrolysis was examined by applying eq.(16) to the pyrolysis chars prepared at several pyrolysis temperatures as shown in Fig. 8. When TC coal was heated to 280 °C, the 2nd phase glass transition temperature, the hydrogen bonding of D_{HB} = 68 to 90 kJ/mol-OH decreased, and the hydrogen bonding of D_{HB} = 42 kJ/mol-OH increased, indicating that the macromolecular network of the coal was altered to a loose network. The strong hydrogen bondings of D_{HB} = 90 kJ/mol-OH was disappeared first when the coal was heated from 386 to 485 °C, then the weak hydrogen bondings disappeared at around 500 °C. These results indicate that the stronger hydrogen bonding sites become the crosslinking site at low temperature. This well coincides with the fact that the value of D_{OH} decreases as the hydrogen bonding becomes stronger.

Thus, the presented equation was found to be very useful for estimating directly the hydrogen bonding in coal. We have made several assumptions and approximations to derive the equation. We will examine the validity of the assumptions and the approximations in future works.

CONCLUSION

A new method was presented for estimating the strength distribution of hydrogen bonding in coal by use of F.T.i.r. and DSC. An equation relating the dissociation energy of hydrogen bonding, D_{HB} , with the OH wavenumber shift, $\Delta\nu_{OH}$, was established by utilizing the change of hydrogen bonding between a Taiheiyu coal and irreversibly swollen coal prepared from the coal. Using the equation, we could estimate the strength distribution of hydrogen bonding in the coal. The peak D_{HB} value of the raw coal was found to be about 68 kJ/mol-OH. The change in the hydrogen bondings through the pyrolysis of coal was well represented by the method.

ACKNOWLEDGMENT

This study was supported by "Research for the Future" project of the Japan Society for the Promotion of Science (JSPS) through the 148 committee on coal utilization technology of JSPS.

REFERENCES

- Lucht, L.M.; Larson, J.M.; Peppas, N.A., *Energy & Fuels*, **1987**, 1, 56-58.
- Mackinnon, A.J.; Hall, P.J., *Energy & Fuels* **1995**, 9, 25-32.
- Yun, Y.; Suuberg, E.M., *Fuel* **1993**, 72, 1245-1254.
- Miura, K.; Mae, K.; Sakurada, K.; Hashimoto, K., *Energy & Fuels* **1992**, 6, 16-21.
- Painter, P.C.; Sobkobiak, M.; Youtcheff, J., *Fuel*, **1987**, 66, 973-978.
- Purcell, K.F.; Drago, R.S., *JACS*, **1967**, 89, 2874-2879.
- Drago, R.S.; Epley, T.D., *JACS*, **1969**, 91, 2883-2890.
- Arnett, E.M.; Mitchel, E.J.; Murty, T.S.S.R., *JACS*, **1974**, 96, 3875-3891.
- Arnett, E.M.; Mitchel, E.J.; Murty, T.S.S.R.; Gorrie, T.M.; Schleyer, P.v.R., *JACS*, **1970**, 92, 2365-2377.
- Larsen, J.W.; Green, T.K.; Kovac, J., *J. Org. Chem.* **1985**, 50, 4729-4735.
- Lucht, L.M.; Peppas, N.A., *Erdol und Kohle-Erdgas* **1987**, 40, 483-485.
- Green, K.; Kovac, J.; Brenner, D.; Larsen, J.W. in *Coal Structure*, Academic Press: New York, **1982**, pp.199.
- Painter, P.C.; Park, Y.; Coleman, M.M., *Energy & Fuels*, **1988**, 2, 693-702.
- Maddams, W.F., *Appl. Spectroscopy*, **1980**, 34, 245-267.
- Painter, P.C., in *Coal and Coal Products: Analytical Characterization Techniques*, *ACS Symp. Ser. 205*, **1982**, pp.47-75.
- Solomon, P.R.; Carangelo, R.M., *Fuel*, **1988**, 67, 949-959.

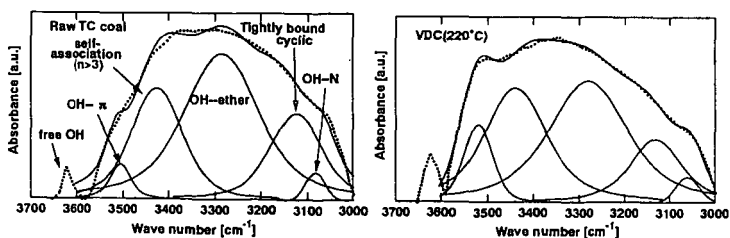


Figure 1 Comparison of the OH stretching vibration between the raw TC and a swollen coal.

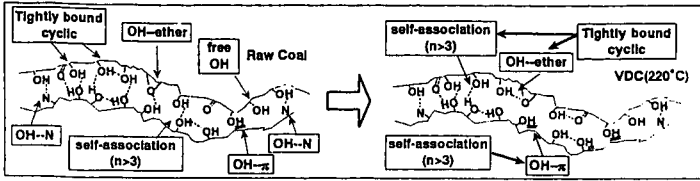


Figure 2 Image of the change in hydrogen bondings in coal through the treatment.

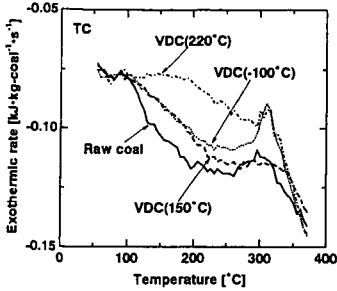


Figure 3 DSC profiles of the raw TC and the VDCs.

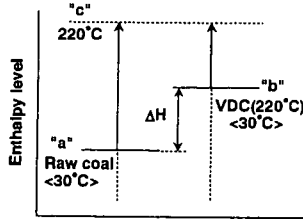


Figure 4 Enthalpy levels of the raw TC and VDC(220°C).

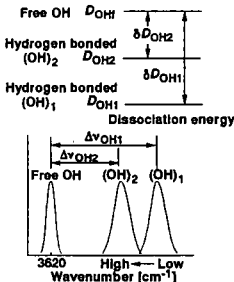


Figure 5 Changes in OH bond energy, D_{OH} , and wavenumber shift, $\Delta\nu_{OH}$, accompanied the change of a hydrogen bonding in coal.

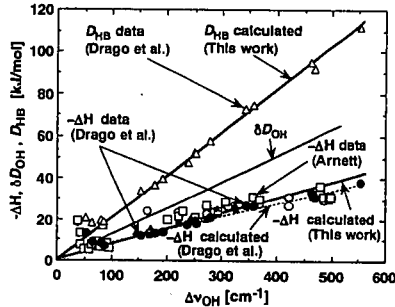


Figure 6 Comparison of the values of D_{HB} and ΔH calculated by eqs.(15), (16) with the experimental data.

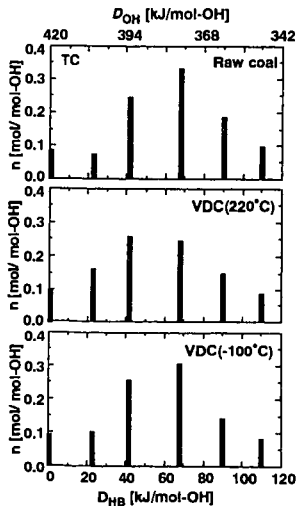


Figure 7 Strength distributions of hydrogen bondings in TC coal and the VDCs.

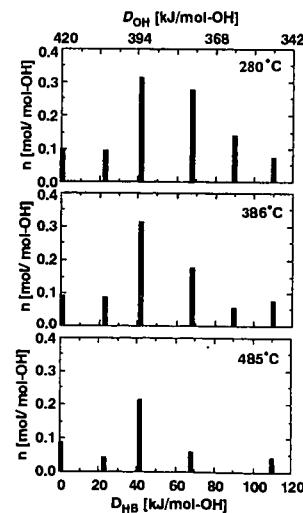


Figure 8 Change in strength distributions of hydrogen bondings in TC coal through the heat treatment.

INFLUENCE OF CHEMICAL STRUCTURE ON THE FLUIDITY OF RAPIDLY HEATED BITUMINOUS VITRINITES

Jonathan P. Mathews, Patrick G. Hatcher, Alan W. Scaroni
Energy & Fuels Research Center and Fuel Science Program, 211 CUL, The Pennsylvania State University, University Park PA 16802

Keywords: Vitrinite, char morphology and thermoplastic transformations.

ABSTRACT

When heated rapidly, many coal particles undergo thermoplastic transformations which change the particle size, shape and morphology. In the current work, vitrinites with subtle differences in rank and bulk chemical composition but significant differences in chemical constitution produced chars with different particle size and helium density. The particle size of an Upper Freeport (UF) sample increased by a factor of 2.5, and the helium density increased to 2.1 g/cm³ (daf). In contrast, a Lewiston-Stockton (LS) vitrinite swelled by a factor of 1.8 and the helium density increased slightly then decreased to 1.3 g/cm³. The LS vitrinite had more aliphatic hydrogen than the UF vitrinite, which should promote thermoplasticity. However, less aromatic hydrogen and more oxygen in the LS sample contributed to increased "cross-linking", presumably increasing the lamella size in the thermoplast, thus reducing the extent of thermoplasticity.

INTRODUCTION

Much of the published work on the properties of chars produced from coals that have undergone thermoplastic transformations has been with whole coals. However, macerals have different extents of thermoplasticity, hence by using whole coals individual maceral behaviour has been masked (1-3). While new separation techniques produce maceral concentrates (4), the associated particle size is typically less than pulverised coal. Although similar in rank and bulk chemical composition, two Illinois No. 6 coal samples were found to develop different extents of thermoplasticity during rapid heating (5). Since maceral analyses were not reported, fluidity differences manifested as different char properties might be explained by differences in the maceral composition. A relationship between chemical structure (total aliphatic hydrogen) and a modified Giesler fluidity has been reported for vitrinites, with an abrupt increase in fluidity over a relatively narrow range of aliphatic hydrogen (6). Furthermore, it has been proposed that three criteria must be met for plasticity to occur in bituminous vitrinites: 1) the presence of lamellae-bridging structures that can be thermally ruptured, 2) a supply of hydroaromatic hydrogen and 3) an initial, intrinsic potential for micellar and lamella mobility (not related to the rupture of chemical bonds), which provides opportunity for the free-radicals formed by bond rupture to contact potentially transferable hydrogen (7). Thus, the relationship between thermoplastic behaviour and chemical constitution can be explored utilizing vitrinites of subtly different bulk composition but different chemical constitution. In this study, particle swelling and helium density of the resulting chars were measured and related to differences in the vitrinite chemical structure.

EXPERIMENTAL

The vitrain samples were collected from *Sigillaria* (a type of Lycopod) tree remains in the roofs of coal mines in the Upper Freeport (UF) and Lewiston-Stockton (LS) coal seams. The samples were comminuted in a Holmes 501XLS pulveriser. A narrow particle size separation was achieved by wet sieving with a series of (U.S. Standard) sieves. Char particles were collected after rapid heating to 1500°C in a drop-tube reactor similar to that discussed previously (8). Coal was fed by an Acrison GMC-60 feeder through a water-cooled injector at a rate of 0.33g/min and entrained by 1.0 L/min of primary nitrogen. The tip of the injector was level with the bottom of a mullite flow-straightener. Secondary nitrogen (3.0 L/min) was preheated to 830 °C and exited the flow straightener with the primary nitrogen. Char particles were collected using a water-cooled probe with a cold suction flow of 4.0 L/min. Char particles were obtained from various locations by raising and lowering the collection probe.

The particle size distributions of vitrinite and collected vitrinite-chars were determined with a laser light scattering instrument (9). Helium densities were obtained using a commercially-available pycnometer. Changes in the morphology of the char were followed using gold-coated samples in a SEM. Ultimate analyses were performed using commercially-available instrumentation. Proximate analyses were determined using a thermogravimetric analyser (5 mg sample size) utilizing a modified ASTM methodology (10). The mean maximum vitrinite reflectance was calculated in accordance with ASTM procedures (11). CPMAS ¹³C NMR and dipolar dephasing experiments were performed in ways similar to those reported previously (12).

RESULTS AND DISCUSSION

The mean maximum vitrinite reflectance values were 0.97 (sd 0.04) and 0.93 (sd 0.08) for the UF and LS vitrinites, respectively. Both samples were determined to be monomaceral in composition using polished briquettes with reflected white and blue light. The elemental compositions of the vitrinites normalized to 100 carbon atoms were $C_{100}H_{75.5}N_{1.2}O_{4.4}S_{0.0}$ and $C_{100}H_{77.9}N_{1.4}O_{6.3}S_{0.6}$ (oxygen determined by difference) for the UF and LS vitrinites, respectively. The elemental compositions differed subtly, however in that, the LS vitrinite was slightly richer in hydrogen, nitrogen, sulphur and oxygen. Aromaticities determined by ^{13}C NMR were 0.77 and 0.81 for the UF and LS vitrinites, respectively (Table 1). Thus, the vitrinites were of the same maceral composition, with close particle size distributions (Table 2), yet subtle differences in the rank (mean maximum vitrinite reflectance) and aromaticities (Table 1). The volatile matter (daf basis) for the 200x400 mesh cuts were 37 and 30% for the UF and demineralized LS vitrinites, respectively. This indicates that, although there were only subtle differences in the bulk chemical composition, the constitution of the two vitrinites was substantially different. Structural parameters derived from the elemental composition and ^{13}C NMR experiments are reported in Table 1. The LS sample was richer in total aliphatic hydrogen (H/Cali) in comparison to the UF vitrinite and had less aromatic bound hydrogen. The lower aromatic hydrogen and higher oxygen content are consistent with a more "cross-linked" structure for the LS vitrinite.

SEM micrographs of the wet sieved 200x400 mesh UF and LS vitrinites and drop-tube generated vitrinite-char particles are presented in Figure 1. The UF vitrinite and chars are shown at different magnifications to aid in following morphological changes. The LS vitrinite and vitrinite-chars are shown at the same magnification to allow visual representation of the swelling. The wet sieved vitrinite fraction for both samples was characterized by angular particles with generally sharp edges. The char particles collected at 13 cm showed that some of the UF particles had undergone thermoplastic transformations, resulting in the rounding of edges and occasional cenosphere formation. However, many of the particles retained their angular shape and sharp edges. In contrast, most of the LS vitrinite chars at the 13 cm sampling location remained angular. The light-scattering-obtained volumetric weighted average size ($D_{[v,0.5]}$) indicated little swelling for both samples at the 13 cm location (Table 2).

The vitrinite-char particles for both samples collected at the 23 cm location displayed the characteristics of greater fluidity, in that very few particles retained their original morphologies and there was a slight increase in the $D_{[v,0.5]}$ (Table 2). The char particles collected at the 33 cm location had increased in size, swelling by a factor of 2.5 for UF vitrinite chars with the distribution of particle sizes increasing by a factor of 3.9 as shown by the Δ value (the difference between the $D_{[v,0.9]}$ and $D_{[v,0.1]}$ diameters). In contrast, the LS vitrinite-chars were less swollen, only expanding by a factor of 1.8 with the Δ value increasing by a factor of 1.6. As both vitrinite particle size cuts had similar Δ 's, indicating similar particle size distributions, the swelling of the UF sample was more sensitive to particle size. For both samples the char particles were almost all cenospheres. The outer skins of the cenospheres appeared wrinkled in many cases, which may be indicative of contraction. Decreasing $D_{[v,0.5]}$ values for both samples after the 33 cm location supports the occurrence of contraction. It might be expected that contraction would occur immediately after the jet release phenomenon (13), where the internal pressure is released suddenly and violently. However, cenospheres collected at the 23 cm location contained rents and blowholes, indicative of a sudden jet-release of volatiles, yet the skins remained smooth. Thus, contraction appears to post-date the jet-release event. It is speculated that the contraction of the particles may therefore be linked to chemical changes affecting fluidity rather than physical changes affecting the internal pressure (3). The cenospheres collected at the 33 cm location contained soot agglomerates on their skins. Chars collected at the 43 and 53 cm locations (not shown) were thin walled, having undergone some structural collapse.

Helium densities for the demineralized vitrinites and vitrinite-chars for both samples are shown in Figure 2, and compared to the reported density of graphite (14). The UF vitrinite chars showed a slight increase in helium density with increasing reactor length until after the 23 cm location where a substantial increase in the helium density occurred. In contrast, the LS vitrinite-chars experienced a slight increase in helium density (at the 13 cm location) and then a decrease to 1.3 g/cm³. A lower helium density is consistent with the observed reduced thermoplasticity of the LS vitrinite.

CONCLUSIONS

Two vitrinites with only subtle differences in bulk chemical composition exhibited different extents of thermoplastic transformations upon rapid heating as manifested by particle swelling and the helium densities of the resulting chars. The Lewiston-Stockton sample, although richer in total aliphatic hydrogen, did not experience enhanced thermoplastic transformations in comparison to the Upper Freeport vitrinite. The higher concentration of oxygen and less aromatic hydrogen in the Lewiston-Stockton vitrinite are consistent with a more cross-linked structure. This appears to reduce the fluidity, presumably by increasing the size of the lamellae, and produced chars with lower helium density and smaller particle size in comparison to the UF vitrinite.

REFERENCES

1. Tsai, C.-Y. and Scaroni, A. W., *Fuel*, 1987, **66**, (2), 200.
2. Street, P. J., Weight, R. P. and Lightman, P., *Fuel*, 1969, **48**, 343.
3. Anson, D., Moles, F. D. and Street, P. J., *Combustion & Flame*, 1971, **16**, 265.
4. Taulbee, D., Poe, S. H., Robl, T. and Keogh, B., *Energy & Fuels*, 1989, **3**, 662.
5. Cai, M. F., Guell, A. J., Dugwell, D. R. and Kandiyoti, R., *Fuel*, 1993, **72**, (3), 321.
6. Senftle, J. T., Kuehn, D. W., Davis, A., Brozoski, B., Rhoads, C. and Painter, P. C., *Fuel*, 1984, **63**, (2), 245.
7. Neavel, R. C., *Coal Agglomeration and Conversion*, West Virginia Geological and Economic Survey, 1975, Morgantown, WV, 120.
8. Artos, V. and Scaroni, A. W., *Fuel*, 1993, **72**, (7), 927.
9. Allen, T., *Particle size measurement*, Vol 4, 1990, London, Chapman and Hall.
10. ASTM, Designation: D 5142 - 90, Standard test methods for proximate analysis of the analysis sample of coal and coke by instrumental procedures, in Annual book of ASTM standards, Section 5, Petroleum products, lubricants and fossil fuels, 1994, 442.
11. ASTM, Standard test method for microscopical determination of the reflectance of vitrinite in a polished specimen of coal, in Annual book of ASTM standards, Section 5, Petroleum products, lubricants and fossil fuels, 1995, 274.
12. Hatcher, P. G., *Energy & Fuels*, 1988, **2**, 40.
13. Grey, V. R., *Fuel*, 1988, **67**, (9), 1298.
14. Franklin, R. E., *Fuel*, 1948, **27**, (1), 46.

Table 1. Chemical parameters

Parameter	UF	LS
f_a (CPMAS)	0.77	0.82
aryl-O content	0.20	0.17
$f_a^{a,H}$	0.49	0.37
H/C	0.76	0.78
H/Cali	1.7	2.7

f_a is the aromaticity, aryl-O content is the ratio of aryl-O bonded carbons to total aromatic carbons, $f_a^{a,H}$ is the fraction of aromatic carbons that are protonated, H/C is the atomic hydrogen to carbon ratio, H/Cali is the aliphatic atomic hydrogen to carbon ratio.

Table 2. Particle size distribution for the vitrinite and vitrinite-chars

Sampling Location (cm)	$D_{[v,0.5]}$ μm	$D_{[v,0.9]}$ μm	$D_{[v,0.1]}$ μm	Δ μm	Swelling
Vitrinite (UF)	65	110	44	66	1.0
13	69	120	48	72	1.1
23	76	132	48	86	1.2
33	160	298	42	255	2.5
43	148	223	54	169	2.3
53	132	210	59	151	2.0
Vitrinite (LS)	61	92	39	53	1.0
13	75	106	49	57	1.2
23	76	139	46	93	1.2
33	109	191	55	136	1.8
43	103	185	49	136	1.7

Analysis is based on volume, $D_{[v,0.5]}$ is the volumetric weighted average size. $D_{[v,0.9]}$ is the particle diameter such that 90% of the total volume is in particles of smaller diameter. $D_{[v,0.1]}$ is the particle diameter such that 10% of the total volume is in particles of smaller diameter, Δ is the difference between the $D_{[v,0.9]}$ and $D_{[v,0.1]}$ diameters, swelling was calculated from the $D_{[v,0.5]}$ diameter, particles were assumed to be spherical and no shape correction was performed. Data were collected in the model independent mode.

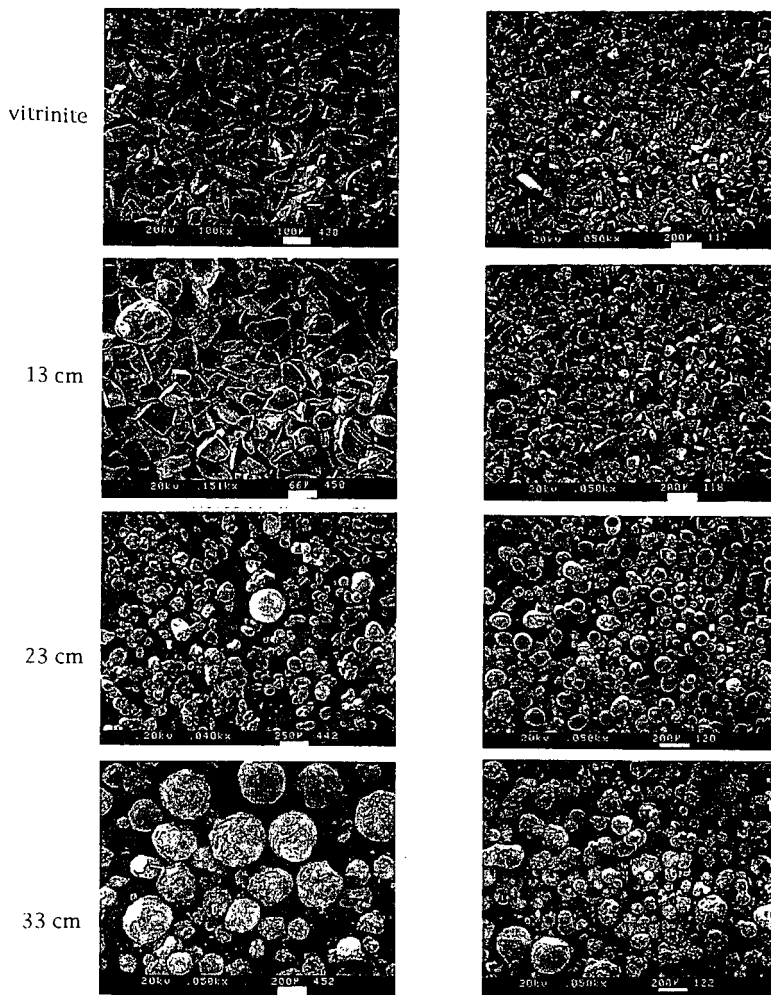


Figure 1. SEM micrographs of Upper Freeport (left) and Lewiston-Stockton (right) vitrinite and vitrinite-chars.

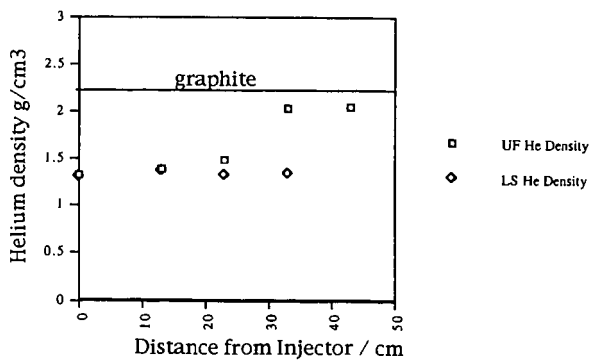


Figure 2. Helium densities for demineralized UF and LS vitrinites and vitrinite-chars

THERMAL BEHAVIOUR OF CARBOXYLIC ACID FUNCTIONALITY IN COAL

Tetsuo Aida, Noriyosi Hiram and Yukinari Tsutsumi
Department of Industrial Chemistry
Faculty of Engineering, Kinki University at Kyusyu
11-6 Kayanomori, Iizuka, Fukuoka 820, JAPAN

Keywords: Coal, carboxylic acid functionality, thermal decomposition

INTRODUCTION

Coal contains various chemical functionalities. Among them, the oxygen-containing functionalities are considered to play very important role to control its physical and chemical properties. Particularly, a carboxylic acid functionality has a relatively strong acidic characteristic comparing with other functionalities such as alcoholic and phenolic hydroxyl functionalities, so that it can make strong cohesive forces with a hydrogen bonding to other functionalities bearing electron negative atoms such as oxygen, nitrogen and sulfur. This means that the solubility of coal extracts for various solvents must be greatly affected by its concentration, as well as the apparent cross-linked structure formation in coal by molecular interactions such as hydrogen bonding, charge-transfer bonding or π - π -bonding.

Nevertheless, it has long been a kind of common-sense in the coal science community that the bonding contribution from a carboxylic acid functionality to the chemical and physical property of coal could be negligible toward higher ranked coals like a subbituminous and a bituminous coals. Simply because the previously reported analytical data concerning a carboxylic acid functionality content was too small, which used to be determined by the chemical method developed by Blom et al.(1) about 40 years ago. Although the recent development of sophisticated instrumentations such as FT-ir, ^{13}C -CP-MAS-NMR, XPS, etc., has made it possible to provide quite reliable informations about such hetero-atom-functionalities as sulfur-, nitrogen- and oxygen-containing functionalities, they seem to have a common problem in the accuracy to determining a small amount of functionality.

At the recent ACS Meeting, we had asked a following question in public with our experimental data obtained by newly developed chemical method(2). However, the low public attention had made us very disappointed.

"Is it true that a bituminous coal contain such a small amount of carboxylic acid functionality in the macromolecular network structure as shown in the Shinn's model(3)(one unit over 660 carbon skelton)?"

In Figure 1, our experimental data determined by the new method are summarized. It is just amazing and unbelievable that a wide range of high ranked coals still have a significant amount of carboxylic acid functionality in their macromolecular network structures. Based on these experimental results, Illinois No.6 coal contains at least 6 units of carboxylic acid functionality over 660 carbon skelton which means 6 times more than the Shinn's Model. Furthermore in the case of its pyridine extract, it reached up to 8 units/660-carbon. Thus, the conclusion in our previous paper was that there was a possibility of very serious misleading preconception concerning the carboxylic acid functionality in coal, particularly to the higher ranked coals.

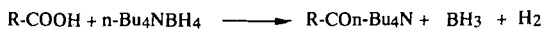
Actually, as Niksa pointed out in his recent personal communication and paper(4), it was well-known contradiction that the most of the CO_2 -release during the pyrolyses of subbituminous and bituminous coals could not rationalize by the unimolecular decomposition chemistry of carboxylic acid functionality in coals, because the previously reported quantity of the functionality was too small to use.

This is the strategical background for us to initiate the study on the thermal behaviour of carboxylic acid functionality in coal by means of the direct chemical determination.

EXPERIMENTAL

The chemical reagents were commercial products(Aldrich's gold label grade) which were used without further purifications. Pyridine for the chemical determination of carboxylic acid functionality was dried over calcium hydride and distilled before use. Coals from the Argonne National Laboratory(premium), the Ames Coal Library and BRAIN-C(5) were ground, seized, dried in a silica-gel desiccator at room temperature under vacuum for three days, and stored under a dry nitrogen atmosphere. The thermal treatment of coals(their analytical data shown in Table 1) and model compounds were carried out by using a thick-wall Pyrex glass sealed tubing of which inside atmosphere was replaced by an argon gas, and heated in a molten salt bath for 30 minutes at an appropriate temperature. After the reaction, the sealed tube was cooled down at a liquid nitrogen temperature, and then broken the seal for analyses.

The principle of our chemical determination method of carboxylic acid functionality is described as follows: The chemical reaction with tetra-n-butylammonium borohydrides was adopted for the determination of the carboxylic acid functionality as shown below. Since this reaction proceeds toward different hydroxyl functionalities with very different reaction rates, we can easily discriminate the carboxylic acid functionality from others. The detailed experimental procedure is available in our previous paper(2).



in pyridine solvent
(R = Aryl, Alkyl)

RESULTS AND DISCUSSION

1. Thermal stability of carboxylic acid functionality in coals

In order to examine the thermal stability of carboxylic acid functionality in coals, we have chosen two young coals (Yalourn, Dietz No.1&2) and two relatively old coals (Illinois No.6, Pittsburgh No.8). These coals were carefully handled under a nitrogen atmosphere to prevent an auto-oxidation by air, and also the heat-denaturation for which the drying operation was performed by using a silica-gel vacuum desiccator at room temperature for three days.

In Figure 2, the degree of the decomposition of the carboxylic acid functionality in each coals for 30 minutes were demonstrated versus temperatures.

Very interestingly, the pattern of the decomposition seems to be quite different between these two groups, that is, the carboxylic acid functionalities in the old coals were relatively stable below 350°C, and started to decompose over 400°C, meanwhile the young coals seemed to contain significant amount of reactive (unstable?) carboxylic acid functionality. Almost 40% of carboxylic acid functionality in coal destroyed under 300°C within 30 minutes heating condition. These results are consistent with a general understanding of a coalification process which is considered to predominantly destroy the reactive functionality in coal. Based on this assumption, the thermal decomposition pattern of the old coal, i.e., Pittsburgh No.8 coal, represents that of the stable form of carboxylic acid functionality in coal. Namely, the decomposition rate is accelerated over 400°C, and about 80% of the total content can be destroyed within 30 minutes at 450°C.

Meanwhile, in the case of the young coals (Lignite) the total content of carboxylic acid functionality are 2-3 times more than those of the old coals, and the most of the functionalities are reactive form which can be decomposed below 400°C. Obviously, the thermal decomposition pattern around 450°C suggest that some amount of stable form of functionality exists in the coal. It is also interesting that the fine structure of the decomposition pattern appeared between 200°C to 350°C suggests that the reactive functional group consisted from further different groups of the functionalities. Although at this moment it will be too early to draw a conclusion, there seems to be interesting coincidence between our data and the CO₂-release rate of the coal pyrolysis reported by Solomon, et al. (6) shown in Figure 3. We have not yet enough stoichiometric data concerning the decomposition of carboxylic acid functionality and the amount of the released CO₂ during the pyrolyses. But, it is quite plausible that the yield of CO₂ in the coal pyrolysis can be rationalized in terms of unimolecular decomposition chemistry of carboxylic acid functionality.

2. Thermal stabilities of model compounds

It has been found that coal contained several groups of carboxylic acid functionalities which had a different thermal stability. So, we have decided to assume the chemical structure of the functionality by comparing with those of the structure-known model compounds.

The first group of the model compounds chosen are the simple aromatic and aliphatic carboxylic acid compounds such as toluic acid, 1- and 2-naphthoic acid, and n-hexanoic acid which are assumed to be thermally quite stable.

Figure 4, summarized the experimental data obtained under the same reaction conditions as used for the coals, previously. The thermal decomposition patterns of the aromatic carboxylic acid, i.e., toluic acid, 1- and 2-naphthol seemed to be quite similar to those of higher ranked coals (Figure 2). The thermal stability of the alkyl derivative seems to be quite stable compared to others, which was decomposed over 450°C.

All of these results strongly suggest that the major component of carboxylic acid functionality in the old coal such as Illinois No.6 and Pittsburgh No.8 coals, must be simple aromatic and/or aliphatic derivatives. This assumption seems to be consistent with our previous understanding, for example, Shinn's model adopted a single aromatic carboxylic acid functionality.

The second group of the model compounds chosen are mainly the nature-oriented form of carboxylic acid compounds such as malic acid and fumaric acid, of which existence in coal are not sure, but it is considered to be one of the candidates for the possible functionality in younger coals like a lignite.

The results obtained are summarized in Figure 5.

As expected, these model compounds started to decompose under relatively mild conditions, around 250-300°C.

Of course it is quite difficult to assume with these data that the actual chemical structure of the reactive carboxylic acid functionality in coals are just like these chemical structure. But at least, we may be able to say that the younger coals like a lignite have much of a nature-oriented (raw) form of carboxylic acid functionality in the macromolecular network structure. Also, the carboxylic acid functionality of which chemical reactivity can be significantly enhanced by the specific substituents or hetero-atoms like a 9-anthracenecarboxylic acid seems to be responsible for such a mild decompositions.

CONCLUSION

It was found that the coal contains both stable form and relatively unstable form of carboxylic acid groups in the macromolecular network structure. The former seem to be a simple aromatic carboxylic acid, and the later is assumed to be more natural product like carboxylic acid functionality. It is also likely that the previous observation of the CO₂-release during the pyrolyses of coals can be rationalized by the unimolecular decomposition chemistry of carboxylic acid functionality in coal.

AKNOWLEDGEMENTS

A part of this research was supported by the grant from The Japanese Ministry of Education through The Nippon Gakujutu Shin-koukai.

REFERENCES

- (1) Blom, L., Edelhause, L., and van Krevelen, D.W., *Fuel*, **36**, 135(1957)
- (2) Aida, T, et al., *Prepr. Am. Chem. Soc. Div. Fuel Chem.*, **41**(2), 744(1996)
- (3) Shinn, J.H., *Fuel*, **63**, 1187(1984)
- (4) Niksa, Stephen, *Energy & Fuels*, **10**, 173(1996)
- (5) Coal Bank sponsored by NEDO through CCUJ(Japan)
- (6) Solomon, P. R., et al., *Energy & Fuels*, **4**, 319(1990)

Table 1. Analytical Data of Coals

Coal	(dmmf wt %)					(mmol / g)		
	Ash	C	H	N	O	S	COOH	Ph-OH
Yallourn*	1.6	66.9	4.70	0.48	27.7	0.26	1.28	4.61
Dietz No.1 & 2	5.5	74.4	5.26	1.09	18.9	0.44	1.27	-
Illinois No.6**	14.3	80.7	5.20	1.43	10.1	4.82	0.67	2.52
Pittsburgh No.8**	9.1	85.0	5.43	1.68	6.90	2.19	0.37	2.04

* Australian brown coal

** Argonne premium coal

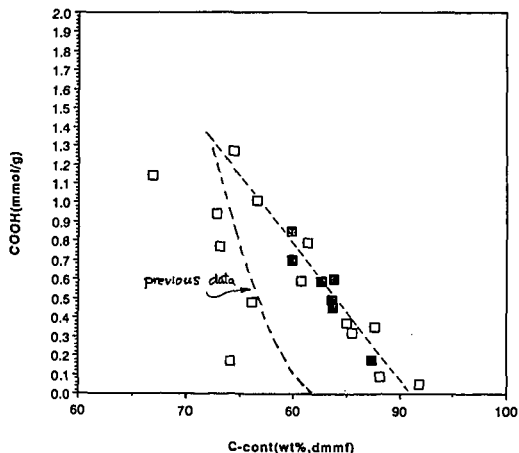


Figure 1. Coal rank dependency of Carboxylic acid functionality content

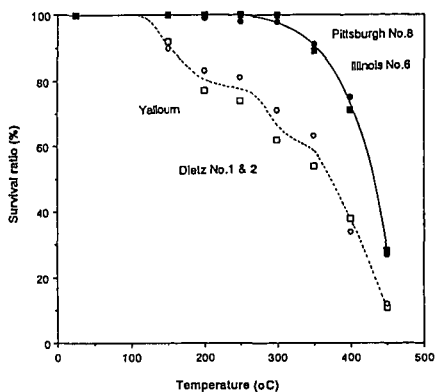


Figure 2. Thermal stabilities of carboxylic acid functionality in coals

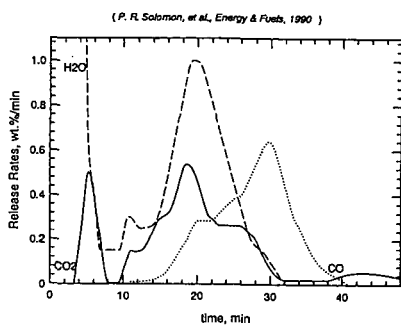


Figure 3. Release rates of gaseous products from thermal decomposition of subbituminous coal (6)

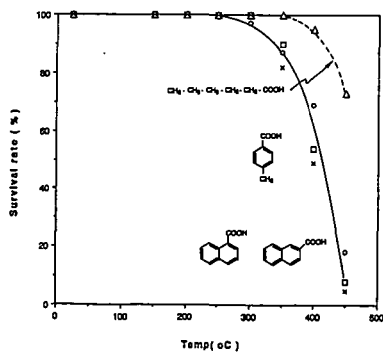


Figure 4. Thermal stabilities of model compounds

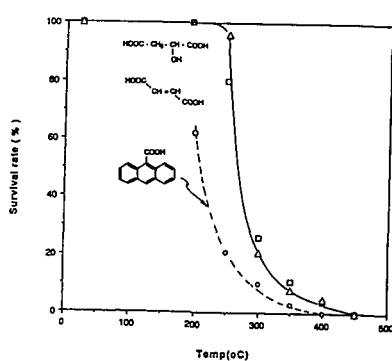


Figure 5. Thermal stabilities of model compounds

THE OXIDATIVE REACTIVITY OF COAL CHARs IN RELATION TO THEIR STRUCTURE

by

M-L Chan*, J. M. Jones, M. Pourkashanian, and A. Williams

Department of Fuel and Energy, The University of Leeds,
Leeds, West Yorkshire, UK, LS2 9JT

*British Gas Research Centre, Ashby Road, Loughborough.

Keywords: coal, porosity, reactivity

Abstract: In the oxidation of highly porous carbons, the internal surface area can increase as a function of conversion due to pore growth and the opening up of sealed internal pores or cavities. Consequently, rate expressions for carbon oxidation are more accurately described in terms of the intrinsic reactivity, where differences in surface area and porosity are accounted for.

The oxidative reactivity of coal chars is complicated by a number of different factors which are explored in this paper. These include (i) the development of the pore structure during devolatilisation of the coal, (ii) the ash content and its distribution in the carbon matrix, (iii) the H and N functional groups present on the solid matrix, and the interrelation with volatile species present, (iv) the graphitic nature of the carbon surface and, the active surface area available for reaction.

Introduction

Coal char structure is influenced, not only by coal properties, but also by the temperature-time history which the coal particles experience within the combustor, i.e. heating rate, maximum temperature experienced, residence time at this temperature, and the gaseous atmosphere. This is because these variables, together with coal properties all influence the amount and nature of the volatile, as well as their rate of release. These factors determine both the macroscopic morphology and the microscopic porosity of the resultant char. The porosity is particularly important because it can control the rates of diffusion of chemical species into and out of the char particle. The rate of combustion of coal chars is an important parameter on combustion efficiency because of its impact on the unburnt carbon in the ash. Rationalization of the relationship between char reactivities in combustion and coal/char chemical and physical properties has therefore been attempted. In the chemical kinetic regime these include structural and chemical properties which increase the active surface area of the chars.

This paper considers the effect of some of these properties on porosity of coal chars and hence active surface area and reactivity. Particular emphasis will be placed on the following: (i) effect of devolatilisation conditions on porosity, (ii) effect of porosity on reactivity of coal chars and (iii) effect of mineral and heteroatoms content, and their distribution, on reactivity

Experimental methods

Coal chars were prepared from three British bituminous coals (70-90 μm), Markham Main (MM), Kiverton Park (KP), and Goldthorpe (G), by heating in an inert atmosphere to different heat-treatment temperatures (400-900 $^{\circ}\text{C}$) and at different heating rates (10 K/min (slow) or $1 \cdot 10^4$ K/s (rapid)). The coal chars were characterized for their surface areas (N_2 and CO_2 adsorption at 77 or 195 K respectively), density, and porosity (mercury porosimetry). Chars were also examined by SEM. Isothermal char reactivities in air were measured in the temperature range 395-764 $^{\circ}\text{C}$ using a Beckman LM 600 microbalance.

Results and Discussion

The physical properties of the coal chars produced at slow pyrolysis are given in Table 1. For all three coals the surface area of the char is seen to pass through a minimum with increasing heat-treatment temperature. The surface areas measured by CO_2 adsorption are much higher than those measured by N_2 adsorption which is indicative of the presence of micropores which are

inaccessible at 77K due to activated diffusion. The density of the chars increase with increasing heat-treatment temperature, while the effect on porosity is more subtle.

The general trends in the changes in surface areas with heat-treatment can be explained in terms of the expected behavior for bituminous coals. At temperatures of between 200-500 °C the coals begin to soften and some volatile gases are evolved resulting in a loss of disordered material within the coal and an improvement in the stacking of the lamellae. A consequence of this is decreasing surface area. Upon further heating (500-600 °C), loss of tars begins resulting in swelling and an increase in the porosity (micro, meso and macro) hence both N₂ and CO₂ surface areas begin to increase again, as do the pore volume and porosity. At still higher temperatures (600-900 °C) resolidification of the coke structure occurs and the lamellae begin to grow with loss of H₂, resulting in increasing meso- and microporosity. These structural changes are validated by the spectroscopic properties and by elemental analysis of the chars. The role of N is also identified in this way.

The reactivity of coals in an oxygen atmosphere were obtained from experimental measurements. These apparent reactivities of the coals were converted into the values per unit surface area of the sample at one atmosphere oxygen partial pressure (i.e. the intrinsic reactivity R_i). The intrinsic reactivity, ρ_i, is used to normalize carbon reaction rates for differences in porosity:

$$\rho_i = R_i P_{O_2}^n \quad (1)$$

$$R_i = \frac{R_c}{A_g \gamma \sigma_a \eta} \quad (2)$$

Where R_i is the intrinsic reaction rate coefficient, P_{O₂} is the oxygen partial pressure, n the reaction order, A_g is the specific (pore) surface area, γ is the characteristic dimension of the particle, σ_a is the apparent density of the char and η is the effectiveness factor, calculated using Thiele's modulus in a unimodal pore system. The chemical rate coefficient, R_c, can be obtained from:

$$R_c = R_D P_{O_2}^{-(n-1)} \frac{X}{(1-X)^n} \quad (3)$$

where, R_D is the rate coefficient for oxygen diffusion to the particle, and X is the ratio of the actual burning rate to the maximum burning rate.

Figure 1 shows the Arrhenius plots of the R_i values not only for the coals examined in present study but includes values collected by the authors (1) for 6 different types of coal including petroleum coke. Figure 1 also includes values of intrinsic reactivity for 32 samples collected by Smith (2). Figure 1 shows R_i at a specific temperature ranging over up to two orders for the coal-types investigated. Values for the char activation-energies obtained from the intrinsic reaction rates were between 172 ± 12 kJ/mole and the pre-exponential factor was approximately 50 g/cm²s for the temperature ranges under investigation. As R_i is the reactivity per unit surface area of the coal, the differences in intrinsic reactivities must be attributed to other factors than porosity of the char sample. To clarify the relative importance of the other factors likely to affect the char oxidation process, relationships between R_i and some physical properties of the coals were examined.

Relationship between char reactivity and ash, H and carbon content: It is well established that overall coal reactivities are affected by the presence of minerals (3,4). The relationship between mineral matters and char reactivity R_i, is explored in (Figure 2). Although the number of coals studied during this investigation is very limited, it appears that reactivities R_i of the chars of higher rank coals are influenced by ash concentration. At low oxidation temperatures (<600 °C) the non-linear behavior of the R_i with ash concentration indicates that char reactivity may be controlled by the catalytic activity of coal minerals. However, at higher oxidation temperature (>600 °C) the intrinsic reactivity depends linearly on the char's ash content which may represent a non-catalytic reaction of carbon. Therefore, reduction in R_i with increasing ash content would be due to an inhibition of the carbon reactivity by the ash.

The relationship between R_i and hydrogen content of the coals is shown in Figure 3. The results imply a relationship very similar to the ash-char reactivity relationship. It is known that coal hydrogen content is directly related to the volatile content of the coal, and the number of carbon active sites on char can be related to the devolatilisation process and volatile concentration.

Therefore, the decrease in reactivity of char with hydrogen content can be related to the reduction in active sites.

Figure 4 shows the relationship between intrinsic reactivity and carbon content of the sample coals. At higher oxidation temperatures the intrinsic reactivity decreases monotonically with carbon content. Lower oxidation temperatures result in a optimum carbon concentration for maximum reactivity.

Reactivity and char structure: In a previous investigation by the authors (5), a correlated chemical reactivity is evaluated for 24 chars and cokes. The correlated chemical reactivity was based on all the chemical and physical variables of the coal. The resulting relationship is:

$$R_c = [1.4 (Vit_m + 0.83 Vit_{ps})] - 0.6(\ln_R + 1.6 \ln_{LR}) \exp^{(-89)} \sigma_a^{(-7.5)} Ag^{(-0.5)} C^{(3.5)} T_p^{(9.5)} \quad (4)$$

where \ln_R and \ln_{LR} are the fractions of low reflectance (reactive) and high reflectance (less reactive) inertinite respectively, and Vit_m and Vit_{ps} is the fraction of matrix and pseudo vitrinite respectively, C the carbon content and T_p the particle temperature.

The class of empirical formulations, of which equation 4 is an example, is of paramount importance to computational modelling. Other investigations have also produced a number of similar classes of formulations (6). Careful consideration of the results indicates that statistical analysis of char burn-out is necessary to describe the reactivity characteristic because of the complicated interplay of factors.

Conclusions

Values for the char activation-energies obtained from the intrinsic reaction rates were between 172 ± 12 kJ/mole for the temperature ranges under investigation. The current studies indicate strong interactions between carbon content, ash, and hydrogen content during the char-oxidation process. These interactions have been quantified for the coals studied.

References

1. Hargrave, G., Pourkashanian, M., and Williams, A., Twenty first Symposium (international) on Combustion, The Combustion Institute, 1987.
2. Smith, I. W., 19th Symposium on Combustion, The Combustion Institute, p1045, 1982.
3. Fung, D.P.C. and Kim, S.D., Fuel, 63, p1197, 1984.
4. Hippo, E.J., Jenkins, P.L. Fuel, 58, p338, 1979.
5. Hampartsoumian, E., Pourkashanian, M. and Williams, A. J. Inst. E. p48, 1989.
6. Charpenay, S., Serio, M.A. and Solomon, P.R., International Conference on Coal Science, Banff, Canada, Vol. II, 189, 1993.

Table 1: Physical properties of Markham Main coal chars produced by slow pyrolysis

Char	HTT (°C)	Surface Area (m ² /g)		Density (g/cm ³)		Pore vol. (cm ³ /g)	Porosity (%)
		N ₂ @ 77K	CO ₂ @ 195 K	He	Hg		
MM-400	400	5.8	257.3	0.99	0.95	0.040	4.04
MM-500	500	0.7	113.7	1.01	0.98	0.030	2.97
MM-600	600	1.1	181.5	1.07	1.02	0.046	4.67
MM-700	700	3.6	179.7	1.15	1.07	0.065	6.96
MM-800	800	10.8	272.1	1.23	1.18	0.034	4.07
MM-900	900	11.3	210.0	1.46	1.33	0.067	8.90
KP-400	400	4.1	91.3	0.98	0.94	0.043	4.08
KP-500	500	0.4	73.1	0.99	0.96	0.032	3.03
KP-600	600	0.8	67.9	1.03	0.98	0.030	2.97
KP-700	700	5.6	221.7	1.01	1.01	0.020	1.94
KP-800	800	8.1	211.6	1.06	1.03	0.030	2.83
KP-900	900	9.6	184.4	1.19	1.12	0.050	5.88
G-400	400	3.6	48.3	1.05	0.95	0.100	9.52
G-500	500	0.3	49.9	1.01	0.97	0.040	3.96
G-600	600	0.2	29.1	1.08	1.01	0.064	6.48
G-700	700	0.9	262.6	1.11	1.09	0.016	1.80
G-800	800	5.9	215.1	1.13	1.10	0.024	2.65
G-900	900	5.1	-	1.27	1.19	0.053	6.30

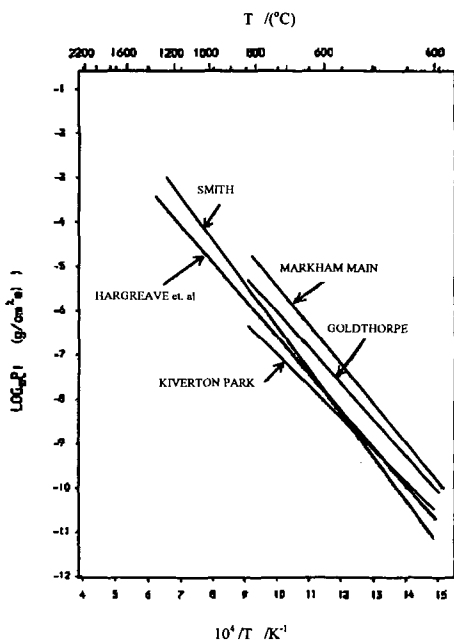


Figure 1: Comparison of intrinsic chars reactivity in air

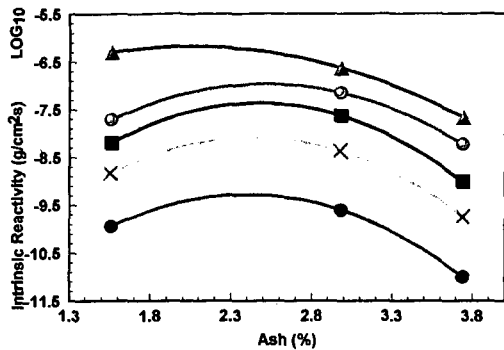


Figure 2: Relationship between Intrinsic reactivity and % ash in char. Oxidation temperature Δ 900C, \circ 800C, \blacksquare 700C, \times 600C and \bullet 500C.

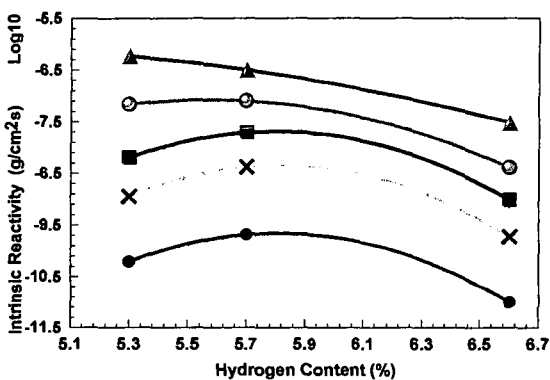


Figure 3. Relationship between Intrinsic reactivity and H in coal samples. Symbols as in Fig. 2.

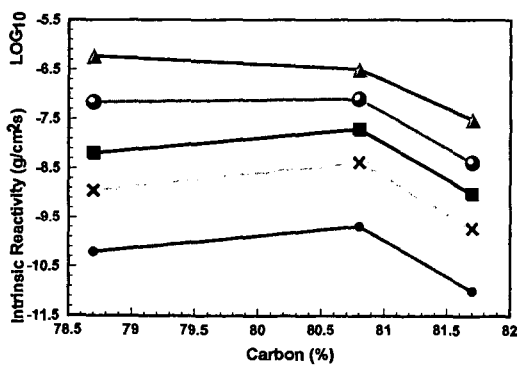


Figure 4: Relationship between intrinsic reactivity and %carbon of the char. Symbols as in Fig. 2.

IN-SITU ^1H NMR STUDY OF FLUIDITY ENHANCEMENT BY HYDROGEN-DONOR AND NON-DONOR PITCHES FOR A BITUMINOUS COAL

M. Mercedes Maroto-Valer, John M. Andrésen and Colin E. Snape

University of Strathclyde, Department of Pure and Applied Chemistry,
295 Cathedral Street, Glasgow G1 1XL, Scotland, UK

Keywords: Hydrogen-donor, pitch, fluid phase, high temperature ^1H NMR.

Hydrogen-donor ability has been ascribed as one of the factors responsible for the stabilisation of the plastic phase during coal carbonisation. In-situ high temperature ^1H NMR has been used here to quantify the interactions between a low-volatile bituminous coal and both a normal coal tar pitch (CTP) and a hydrogen-donor pitch (HDP) obtained from a coal liquefaction process. When the CTP was added to the coal (25% w/w, 150-250 μ), the amount of fluid material increased by nearly 20% more than that predicted at maximum fluidity close to 450°C. Indeed, a larger synergistic effect was observed with the HDP. By 400°C, 90% of the fluid phase concentration observed at 450°C had already been generated, corresponding to an enhancement of 50% over that predicted. However, particle size appears to be a dominant factor under the slow heating regime used in that no enhancement in fluidity was detected when the coal size was <45 μ .

INTRODUCTION

Coal and pitch carbonisation has previously been investigated using high temperature in-situ ^1H NMR by Sanada and coworkers⁽¹⁾ and, more recently, by Lynch et al, who refer to the technique as "Proton Magnetic Resonance Thermal Analysis" (PMRTA)^(2,3). The thermoplastic stage of coal is characterised by a ^1H NMR signal that consists of a mobile (Lorentzian) and a rigid (Gaussian) component⁽²⁻⁵⁾. The authors recently have used a high temperature Doty NMR probe to rationalise a number of coal carbonisation phenomena, including the effects of particle size and mild oxidation, in terms of both the concentration of rigid and fluid material present, as well as the mobility or T_2 of the later^(4,5).

The stabilisation of the plastic phase present during coal carbonisation has been reported to be connected with its hydrogen transfer and donor abilities^(6,7). Indeed, aromatic additives that soften upon heating and include coal extracts, pitch and individual polycyclic aromatic compounds can improve fluid properties considerably. For example, using Gieseler fluidity measurements for a series of New Zealand coals, Clemens and Matheson⁽⁸⁾ reported that both decacyclene and solvent extracts can improve plasticity development. Fortin and Rouzaud used TEM to view the beneficial effects of N-methyl-2-pyrrolidone and boiling anthracene oil extracts on the formation of coke microtexture⁽⁹⁾. Indeed, the addition of coal tar pitch (CTP) to coal blends is widely used as a means of enhancing fluidity in coke production. To rationalise the role of solvent extractable material present on the development of a potentially much larger pool of fluid material, Neavel and Marsh⁽¹⁰⁾ proposed a parallel between coal liquefaction and carbonisation. The development of plasticity can be considered as a pseudo liquefaction process, in the sense that the extractable material acts as a hydrogen-donor and transfer agent, stabilising the unstable radical species produced by pyrolytic-reaction pathways. In this study, in-situ high temperature ^1H NMR has been used here to quantify the interactions between a low-volatile

bituminous coal and both a normal (CTP) and a hydrogen-donor pitch (HDP) obtained from a coal liquefaction process.

EXPERIMENTAL

Table 1 lists the atomic H/C ratios, aromaticity and softening points for the low volatile Australian coal (20% daf volatile matter, $R_{o,max}$ of 1.46), the CTP and the HDP investigated. The CTP was obtained by distillation of a coal tar at 380°C and under 125 mm Hg vacuum for 2 hours. The HDP was produced in the liquid British Coal Liquid Solvent Extraction (LSE) process at the Point of Ayr facility, and comprises material boiling above 450°C in the product from the hydrocracker. The coal was ground manually using a mortar and pestle to give <45 and 150-212 μ fractions. Mixtures of coal and pitch (4:1 w/w) were prepared and stirred for one hour to ensure homogeneous blends were obtained.

The high temperature measurements were carried out using a Doty probe on a Bruker MSL-100 spectrometer as described previously (4,5). Approximately 50 mg of sample was packed in a zirconia container, except for the pitch samples, where only around 30 mg was used due to their high fluidity and the fact that a significant amount of sample distills off below 450°C. The average heating rate was around 4°C min⁻¹. Spectra were obtained at a number of different temperatures and fitted to Lorentzian and Gaussian components, as appropriate.

RESULTS AND DISCUSSION

General aspects Figure 1 compares the peak widths at half height, $\Delta H_{1/2}$, at temperatures up to 550°C for the coal, CTP and their mixture (4:1 w/w) with a particle size of 150-212 μ . The softening process for the coal is similar to other coking coals (4,5); the maximum fluidity at 470°C is reflected by the minimum in $\Delta H_{1/2}$, corresponding to a maximum in T_2 . During the fluidity range, the peak width of the plastic phase (this dominates $\Delta H_{1/2}$) is only 20-35% of that for the initial coal. At maximum fluidity, the fluid phase accounts for 26% of the hydrogen observed (Table 2). After the onset of resolidification at 490°C, the peak width increases to reach a value similar to that of the initial coal. As anticipated for the CTP, the overall $\Delta H_{1/2}$ decreases markedly after softening at ca. 190°C and then stays constant close to 1000 Hz (Figure 1). Indeed, as discussed later, the overall peak width of only 10 ppm for both pitch samples means that aromatic and aliphatic hydrogen peaks are resolved. No rigid material was observed in the spectra of the pitch samples above their softening points.

Particle size effect Figure 1 shows that for the peak width for the coal (150-212 μ)/CTP mixture below 350°C is dominated by the softening of the pitch. For the mixture, the $\Delta H_{1/2}$ of ca. 1100 Hz is the same as for the pitch alone indicating that the coal particles do not impair the motion of the pitch constituents. In contrast, for the mixture with <45 μ particles, the $\Delta H_{1/2}$ (ca. 10 kHz) is nearly ten times larger between 200 and 400°C. This difference in halfwidth is also apparent in the ¹H NMR spectra obtained at maximum fluidity (460°C) for the two mixtures (Figure 2). The increase in peak halfwidth with decreasing particle size has previously been reported as playing an important role in fluidity development (4,5). The mobility or T_2 of the fluid material falls with decreasing particle size, but the amount of fluid material remains constant. These findings suggest that the fluid material - both pitch and coal extract - is weakly adsorbed on the coal and the extent of this interaction increases with decreasing particle size as more of the surface becomes available.

Synergism with coal tar pitch In order to ascertain whether there was any synergism between coal and CTP in terms of plasticity development, the spectra obtained at maximum fluidity were deconvoluted to derive the proportions of fluid and rigid material. The observed and predicted values for the proportion of

hydrogen in the fluid phase are listed in Table 2. The latter were derived from the amounts of fluid material generated when the coal and CTP were heated separately, the hydrogen contents of the coal and CTP and the hydrogen lost during the heating. For the smaller particle size ($<45 \mu$), the predicted value of 37% is extremely close that of 38% for the proportion of fluid hydrogen at maximum fluidity, indicating no synergism has occurred. In contrast, the predicted proportion of 37% for the fluid hydrogen was significantly lower than that of 45% observed with the larger particle size (150-212 μ , Table 2). This difference corresponds to an enhancement of 20% in the amount of fluid material generated (Table 2). The same treatment at 400°C indicates that the enhancement in fluidity is 15%, although the total concentration is only about two-thirds that observed at 450°C (Table 2). Thus, a synergistic effect is evident only when the coal particles are sufficiently large (ie. 150-212 μ) so as not to impair the motion of the pitch.

Hydrogen-donor pitch The structural differences of the two pitches are listed in Table 1, the HDP having a higher atomic H/C ratio and lower carbon aromaticity (0.75 compared to 0.99 for the CTP). Figure 3 presents the ^1H NMR spectra for the two pitches obtained in the fluid stage at 300°C before any significant proton weight loss. Both pitches display two peaks from aromatic (5-10 ppm) and aliphatic (0-5 ppm) hydrogen, respectively. As expected from the relatively low aromaticity, the HDP spectrum is dominated by the aliphatic peak.

The amount of fluid material generated at 460°C from the coal (150-212 μ)/HDP mixture is 44% (Table 2), indicating a positive interaction as for the coal/CTP mixture. However, since the HDP loses more weight during the heating process (ca. 60% of its hydrogen) than the more aromatic CTP (only 25%), the degree of synergism is larger with 30% more fluid material being generated than predicted (Table 2). By 400°C, 90% of the fluid phase concentration observed at maximum fluidity (460°C) has already been generated, corresponding to an enhancement of 50% over that predicted. Thus, the HDP extends the range of high fluidity to a significant degree. Moreover, the halfwidths of the fluid components at maximum fluidity for the coal (150-212 μ)/pitch mixtures (Table 3) indicate that the HDP also mobilises the fluid phase to a much greater extent than the CTP, further demonstrating the ability of this pitch to solubilise the coal.

CONCLUSIONS

This study has confirmed the ability of high temperature ^1H NMR to quantify the enhancement of coal fluidity by pitch additives. Particle size appears to be a dominant factor with slow heating, in that positive interactions were not detected with the $<45 \mu$ coal fraction. The synergistic effect observed with the HDP was considerably larger than that with the normal CTP, particularly at temperatures below maximum fluidity with the proportion of fluid material being 50% more than that predicted at 400°C.

ACKNOWLEDGEMENTS

The authors thank the European Coal & Steel Community (Contract No. 7220-EC/870) and the Basque Government (studentship for M.M. Maroto-Valer) for financial support. We are also grateful to British Steel and CRE for supplying the coal and HDP, respectively.

LITERATURE CITED

- 1 K. Miyazawa, T. Yokono and Y. Sanada, Carbon, 1979, 17, 223.
- 2 L.J. Lynch and D.S. Webster, American Chemical Society Symposium Series, 1983, 230, 353.

- 3 L.J. Lynch, D.S. Webster, R. Sakurovs, W.A. Barton and T.P. Maher, Fuel, 1988, **67**, 579.
- 4 M.M. Maroto-Valer, J.M. Andrésen and C.E. Snape, Prep. Am. Chem. Soc., Division of Fuel Chemistry, 1996, **41**, 1147.
- 5 M.M. Maroto-Valer, J.M. Andrésen and C.E. Snape, Energy & Fuels, in press.
- 6 R.C. Neavel, in Coal Science, vol 1, M.L. Gorbaty, J.W. Larsen, and I. Wender, 1982, Academic Press.
- 7 T. Yokono, T. Obara, Y. Sanada, 1984, Carbon, **22**, 2, 169.
- 8 A.H. Clemens, and T.W. Matheson, 1992, Fuel, **71**, 193, and 1995, Fuel, **74**, 57.
- 9 F. Fortin and J.N. Rouzaud, 1993, Fuel, **72**, 245, and 1994, Fuel, **73**, 795.
- 10 H. Marsh and R.C. Neavel, 1980, Fuel, **59**, 511.

Table 1 Atomic H/C ratios, aromaticities and softening points for the coal and pitches investigated.

	Atomic H/C	Aromaticity ^a	Softening point / °C
Coal	0.61	0.89	470 ^b
Coal tar pitch (CTP)	0.49	0.99	190
Hydrogen donor pitch (HDP)	0.78	0.75	175

^a The aromaticity fraction was determined by using the quantitative ¹³C NMR SPE methodology.

^b The softening temperature for the coal refers to the maximum fluidity temperature as determined by the standard Gieseler plastometer.

Table 2 Proportion of the fluid component at maximum fluidity temperature for the coal, pitches and coal/pitch mixtures (4:1 w/w).

	Observed mobile H / %		Weight average mobile H / %		Enhancement	
	400°C	460°C	400°C	460°C	400°C	460°C
Coal	12	26	10 / 10 ^a	22 / 23 ^a		
CTP	100	100	16	15		
HDP	100	100	17	11		
Coal (<45 μ) / CTP	27	38	26	37	NONE	NONE
Coal (150-212 μ) / CTP	31	45	26	37	15 %	20 %
Coal (150-212 μ) / HDP	41	44	27	34	50 %	30 %

^a The first and second values are for the coal in the coal/CTP and coal/HDP mixtures, respectively.

Table 3 Peak widths at half height, $\Delta H_{1/2}$, of the fluid component at maximum fluidity for the coal, pitches and coal/pitch mixtures (4:1 w/w).

	Observed $\Delta H_{1/2}$ / Hz	Calculated $\Delta H_{1/2}$ for mixtures / Hz	Enhancement
Coal	5260		
CTP	1000 ^a		
HDP	1000 ^a		
Coal (150-212 μ) / CTP	3000	4700	36%
Coal (150-212 μ) / HDP	1920	4800	60%

^a Peak width is for aromatic and aliphatic hydrogen bands combined, each band having a $\Delta H_{1/2}$ of only 300-400 Hz.

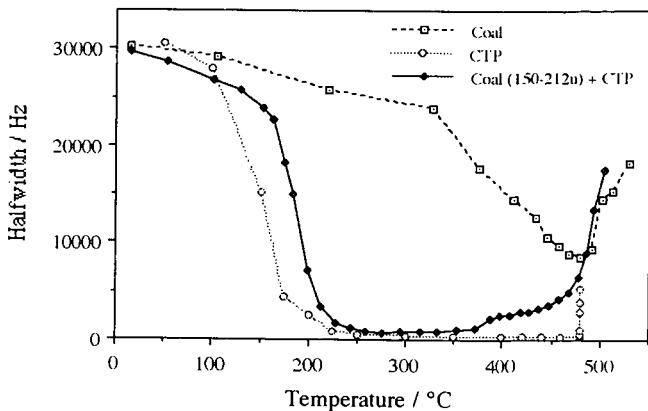


Figure 1 Evolution of the peak halfwidth for the coal (150-212 μ), CTP and the coal / CTP mixture.

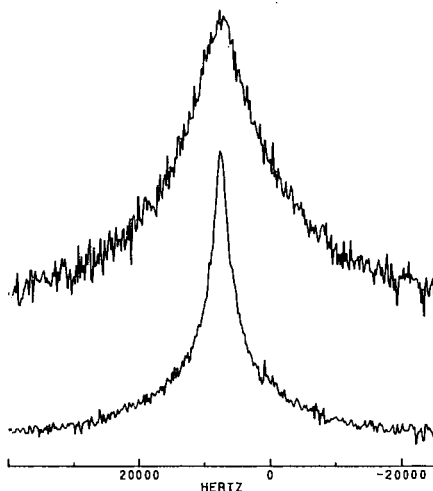


Figure 2 ^1H NMR spectra at maximum fluidity (460°C) for the coal / coal tar pitch mixtures (4:1), coal particle size <45 μ (top) and 150-212 μ (bottom).

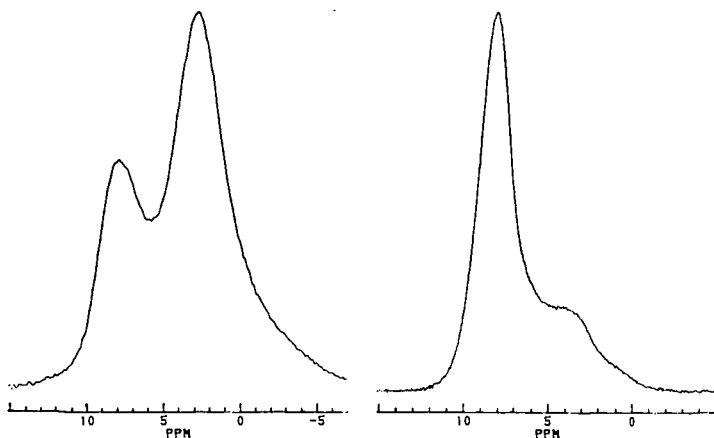


Figure 3 ^1H NMR spectra at 300°C prior to significant weight loss for the CTP (right), and HDP (left).

AN ^{19}F AND ^{13}C NMR STUDY OF CF_x PREPARED BY VARIABLE TEMPERATURE FLUORINATION OF CHARCOAL WITH ELEMENTAL FLUORINE.

D. K. Murray, E. W. Hagaman and G. D. Del Cul,
Chemical & Analytical Sciences Division, Oak Ridge National Laboratory,
P. O. Box 2008, Oak Ridge, TN 37831-6201.

Key Words: charcoal, fluorine, carbon monofluoride, nmr

Abstract

The preparation of CF_x by elemental fluorination of charcoal is studied using solid state ^{13}C and ^{19}F NMR spectroscopy. ^{19}F - ^{13}C CP/MAS NMR experiments are used to determine the extent of fluorination vs. reaction temperature. Four types of carbon species are observed over the temperature range -80°C to 350°C , assigned to graphitic carbon (C), CF, CF_2 and CF_3 . These species are assigned and quantified using dipolar dephasing and variable contact time experiments. NMR results are presented along with gravimetric and ESCA results to provide new insights into charcoal structure and fluorination.

Introduction

Probing heterogeneous carbonaceous solids with selective reagents is a useful approach to study their chemical and physical properties.¹ Elemental fluorine is a particularly effective probe, adding to unsaturated carbon, and displacing O and H from organic materials.^{2,3} Fluorine is easily detected by ^{19}F NMR spectroscopy.⁴ It also provides a useful polarization source for investigating carbon structure by ^{19}F - ^{13}C CP NMR spectroscopy.⁵

Here we describe changes in the structure of charcoal as it is converted to CF_x by reaction with elemental fluorine. These studies demonstrate the utility of fluorine as a probe and provide insight into the fluorination process in more complex solids. Both radical and ionic mechanisms are reported upon elemental fluorination of model organic compounds.^{2,3} CF_x made from graphite is reported as a solid lubricant and as an excellent cathode material for Li batteries.⁶ Gravimetric, NMR and ESCA analyses are used to investigate charcoal structure and the fluorination process.

Experimental

Preparation of CF_x . Coconut-based activated charcoal (6x16 mesh size) was provided by Calgon Carbon Corporation. The microstructure is that of graphite, consisting of stacked planar platelets of fused aromatic carbon.⁷ The C-C bond distance is 0.141 nm and the interplatelet distance is 0.335 nm. According to the manufacturer's data a large portion of the micropore volume consists of pores in the range 1.5 to 2.0 nm and a system of macropores larger than 100 nm. A suite of ten CF_x samples were prepared over the temperature range -80 to 350°C using the following method. Ten to fifteen gram batches were loaded into a passivated-nickel U-tube reactor (1/2" OD) having monel bellows vacuum valves at each end. The activated charcoal was pre-conditioned by heating to 200 - 250°C under helium flow. The reactor was then fully immersed in a thermostatic bath to maintain the desired fluorination temperature. To minimize formation of gaseous products and to better control the highly exothermic reaction, dilute fluorine gas was used. A 5 % by volume F_2/He

gas mixture was prepared in three liter batches in a passivated-nickel tank. The preparative manifold has a titanium getter to remove water, oxygen or nitrogen impurities. Dilute fluorine was introduced into the reactor at a very low flow rate. A temperature difference of $<3^{\circ}\text{C}$ was maintained between the charcoal and reactor wall by controlling gas flow. Flow was maintained for several days until these temperatures equalized. Finally, pure fluorine was slowly flowed for several hours to ensure complete reaction. The reaction vessel was then purged with helium and transferred to a dry-helium glove box for disassembly and storage of the fluorinated product.

NMR Spectroscopy. NMR spectroscopy was performed on 50-100 mg samples in a Bruker MSL-100 (2.35 T) spectrometer. The samples were spun at 5 kHz in a doubly tuned single coil magic angle spinning probe. Single pulse ^{19}F spectra were obtained at 94.200 MHz and MAS = 12 kHz. ^{13}C spectra were obtained at 25.184 MHz by ^{19}F - ^{13}C cross polarization (CP) with ^{19}F decoupling during acquisition. Dipolar dephasing (DD) delays in the range of 0-100 μs were used to aid in assignment of fluorinated species, while 0-2 ms delays were used for graphitic carbons. To obtain quantitative CP data, variable contact time (VCT) experiments were performed.⁸ Signal intensity (I) is acquired vs. contact time (τ) over a wide range of contact times (25 μs to 100 ms), and fit to equation (1) to

$$I = \frac{I_0}{T_{\text{CF}}} * \frac{e^{-(\tau/T_{1\rho})} - e^{-(\tau/T_{\text{CF}})}}{(1/T_{\text{CF}}) - (1/T_{1\rho})} \quad (1)$$

obtain I_0 , T_{CF} and $T_{1\rho}$. I_0 represents the $T_{1\rho}$ relaxation-independent intensity of the resonance, while T_{CF} and $T_{1\rho}$ are the time constants associated with the buildup and decay of intensity. Fitting is accomplished by least squares minimization. Composition of each carbon type is reported as a percentage of total observed carbon. The precision of the percentage composition reported are on the order of $\pm 5\%$.

ESCA Analysis. ESCA data were obtained using a PHI (Perkin Elmer) 5000 series XPS spectrometer equipped with a dual anode (Al: $h\nu = 1486.6$ eV and Mg: $h\nu = 1253$ eV). The Al anode was utilized at a power of 400 W (15 kV). The instrument was operated in the fixed analyzer transmission (FAT) mode with a pass energy of 17.9 eV for high resolution scans. Pressure was $< 1.0 \times 10^{-7}$ torr.

Results and Discussion

NMR Analysis. ^{13}C NMR spectra of charcoal fluorinated at different temperatures are presented in Figure 1. Four distinct resonances are observed, assigned to graphitic C, CF, CF_2 and CF_3 species. In the -80°C spectrum, the downfield feature found at 129 ppm is initially assigned to graphitic carbon (C). This chemical shift is consistent with model fused aromatic carbons (121-133 ppm). Its relatively slow signal accrual ($T_{\text{CF}} > 100 \mu\text{s}$) and decay ($T_{\text{DD}} \approx 500 \mu\text{s}$) indicate that these carbons are at least 0.3 nm (2-3 bonds) from fluorine nuclei. The resonance observed at 86 ppm is assigned to CF. Fast signal accrual and dephasing (T_{CF} and $T_{\text{DD}} \approx 50 \mu\text{s}$) confirm that these carbons are strongly coupled (directly bonded) to fluorine. A third resonance (CF_2) becomes apparent at 112 ppm in charcoal fluorinated at higher temperatures. A fourth resonance (136 ppm) is observed only in the charcoal fluorinated at 250°C and is assigned

to CF_3 . A ^{19}F spectrum of the charcoal fluorinated at 250°C (Figure 2) supports these ^{13}C CF_x assignments. The broad feature in the region -60 to -220 ppm contains unresolved isotropic peaks which are flanked by spinning sidebands outside this range. The isotropic peaks indicate the presence of CF (-170 ppm), CF_2 (-128 ppm) and CF_3 (-85 ppm).

The relative percentages of each carbon type in the ^{13}C spectra are listed in Table 1. The F/C atomic ratio indicates the extent of fluorine incorporation. Fluorination is evident even at -80°C , but is not complete until 350°C . CF, CF_2 , and CF_3 percentages determined by ^{13}C NMR and ^{19}F NMR are comparable (within 5 %), supporting structural assignments and justifying the fitting procedure used to quantify species in CP spectra. CF_3 is lost upon fluorination at 350°C , indicating platelet degradation above 250°C . Carbons at the platelet edge produce CF_2 rather than CF upon fluorination. The CF_2/CF ratio is a measure of edge to bulk carbon and is thus useful in determining platelet size. A simple hexagon-shaped model platelet with 5 aromatic rings per side (assuming a C-C distance of 0.14 nm) has an edge to bulk carbon ratio of 0.20 and a 2.2 nm diameter. The CF_2/CF ratio obtained by NMR studies of the 250°C material is 0.19 ± 0.09 . A platelet diameter of 2 ± 1 nm is obtained if a hexagonal shape is assumed. Small angle neutron scattering experiments gave a platelet size of roughly 2 nm.

Two graphitic carbon species are assigned to the 129 ppm resonance based on VCT results. This bimodal character is revealed in a plot of intensity vs. contact time for the charcoals fluorinated at -80°C , 23°C and 65°C (Figure 3). Bulk graphitic carbon (C_b), with $T_{\text{CF}} = 5$ ms and $T_{1\rho} = 30$ ms, dominates the -80°C plot. It consists of carbon further than 0.32 nm from fluorine nuclei. At higher preparation temperatures, an increasing amount of graphitic carbon displays $T_{\text{CF}} = 0.2$ -1 ms and $T_{1\rho} = 1$ -5 ms. This species becomes dominant at 65°C as indicated by the change in lineshape and is defined as interfacial graphitic carbon (C_i). C_i is adjacent to CF with a $\text{C}_i\text{-C-F}$ distance estimated at 0.24 nm. Fluorine must be widely dispersed in small CF clusters at -80°C to account for the percentage C_i observed. The C_i/CF ratio is an indicator of CF cluster size. It shows the growth of CF regions in the graphitic plates with increasing temperatures. Initially, 2-3 F/cluster are indicated, increasing to about 8 F/cluster at 23°C , and >40 F/cluster at 180°C .

ESCA Analysis. Results of ESCA analyses are given in Table 2. The generation of fluorinated carbon species follow trends observed in the NMR data, although relative percentages are lower by 10-20 %. CF_2 is detected even at -80°C , but is never more than 4 %. Two species of graphitic carbon are also observed. Bulk graphitic carbon (C_b), analogous to C_b , is initially the dominant species but is entirely consumed at 250°C . $\text{C}(\text{CF})$ is analogous to C_i . Its concentration (35-40 %) is remarkably constant over the sample temperature range. The ratio $\text{C}(\text{CF})/\text{CF}$ follows trends observed for C_i/CF . CF_2/CF is nearly constant at 0.11 throughout the temperature range. Assuming a hexagon-shaped platelet, the platelet diameter that produces this ratio is about 4 nm.

Comparison of Analyses. Gravimetric analysis is the most direct measure of fluorine incorporation into charcoal. The F/C ratios determined by attributing net weight gain to fluorine (See Tables 1 & 2) are very similar to results from NMR and ESCA. Gravimetry does not take into account weight loss from the displacement of edge oxygen and hydrogen by fluorine. This atomic replacement can lower the F/C ratio measured

gravimetrically by as much as 20 %. Differences in F/C ratios are generally within experimental error except at 250°C where the F/C ratio from the ESCA analysis is significantly lower than the NMR result. The F/C ratio is very sensitive to CF₂ and CF₃ concentrations which are consistently lower in the ESCA results. This lower ratio is most pronounced in studies of the sample fluorinated at 250°C where the CF₂ and CF₃ concentrations is greatest. An F/C ratio of 1.1-1.25 is calculated for fluorinated charcoal with platelets roughly 2-3 nm, a value more consistent with NMR results.

Structural Features and Fluorination Mechanism. Charcoal consists of planar fused aromatic carbon platelets having an average diameter on the order of 2-4 nm. The platelet interlayer distance (0.33 nm) is large enough for F₂ to diffuse between platelets. F₂ is not limited to surface reaction in micropore void spaces. The platelets separate to 0.57 nm upon complete fluorination.⁶ Paramagnetic sites were detected based on NMR observations. Carbonaceous materials generally contain free electron spin density as a result of their aromatic character and/or the presence of trace amounts of metals. A ¹H-¹³C CP experiment was attempted on the original charcoal used in this study to search for edge functionality. Edge sites in this material are assumed to consist of hydrogen and oxygen containing functional groups. Edge resonances were not detected, but the experiments did confirm the presence of free spin density. The probe tuning characteristics changed significantly with this material, an effect sometimes observed for conductive or paramagnetic materials. A ¹H-¹³C CP spectrum could not be obtained. The spinning sample also slowed significantly (4953 Hz to 4860 Hz) when the probe was raised into the magnetic field. This effect was reversible. ¹⁹F T_{1ρ} time constants were on the order of 50 ms for the charcoal fluorinated at -80°C, a value common for diamagnetic materials. The free spin density present in the charcoal had evidently been quenched by fluorine reaction at -80°C. At higher CF_x preparation temperatures, ¹⁹F T_{1ρ} grows significantly shorter (to 1 ms for the 250°C material) and returns to 50 ms for the 350°C material. Iron is also present in this charcoal (1 %) as a possible paramagnetic source. Demineralization did not remove the paramagnetic sites, so we conclude that iron is not the source of free spin density in the charcoal or its fluorination products. The tuning, spinning, and T_{1ρ} behavior strongly suggest the presence of paramagnetic organic radicals.

Summary

Carbon monofluoride is prepared by elemental fluorination of charcoal. Two graphitic and three fluorinated carbon species are quantified in NMR studies and confirmed by ESCA analysis. Fluorination occurs to a limited extent at -80°C by a radical mechanism. Small widely dispersed CF regions grow larger and more numerous when charcoal is fluorinated at higher temperatures. CF_{1.1-1.2} is produced above 250°C. The charcoal platelet has an average diameter on the order of 2-4 nm and is stable to at least 250°C.

Acknowledgments

This research was sponsored by the Division of Chemical Sciences, Office of Basic Energy Sciences, U. S. Department of Energy, under Contract No. DE-AC05-84OR21400 with Lockheed Martin Energy Research. The ESCA analysis was done by Joeseph Fiedor.

References

- (1) Hagaman, E. W.; Lee, S. K. *Energy & Fuels*, **1995**, *9*(5), 727-734.
- (2) Purrington, S. T.; Kagen, B. S.; Patrick, T. B. *Chem. Rev.* **1986**, *86*, 997-1018.
- (3) Wilkinson, J. A. *Chem. Rev.* **1992**, *92*, 505-519.
- (4) Harris, R. K.; Jackson, P. *Chem. Rev.* **1991**, *91*, 1427-1440.
- (5) Hagaman, E. W.; Burns, J. H. *Fuel*, **1993**, *72*(8), 1239-1243.
- (6) Kamarchik, P.; Margrave, J. L. *Acc. Chem. Res.* **1978**, *11*, 296-300.
- (7) Greenwood, N. N. And Earnshaw, *Chemistry of the Elements*, Pergamon Press, New York, 1984; p304.
- (8) Hagaman, E. W.; Chambers, R. R.; Woody, M. C. *Anal. Chem.*, **1986**, *58*(2), 387-394.

Table 1. Composition and ratios of carbon components in fluorinated charcoal as determined by ^{19}F - ^{13}C CP/MAS NMR

Carbon Component	Fluorination Temperature							
	-80	0	23	65	120	180	250	350
C _i	27%	38%	33%	36%	29%	21%	0%	0%
C _b	57%	37%	33%	21%	17%	5%	0%	0%
C (=C _i + C _b)	84%	75%	66%	57%	46%	26%	0%	0%
CF	16%	25%	34%	39%	48%	67%	81%	78%
CF ₂				4%	6%	8%	15%	22%
CF ₃							4%	0%
C _i /CF	1.64	1.50	0.96	0.91	0.61	0.31	0	0
CF ₂ /CF				0.10	0.12	0.11	0.19	0.28
F/C by NMR	0.16	0.25	0.34	0.47	0.59	0.82	1.19	1.22
F/C by Wt.	0.27	0.32	0.38	0.45	0.50	0.77	0.91	

Table 2. Composition and ratios of carbon components in fluorinated charcoal as determined by ESCA Analysis

Carbon Component	Fluorination Temperature						
	-80	0	23	65	120	180	250
C(CF)	38%	39%	34%	39%	43%	38%	35%
CC	43%	39%	36%	13%	9%	10%	0%
Total C	81%	78%	70%	52%	52%	48%	35%
CF	19%	18%	22%	32%	44%	47%	60%
CF ₂	2%	2%	2%	4%	4%	4%	4%
CF ₃	0%	0%	0%	0%	1%	1%	1%
C(CF)/CF	2.00	2.17	1.55	1.22	0.98	0.81	0.58
CF ₂ /CF	0.11	0.11	0.09	0.13	0.09	0.09	0.07
F/C by ESCA	0.24	0.26	0.30	0.42	0.53	0.56	0.77
F/C by Wt.	0.27	0.32	0.38	0.45	0.50	0.77	0.91

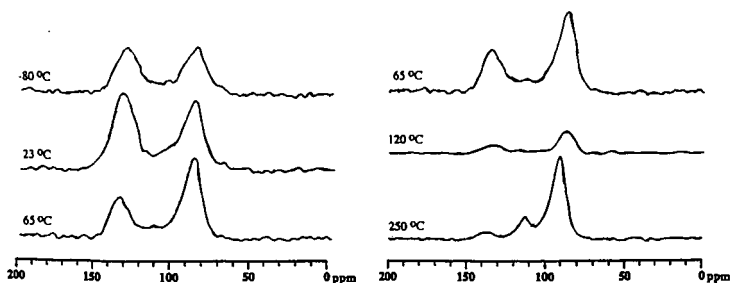


Figure 1. ^{19}F - ^{13}C CP/MAS NMR spectra of charcoal fluorinated at various temperatures. Typically 20k scans were signal averaged using a 2.5 ms contact time and a 2 s recycle delay.

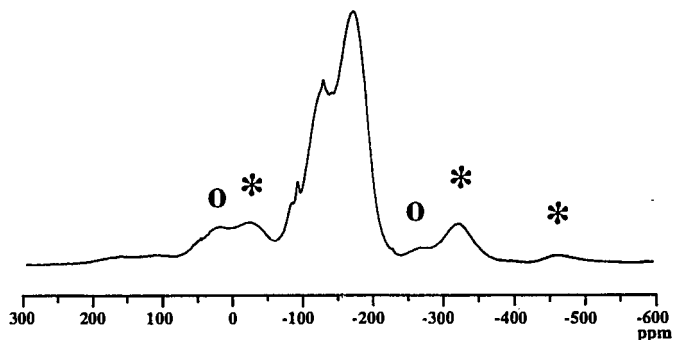


Figure 2. ^{19}F MAS NMR spectrum of charcoal fluorinated at 250°C. Spin rate is 12 kHz (127 ppm). * indicates spinning sidebands of the CF peak (-170 ppm). O indicates sidebands of the CF_2 peak (-128 ppm).

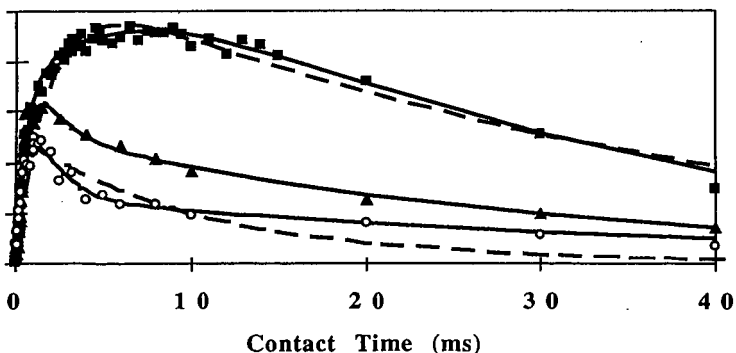


Figure 3. Graphitic carbon intensities from ^{19}F - ^{13}C CP/MAS NMR studies plotted vs. contact time for several fluorinated charcoal samples: (■) -80°C, (▲) 23°C, (○) 65°C. Two component fits are displayed as solid lines. Selected one component fits are displayed as dashed lines.

TYPE OF WATER ASSOCIATED WITH COAL

K. Norinaga, H. Kumagai, J.-i. Hayashi and T. Chiba
Center for Advanced Research of Energy Technology (CARET), Hokkaido University
N13, W8, Kita-ku, Sapporo 060, Japan

M. Sasaki
Hokkaido National Industrial Research Institute (H-NIRI)
2-17, Tsukisamu-Higashi, Toyohira-ku, Sapporo 062, Japan

Key words: crystallization, proton mobility, non-freezing water

INTRODUCTION

The authors¹ have evaluated changes in physical structure of a lignite induced by drying by means of swelling in water and proton NMR relaxation measurements. They have found that the water removal reduces considerably and irreversibly the swelling ratio and the relaxation time of protons in the macromolecular phase meaning that it makes the macromolecular network more rigid, as has been observed for solvent loading and removal processes.² It has been also found that the dryings carried out at different temperatures of 303K and 380 K give rise to difference in the above properties even at the same extents of water removal. This result reveals that physical structure of macromolecules in the lignite is not determined only by the water content but also other factors such as properties of water in its matrix. The systematic analysis of water sorbed on coal should be therefore established for understanding its roles in physical structure of coal.

Differential scanning calorimetry (DSC) has been applied to evaluate the crystallization property of water sorbed on polymers carrying polar functional groups. Nakamura et al.³ investigated the property of water in polyhydroxystyrene employing this technique. When the water content reached a certain level, they observed two exothermic peaks due to the crystallization of water centering at 273 K and 235 K respectively arisen from bulk (or free) water and freezable bound water. They also found another type of water, called as non-freezing water, no crystallization of which was observed. An advantage of this technique is that water can be quantitatively classified by assuming its crystallization heat and it can be also applied for characterization of water sorbed on coal.⁴ The freezing-point temperature depends on the size of space where water is condensed and it is not observed when the size is smaller than a critical value. The distribution of water elucidated by DSC may give informations on the size distribution of assemblies of water molecules. The non-freezing water has been recognized to be directly hydrogen-bonded to polymer functionalities and would be the most important type of water relevant to properties of the macromolecular network of coal. However, the non-freezing water is not directly observed by DSC.

The crystallization of free and bound waters is also expected to be observed in proton NMR relaxation measurements as the conversion of 'mobile proton' giving Lorentzian magnetization decays into 'immobile proton' doing Gaussian ones. Furthermore, the non-freezing water would be observed and its abundance and mobility would be also evaluated. Recently the NMR measurements have been adopted for determination of water content in coal^{5,7}. Lynch et al.⁷ observed a Lorentzian-Gaussian transition in a brown coal around 273 K and thereby estimated the content of free water contained in the coal.

The present study aims first to quantify the amounts of free, bound and non-freezing waters sorbed in coals ranging from lignite to bituminous ranks on the basis the crystallization characteristics measured by DSC. The second objective is to observe the non-freezing water and to evaluate changes in its mobility in the course of cooling as well as the other types of water and coal hydrogen.

EXPERIMENTAL

Coal samples

Table 1 presents the moisture and ash contents as well as the elemental compositions of coal samples so far used. Experiments were conducted with four Argonne PCSP coals and four brown coals supplied from the Nippon Brown Coal Liquefaction Co. Ltd.. The particle sizes were smaller than 150 μm for all samples. The samples other than the PCSP ones were stored in a gas tight vessel which was filled with atmospheric nitrogen saturated by water vapor at 293 K for a week prior to analyses. The moisture contents in the brown coals were determined from fractional mass release from them by a drying under nitrogen flow at 380 K for 2 h, while for the PCSP coals the literature values were used⁸. The PCSP samples were subjected to analyses immediately after opening the ampules.

Drying

Among the coal samples BZ coal was partially or completely dried at 303 K under dried or humidified nitrogen atmosphere. The extent of water removal was controlled by varying the relative humidity in a drying vessel from zero to 84% using conc. H_2SO_4 and aqueous solutions

saturated by selected salts.¹

DSC

DSC measurements were made employing a calorimeter (DSC 200, Seiko Co. Ltd.) equipped with a liquid nitrogen cooling accessory. The coal sample was cooled from 293 K to 123 K at a rate of 2 K/min and then heated up to 293 K at 2 K/min under atmospheric nitrogen gas flow of 80 ml/min.

Solid-state proton NMR

A proton magnetic resonance was adopted to elucidate spin-spin relaxation characteristics for the coal samples. The relaxation measurements were carried out on a JEOL Mu-25 spectrometer operated at 25 MHz. A $90^\circ_x - \tau - 90^\circ_y$ solid echo sequence was used to obtain the entire free induction decays (FID). The FID was measured at temperature intervals of 2-5 K in the course of cooling from 293 K to 203 K. At each temperature the signal was recorded after a time period of 15 min since the temperature was reached for confirming homogeneous temperature distribution in the specimen. The FID curves were analyzed by a sequential linear-least-squares fitting method which has been commonly employed to deconvolute the total FID into two Gaussian and a Lorentzian functions with different specific relaxation times, i.e., T_2 . The following equations were used to fit the FID signal.

$$I(t) = I_1(t) + I_2(t) \quad (1)$$

$$I_1(t) = I_1(0) \exp[-t/T_{2L}] \quad (2)$$

$$I_2(t) = I_2(0) \exp[-t^2/2T_{2G1}] + I_2(0) \exp[-t^2/2T_{2G2}] \quad (3)$$

where $I(t)$ and $I_i(t)$ are the intensity observed and that attributed to the component i at time t . In Figure 1 natural logarithm of the FID intensity of YL, BZ and WY coals at 293 K are shown versus the relaxation time. The long-decaying component observed after 30 μ s for each coal is evidently a Lorentzian function. After fitting the Lorentzian component by Eq. (2) to determine $I_1(0)$ and T_{2L} and subtracting it from the signal, the rest was further fitted by Eq. (3) to obtain $I_2(0)$, $I_{G1}(0)$, T_{2G1} and T_{2G2} . This procedure was successful for all curves observed. FID curves of dried BZ coal shown in Figure 2 were also analyzed by the same procedure.

RESULTS AND DISCUSSION

DSC results

Figure 3 exhibits the DSC curves for four different coals together with that for pure water. The positive peaks appearing on the curves mean exothermic processes. Though not shown here such peaks were never observed for the coals dried at 380 K. Negligible weight change was confirmed for all samples during the measurements. These peaks are thus arisen from a transition of water sorbed on the coal into ice, i.e., crystallization. For YL coal two peaks centering at 226 K and 258 K are evident. The larger one appears in the same temperature range as that for pure water and is ascribed to the crystallization of water having no specific interactions with the coal. The water can be defined as 'free water' or 'bulk one'. On the other hand, the smaller peak is attributed to 'bound water' being frozen at temperatures lower than that for the free water. Water condensed in capillaries with diameters of less than several microns has been known to be frozen around 220-230 K. Hence the bound water defined here can be also regarded as water condensed in macropores. The curves for the other coals indicate the existence of the bound water, while no free water. The peaks around 226 K are common among the curves for all coals, and in addition, for BZ and SB coals they overlap with the peaks observed at higher temperatures which are also assigned to the bound water.

The amounts of the free and bound waters can be estimated by assuming their crystallization heat. The heat for the free water was calculated as 333 J/g by analyzing the DSC curve for pure water. The value is nearly equivalent to that for the transition of bulk water into ice having Type-I polymorphic form, an only one that can be formed under the present conditions, i.e., 334 J/g.² This literature value was thus employed for estimating the free water content. This was also used to estimate that of the bound water content assuming its crystallization into Type-I ice.

Calculated fractions of the free and bound waters are summarized in Table 2. It should be noted that these types of waters account only for a portion of total for the all coals tested. This means the existence of another type of water that is not frozen at any temperatures examined. This type of water is here defined as 'non-freezing one' according to Nakamura et al.³ as well as the other types of waters.

In Figure 4(a) the amount of the non-freezing water per unit mass of coal on a dry basis is plotted against the sum of oxygen and nitrogen molar contents in them, which is a measure for the amount of polar and hydrophilic functional groups. The non-freezing water seem to be more abundant in the coal carrying more oxygen and nitrogen. This tendency can be reasonably explained by that water molecules as the non-freezing water are dispersed in the coal matrix at molecular levels being hydrogen-bonded to polar functional groups, a necessary condition of which is that the water is not frozen at any temperatures scanned in the DSC measurements. It is also noted in Figure 4(b) that the coal having more oxygen and nitrogen functionalities binds the larger number of water molecules as the non-freezing water per that of oxygen and nitrogen atoms. There is a wide variation in the number ranging from 0.3 for IL coal to 1.5-1.8 for the brown coals. Although the values indicated

in the figure are averaged ones, they are small enough to support that water molecules directly interact with oxygen and nitrogen-containing groups.

The above DSC results reveal that the coals contain freezable water which is classified into the free water and bound one based on their crystallization temperature. They also indicate the existence of the non-freezing water, the crystallization of which is not observed. As suggested from the result shown in Figure 4(b), when water molecules are dispersed on a molecular scale, the crystallization as a phase transition should be not observed even if their mobility as liquid is lost by the cooling. The NMR relaxation measurements were therefore made to examine the mobility of molecules as the non-freezing water and its temperature dependence as well as to observe the crystallization of the free and bound waters as the conversion of the Lorentzian component into Gaussian one.

NMR results

In Figure 5 are shown relationships between the amount of proton assigned to the Lorentzian component at 293 K and that as water sorbed on the coals. The former, given as $I_L(0)/I(0)$ multiplied by the total amount of hydrogen in water-containing coal, is larger than the latter without an exception, suggesting that a portion of coal hydrogen has mobilities characteristic to those in a liquid environment. Under an assumption that all protons as water are attributed to the Lorentzian component at 293 K, fractions of coal hydrogen having such mobility to the total are 9-38 % as indicated in the figure. The effect of water content on the amount of mobile coal hydrogen is shown for BZ coal in Figure 6. It is seen that the amount increases with an increase in the water content. This suggests that both non-freezing and bound waters mobilize coal hydrogen. The authors previously reported that water contained in the coal plays a role of solvent as a swelling agent based on volumetric shrinkage due to its removal.¹ Yang et al.,¹⁰ who studied the proton relaxation characteristics of dried and pyridine-swollen high-volatile bituminous coals by means of a spin-echo NMR technique, found that the fraction of the Lorentzian component in the coals increases from zero to 70-80% due to the swelling. The results shown in Figs. 5 and 6 are therefore quite reasonably accepted.

Figure 7 presents the amount of hydrogen giving the Lorentzian decay, H_L , normalized by that as water contained in the coal as a function of temperature ranging from 213 K to 293 K. For MW coal, the reduction of H_L is first observed at 273 K. There seems to be two different temperature dependences of the H_L reduction in the ranges of 263-273 K and 213-263K. Similar profiles were obtained for LY and YL coals. Considering that such sharp decrease in H_L at 263-273 K is not observed for the other coals, it can be mainly attributed to the crystallization of free water which is also observed in the DSC measurements. The liquid-solid transition should be observed as the conversion of the Lorentzian component to the Gaussian one. Moreover, the decrease in H_L in the range of 213-263 K should involve that due to the phase transition of the bound water, while it may also involve other Lorentzian-to-Gaussian transitions for hydrogen as the non-freezing water and/or coal hydrogen. The total decrement of H_L is thus expected to be at least equivalent to the amount of hydrogen as the free and bound waters, or larger if other transitions are also observed. The extents of H_L reduction for MW and YL coals are respectively 52 and 57 % and are in good agreement with the total fractions of the free and bound waters in these coals, i.e., 52 and 58 %. Hence the decrease in H_L can be referred to the crystallization of these types of waters, and hydrogen of the non-freezing water and coal hydrogen being mobile at 293 K both give the Lorentzian decay even at 213 K.

Table 3 summarizes the decrement of H_L in the range of 213-293 K for six different coals. For the coals other than the brown ones, the decrement is evidently larger than the amount of hydrogen as the bound water, while H_L at 213 K also appears to be larger than that as the non-freezing water. The result means that the reduction of H_L involves the transition of a portion of coal hydrogen being mobile at 293 K, that of hydrogen as the non-freezing water or both of them. Although their contributions to the reduction are not clear at present, it can be said that at least most of the non-freezing water is in a liquid environment even at 213 K by postulating higher mobility of water molecules than that of coal macromolecules based on much smaller mass of the former than the latter.

Figure 8 shows T_{2L} of the four different coals as a function of temperature. Although there is a wide variation in the temperature dependence of T_{2L} with the coals, the relaxation time seems to reach a value of 60 μ s at 213 K for the all coals. Such a coal-independent relaxation time implies that the Lorentzian components observed for the different coals at the temperature, which consist mainly of the non-freezing water, have similar mobilities.

CONCLUSIONS

The eight coals were subjected to the DSC and proton solid-state NMR relaxation analyses. Water sorbed on/in their matrices can be classified into three types on the basis of the crystallization characteristics, namely free water, bound water and non-freezing water. The abundances of the free and bound waters can be quantified using the crystallization heat of water, while the non-freezing water by difference. The crystallization of the freezable waters is also observed in the NMR as the conversion of the Lorentzian component into Gaussian one at 213-273 K where the conversion for coal hydrogen is also observed for the coals other than the brown ones. All or at least most of the non-freezing water is in a liquid environment to give Lorentzian decays even at 213 K.

REFERENCES

1. K. Norinaga, H. Kumagai, Y. Sanada, M. Sasaki and T. Kotanigawa, *Coal Science and Technology* 1995, 24, 35.
2. R. P. Warzinski and G. D. Holder, *Fuel* 1992, 71, 993.
3. K. Nakamura, T. Hatakeyama and H. Hatakeyama, *Polymer* 1983, 24, 871
4. S. C. Mraw, D. F. Orourke, *Science* 1979, 205, 901.
5. B. C. Gerstein, C. Chow, R. G. Pembleton, R. C. Wilson, *J. Phys. Chem.* 1977, 81, 565
6. X. Yang, A. R. Garcia, J. W. Larsen, B.G. Silbernagel, *Energy Fuels* 1992, 6, 651.
7. L.J. Lynch, D. S. Webster, *Fuel* 1979, 58, 429.
8. K. S. Vorres, 1993. *USERS HANDBOOK FOR THE ARGONNE PREMIUM COAL SAMPLE PROGRAM*. Argonne National Laboratory, Argonne, Illinois, p. 20.
9. D. Eisenberg and W. Kauzmann, 'The Structure and Properties of Water', Oxford University Press, London, 1969
10. X. Yang, J. W. Larsen, B.G. Silbernagel, *Energy Fuels* 1993, 7, 439.

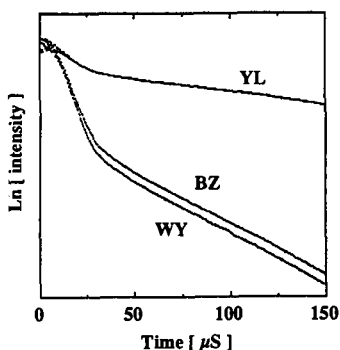


Figure 1. Natural logarithm of FID intensity versus relaxation time at 293 K for LY, BZ and WY coals.

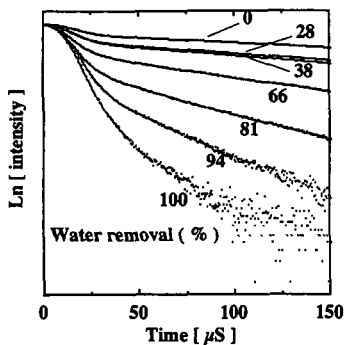


Figure 2. Natural logarithm of FID intensity versus relaxation time at 293 K for BZ coal with different water removal.

Table 1. Properties of coals so far used.

Coal	(Symbol)	Moisture [wt. % -sample]	Ash [wt. % db-coal]	C H N S O(diff.)				
				[wt. % daf-coal]				
Blind Canyon	(BL)	4.6	4.7	80.7	5.8	1.6	0.4	11.6
Illinois #6	(IL)	8.0	15.5	77.7	5.0	1.4	2.4	13.5
Wyodak	(WY)	28.1	8.8	75.0	5.4	1.1	0.5	18.0
Beulah Zap	(BZ)	32.2	9.7	72.9	4.8	1.2	0.7	20.3
South Banko	(SB)	31.5	3.2	70.4	5.8	1.2	0.4	22.2
Yallourn	(YL)	57.5	1.4	62.6	4.6	0.7	0.3	31.9
Loy Yang	(LY)	56.7	1.1	62.7	4.7	0.7	0.3	31.6
Morwell	(MW)	55.5	2.6	64.2	4.7	0.7	0.3	30.1

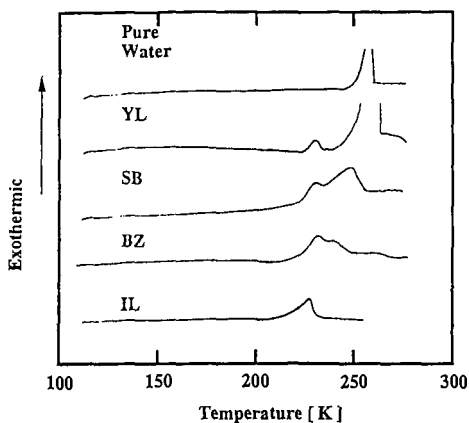


Figure 3. DSC profiles of LY, SB, BZ and IL coals and pure water.

Table 2 Summary of DSC results

Coal	Peak at higher temp.		Peak at lower temp.		Water type		
	ΔH J/g	Temp. K	ΔH J/g	Temp. K	Free	Bound	Non freezing
					[% to total]		
BL	0	-	1.1	226.2	0	7	93
IL	0	-	5.0	227.0	0	19	81
WY	0	-	25.1	227.6	0	27	73
BZ	0	-	23.0	226.4	0	21	79
SB	0	-	31.0 (248.1, 227.6)	0	29	71	
YL	86.7	258.5	25.4	226.3	45	13	42
LY	93.6	258.4	18.4	227.1	49	10	41
MW	83.6	257.9	13.9	227.0	45	7	48

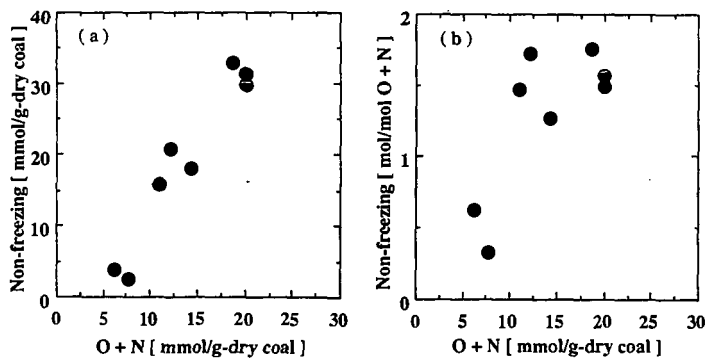


Figure 4. Plots of abundance of non-freezing water against sum of molar oxygen and nitrogen contents (a) and those of number of water molecules as non-freezing water per that of oxygen and nitrogen atoms (b).

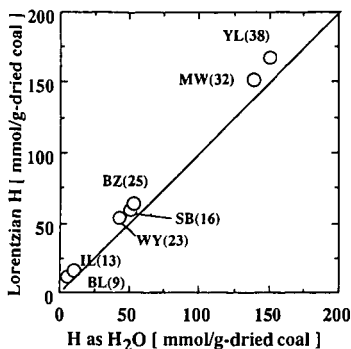


Figure 5. Comparison of amount of proton giving Lorentzian decay with that as water sorbed on coals. Values in (): % fraction of Lorentzian coal hydrogen to total.

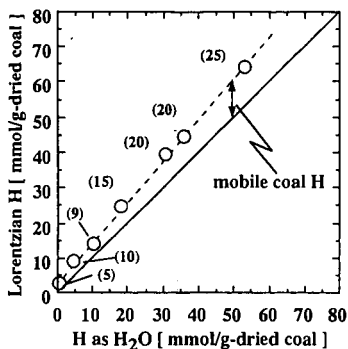


Figure 6. Comparison of amount of proton giving Lorentzian decay with that as water for BZ coal with different water contents. Values in (): % fraction of Lorentzian coal hydrogen to total.

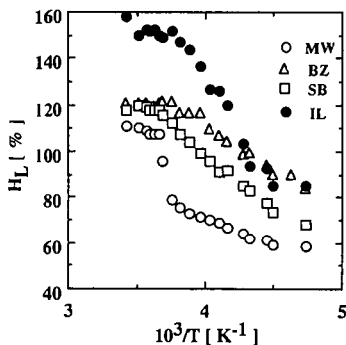


Figure 7. Temperature-dependent changes in H_L being amount of Lorentzian proton normalized by molar amount of proton

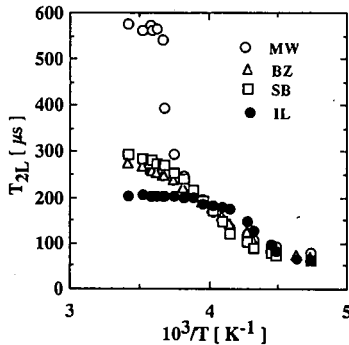


Figure 8. Temperature-dependent changes in relaxation time of Lorentzian component.

Table 3. H_L 's at 293 and 213 K and difference between them.

Coal	H as H ₂ O [mmol/g-dried coal]	H_L [%]		
		293 K (1)	213 K (2)	(1)-(2)
IL	9.6	158	85	73
WY	43.4	126	79	47
BZ	52.9	120	84	36
SB	51.1	118	68	50
YL	150.6	112	55	57
MW	138.7	111	59	52

THE PREPARATION AND CHARACTERIZATION OF LINEAR AND CROSS-LINKED POLY(FLUORENYL).

Edward W. Hagaman and Suk-Kyu Lee.

Chemical and Analytical Sciences Division
Oak Ridge National Laboratory
Oak Ridge, Tennessee 37831-6201

Keywords: Cross linking, Poly(fluorenyl), CP/MAS ^{13}C NMR

INTRODUCTION

Retrogressive reactions in coal processing are that class of reactions that lead to the formation of high molecular weight materials that are more intractable than those present in the coal prior to processing. This outcome almost always is regarded as deleterious. The present work focuses on the characterization of the acid-catalyzed polymerization of benzylic fluorides, and in particular the synthesis of poly(fluorenyl), as an example of the type of chemistry that may occur in the cross-linked organic matrix of coals when in contact with strong acids. Solution and solid state ^{13}C NMR spectroscopy was used to characterize the soluble and insoluble polymers. The change in the value of $f_{\text{A}^{\text{H}}}$, the fraction of aromatic carbon that is protonated¹, is the criterion used to monitor the extent of cross-linking in these polymer preparations.

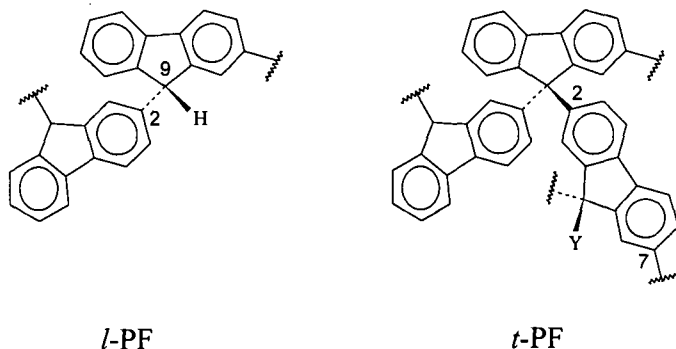
Benzylic fluorides are sensitive substances, prone to further reaction via acid catalyzed heterolytic scission of the C-F bond. The electron deficient reactive intermediate formed in this reaction undergoes electrophilic aromatic substitution. This reaction can be started with catalytic traces of acid and is self-sustaining as HF is generated in equivalent concentrations as the reaction proceeds. The relevance of this naturally non-occurring functional group in coal processing stems from the similar reaction pathway followed by both benzylic fluorides and benzylic alcohols. In the coal matrix, the operation of two exogenous processes- air oxidation and strong acid treatment of the coal (deminerallization) creates a situation in which the polymerization discussed herein may occur in the coal. In addition to the polymerization reactions that produce poly(fluorenyl), the subsequent cross-linking of the linear polymer is also reported. In subsequent work, similar chemistry will be applied to soluble lignin as a model more similar to low rank coals.

RESULTS AND DISCUSSION

The generation of poly(fluorenyl), PF, is most easily effected by impurity- or self-catalyzed decomposition of solid 9-fluorofluorene. The solid state reaction proceeds unattended by storing the monomer in a closed, dry glass container at room temperature. In a matter of days the white, crystalline 9-fluorofluorene is completely converted into a white, fluorine-free, *soluble* polymer. This material is identical (except in molecular weight distribution) to the polymer generated from 9-fluorofluorene in hexane or THF solution that has been treated with catalytic trifluoroacetic acid. A polymer that is virtually indistinguishable from that derived from 9-fluorofluorene is obtained from the reaction of 9-hydroxyfluorene in HF/pyridine.

The gross structure of the polymer follows from the change in $f_{\text{A}^{\text{H}}}$ between the monomer, 9-fluorofluorene (0.67 ± 0.02) and the polymer (0.59 ± 0.02), i.e., a change from 8 to 7 aromatic methines out of 12 aromatic carbons. The identification of protonated and non-protonated aromatic carbon resonances is made through dipolar dephasing experiments.² In Figure 1 the two resonances with chemical shifts greater than 140 ppm represent the non-protonated aromatic carbons in this polymer. In addition, the C(9) fluoromethine resonance (92.6 ppm, $^1J_{\text{CF}} = 180$ Hz) of 9-fluorofluorene is absent in the polymer. Indeed, no fluorocarbon resonance appears in the polymer.

The tetrahedral carbon resonance in the polymer occurs at 54.5 ppm (Figure 1a). These data indicate the loss of the carbon-fluorine bond and the formation of a carbon-carbon bond between C(9) and an aromatic carbon of another fluorene moiety. The C(9) resonance of the model 9-phenylfluorene is 54.4 ppm, an excellent match for the corresponding resonance in the polymer. The site of attachment of C(9) of one residue to the aromatic ring of the next monomer unit is C(2) [see the structure for numbering]. This attachment is supported by (1): chemical shift additivity arguments, (2): the well established electrophilic substitution pattern observed in fluorene, e.g., nitration of fluorene produces solely 2-nitrofluorene, and (3): a proof of structure based on long range ^1H - ^{13}C coupling in 2-(pentamethylbenzyl)fluorene, prepared by the acid-catalyzed reaction of pentamethyl benzyl fluoride with fluorene. The polymer has the structure shown below labeled linear PF, *l*-PF. The line widths of the resonances in the solid state spectrum are on the order of 125 Hz. The high resolution ^{13}C NMR spectrum of this highly soluble *l*-PF, obtained at low concentration in CDCl_3 , to keep solution viscosity low, shows an order of magnitude better resolution than the solid state spectrum. The spectrum contains evidence of conformational heterogeneity of the polymer, with most carbons represented by a narrow manifold of chemical shifts that produces an asymmetric or split resonance band shape. This distribution in chemical shifts is too small to be an indication of the presence of structural isomers.



The *l*-PF formed from the solid state reaction of 9-fluorofluorene has a number average molecular weight, $M_n = 568$ and polydispersity, $M_w/M_n = 2.5$ determined by GPC. The weight average molecular weight, 1420, is in good agreement with that determined from end group analysis in the solid ^{13}C NMR spectrum, 1245. The end group resonance in this spectrum occurs at 36.0 ppm, the chemical shift of C(9) in the fluorene itself. It is possible that the polymer could bite back on itself, generating a ring or branch point in the polymer. The linkage so generated would be indistinguishable from the linear C(9) polymer resonances on the basis of chemical shift. Such structures, if present in high concentration would be reflected in low f_a^{CH} values.

Treatment of *l*-PF with F-TEDA or with $\text{HF/pyridine/NO}\cdot\text{BF}_4^-$, reagents used to introduce a fluorine substituent at unactivated aliphatic sites, fails to generate the intended product, poly(9-fluorofluorenyl). The products are *fluorine-free*, have a ^{13}C NMR spectrum similar in appearance to the starting material (cf. Figure 1a,b), and are *highly insoluble*. Integration of the aromatic resonances reveals $f_a^{\text{CH}} = 0.56 \pm 0.020$.³ These facts indicate that the polymer has been cross-linked by this chemical treatment. The implication is that the reagents do in fact generate the 9-fluoro *l*-PF, but that this product, like the 9-fluoro monomer, undergoes cationic polymerization. The f_a^{CH} of the product indicates that one of every three fluorenyl residues in the product, *l*-PF, has a new intra- or inter-chain C(9)-C(2) connection. The statistical repeating structural unit

of *t*-PF is shown above. In the limit of complete cross-linking the aromatic CH/C ratio would become 6/6, i.e., $f_a^{aH} = 0.50$. The inter-chain cross-links imbue the polymer with its high insolubility. All samples of *t*-PF that we have synthesized are cross-linked to about the same extent ($f_a^{aH} = 0.55 \pm 0.02$). This may represent a limiting degree of polymerization dictated by the physical constraints of the polymer chain. In addition to the 54 ppm resonance representing mono- and di-aryl substituted C(9) carbons of the fluorenyl residues, a new resonance at 83 ppm appears in the spectrum of *t*-PF produced using F-TEDA (Figure 1b). This is the region of the spectrum for oxygenated aliphatic carbon resonances. The resonance represents the incorporation of 9-aryl-9-fluorenol residues in the *t*-PF polymer (Y = OH in the above structure). The C(9) resonance of the model, 9-phenyl-9-hydroxyfluorene, is 83.4 ppm. This functionality likely arises from quenching of fluorenyl cation sites with water during reaction work-up, sites that can not react by the usual pathway due to physical constraints built into the cross-linked polymer.

REFERENCES

1. M. A. Wilson, R. J. Pugmire, J. Karas, L. B. Alemany, W. R. Woolfenden, and D. M. Grant, *Anal. Chem.*, **56**, 933, (1984).
2. P. D. Murphy, B. C. Gerstein, V. L. Weinberg, and T. F. Yen, *Anal. Chem.*, **54**, 522, (1982).
3. The error limits on the aromaticity determinations reflect the absolute error in this quantity. The theoretical value of f_a^{aH} for the linear polymer is 0.583. The value from the direct NMR integral, splitting the area at the saddle point, is 0.60. Peak fitting with an assumed Gaussian line shape yields 0.59, while allowing the line shape to be treated as a mixed Gauss-Lorentz line produces the best line fit (smallest residuals) and a value of 0.61. The ± 0.02 error limits reflect these uncertainties as well as the deviations from linear response that may accrue in the actual experiment. However, in comparisons between two similar materials, taking care to use the same evaluation criterion for both, the relative error is small. The 0.03 difference in f_a^{aH} between *l*-PF and *t*-PF is reproducible, indicating a small relative error.

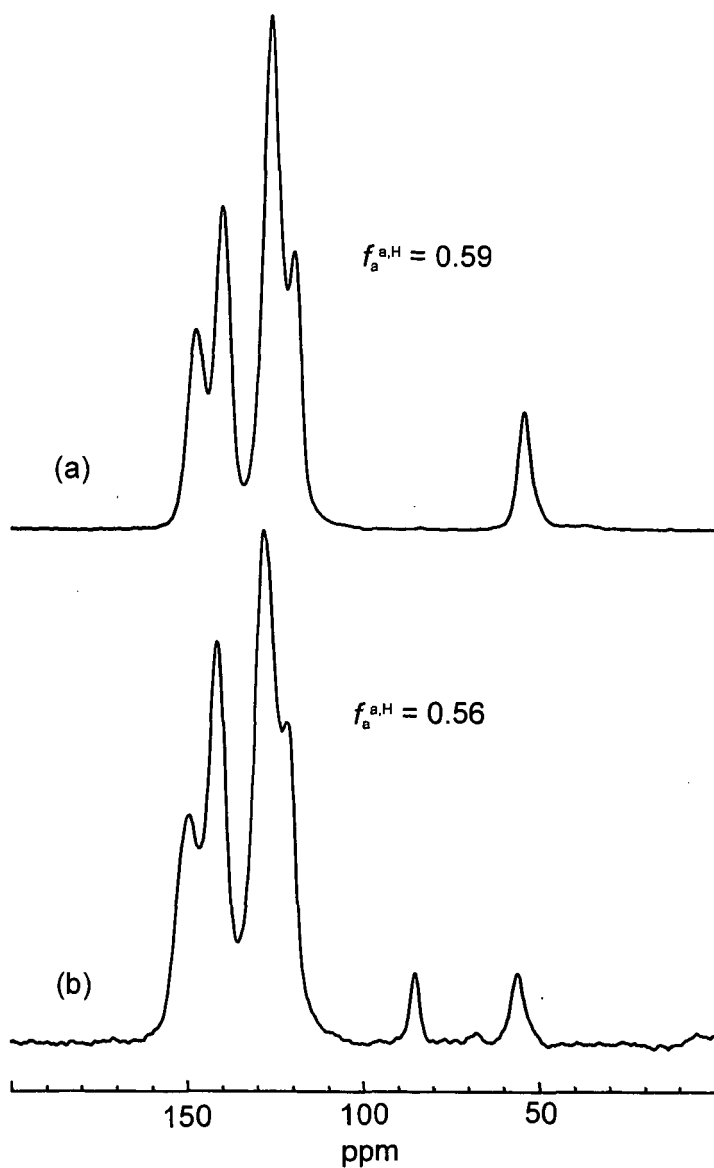


Figure 1. ^{13}C NMR spectra of (a) *t*-PF from the solid state polymerization of 9-fluorofluorene and (b) *t*-PF from the reaction of *t*-PF with F-TEDA. Broadening of the aromatic peaks in 1b relative to 1a and the change in $f_a^{a,H}$ evidence the increase in conformational heterogeneity and cross linking in *t*-PF. The $f_a^{a,H}$ values are calculated from areas derived from peak deconvolution of the aromatic resonances.

THE INCREASE OF THE EXTRACTION YIELD OF COALS BY THE ADDITION OF AN ELECTRON ACCEPTOR

Masashi Iino, Hongtao Liu, Nobuyuki Hosaka, Hideyuki Kurose, and Toshimasa Takanohashi
Institute for Chemical Reaction Science, Tohoku University
Katahira, Aoba-ku, Sendai 980-77, JAPAN

KEYWORDS: Coal extraction, additives, electron acceptor

INTRODUCTION

We have reported(1) that the extraction yield with carbon disulfide - *N*-methyl-2-pyrrolidinone (CS₂-NMP) mixed solvent (1:1 by volume), which gave very high extraction yields for bituminous coals at room temperature(2), increases by the addition of a small amount of tetracyanoethylene(TCNE) to the solvent. The yield of the room temperature extraction of Upper Freeport coal with the 1:1 CS₂-NMP mixed solvent increases from 59 wt%(daf) to 85 wt%(daf) by adding only 5%(based on coal) of TCNE to the mixed solvent. *p*-Phenylenediamine is also an effective additive for the mixed solvent extraction (3).

We have also found (4) that when the extracts obtained with the CS₂-NMP mixed solvent were fractionated with pyridine to yield pyridine-insoluble (PI) and -soluble (PS) fractions, part of PI became insoluble in the mixed solvent. The addition of a small amount of TCNE, tetracyanoquinodimethane (TCNQ) or *p*-phenylenediamine to the mixed solvent, PI became soluble in the mixed solvent.

While, the aggregation state of coal molecules and its change with heating or contact with solvent and reagent play an important role in structure and reactivity of coal, but the details on them are still unknown. Coal extracts and coal-derived liquids are known to readily associate between themselves to form complex aggregates(5-7). The effect of TCNE on the extraction yields above mentioned can be explained by its breaking ability of noncovalent bonds through which the aggregates form(1). However, another explanation is possible, i. e., covalent bonds in coal such as ether bonds break after electron transfer from coal to TCNE, which is a strong electron acceptor. Solubility limit of coals, i. e., maximum extraction yield without the breaking of covalent bonds is one of the key points to clarify a kind of cross-linking bonds, i. e., covalent or non-covalent (physical)cross-links. If coal has developed covalent cross-links, its extractability is low, as observed in the extraction with conventional solvents such as pyridine which gave the yields less than 30-40wt% (daf) of coal. So, 85wt% of the extraction yield for CS₂-NMP-TCNE solvent system suggests that Upper Freeport coal has little covalent cross-links, if no covalent bond breakings occur during this extraction.

In this study the effect of various electron acceptors on solubility of PI in the mixed solvent and also the effect of TCNE retained in PI on the solubility of PI were investigated. The mechanisms for the enhancement of the extraction yield of coal and solubility of PI by electron acceptors are discussed.

EXPERIMENTAL

Upper Freeport(Argonne Premium coal, 86.2 wt% C(daf)) and Zao Zhuang(Chinese coal, 87.8 wt% C(daf)) coals were extracted with the 1:1 CS₂-NMP mixed solvent repeatedly at room temperature (2). The extract obtained was fractionated with acetone and pyridine, respectively, to give acetone-soluble(AS), pyridine-soluble and acetone-insoluble(PS), and pyridine-insoluble (PI) fractions, as shown Figure 1. Solubility of PI in the CS₂-NMP mixed solvent was examined using 0.4g of PI and 50ml of the mixed solvent at room temperature under ultrasonic irradiation with or without an electron acceptor such as TCNE. The quantity of an electron acceptor added is 8×10^{-5} mol to 0.4g of PI. This quantity corresponds to 2.5wt% (10wg) of TCNE to 0.4g of PI.

RESULTS AND DISCUSSION

The Effect of Electron Acceptors on the Solubility of PI

Table I shows the solubility of PI in the mixed solvent when an electron acceptor was added, together with its electron affinity, which is a measure of the electron acceptability of electron acceptor. Table I shows that only TCNE and TCNQ gave high solubility as expected from their high electron affinities. However, other electron acceptors used here do not show the solubility enhancements. So, it is not clear whether charge-transfer (donor-acceptor) interactions is responsible for the solubility enhancement by the addition of TCNE and TCNQ, or not.

The Effect of TCNE Retained in PI on the Solubility of PI

Figure 2 shows the result of the repeated dissolution experiments of PI(PI-1 in Figure 2) from Zao Zhuang coal in the 1:1 CS₂-NMP mixed solvent with or without TCNE. A part(40.4%) of PI becomes insoluble in the mixed solvent, though PI is a part of the mixed solvent extract, but almost completely(97.6%) soluble in the mixed solvent containing TCNE, as already reported (4). Figure 1 shows that PS(PS-2) and AS(AS-2), in addition to PI(PI-2), were also obtained from PI-1 in the yield of 9.2% and 5.0%, respectively, probably due to the change of the aggregation state, as described later. PI-2 was well washed with pyridine to remove PS. It was reported that most of TCNE retained in PI could be removed by its washing with pyridine (1). In fact, from Figure 3, which shows that the FT-IR spectra of soluble and insoluble fractions of PI in the CS₂-NMP-TCNE solvent, PI-2, and PS-2, the peak at 2200cm⁻¹ due to TCNE (nitrile group) was almost disappeared in PI-2 (Figure 3-c), compared to soluble fraction (Figure 3-a) and PS-2 (Figure 3-d), indicating the removal of TCNE retained in PI-2 by washing with pyridine. PI-2 was then tried to redissolve in the CS₂-NMP mixed solvent and again a considerable part(31.6%) of PI-2 became insoluble, and 99.0% of PI-2 was dissolved in the mixed solvent containing TCNE, as shown in Figure 2. Fractionation of PI soluble in CS₂-NMP-TCNE solvent gave again 9.1% of PS+AS. A similar result was obtained for the PI from Upper Freeport coal, as shown in Figure 4.

If the solubility increase by TCNE addition is caused by the covalent bond breaking through the electron transfer from coal to TCNE, the insolubilization of PI in the mixed solvent after the removal of TCNE from the PI, just described above, should not be observed. So, the solubility increase of PI by TCNE is considered to be caused by the breaking of noncovalent bonds in the aggregates among coal molecules and the new associates with TCNE is more soluble than the original aggregates, as shown in Figure 5. In Figure 5, two kinds of noncovalent bonds, weak and strong, are assumed. The CS₂-NMP mixed solvent can break the weak bonds, but not the strong bonds, and the mixed solvent containing TCNE, which has strong interaction with coal molecules, can break even the strong bonds. The interaction between TCNE and coal molecules may be charge-transfer (donor-acceptor) and/or other interactions. The solvents such as pyridine and THF seem not to break easily even the weak noncovalent bonds, resulting in low extraction yields. The mechanism shown in Figure 5 can also explain the reason why the extraction yield increased by TCNE addition.

Figures 2 and 4 show that lighter fractions such as AS and PS formed from PI by the treatment with CS₂-NMP mixed solvent containing TCNE. This suggests that they are included in PI due to the formation of the aggregates which are not soluble in pyridine nor acetone and became soluble in those solvents by the change of the aggregation state. So, the fraction distribution obtained here is considered to be a reflection of not only solubility of coal molecules themselves, but aggregation state among coal molecules.

TCNE is very efficient for the extraction yield enhancement of Upper Freeport coal. The addition of TCNE more than 0.05g to 1g of the coal reached an almost constant extraction yield of about 85 wt% (daf). Using the structural parameters of *f*_a and degree of aromatic ring condensation for Upper Freeport coal reported by Solum et al.(8), 0.05g of TCNE per 1g of coal is calculated to correspond to 1 molecule of TCNE per about 8 aromatic clusters of the coal.

These results obtained strongly suggest that at least some bituminous coals, which gave high extraction yields with the CS₂-NMP-TCNE solvent, have chemical structure consisting of complex mixture of the aggregates among coal molecules, and having no giant covalently bound cross-linked network.

CONCLUSIONS

The effect of various electron acceptors on the solubility of pyridine-insoluble extract fraction (PI) in the CS₂-NMP mixed solvent was investigated. The other electron acceptors than TCNE and TCNQ do not show the solubility enhancement. So, it is not clear whether the solubility enhancement by TCNE and TCNQ is ascribed to their charge-transfer interactions with coal molecules or not. The results obtained for the effect of TCNE retained in PI on solubility of PI suggest that the solubility increase by the electron acceptors is caused by the breaking of noncovalent interaction in aggregates of coal molecules.

ACKNOWLEDGEMENT

This work was supported by "Research for the Future" project of Japan Society for the Promotion of Science (JSPS) through the 148 committee on coal utilization technology of JSPS.

REFERENCES

1. Liu, H., Ishizuka, T., Takanohashi, T., and Iino, M. *Energy Fuels*, 1993, 7, 1108-1111.
2. Iino, M., Takanohashi, T., Osuga, H., and Toda, K. *Fuel*, 1988, 67, 1639-1647.
3. Ishizuka, T., Takanohashi, T., Ito, O., and Iino, M. *Fuel*, 1993, 72, 579-580.
4. Sanokawa, Y., Takanohashi, T., and Iino, M. *Fuel*, 1988, 69, 1577-1578.
5. Sternberg, H. W., Raymond, R., Schweighardt, F. K., *Science*, 1975, 188, 49-51.
6. Sternberg, V. I., Baltisberger, R. J., Patel, K. M. et al. in *Coal Science*; Gorbarty, M. L., Larsen, J. W., Wender, I., Ed.; Academic Press: New York, 1983; pp125-171.
7. Nakamura, K., Takanohashi, T., Iino, M. et al. *Energy Fuels*, 1995, 9, 1003-1010.
8. Solum, M. S., Pugmire, R. J., Grant, D. M. *Energy Fuels*, 1989, 3, 187-192.

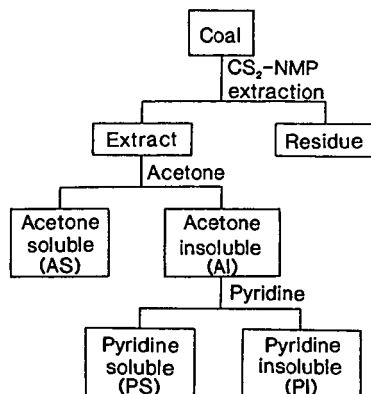


Figure 1 Extraction and fractionation procedures

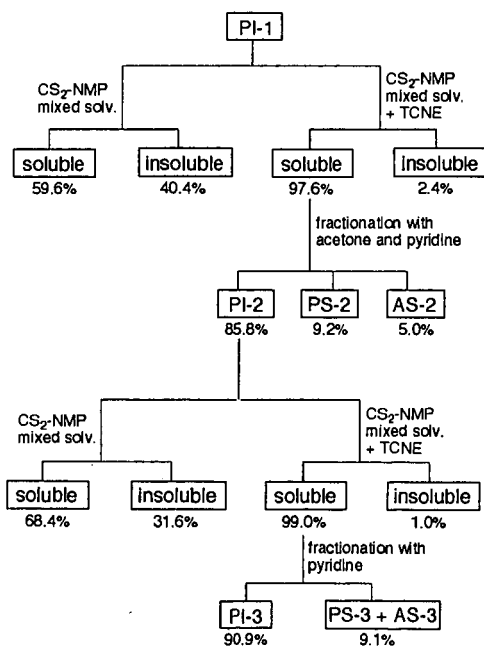


Figure 2 Repeated solubility experiments for PI from Zao Zhuang coal in the CS_2 -NMP mixed solvent with or without TCNE (2.5 wt% based on PI).

Table 1 The effect of the addition of electron acceptors on the solubility^{a)} of PI from Zao Zhuang coal in the CS₂-NMP mixed solvent at room temperature

Electron acceptor	Solubility of PI (wt%)	Electron affinity ^{b)} (eV)
None	51.0	—
Tetracyanoethylene(TCNE)	99.5	2.2
7,7,8,8-Tetracyanoquinodimethane(TCNQ)	81.0	1.7
2,3-Dichloro-5,6-dicyano- <i>p</i> -benzoquinone(DDQ)	53.8	1.95
1,2,4,5-Tetracyanobenzene	47.7	0.4
<i>p</i> -Benzoquinone	44.1	0.77
2,6-Dichloro- <i>p</i> -benzoquinone	37.0	1.2
<i>p</i> -Chloranil	34.8	1.37

a) Wt% of PI soluble in the mixed solvent when 8×10^{-5} mol of an electron acceptor was added to 0.4g of PI in 50ml of the mixed solvent.

b) Electron affinity of the electron acceptor.

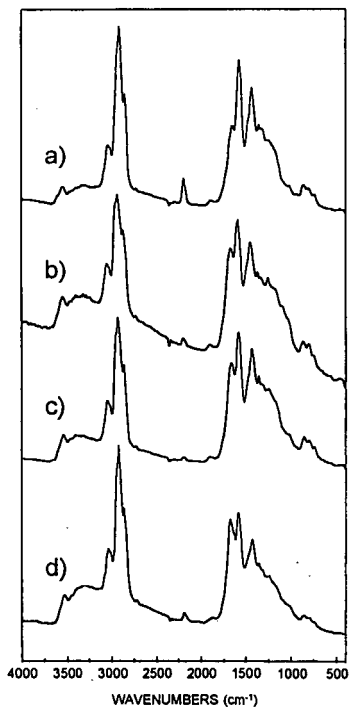


Figure 3 FT-IR spectra of soluble(a) and insoluble(b) fractions of PI-1 in the CS₂-NMP-TCNE solvent, PI-2(c) and PS-2(d).

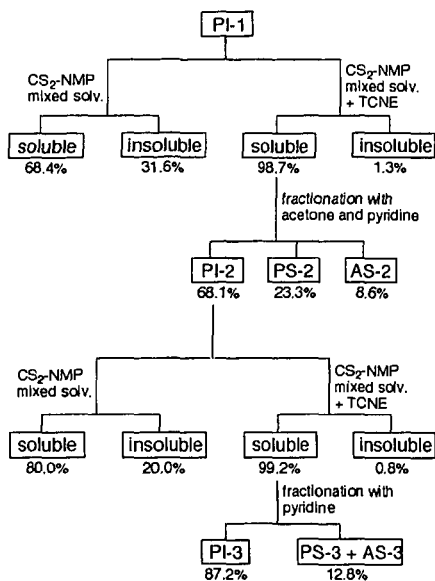


Figure 4 Repeated solubility experiments for PI from Upper Freeport coal in the CS₂-NMP mixed solvent with or without TCNE(2.5 wt% based on PI),

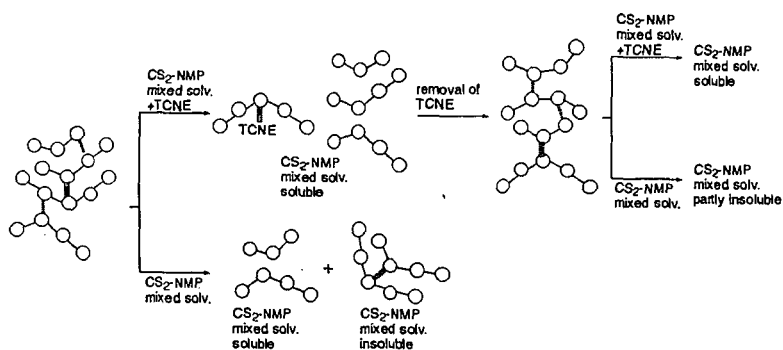


Figure 5 Solubilization mechanism of PI in the CS₂-NMP mixed solvent with or without TCNE. ○: aromatic cluster, —: covalent bond, |||||: non-covalent bond(strong), ———: non-covalent bond(weak)

SMALL ANGLE NEUTRON SCATTERING STUDIES OF COAL-EXTRACT SOLUTIONS

P. Thyagarajan Intense Pulsed Neutron Source, Argonne National Laboratory Argonne, IL 60439 George D. Cody, Geophysical Laboratory Carnegie Institution of Washington 5251 Broad Branch Rd. Washington, DC 20015

key words SANS, Coal Extracts, Fractals

INTRODUCTION

Interest in the physics and chemistry of coal extracts has extended for over 100 years. Early on it was recognized that pyridine was a particularly good solvent capable of extracting a significant weight percent of intermediate rank coals. Many of the current theories regarding the macromolecular structure of coals (type III kerogens) are based on the fact that there exists a physically definable limit in the extractability of soluble organics from coal in pyridine¹. The non-extractable residue is generally considered to be a cross-linked macromolecular network². The extract-solvent "solutions", although acknowledged to be far from ideal (thermodynamically), are presumed to be "molecular solutions" in the sense that random mixing of the constituents occurs within a single solution phase³.

Recently, a number of investigations have challenged this established model of coal structure. In particular, studies by Iino and colleagues⁴, using mixed solvent systems (most notably, a *n*-methyl-2-pyrrolidinone (NMP) mixture with CS₂), have demonstrated increases in extractabilities of more than twice that by pyridine in the case of some coals⁴. These results suggest that either there exists a set of non-covalent interactions unperturbed by pyridine but disrupted by the mixed solvents or that the mixed solvents are degrading the network and enhancing the extraction yields through some, as yet unknown, chemical reaction.

In the present work we set out to characterize the solution structures of coal extracts to gain insight on the nature of coal-solvent interactions. The characterization of solution structures of dilute mixtures of macromolecules in various solvents is readily attainable using small angle neutron scattering⁵⁻¹⁷. The theory of small angle scattering is well established and the method has been used by many researchers for the purpose of elucidating the configurational state of polymers in solution⁶, the structure of asphaltenes in apolar solvents⁷⁻¹², the study of proteins¹³, as well as dilute coal extract "solutions"^{5,14,15}.

Neutron scattering is particularly useful in revealing the spatial characteristics of structures composed of low atomic number (*Z*) elements. This is due to the fact that neutrons, uncharged and with spin (*I*) = 1/2, interact with a given element through their respective angular momenta. The magnitude of this interaction has no correlation with *Z*. X-rays, on the other hand, interact with the electronic shell surrounding the nuclei and the magnitude of the coherent scattering amplitude varies as a strong function of *Z*. Although lighter elements are nearly "invisible" to X-rays, the unique nature of the interaction of the neutron with spin (*I*) > 0 nuclei results in the coherent scattering cross-section of low *Z* elements being similar in magnitude to that of many of the higher *Z* elements¹⁶; e.g. deuterons scatter neutrons as efficiently as gold.

In the following the results of small angle neutron scattering (SANS) experiments are described in reference to assessing the solution structure of solvent extract "solutions" from a number of coals. The goal of this study is to identify features or characteristics of the mixtures which may highlight the mechanism behind the exceptional solvating capabilities of the mixed solvents as compared with other polar solvents such as pyridine. For the present study we chose a lignite (APCS No. 8), a sub bituminous C rank coal (APCS No. 2), a High volatile bituminous coal (APCS No. 3), and a medium volatile bituminous coal (APCS No. 1) (see Table I).

In addition to characterizing the solution structure of the neat extracts, O-methylated extracts were also studied. The purpose of O-methylation was to neutralize the predominant interaction between coal and pyridine. The medium volatile coal was not O-methylated.

Experimental Section

Solvent Extraction: In the case of pyridine extraction, approximately 5 grams of 100 mesh coal was extracted with pyridine in a Soxhlet extraction apparatus for periods exceeding 24 hours. The extract was separated from the solvent using roto-evaporation. The extractability of the Upper Freeport (UF) coal in the mixed solvent (NMP/CS₂) is over twice that in pyridine as is presented in Table I. Extraction of the Upper Freeport coal (APCS No. 1) with NMP/CS₂ follows the procedure of Iino et al.⁴ with minor

modifications. Approximately 5 grams of 100 mesh APCS No. 1. was stirred in 150 ml of a 1:1 mixture (by volume) of n-methyl-2-pyrrolidinone (NMP) and carbon disulfide (CS₂) (mixed solvent, MS) for approximately 6 hours. The solvent extract was decanted and then centrifuged up to 14 K rpm to sediment out any entrained solids.

Throughout the paper below, the various soluble fractions from different coals are designated as presented in Table II.

Small Angle Neutron Scattering: Solutions of the extracts (5 wt. %) were prepared by mixing dry extract with either of the per-deuterated solvents. This concentration was selected to yield sufficient scattering intensity without introducing scattering intensity due to interparticle interactions. Previous work on the SANS behavior of coal extract solutions in pyridine exhibited no dependence on scattering behavior with solvent concentration (at 1, 5, and 10 wt. %) other than a linear increase in incoherent and coherent scattering intensity with increasing wt. % of extract.⁵

Solutions were contained in Suprasil cylindrical cells with a 2 mm path length (volume = 0.7 ml) for the SANS analysis. SANS data were measured at the Intense Pulsed Neutron Source of Argonne National Laboratory, using the Small Angle Diffractometer (SAD). This instrument uses pulsed neutrons derived from spallation with wavelengths in the range of 1-14 Å and a fixed sample-to-detector distance of 1.54 meters. The scattered neutrons are measured using a 64 x 64 array of position sensitive, gas filled, 20 x 20 cm², proportional counters with the wavelengths measured by time-of-flight by binning the pulse to 67 constant $\Delta t/t = 0.05$ time channels. The size range in a SANS experiment is constrained by both the geometry of the instrument and the wavelength of the neutrons which determine the working range of momentum transfer Q.

$$Q = 4\pi\lambda^{-1} \sin \theta \quad (1)$$

where θ is half the Bragg scattering angle and λ is the wavelength of the neutrons. Given the characteristics of the SAD¹⁷ at the Intense Pulsed Neutron Source (IPNS), useful SANS data in the Q range of 0.006-0.25 Å⁻¹ can be obtained in a single measurement. The reduced data for each sample is corrected for the backgrounds from the instrument, the Suprasil cell, and the solvent as well as for detector nonlinearity. Data are presented on an absolute scale by using the known scattering cross-section of a silica gel sample. The absolute cross-section for this sample has been measured at the SANS instrument at ORNL. Standard Guinier analysis in the region of $QR_g < 1.0$ can be used to extract the radius of gyration, R_g and $I(0)$ values by using the equation below.

$$I(Q) = I(0)\exp(-Q^2 R_g^2 / 3) \quad (2)$$

R_g is the root-mean-squared distance of all of the atoms from the centroid of neutron scattering length density of the particle and $I(0)$ is the absolute scattering cross-section at $Q=0$ which is defined as follows.

$$I(0) = N_p (\rho - \rho_s)^2 V^2 \quad (3)$$

Here N_p corresponds to the number density of particles, V is the volume of the particle, and ρ and ρ_s are the scattering length densities of the particle and the solvent, respectively. The absolute scattering data of the silica gel standard give $R_g = 44.7 \pm 0.2$ Å and $I(0) = 70$ cm⁻¹. The magnitudes of R_g and $I(0)$ for this sample are routinely measured in the same Q region and are used to determine scale factors to place the scattering data on an absolute scale in units of cm⁻¹.

RESULTS

SANS of Soluble Fractions in Organic Solvents:

The SANS data, on an absolute scale, for each coal extract in pyridine-d₅ is presented in Figures 1-4, where the intensity of the scattered neutrons $I(Q)$ is plotted against the magnitude of the momentum transfer (Q); note that all of the plots are log-log. The SANS data for UF-PyS/dPy, UF-MS/dPy and UF-MS/dM solutions on an absolute scale are presented in figure 5.

The scattering behavior of the lowest rank coal (APCS No. 8) (Figure 1) exhibits power law scattering behavior in the low Q region; the power law exponent is 2.13 for the

untreated extract and 2.29 for the O-methylated. Similar behavior is observed for the sub bituminous extract (APCS No. 2) (Figure 2), with exponents of 1.79 and 2.46, for the untreated and O-methylated extracts, respectively. The high volatile C rank coal exhibits scattering behavior that is "bounded" at low Q for the untreated extract, but exhibits power law scattering at low Q in the O-methylated case ($d = 1.7$) (figure 3). The medium volatile bituminous coal (APCS No. 1) exhibits scattering behavior that is remarkably similar to that of the (APCS No. 3) (Figure 4). The scattering behavior of the medium volatile coal (APCS No. 1) in the mixed solvent (Figure 5) exhibits only incoherent scattering, i.e. there are no large structures in this particular system.

Discussion

In a number of liquid-phase systems there exist random solution structures that exhibit scattering behavior resulting from self similar or fractal topology. An elegant theory, formulated by Freltoft et al¹⁴, accounts for power law scattering behavior, with $d < 3.0$, to systems with mass fractal characteristics. Such solution structures are aggregates with structure factors governed by interparticle correlations which decay exponentially from the center of the aggregate. Thus, changes in d , as seen in figures 1-3 reveal changes in the density of the mass fractal aggregates.

In the case of APCS No.s 3 and 1, in pyridine, aggregates also exist, however, they do not exhibit mass fractal characteristics, rather they are readily described using the Guinier approximation. Incidentally, The remarkable similarity between the SANS behavior of the two extracts exhibited in Figure 4 strongly suggests that, in both the IL-PyS/dPy and UF-PyS/dPy samples, the molecular aggregates are nearly identical in their chemical composition, size, shape, and number density.

In complete contrast to the aforementioned results, the solution of mixed solubles in NMP/CS₂ (UF-MS/dM) exhibits virtually no coherent scattering intensity across the accessible Q range of the SAD. SANS analysis of the UF-MS/dM solution, therefore, reveals a well dispersed "molecular" solution of small particles. The fact that aggregation does not occur in UF-MS in NMP/CS₂ indicates that the mixed solvent solvates the extractable molecules much more effectively than pyridine, a result which is clearly consistent with the observation of overall enhanced extractability.

The presence of aggregated structures in solutions of coal extracts with pyridine is contradictory to the hypothesis that pyridine is an exceptionally good solvent for coal in a thermodynamic sense. Although, pyridine clearly exhibits a strong interaction with acidic functional groups in coal, in the case of coal extracts, pyridine does not appear to have exceptional solvating capabilities. The clustering or aggregation, clearly evident in all of the pyridine solutions suggests that coal-pyridine interactions may not be sufficient to solvate all non-covalently bound material in coal. This implies that the limits in extractability may be the result of limits in pyridines solvating capability, rather than limits dictated by a covalently cross-linked, "infinite", macromolecular network.

Acknowledgments

The neutron scattering experiments were performed at the Intense Pulsed Neutron Source at Argonne National Laboratory. The authors gratefully acknowledge the help of Denis Wozniak of IPNS, Argonne National Laboratory. Insightful discussions related to the mixed solvent/Upper Freeport system with Profs. Masashi Iino and Toshimasa Takanohashi of the Institute of Chemical Reaction Science, Tohoku University, Sendai Japan, are greatly appreciated. This work was performed under the auspices of the Office of Basic Energy Sciences, Division of Chemical Sciences, U. S. Department of Energy, under contract No. W-31-1090ENG-38. The Intense Pulse Neutron Source is a Department of Energy supported facility.

References

- (1) van Krevelan, *Coal*, Third Edition, Elsevier, Amsterdam, 1993, 979.
- (2) Larsen, J. W.; Green, T. K.; Kovac, J., *J. Org. Chem.*, 1985, **50**, 4729
- (3) Painter, P. C.; Park, Y.; Coleman, M. M., *Energy & Fuels*, 1988, **2**, 693-702
- (4) Iino, M.; Takanohashi, T.; Ohsuga, H.; Toda, K., *Fuel*, 1988, **67**, 1639-1647
- (5) Cody, G. D.; Thiyagarajan, P.; Botto, R. E.; Hunt, J.E.; Winans, R. E., *Energy & Fuels*, 1994, **8**, 1370-1378
- (6) Bates, F. S., *J. Appl. Cryst.*, 1988, **21**, 681.
- (7) Herzog, P.; Tchoubar, D.; Espinat, D., *Fuel*, 1988, **67**, 245
- (8) Ravey, J. C.; Ducoiret, C.; Espinat, D., *Fuel*, 1988, **67**, 1560.
- (9) Overfield, R. E.; Sheu, E. Y.; Sinha, S. K.; Liang, K. S. *Fuel Sci. Technol. Int.*, 1989, **7**, 611.
- (10) Senglet, N.; Williams, C.; Faure, D.; Des Courieres, T.; Guillard, R. *Fuel*, 1990, **69**, 72
- (11) Storm, D. A.; Sheu, E. Y.; DeTar, M. M. *Fuel*, 1993, **72**, 977.
- (12) Thiyagarajan, P. Hunt, J. E., Winans, R. E., Anderson, K. B.; Miller, J. T. *Energy & Fuels*, 1995, **9**, 829.

- 13) Stuhmann, H. B.; Miller, A. *J. Appl. Cryst.*, 1978, **11**, 325.
 (14) Ho, B.; Briggs, D. E. *Colloids Surf.*, 1982, **4**, 285.
 (15) Triolo, R.; Child, H. R. *Fuel*, 1984, **63**, 274.
 (16) Bacon, G. E. in *Neutron Diffraction*, Clarendon Press, Oxford, 1975, pp.38-40
 (17) Thiyagarajan, P.; Epperson, J. E.; Crawford, R. K.; Carpenter, J. M.; Hjelm, R. P. In *Proceedings of International Seminar on Structural Investigations on Pulsed Neutron Sources*; Dubna, 1993; pp 194.
 (18) Freltoft, T.; Kjems, J. K.; Sinha, S. K., *Phys. Rev. B*, 1986, **33**, 269

Table I

Sample	Rank	Samples and Their Physical Characteristics					
		%C*	%H	%O	%S	%E(NMP/CS ₂)**	%E(PyT)***
APCS No. 8	Lignite	73	4.8	20	0.8	NA	15.0
APCS No. 2	Sub.bit	75	5.4	18	0.6	NA	29.0
APCS No. 3	HvC	78	5.0	14	4.8	NA	29.0
APCS No. 1	mv	86	4.7	8	2.3	56.0	25.5

*Dry ash free basis

**percent extractable (wt.) in NMP/CS₂

***percent extractable (wt.) in pyridine

Table II

Sample Designations

Sample:	Lignite (Lig)	Sub.bit (Sub)	HvC Bit (HV)	Med. Vol.(MV)
Solvent				
Pyridine	Lig-PyS/dPy*	Sub-Pys/dPY	HV-PyS/dPy	MV-PyS/dPy
NMP/CS ₂	-	-	-	MV-PyS/dM**

* where PyS - pyridine solubles, dPY-deuteropyridine

** where dM - perdeutero-n-methyl-pyrrolidinone and carbon disulfide

Figure Captions.

Figure 1: Absolute differential SANS cross-section of APCS No. 8 pyridine extract 5 % (wt.) in pyridine D₅, Untreated (filled) and O-methylated (unfilled).

Figure 2: Absolute differential SANS cross-section of APCS No. 2 pyridine extract 5 % (wt.) in pyridine D₅, Untreated (filled) and O-methylated (unfilled).

Figure 3: Absolute differential SANS cross-section of APCS No. 3 pyridine extract 5 % (wt.) in pyridine D₅, Untreated (filled) and O-methylated (unfilled).

Figure 4: Absolute differential SANS cross-section of APCS No.1 pyridine extract 5 % (wt.) dispersed in pyridine-D₅ (filled o) and APCS #.3 pyridine extract 5 % (wt.) dispersed in pyridine-D₅ (o).

Figure 5: Absolute differential SANS cross-section of APCS No.1 pyridine extract 5 % (wt.) dispersed in pyridine-D₅ (Square), APCS No. 1 pyridine extract 5 % (wt.) in NMP/CS₂ (filled o) APCS No. 1 NMP/CS₂ extract 5 % (wt.) in NMP-D₉/CS₂ ((o).

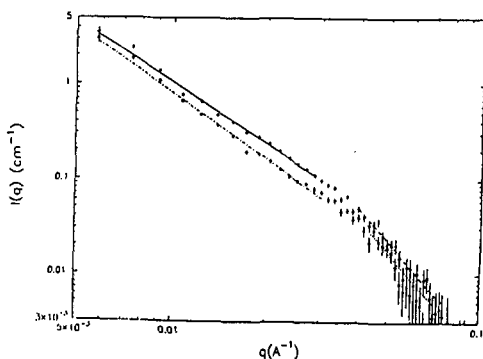


Figure 1

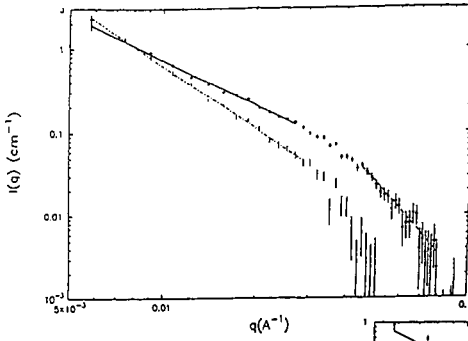


Figure 2

Figure 3

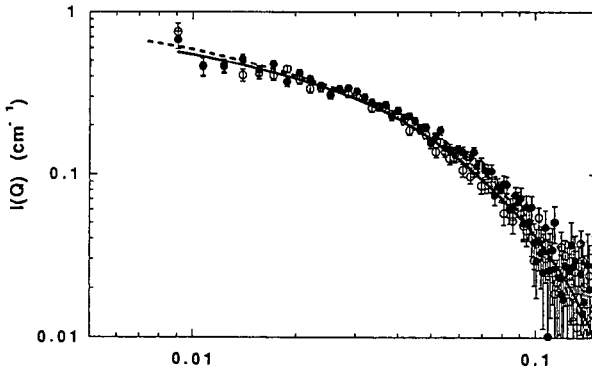
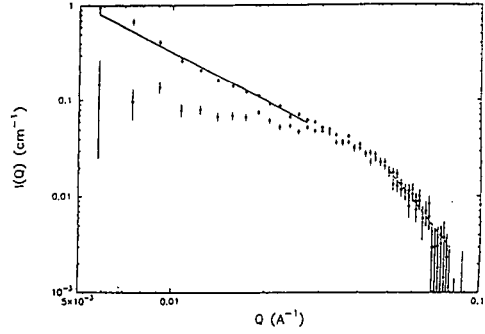
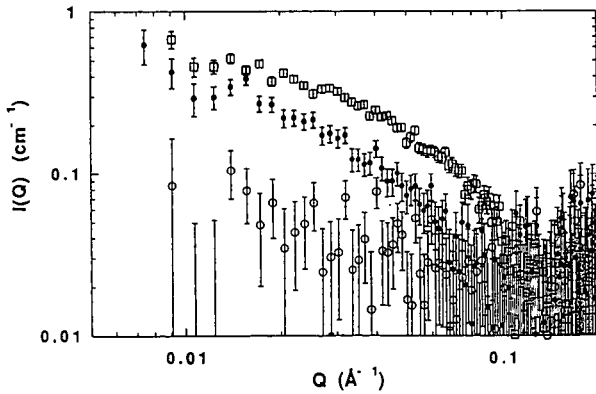


Figure 4

Figure 5



EFFECTS OF LITHIUM IODIDE DOPING ON
THE ASSOCIATED MOLECULAR STRUCTURE OF BROWN COAL.

H.Kumagai, J.-i.Muraoka, J.-i.Hayashi, T.Chiba,
Center for Advanced Research of Energy Technology, Hokkaido
University,
Kita-ku, Sapporo 060, Japan,

D.S.Webster, R.Sakurovs, D.Phan,
CSIRO, Division of Coal and Energy Technology,
North Ryde, NSW 2113, Australia

Keywords:Associated molecular structure, Hydrogen bonding, Low rank coal

ABSTRACT

Effects of lithium iodide (LiI) doping on the associated molecular structure of brown coal have been investigated. Devolatilization of the coal is enhanced with LiI doping at lower temperature range (<300°C). The devolatilization enhanced with LiI doping proceeds without thermal decomposition and cleavage of cross-linkage structure. High temperature ¹H-NMR results indicate that the LiI doping increases the fractions of mobile structure, and also enhances the mobility of molecules. During heat treatment, LiI maintains the enhanced molecular mobility resulting in an increase in the evolution of volatile matter.

INTRODUCTION

Coal is complex macromolecular compounds containing several types of noncovalent interactions, such as hydrogen bonding, van der Waals, aromatic π - π and charge transfer interaction. Chemical and physical properties of coal are strongly affected with associated structure as well as chemical structure of coal molecules. The associated structure of coal molecules is governed the type and strength of noncovalent interactions exist in coal. Low rank coals, such as lignite and brown coal, have a high oxygen content, and a considerable proportion of the oxygen is present in the form of carboxyl and phenolic functional groups. These oxygen containing groups are forming hydrogen bonds with each other resulting in the associated structure of molecules. Thus, it can be considered that inter- and intra-molecular hydrogen bonding interactions are responsible for the properties of low rank coal.

The role of hydrogen bonding in the properties of coal has already been recognized. Painter and co-workers [1] have discussed the band assignment of hydroxyl groups forming hydrogen bonding interaction in coal. They also discussed the significance of hydrogen bonding on the structure of coal. The classical solvent induced swelling techniques of polymer chemistry have been applied to investigate the associated structure of coal molecules [2-6]. Larsen et al. [4] estimated that bituminous coal contain about 5 times as many hydrogen bond cross-link as covalent cross-link. Brenner [3] pointed out the effects of hydrogen bonding interaction on the glass transition temperature and glassy properties of coal. The importance of the hydrogen bonding interaction in the formation and stabilization of coal macromolecular structure has also demonstrated by computer aided molecular design technique [7,8].

Cross-linking reactions at hydroxyl sites during heat treatment have been postulated to suppress the fluidity and volatile matter formation of coals [9-14]. Van Krevelen and co-worker [9] provided direct evidence on the role of hydroxyl groups in suppressing fluidity by model compound study. The mechanism of the suppression by the presence of hydroxyl groups has been modeled as involving cross-linking reactions at hydroxyl sites. The solvent induced swelling techniques have been employed also to determine cross-link density changes during heat treatment. The results obtained from the swelling techniques have demonstrated that cross-linking in low rank coals occurs prior to tar evolution, and the temperature is lower than that for bituminous coals [10-12]. Comparison of char solvent swelling behaviour and gas evolution has indicated that the low temperature cross-linking occurs simultaneously with CO₂ and H₂O evolution [13]. The cross-linking at lower temperature was also inferred with the Proton Magnetic Resonance Thermal Analysis (PMRTA) [15,16]. The mobile phase of low rank coal determined from NMR

relaxation time decreased at a substantially lower temperature, below that for tar evolution.

In this paper, to clarify the effects of hydrogen bonding interaction on the associated molecular structure of Loy Yang brown coal, the devolatilization of the coal subjected to modification of hydrogen bonding interaction with lithium iodide doping have been investigated by means of a thermogravimetric analysis (TGA), a high temperature electron paramagnetic resonance spectroscopy (HT-EPR) and PMRTA.

EXPERIMENTAL SECTION

Coal Sample and Reagents.

The coal sample used for the present study is Loy Yang brown coal (LY, C;70.6wt%, H;5.0wt%, N;0.8wt%, O+S;23.6wt% diff.). The sample coal was ground to pass through 100 Tyler mesh and dried under a vacuum at 40°C for 24 hours. Methanol (G.R. grade) as a solvent and lithium iodide (G.R. grade) were used without further purification.

Preparation of LiI Doped Coal.

A known amount of lithium iodide (LiI), i.e., 4.17×10^{-3} mol/g-coal, dissolved in methanol was added to dried coal particles. The coal suspension was placed in an ultrasonic bath for 10 minutes and stirred for 2 hours at room temperature. After standing the suspension over night, the solvent was evaporated off. The LiI doped sample thus obtained, was dried under a vacuum at 40°C for 24 hours and then cooled down in a flow of nitrogen.

TGA.

Typically, 10mg of sample in platinum TG cell was placed in a thermogravimetric equipment (ULVAC TGD 5000). The sample was heated at 105°C under a flow of nitrogen for 2 hours to remove moisture. TG curves of the sample were measured at a heating rate of 5°C/min up to 500°C in a flow of nitrogen. For kinetic studies, the sample removed moisture at 105°C was heated at a rate of 200-400°C/min to a prescribed temperature of 200-400°C and kept at final temperature for 30 minutes.

HT-EPR.

The sample in a HT-EPR quartz tube of 6mm o.d. was inserted directly into a cavity where the sample was heated at 105°C in a flow of nitrogen to remove moisture. The variation in EPR spectra was monitored with a Varian E-109 EPR spectrometer equipped with a cylindrical high temperature cavity (Micro-device Co.Ltd.) in a flow of nitrogen at a heating rate of 5°C/min. The details of the HT-EPR operation have been reported previously [17].

PMRTA.

For a PMRTA experiment, 500mg of sample was contained in a 10mm o.d. glass tube and dried at 105°C in a flow of nitrogen prior to analysis with PMRTA. The solid-echo pulse sequence (90°x-t-90°y) was used to generate ¹H-NMR transverse magnetization signal. The solid-echo signal, I(t), was recorded at regular intervals (1-2 minute) while the sample was heated from room temperature to 500°C at a rate of 4°C/min in a flow of nitrogen. The details of PMRTA operation have also been reported previously [17].

RESULTS AND DISCUSSION

TGA Studies

The effects of LiI doping on the devolatilization properties of Loy Yang brown coal (LY) were investigated with TGA. TGA curves for LY and LiI doped LY (LILY) are shown in Figure 1 where the weight loss of coal sample is expressed on an ash and LiI free basis. The weight loss of LY starts at about 200°C, and increases gradually with increasing temperature. LILY always shows higher weight loss than that for LY over the range of measurement temperatures. The weight loss of LY increases from 25wt% to 44wt% at 400°C with LiI doping.

In Figure 2, the variation in the differential weight loss curves, i.e., the rates of volatile matter evolution, for LY and LILY are plotted as a function of temperature. The rate of evolution for LY monotonously increases, and reaches a maximum value at 400°C. In contrast, the rate for LILY increases immediately at the initial stage of heating. These results indicate that LiI doped in LY enhances the evolution of volatile matter at lower temperatures. It should be noted that the temperature at which the maximum rate of

volatile matter evolution is obtained shifts down from 400°C to 250°C with LiI doping and the temperature for LILY seems to be much lower than that of thermal decomposition and cleavage of cross-linkage structure in the coal.

For kinetic analysis of the devolatilization, a systematic series of experiments were carried out on change of the yields of devolatilization products (weight loss), Y , with time, t , at different temperature. Considering the appreciable and rapid decrease in the weight of coal, the reactions in early stage appear to proceed mainly with evolution of volatile matter. Figure 3 shows a typical result of analysis where $\ln(1-Y)$ are plotted against t assuming a first-order irreversible reaction. In the figure, straight line can be seen within the first 1 minutes, implying that evolution of volatile matter in the early stage can be described by a first-order irreversible reaction.

The first-order reaction rate constant, k , for evolution of volatile matter was obtained analyzing data of Y at different time and temperature for LY and LILY. The Arrhenius plots of these reaction rate constants are shown in Figure 4. It is seen that k 's for LILY is higher than k for LY within the present range of reaction temperature, reflecting the promotion of volatile matter evolution by LiI doping. The activation energy, E , for LILY (34.3kJ/mole) is found to be appreciably smaller than that for LY (50.3kJ/mole). This less temperature-sensitive devolatilization may be attributed to the modification of associated molecular structure of the coal with LiI doping

HT-EPR Studies

The spin concentrations for LY and LILY were monitored by using HT-EPR. With HT-EPR technique, relatively stable radicals are detected, such as stable π and/or s radicals with relatively long life. As shown in Figure 5, the spin concentration for LY starts to increase at about 170°C and increases drastically beyond 380°C. The drastic increase in the spin concentration observed beyond 380°C in LY may be attributed to the increase in stable π and/or s radicals produced with thermal decomposition and cleavage of cross-linkage structure during heat treatment [18]. For LILY, however, the spin concentration remains almost constant at temperature below 350°C, where marked increase in weight loss is seen. A drastic increase in the spin concentration similar to that for LY is seen beyond 380°C. This result suggests that the reaction mechanism for weight loss for LILY at lower temperature is somewhat different from that for LY and evolution of volatile matter at lower temperature proceeds without thermal decomposition and cleavage of cross-linkage structure. Since the temperature at which LILY gives the maximum evolution rate is much lower than usual pyrolysis temperature, the enhancement of devolatilization at lower temperature, therefore, might be resulted from the evolution of volatile matter which linked physically and/or noncovalently to the coal.

PMRTA Studies

Residual Hydrogen

The PMRTA technique was employed to elucidate the effects of LiI doping on the thermal transformation behaviour of LY. The initial amplitude of solid-echo signal, $I(0)$, is closely proportional to the hydrogen content in the specimen. Therefore, the variation in $I(0)$ plotted in Figure 6 is akin to that of weight loss (TG curves) in Fig. 1. For LY, $I(0)$ decreases rapidly as heating above 350°C relative to the decrease in weight loss. This fact means that disproportionation of hydrogen in the specimen occurs at this temperature range. From the HT-EPR study, the disproportionation is considered due to the evolution of hydrogen rich compounds, such as methane and water, produced by the thermal decomposition and cleavage of cross-linkage structures. The variation in $I(0)$ for LILY is nearly in accordance with that in the weight loss at temperatures below 350°C (Fig.1), where a significant increase in volatile matter was observed. Thus, it appears that the composite of volatile matter evolved at lower temperature (<350°C) is analogous to that of parent coal (LY). The disproportionation is seen to occur slightly above 350°C.

Mobile Remaining Hydrogen

The separation of the solid-echo signals permits hydrogen-weighted mobile and rigid fractions of the molecular structure in coal [17]. The fractions of remaining hydrogen in mobile structures, H_m , on the

basis of the initial amplitude of signal are plotted in Figure 7 against temperature. H_a for LILY is high even at the initial stage of heating, increases with temperature, and then reaches a maximum value at about 150°C. On further heating, H_a maintains the high value up to 400°C where evolution of volatile matter occurs. The result indicates that the LiI doping increases the fraction of mobile structures in LY and keeps it at the higher level up to 400°C. H_a for LY shows a maximum value at about 320°C, and then decreases rapidly on further heating. For LY, the drastic increase in the spin concentration (>380°C) and the rapid decrease in $I(0)$ (>350°C) were observed at a higher temperature range. The rapid decrease in H_a , therefore, could be attributed not only to the evolution of volatile matter, but also to the condensation and recombination reactions, which follow the thermal decomposition and cleavage of cross-linkage structures in coal.

CONCLUSIONS

1. Devolatilization of LY is enhanced with LiI doping at lower temperature range (<300°C).
2. The activation energies for the devolatilization decrease with LiI doping. This less-temperature sensitive devolatilization may be attributed to the modification of associated molecular structure of the coal with LiI doping.
3. The devolatilization enhanced with LiI doping proceeds without thermal decomposition and cleavage of cross-linkage structure.
4. The doping LiI increases the fractions of mobile structure, and also enhances the mobility of LY molecule.
5. During heat treatment, LiI maintains the enhanced molecular mobility resulting in an increase in the evolution of volatile matter.

ACKNOWLEDGMENT

H.K. gratefully acknowledge the financial support of Ministry of Education, Science and Culture, Japan (Japan-Australia Joint Research Program, No. 06044017, Coordinator: Prof. Y. Nishiyama of Tohoku University).

REFERENCE

- (1) Painter, P.C.; Sobkowiak, M.; Youtcheff, J. *Fuel* 1987, 66, 973
- (2) Brenner, D. *Fuel* 1984, 63, 1324
- (3) Brenner, D. *Fuel* 1985, 64, 167
- (4) Larsen, J.W.; Green, T.K.; Kovac, J. *J. Org. Chem.* 1985, 50, 4729-4735
- (5) Cody, G.D.; Larsen, J.W.; Siskin, M. *Energy Fuels* 1988, 2, 340
- (6) Aida, T.; Fuku, K.; Fujii, M.; Yoshihara, M.; Maeshima, T.; Squires, T. *Energy Fuels* 1991, 5, 79-83
- (7) Carlson, G.A. *Energy Fuels* 1992, 6, 771
- (8) Kumagai, H.; Nakamura, K.; Sasaki, M.; Yoneda, J.; Sanada, Y. *Proc. Int. Conf. Coal Sci.* 1993, Vol. 1, 136
- (9) Wolfs, P.M.J.; van Krevelen, D.W.; Waterman, H.I. *Fuel* 1960, 39, 25
- (10) Suuberg, E.M.; Lee, D.; Larsen, J.W. *Fuel* 1985, 64, 1668
- (11) Suuberg, E.M.; Unger, P.E. Larsen, J.W. *Energy Fuels* 1987, 1, 305
- (12) Solomon, P.R.; Hamblen, D.G.; Carangelo, R.M.; Serio, M.A.; Deshpande, G.V. *Energy Fuels* 1988, 2, 405
- (13) Solomon, P.R.; Serio, M.A.; Deshpande, G.V. Kropo, E. *Energy Fuels* 1990, 4, 42
- (14) Ibarra, J.V.; Moliner, R.; Gavilab, M.P. *Fuel* 1991, 70, 408
- (15) Sakurovs, R.; Lynch, L.J.; Maher, P.; Banerjee, R.N. *Energy Fuels* 1987, 1, 167
- (16) Lynch, L.J.; Webster, D.S.; Sakurovs, R.; Barton, W.A.; Maher, P. *Fuel* 1988, 67, 579
- (17) Sanada, Y.; Lynch, L.J. In *Magnetic Resonance of Carbonaceous Solids*; Botto, R.E.; Sanada, Y., Eds.; ACS Symposium Series 229; American Chemical Society: Washington, DC, 1993; 139
- (18) Petrakis, L.; Grandy, D. In *Free radicals in Coals and Synthetic Fuels*; Coal Science and Technology Series No. 5; Elsevier: Amsterdam, Netherlands, 1983; 71

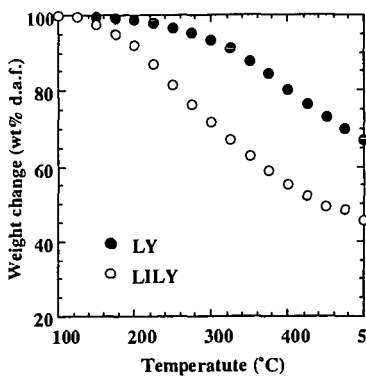


Figure 1. Effects of LiI doping on the devolatilization properties of LY

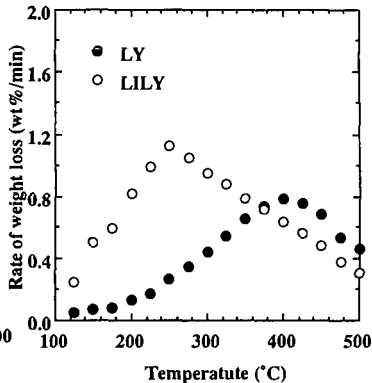


Figure 2. Differential weight loss curves for LY and LILY

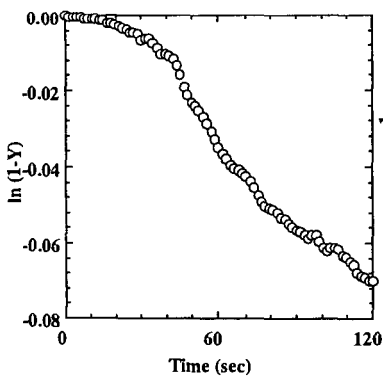


Figure 3. Variation of $\ln(1-Y)$ against reaction time for LILY at 250°C

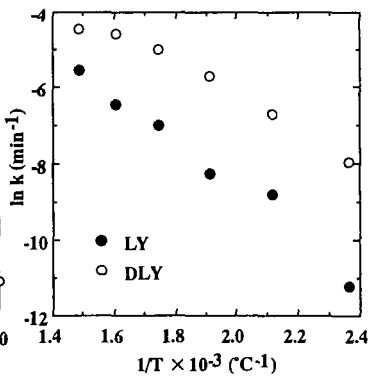


Figure 4. Arrhenius plots of weight loss rate constants for LY and LILY

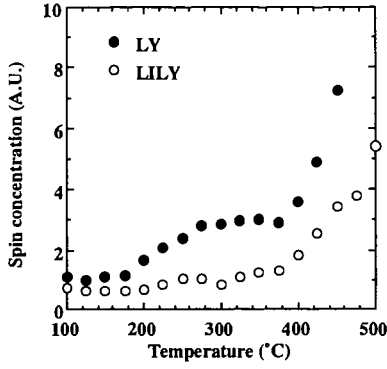


Figure 5. Variation in spin concentration for LY and LILY

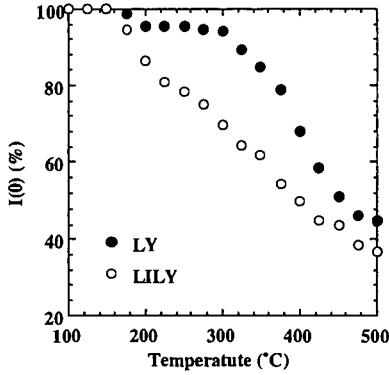


Figure 6. Residual hydrogen, $I(0)$, pyrograms derived from PMRTA data for LY and LILY

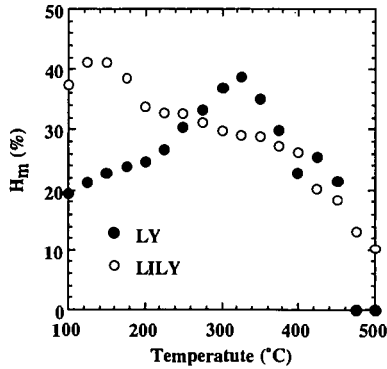


Figure 7. Mobile remaining hydrogen, H_m , pyrograms derived from PMRTA data for LY and LILY

COAL; CROSS-LINKED NETWORKS OR ASSOCIATED STRUCTURES?

Paul Painter, Maria Sobkowiak and Mike Coleman

Polymer Science and Engineering Program
Penn State University
University Park, PA 16802

Introduction

For many years the "standard model" for coal structure has essentially considered most coals to consist of covalently cross-linked networks with a cross-link density and "sol" fraction that varies systematically with rank (this model excludes anthracites and high rank coals that are more graphitic in their structure). Recently, this view has been challenged on a number of grounds. One view, based on some seminal and very important experiments on the mechanical response of swollen coal particles, is that coal is indeed a macromolecule but the network essentially consists of entangled rather than covalently linked chains (1). We have remained somewhat skeptical of this model because it would suggest that there should be a solvent that could completely dissolve coal. More on this later. Another fairly recently proposed model considers coal to be an associated structure, held together by secondary forces acting in some undefined cooperative manner (2-6). Although space in this preprint does not allow us to fully review the evidence for this view, it is largely based on three lines of evidence

1) There is a solvent induced association that occurs upon soaking in organic solvents 2) There is an increase in extraction yields using certain mixed solvents 3) Experiments involving the swelling of extracts compared to the swelling of residues

The latter experiments have been largely interpreted in terms of secondary forces such as hydrogen bonds acting as cross-links, thus by extension indicating that the parent coal itself may be held together by such forces.

We have addressed this latter point in a note (7). If, for example, one were to take a pyridine soluble extract and then try to swell it in pyridine, one would not get any useful result, because the extract would simply redissolve. In this type of work the extracts are placed in contact with a *poor solvent*, like benzene or methanol. The phase behavior of such mixtures is such that there will be a solvent rich phase (e.g., benzene with some dissolved extract) and a solvent poor phase (a "swollen" extract rich phase). It is not our intention in this paper to rehash this issue but to consider some of the other evidence that has been cited as favoring an associated structure. Some recent work in the polymer literature will also be discussed because of the light it throws on what role secondary interactions can play in terms of forming crosslinks.

Solvent Soaking and Extraction of Coal

Nishioka (2-5) has argued that the evidence for associative equilibria in coal has not been fully recognized. The basis for this view is the change in extraction yields upon pre-soaking in pyridine (or other solvents) and the enhanced yields obtained in multi-step extraction. These experiments, however, are seriously flawed. Take, as an example, the soaking experiments. A coal is soaked in pyridine for various periods of time. The pyridine is evaporated and the treated coal is washed with methanol. This coal is then Soxhlet extracted with pyridine. The yield of soluble material obtained in this latter step is found to be less than the yield obtained by Soxhlet extraction of the original untreated coal. It is then argued that there is some solvent induced conformational change that results in the coal being more "associated" than the original structure.

We have repeated these experiments with an Illinois #6 coal and obtained very similar results. We found 20.1% of the weight of the original coal could be extracted with pyridine (the residue accounted for 80.7 wt%, giving a total of 100.8% because of tightly bound residual pyridine). The pyridine soaked coal only gave an extraction yield of 16.9%, however, an apparently significant reduction. The problem is that Nishioka ignored the material that dissolves in the methanol washing step, which accounts for 2.8% of the original coal, giving a total extraction yield of 19.7%, within error of the extraction yield of the original coal. Of course methanol by itself does not extract appreciable amounts of soluble material from the original coal, but this is because it does not swell the coal to any detectable amount, so that low molecular weight material that may be soluble remains trapped in the network. Upon treating with pyridine, soluble material is extracted from the coal particles into the solvent phase and upon evaporation of solvent this material remains sitting on the surface of the coal particles. A portion of this, probably the low molecular weight end, can then be dissolved in the methanol wash step. In other words, the arguments concerning the effect of soaking immediately collapse once a complete mass-balance is performed.

The evidence concerning multi-step extraction is similarly flawed. For example, Nishioka asserts, with no evidence, that covalent bonds are not broken in these experiments. However, reactive solvents, such as phenol at 180°C, are used! At these temperatures phenol can break ether linkages.

Experiments involving mixed solvents, particularly the CS₂/NMP mixture used by Iino and co-workers (8), provide far more compelling evidence that many coals have a much larger soluble fraction than originally suspected. This does not mean that they are associated structures simply held together by secondary forces, however. Figure 1 shows the extraction yields obtained from just U.S. Eastern and Interior coals (we have found in previous work that comparing coals from similar sources gives superior correlations). In this figure the yields obtained using a CS₂/NMP mixture are compared to pyridine extraction yields as a function of coal rank. The first thing to note is that many samples of equivalent rank give comparable yields. However, a large proportion gave significantly high yields, the largest being an Upper Freeport Coal giving a 54% extraction yield in CS₂/NMP. (Iino et al (8) also reported a Zao Zhuang coal that gave a 65% extraction yield). As we mentioned above, this does not mean that these coals are purely associated structures. At the gel point in the formation of polymer networks only about 16% of the material (by volume) needs to be in the "gel" or network phase to give a continuous structure, the rest can be the "sol" or soluble phase (9,10). Furthermore, it would not be surprising, giving the heterogeneous character of coal, that a few coals are indeed significantly different in their structure to most of their counterparts, being largely soluble in the appropriate solvents. Finally, there are other compelling reasons to believe that coal is not a collection of relatively small molecules held together by secondary forces such as hydrogen bonds and these relate to the nature and character of these interactions.

The nature of cross-linking and cooperative processes in physical gels

There are various types of cross-links that can exist in networks. It is useful to subdivide these into two categories, "point" cross-links and junction zones. In the first category are covalent cross-links, entanglements and specific interactions such as hydrogen bonds. The first of these, covalent linkages, can be considered "permanent", in the sense that if we confine our experiments to conditions of temperature, stress, etc., where bond rupture does not occur, then they confer certain elastic properties on the network (e.g., reversible deformation). Entanglements and non-covalent linkages are dynamic, so that in the "melt" or liquid state (i.e., above the T_g of the system), they have a "lifetime" or, more precisely, there is a relaxation time associated with their behavior. Thus under fast loads a non-covalently cross-linked polymer like "silly putty" behaves elastically, because the rate of loading is much faster than the "disentanglement" time. Under slowly applied loads the material deforms permanently, because the chains have time to disentangle.

This brings us to secondary interactions such as hydrogen bonds; can they act as crosslinks? We have to be careful about semantics here. Of course, there is a "network" of hydrogen bonds in materials such as coal, but in order for them to act as cross-links they must maintain their integrity during the course of a deformation experiment (e.g., swelling), thus causing the interlinked segments to be displaced in such a way as to maintain a certain spatial relationship with respect to one another (i.e., there are configurational constraints relative to a non cross-linked system). As with entanglements, this comes down to the dynamic properties of the cross-link relative to the time frame of the mechanical experiment. For small molecules in the liquid state the lifetime of hydrogen bonds appears to be in the range 10⁻⁵ to 10⁻¹¹ secs, much too short to act as a cross-link. In macromolecular systems the dynamics of the hydrogen bond can be coupled to those of the chain, so that the situation may be very different. The work of Stadler and co-workers (11-13), however, demonstrates unequivocally that at temperatures well above the T_g the lifetimes are still very short (~ 10⁻³ to 10⁻⁶ secs, depending on the experiment).

Stadler and his group have published an extensive body of work concerning the effect of hydrogen bonds on mechanical and rheological properties. They introduced urazole groups, which form hydrogen bonded pairs with an enthalpy of about -7 kcal/mole (i.e., somewhat stronger than most of the hydrogen bonds found in coal), into various elastomers and compared properties to those of the unmodified rubbers. The transient network formed by the hydrogen bonds was found to affect viscoelastic properties through an apparent increase in the viscoelastic effective molecular weight, but the equilibrium network modulus remained unaffected (i.e., the hydrogen bonds were not behaving like covalent cross-links). In a theoretical analysis Leibler et al. (14) demonstrated how the properties of these transient networks depend upon the dynamics of the hydrogen bonded complex. At frequencies that are higher than the characteristic frequency of the complex, the hydrogen bond acts like a covalent cross-link, but at lower frequencies they hydrogen bonds simply retard the terminal relaxation. However, as a system is cooled through the T_g there is a point where the dynamics are such that a hydrogen bond could act as a cross-link (11-13).

Now we must consider the implications of this work for coal extraction and swelling. The quantity we work with is the change in free energy of the swollen coal/solvent gel relative to that of the initial pure coal and pure solvent. The initial coal is a glassy solid. Are the hydrogen bonds and perhaps other interactions acting as cross-links in this state? If we neglect various relaxation processes we can argue that all contacts are essentially frozen in place, so they are all cross-links! What is important is this; we must consider the change in free energy on going to the swollen state. Larsen and co-workers (15,16) have demonstrated that swollen in a good solvent a coal such as Illinois #6 has a T_g of about 210°K, well below room temperature (naturally, we are only discussing coals that are capable of appreciably swelling in a good solvent). In this state point interactions such as hydrogen bonds (and anything weaker such as π - π^* interactions) cannot act

as cross-links in the time-frame of a swelling measurement. Covalent cross-links, however, contribute to the free energy through terms that account for the distribution of chain configurations between cross-link points and the distribution of cross-link junctions over the volume of the swollen gel relative to volume of the initial coal (at least in the Flory model). In other words, it is only those contacts that are crosslink points or junctions in both the original pure coal and the swollen coal gel that determine the free energy change. Other types of contacts contribute to the free energy through mixing terms, where a proportion of coal/coal contacts are replaced by coal/solvent contacts to an extent that depends upon composition. We have made this point before, although not in this way, and demonstrated how coal will not swell in a non-hydrogen bonded solvent because the mixing part of the free energy changes are unfavorable, not because the hydrogen bonds act as cross-links (i.e., if the coal and solvent don't mix, the hydrogen bonds don't break!)

This finally brings us to the question of whether secondary forces can act in a cooperative manner to give so-called "junction zones". In various coal papers such cooperative processes are often invoked, but never specified. This should be against the law, because the types of cooperative processes that occur in physical gels are well-known and occur through specific identifiable mechanisms, such as the formation of triple helical regions, as in gelatin; microcrystalline regions, as in poly(vinyl chloride) gels; or by the intersection of a liquid-liquid phase separation and a glass transition, as in polystyrene gels formed upon cooling certain solutions (see reference 17). These processes are all subject to physical characterization and detection. If cooperative processes are to be invoked in coal, their nature must be specified, together with the evidence leading to this conclusion, otherwise we are left with the "standard model"; coal is a covalently cross-linked network.

Acknowledgments

The authors gratefully acknowledge the support of the Office of Chemical Sciences, U. S. Department of Energy, under grant No. DE-FG02-86ER13537.

References

- 1 Cody, G. D., Davis, A. and Hatcher, P. G. *Energy and Fuels*, 1993, 7 455.
- 2 Nishioka, M., Gebhard, L. A. and Silbemagel, B. G. *Fuel*, 1991, 70, 341.
- 3 Nishioka, M. *Fuel*, 1991, 70, 1413.
- 4 Nishioka, M. *Fuel*, 1992, 71, 941
- 5 Nishioka, M. *Energy and Fuels*, 1991, 5, 487.
- 6 Takanoashi, T., Iino, M., and Nishioka, M. *Energy and Fuels*, 1995, 9, 788
- 7 Painter, P. C. *Energy and Fuels*, 1992, 6, 863.
- 8 Iino, M., Takanoashi, t., Ohsuga, H. and Toda, K. *Fuel*, 1988, 67, 1639.
- 9 Flory, P. J. *Principles of Polymer Chemistry*. Cornell University Press, 1951.
- 10 Zallen, R. *The Physics of Amorphous Solids*. John Wiley and Sons, 1983.
- 11 Muller, M., Kremer, F., Stadler, R., Fischer, E. W. and Seidel, U. *Colloid Polym. Sci.*, 1995, 273, 38
12. Muller, M., Stadler, R., Kremer, F. and Williams, G. *Macromolecules*, 1995, 28, 6942.
- 1 3 Muller, M., Seidel, U. and Stadler, R. *Polymer*. 1995, 36 3143
14. Liebler, L., Rubinstein, M., and Colby, R. H., *Macromolecules*, 1991, 24, 4701
15. Hall, P. J., and Larsen, J. W., *Energy and Fuels*, 1993, 7, 47
16. Yang, X., Silbemagel, B. G., and Larsen, J. W., *Energy and Fuels*, 1994, 8, 266
17. Burchard, W. and Ross-Murphy, S. B. *Physical Networks*, Elsevier Applied Science, London and New York, 1990.

Plot of the extraction yield versus carbon content of coals

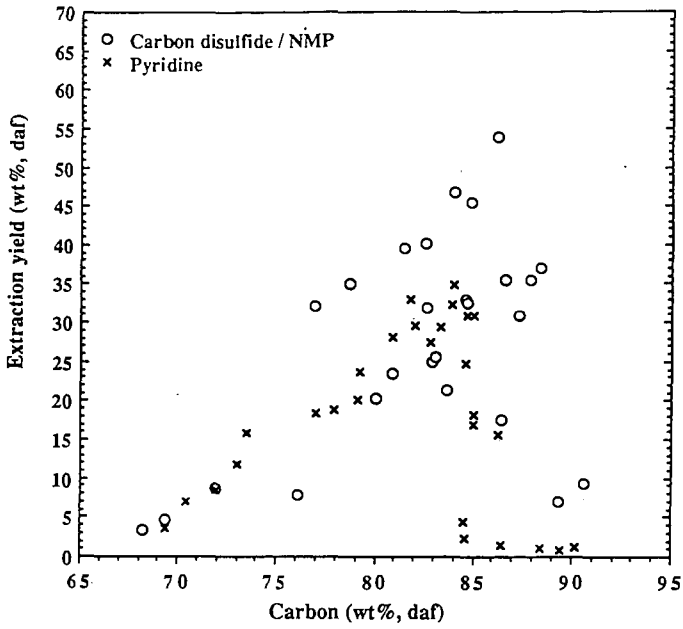


Figure 1.

THE TEMPERATURE DEPENDENCE ON THE STRAIN DYNAMICS OF SOLVENT-DILATED COAL

George D. Cody
Geophysical Laboratory
Carnegie Institution of Washington,
5251 Broad Branch Rd., NW
Washington, DC 20015

Key Words: Coal, Viscoelastic, Solvent Swelling

Introduction

The "rubbery" properties of pyridine dilated coals has been recognized for several decades (1). The physical properties of rubbery materials are related to macromolecular structure. For example, measurement of the time-dependent response of a rubber material to applied stresses is one means of obtaining fundamental information on macromolecular structure, such as short range chain flexibility, and long range network topology (2). Previous work exploring the time-dependent compliance of solvent-dilated coals revealed upon the application of a uniaxial compressive stress, numerous coals exhibited both a reversible, viscoelastic strain and an irreversible, viscous strain (3); the irreversible strain was confirmed with creep recovery experiments. This later observation was unexpected as it requires that the coal macromolecule not be covalently cross-linked. It was further noted, however, that the enormity of the viscous coefficients ($\eta \sim 10^{12}$ Poise), coupled with the relatively short time required to reach steady state compliance indicated a structure composed of highly entangled chains with long chain branches. Thus, although the coals are technically not cross-linked, the very small self diffusion coefficients of the entangled macromolecules preclude extraction over reasonable time scales.

In order to characterize the viscoelastic and viscous behavior further, creep compliance experiments have been applied as a function of temperature. By monitoring the temperature dependence on the various dynamic parameters insight can be gained on the molecular scale features that constitute the building blocks of coals macromolecular structure.

Experimental

A sample of the Illinois No. 6 coal, PSOC 1539 was selected for study. This coal is characterized with 81.9 % C, 5.5 % H, 9.4 % O, 1.4 % N, and 2.2 % S. Sections of vitrain (over 95 % vitrinite) were identified and separated from larger blocks with a wafer saw. Small rectangular blocks were sectioned with dimension on the order of 1 x 2 x 2 mm. The blocks were exhaustively extracted in pyridine prior to analysis. Uniaxial stress ($\sim 0.5 \text{ Kg/cm}^2$) was applied to the sample, strain was measured using a microdilometer employing a linearly variable differential transformer (LVDT). Details on measuring apparatus have been published previously (4). To control temperature, the entire sample holder was placed within a reservoir of pyridine, which was surrounded by an oil bath. Heating tape and a temperature controller were used to establish the temperatures of interest; 25, 50, and 76° C, in this case. During the experiment the inner bath temperature was monitored with a thermocouple; details on the measuring protocol for the variable temperature experiments have been published elsewhere (5).

Results

Figure 1 presents data from a typical creep compliance run. Following the application of uniaxial compressive stress, the swollen coal exhibits a rapid, essentially instantaneous, initial compliance. This evolves into a more gradual viscoelastic compliance spanning several tens of minutes. After approximately 40 minutes the system has reached steady state viscous flow characterized by a constant strain rate. The strain in this during time is totally irreversible. Previous creep experiments were monitored for up to 72 hours. The present experiments were run only long enough to establish steady state deformation.

In general, creep compliance data can be decomposed as the sum of three independent strain components, e.g.

$$J(t) = \frac{t}{\eta} + J_i + \sum_{i=1}^n J_n(1 - e^{-t/\tau}) \quad (1)$$

Where the first term corresponds to viscous strain, governed by the coefficient of viscosity, η ; the second term corresponds to instantaneous compliance, i.e. very high frequency or glassy strain; the third term corresponds to viscoelastic strain in the so-called "transition

zone", i.e. in the frequency range spanning the "glass transition" (2). This final term is expressed as a sum of exponentially relaxing strain elements. In reality, it would be more appropriate to consider a continuous spectrum of relaxation times as opposed to this discrete representation, e.g.

$$\int_0^{\infty} J(\tau_n)(1 - e^{-t/\tau_n}) d\tau \quad (2)$$

The creep compliance, $J(t)$, can be separated into purely viscoelastic and viscous contributions using equation 1, given data that is acquired over a sufficiently long interval of time. Figure 2 presents the purely viscoelastic strain at $T = 25, 50, \text{ and } 76^\circ\text{C}$. The data are normalized to magnitude of the final steady state reversible compliance.

$$\alpha(t)/\alpha_f; \alpha(t) = \Delta L(t)/L; \alpha_f = \Delta L_f/L \quad (3)$$

Each curve is best described by a multiexponential "spectrum" of viscoelastic elements (equation 1 or 2). Significant shifts in the relaxation "spectra" with temperature are clearly evident. One question that arises is whether the different viscoelastic strain elements have the same temperature dependence. For example, a simple chain may exhibit Rouse-like (2) dynamics, where backbone vibrations all contribute to the viscoelastic response. In this case the viscoelastic spectrum is given as proportional to the normal mode frequencies of the coupled oscillators that constitute the simple polymer chain. Of course the temperature dependence of the viscoelastic elements across the frequency spectrum will be the same in such a system. As a consequence of such behavior, each creep compliance curve will be self-similar, when scaled by a time-temperature shift factor a_T^{-1} (6). Indeed, many simple polymers exhibit such behavior.

To test if such behavior is exhibited by the Illinois No. 6 Coal we attempt to scale each curve to match the $T = 76^\circ\text{C}$ viscoelastic curve. We plot the natural log of the shift factors, a_T^{-1} , obtained for the time it takes to reach 50 % and 80 % of the steady state compliance. These are plotted against, $1/T$ (K), in figure 3. If all of the strain viscoelastic strain elements shared the same temperature dependence, then $\ln(a_T^{-1})$ vs $1/T$ for 50% should equal that for 80%. The fact that they do not equate, reveals that viscoelastic elements in different frequency regimes exhibit different temperature dependences. Clearly, the lower frequency modes exhibit a stronger temperature dependence than the higher frequency modes.

This type of behavior has been observed in the case of polymers with side chains, e.g. poly[ethylmethacrylate]. The favored interpretation is that the side chain motion dominates the high frequency, "glassy", deformation, while chain backbone motions dominate the lower frequency, "transition zone", deformation. One can only speculate as to the molecular origin of such variations in the temperature dependence of the viscoelastic properties of solvent dilated coals. It is likely that in place of side chains, oscillations of phenyl groups along the molecular chains within coal may contribute to the high frequency deformation. The lower frequency backbone motion, including the coupled motion of the "virtual" bonds that span the phenyl groups, contributes to the stronger temperature dependence of strain at longer times. This simple picture is complicated, however, by additional factors as described in the discussion section below.

In consideration of the temperature dependence on the viscous deformation it is generally noted that viscous strain (terminal relaxation) follows Arrhenius type behavior, with the temperature dependence being governed by an apparent activation energy given by

$$\eta \propto e^{E_a/RT}$$

Figure 4 presents the viscous coefficients, η , plotted as the natural log of η against $1/T$ (K). Apparent Arrhenius behavior is observed yielding an apparent activation energy of 6.9 Kcal/mol. This value is similar to that of high molecular weight polymer melts and solutions. In general the magnitude of the viscous coefficient in polymeric systems is considered to be related to a molecular friction coefficient (2). Reduction in the molecular friction coefficient with increases in temperature is classically interpreted to be the result of an increase in "free volume" within the system. The viscous data is therefore interpreted to indicate that there is a small positive coefficient of expansion for this solvent dilated coal.

Discussion

At the molecular level, the exact nature of creep in solvent dilated polymers is complex. In general there are two different moduli (both time dependent) that warrant consideration. It is important to recognize the the swelling equilibrium is a balance between

the osmotic stress given by mixing component of the chemical potential and the elastic "pressure" given by the elastic component of the chemical potential (6). Stress applied to one surface of the sample will act with the elastic "pressure" to oppose the osmotic stress leading to compression of the swollen gel through the expulsion of solvent. Calculation of the pure osmotic compressibility for a sample with the dimensions described above, an equilibrium swelling value of $v_2 = 0.42$, and subjected to a uniaxial stress of 0.5 Kg/cm^2 indicates that up to 22 % of the elastic/viscoelastic compliance may be the result of osmotic deswelling.

The osmotic deswelling is clearly time-dependent, subject to requirement that the solvent diffuse out of the network to restore "swelling" equilibrium. The small osmotic strain component corresponds to a 1.4 mol% reduction (calculated) in pyridine. Given that rate of diffusion will be proportional to the chemical potential gradient of solvent inside and out of the network, it is clear that the osmotic deswelling contributes only to the low frequency strain behavior. It is quite possible that the rate of osmotic deswelling is so slow as to be buried within the viscous strain. For example, De-swelling kinetics experiments on similarly sized samples required many hours for full solvent expulsion (7). Additional experiments will need to be run to fully account for the time dependences of the various strain mechanisms. It is clear, however, that the temperature dependence of viscoelastic strain in solvent diluted coals is complex, hence may be some value in characterizing the macromolecular structure of coals.

References

- 1) van Krevelan, Coal, Elsevier Scientific, New York, 1981.
- 2) Ferry, J. D., The Viscoelastic Properties of Polymers; John Wiley & Sons, New York, 1980.
- 3) Cody, G. D., Davis, A., Hatcher, P. G., Energy & Fuels, 7, 455-462
- 4) Cody, G. D., Davis, A., Hatcher, P. G., Energy & Fuels, 1993, 7, 463-468.
- 5) Cody, G. D., Eser, S., Hatcher, P.G., Davis, A., Sobkowiak, M., Shenoy, S., Painter, P. C. Energy & Fuels, 1992, 6, 716
- 6) Flory, P.J., Rehner, J. Chem. Phys., 1944, 12, 412.
- 7) Lei, H., Cody, G. D., French, D. C., Botto, R. E., Hatcher, P. G, Energy & Fuels, 1995, 9, 84

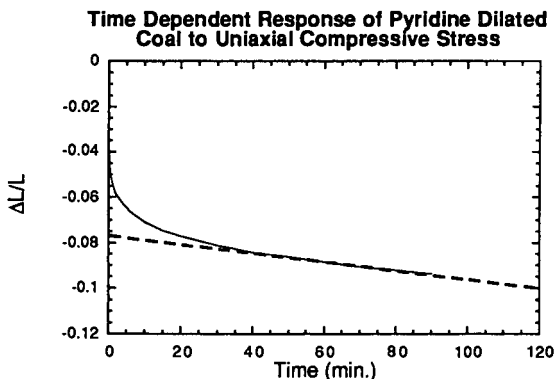


Figure 1: Time dependent Compliance of Solvent Dilated Illinois No. 6 Coal following application of uniaxial compressive stress (-0.5 Kg/cm^2). Rapid (high frequency) elastic strain grades into viscoelastic (Transition zone) strain, followed by purely viscous (terminal zone) strain. The viscous strain is irreversible.

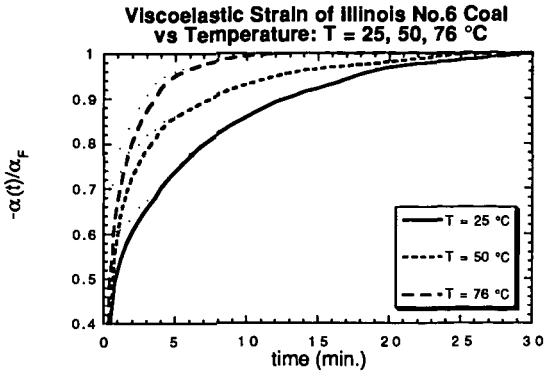


Figure 2: Purely viscoelastic strain (scaled). Temperatures are 25, 50, 76°C. Large shifts towards the higher frequency strain components is clearly evident.

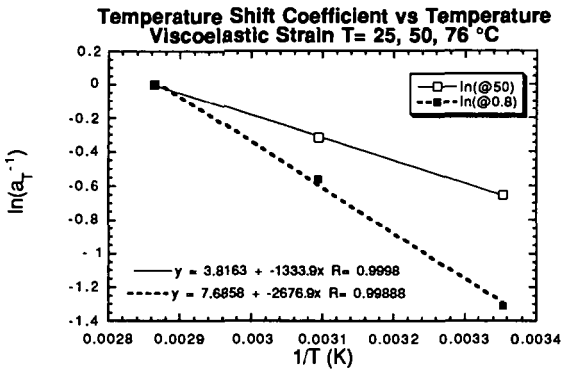


Figure 3: The temperature dependence of the inverse time-temperature shift factor, a_T^{-1} . The different slopes at different extents of total viscoelastic strain reveal that the viscoelastic deformation is not self-similar at different temperatures. The lower frequency modes clearly, exhibit a stronger temperature dependence than the higher frequency modes. This may indicate that different structural elements are dominating different regions of frequency response.

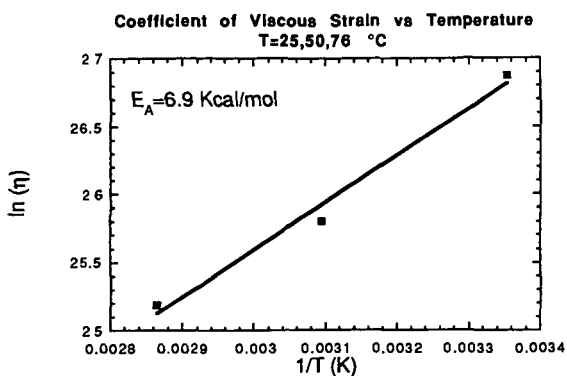


Figure 4: The inverse temperature dependence of the viscous coefficient. The viscosity of polymer/macromolecular melts and solutions typically exhibit Arrhenius type temperature dependences described by an apparent activation energy, E_A . The magnitude of E_A is similar to that of high molecular weight polymer melts, e.g. polyethylene. The positive slope is generally considered to indicate a reduction in the molecular friction factor through a temperature dependent increase in the free volume of the system.

VISCOELASTICITY OF COAL GEL FILMS PREPARED FROM SOLVENT-SOLUBLE CONSTITUENTS OF COALS

Toshimasa Takanoashi, Shigeki Isoda, Satoshi Doi, and Masashi Iino
Institute for Chemical Reaction Science, Tohoku University
Katahira, Aoba-ku, Sendai 980-77, JAPAN

KEYWORDS: Coal, Gel Film, Viscoelasticity

ABSTRACT

A large amount of solvent-soluble constituents of coals were mildly extracted with a carbon-disulfide - *N*-methyl-2-pyrrolidinone mixed solvent at room temperature. Various gel films containing a solvent was successfully prepared by using the solvent-soluble constituents and polar solvents such as *N*-Methyl-2-pyrrolidinone and *N,N*-dimethyl-formamide. A thermomechanical analysis (TMA) of the gel films was carried out and the creep compliance behaviors of the gel films showed the viscoelastic properties, suggesting that the gel films have mainly physical cross-linked networks through coal - coal interaction and coal - solvent interaction, since the solvent-soluble constituents have little original covalent cross-links. When the weight fraction of solvent in the gels was decreased, the viscous strain and the viscoelastic strain decreased, while the elastic strain was almost unchanged, suggesting no participation of a solvent. The network structure of homogeneous coal - solvent gel films and the coal - solvent interactions are discussed.

INTRODUCTION

Coal is considered to have cross-linked network structure consisting of various macromolecules, but the nature of network structure has not been well understood. Recently, it has been reported¹⁻³ that the network consists of physical cross-links through noncovalent interactions between coal molecules, not a covalently bound cross-linked network. The study on viscoelasticity of coal and coal-derived materials is one of the key to clarify cross-link structure of coal. To investigate the elasticity of coal network, coal thin sections were prepared and viscoelasticity of the pyridine swollen coal has been measured by Brenner⁴ and Cody et al.^{1,5} The pyridine swollen coals have been reported^{4,6} to show a rubbery elasticity. However, raw coal contains mineral matter and has a significant amount of pores and cracks on the surface, being liable to influence the measurement of elasticity of coals.

In our research groups, it has been found^{6,8} that by using a carbon disulfide - *N*-methyl-2-pyrrolidinone (CS₂-NMP) mixed solvent 40 wt % - 79 wt % of organic components in coals can be extracted at room temperature. The extract obtained is relatively homogeneous and has no ash.⁹ Since the extraction procedure includes no chemical reaction such as cleavage of covalent bonds in coals and addition reaction of the solvents with coals, the organic constituents originally existing in the raw coals are extracted.^{6,9} Recently, it has been succeeded¹⁰ to prepare gel films by mixing the homogeneous solvent-soluble constituents and polar solvent such as NMP or *N,N*-dimethyl-formamide at room temperature. In the present study, viscoelasticity of the gel films is measured and the network structure is discussed.

EXPERIMENTAL

Sample Preparation.

Upper Freeport coal (Argonne Premium Coal, 86.2 Cwt%) and Zao Zhuang coal (Shan Tong Province in China, 86.9 Cwt%) were used in this study. The coals (-150 μm) were extracted with the mixed solvent under ultrasonication at room temperature. The two bituminous coals have been reported^{6,7} to give the high extraction yields with the CS₂-NMP mixed solvent, 59 wt% (daf), and 63 wt% (daf), respectively. The extract obtained was further fractionated with acetone and pyridine into acetone soluble (AS) fraction, acetone insoluble-pyridine soluble (PS) fraction and pyridine insoluble (PI) fraction under ultrasonication at room temperature. The PS and PI fractions were washed with acetone, while AS fraction was washed with acetone-water mixed solvent to remove the retained solvents. The extract fractions (AS, PS, PI) were dried under vacuum at 80 °C for 12 h. The fractionation procedure and the yields of each fraction of two coals are shown in Figure 1.

Gel Film Preparation.

Approximately 2 mL of solvent was added to 0.1 g of the coal extract fraction and was mixed under ultrasonication. After filtration with a membrane filter (0.8 μm), the solution was placed in a glassware. The solvent in the solution was gradually removed under vacuum at room temperature. At some range of solvent wt % in the mixture, the

mixture became a lustrous gel film. By changing the evacuation time of solvent, the gel films containing different solvent composition (W_s) were prepared. The thickness of the films are the range of 50 μm – 200 μm .

Thermomechanical Analysis.

Viscoelasticity of the gel film was measured by a thermomechanical analysis apparatus (Shimadzu-TMA50). The small section of gel film was placed on the bottom plate. A load (stress) of 1 g was applied to the film section by using a detector bar, and a strain was measured from the decreased thickness of the film. Creep compliance measurements in which constant stress (5 g or 10 g load) was applied to the film, and stress-strain analyses in which the weight of load was changed were carried out.

RESULTS AND DISCUSSION

The Nature of Gel Film.

Figure 2 shows the weight fraction of NMP (W_s) in the Upper Freeport-PS fraction + NMP mixture (UFPS-NMP) when NMP was vaporized under vacuum. The W_s was decreasing with time by vaporization of NMP from the mixture and the slope became small around at $0.35 > W_s > 0.25$. In this range of W_s , it was observed that the mixture became lustrous gel film. For other fractions, PI, AI (PS+PI), the formation of similar gel films was observed, while for AS fraction which is a lighter fraction than the others, the mixture kept pasty even when W_s became little unchanged, i.e., no gel film formation. It has been reported that the AS fraction has lower average molecular weight and lower polar functional groups than other heavy fractions, suggesting that a physical cross-linked network by coal-solvent interaction and coal-coal interaction is important for the formation of gel films.

Creep measurements.

Figure 3 shows the creep compliance behaviors of three gel films with different W_s (0.70, 0.47, 0.30) which were obtained from UFPS-NMP mixture. The load of 5 g applied on the film was kept for 15 min, and then the load was released and the relaxation behavior was also measured. The procedure was repeated three times. In the case of $W_s = 0.70$, the strain was greatly changed with an increase and a decrease in the load, showing the breaking of gel structure due to the stress. The strain is considered to be mainly due to viscous strain by the flow of solvent. On the other hand, for $W_s = 0.47$ and 0.30, in the second and third scans, the reproducible data was obtained. Cody et al. analyzed² the creep compliance behavior of pyridine-swollen coal using a four-element Kelvin-Voigt model, which separates the strain into three strain elements, i.e., instantaneous elastic strain, ϵ_E , time-dependent viscoelastic strain, ϵ_{VE} , which decayed exponentially to a constant strain rate, and irreversible viscous strain ϵ_v , which was linear with time.

We also treated similarly. For the second and third scans for two gel films ($W_s = 0.47$ and 0.30), total strain is represented as the following equation.

$$\epsilon(t) = \epsilon_E + \epsilon_{VE}(1 - \exp(-t/\tau)) + 100\sigma t/\eta \quad (1)$$

where t is time (s), τ is retardation time constant (s), σ is stress (Pa), and η is coefficient of viscosity (Pa s). In the eq. (1), the third term on the right describes viscous strain, $\epsilon_v(t)$. The calculated lines assuming ϵ_E , ϵ_{VE} , ϵ_v , τ and η in the eq. (1), for the second and third scans on the UFPS-NMP gel film ($W_s = 0.30$) are shown in Figure 4. It was found that the calculated lines are well consistent with the experimental points for the both scans. A half of total strain is produced near $t = 0$, i.e., instantaneous elastic strain. The strain at the second scan is more greatly increasing with time than that for the third one. The values of elastic strain, ϵ_E , viscoelastic strain, ϵ_{VE} , and coefficient of viscosity, η , are shown in Table I. For both samples, the changes of elastic strain, ϵ_E and viscoelastic strain, ϵ_{VE} were small between the second and the third scan, while coefficient of viscosity, η greatly increased, showing that the viscous strain is gradually decreasing. In $W_s = 0.30$, the viscoelastic strain and the viscous strain were small, while the elastic strain was a little large, compared to the case in $W_s = 0.47$, suggesting that the elastic strain may originate from physical cross-links through noncovalent interactions between macromolecules in the heavy extract fraction, as well as relatively strong interactions between coal macromolecules and the solvent.

Stress-Strain Curve.

A load was increased from initial 1 g to 10 g at a constant rate, 1 g/min, and then the load was decreased at the same rate. The procedure was repeated several times. The stress-strain curves of UFPS-NMP gel films with $W_s = 0.53$ and 0.30, are shown in Figure 5 and 6,

respectively. Figure 5 shows that the first and the second scan gave a large strain. The first large strain is considered to be attributed to the structural changes by the viscous strain. While after the fourth scan a similar stress-strain curve was obtained, suggesting that the structural changes of gel becomes reversible with repeating the increase and decrease in the stress. Figure 6 shows that the strain change is small compared to that for $W_s = 0.53$ shown in Figure 5. This result suggests that the gel film is more elastic, since the amount of the solvent is small and relatively strong interactions must have still remained in the gel film, resulting in the large contribution of the elastic component.

CONCLUSIONS

Homogeneous gel films containing no mineral matter could be prepared from the mixture of the solvent-soluble constituents with polar solvents such as *N*-methyl-2-pyrrolidinone and *N,N*-dimethyl-formamide. It is suggested that the gel films have physical cross-linked networks through coal-coal interaction and coal-solvent interaction, since the solvent-soluble constituents themselves have little extended covalent cross-links. When the weight fraction of solvent in the gels was decreased, the viscous strain and the viscoelastic strain decreased, while the elastic strain was almost unchanged. It was found that a similar stress-strain curve is obtained after several cycles of the increase and decrease in the stress, indicating that a constant structural change with changing the stress occurs.

ACKNOWLEDGMENT

This work has been carried out as one of "Research for the Future" project of the Japan Society for the Promotion of Science (JSPS) through the 148 committee on coal utilization technology of JSPS.

REFERENCES

1. Cody, G. D. J.; Davis, A.; Hatcher, P. G. *Energy Fuels* **1993**, *7*, 463.
2. Fujiwara, M.; Ohsuga, H.; Takanohashi, T.; Iino, M. *Energy Fuels* **1992**, *6*, 859.
3. Takanohashi, T.; Iino, M.; Nishioka, M. *Energy Fuels* **1995**, *9*, 788.
4. Brenner, D. *Fuel* **1985**, *64*, 167.
5. Cody, G. D. J.; Davis, A.; Hatcher, P. G. *Energy Fuels* **1993**, *7*, 455.
6. Iino, M.; Takanohashi, T.; Ohsuga, H.; Toda, K. *Fuel* **1988**, *67*, 1639.
7. Takanohashi, T.; Iino, M.; *Energy Fuels* **1990**, *4*, 452.
8. Iino, M.; Takanohashi, T.; Ohkawa, T.; Yanagida, T. *Fuel* **1991**, *70*, 1236.
9. Iino, M.; Takanohashi, T.; Obara, S.; Tsueta, H.; Sanokawa Y. *Fuel* **1989**, *68*, 1588.
10. Iino, M.; Watanabe, H.; Takanohashi, T. *Inter. Conf. Coal Sci.*, Oviedo, **1995**, vol. 1, p.59.

Table 1 The Values of Elastic Strain(ϵ_E), Viscoelastic Strain(ϵ_{EV}), and Viscosity (η)

	$W_s = 0.30$		$W_s = 0.47$	
	second	third	second	third
ϵ_E (%)	0.55	0.53	0.47	0.43
ϵ_{EV} (%)	0.08	0.06	0.13	0.13
$\eta \times 10^{10}$ (Pa s)	11.3	19.0	5.0	8.5

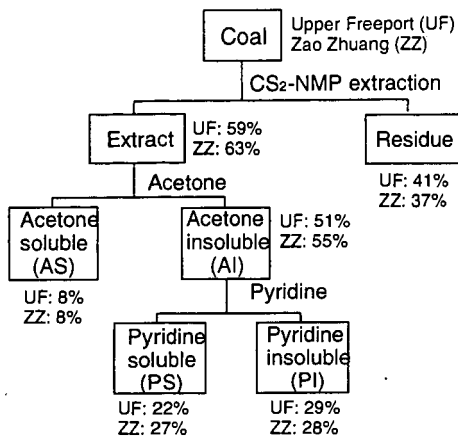


Fig.1 Extraction and Fractionation Procedures

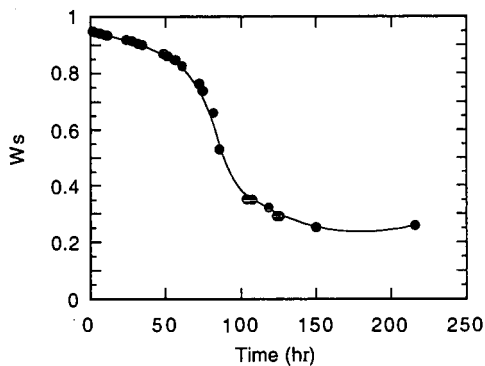


Fig.2 Weight Fraction Change of UFPS+NMP under vacuum at room temperature

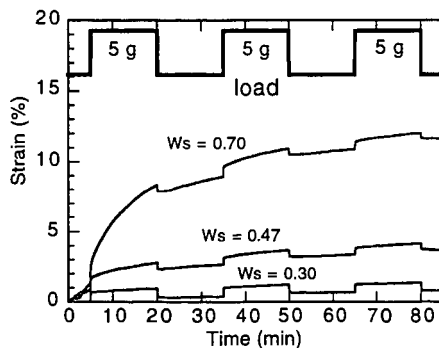


Fig.3 Creep Compliance of UF-PS - NMP gel: (Ws = 0.30, 0.47, 0.70)

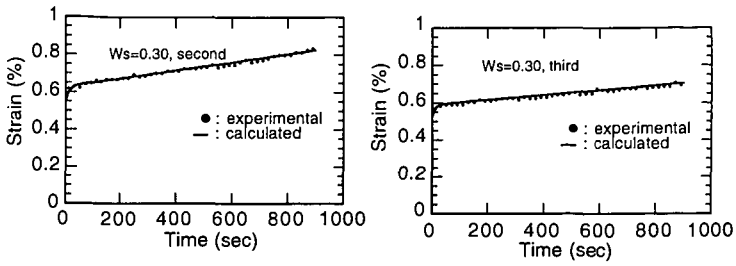


Fig.4 The Fitting Curves for the Second Scan (a) and the Third Scan (b) of Creep Compliance of UFPS - NMP Gel ($W_s = 0.30$)

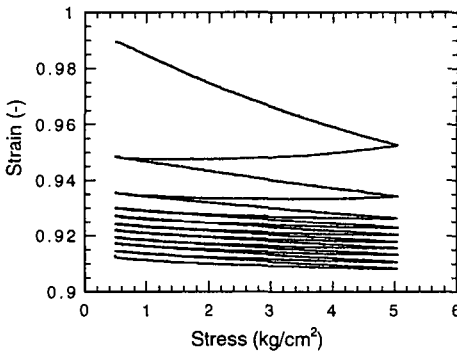


Fig. 5 The Stress-Strain Curve of UFPS - NMP Gel Film ($W_s=0.53$)

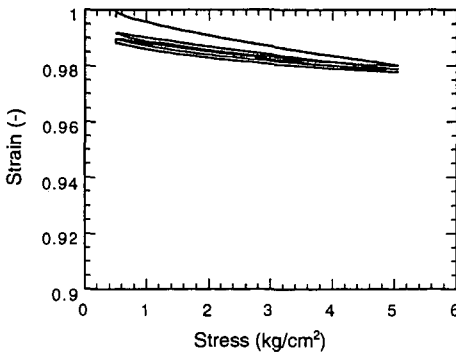


Fig.6 The Stress-Strain Curve of UFPS - NMP Gel Film ($W_s=0.30$)

DIFFUSION RATES OF ORGANIC SOLVENTS IN COALS: ACTIVATION ENERGIES

Yoshinobu Otake and Eric M. Suuberg
Division of Engineering
Brown University, Providence, RI, 02912

Keywords: Coal, Diffusion, Swelling

INTRODUCTION

Diffusional limitations are of concern in virtually all aspects of coal utilization. As a result, over the last few years there have been a number of studies of the factors that influence diffusion [1-24]. These studies, which have been mostly concerned with transport of solvents through coals, have generally indicated that diffusion in coals is similar in many respects to the diffusion of solvents through glassy polymers. The process of relaxation of coal structure by the solvents plays an important role in determining how fast the coal can take up additional solvent. The rates of solvent uptake are strongly influenced by factors such as the nature of the coal, the size of the coal particles [1], the strength of the solvent [15,17,18], the size and shape of the solvent molecules [7,8, 24], the temperature [5,6,17-19,23], the moisture content of the coal [19], and other features of its pretreatment [9,10,14,19,20,21]. The present paper presents results that shed further light on the role of temperature on the rates of diffusion. This is a key aspect of the process that requires further consideration, since most coal conversion processes are performed at elevated temperatures.

It is important to note at the outset that the diffusional processes that are of concern in this study involve movement of individual molecules of solvent through molecular scale openings in the coal. Thus we are not concerned with diffusion or flow in the macropores of coal, which would generally be much faster processes than those of interest here.

The main experimental method that is applied in this study is solvent swelling of coal. This method has been applied in earlier studies of diffusion in coals [7,8,15,17-21,23,24]. To be useful, this technique requires working with coal-solvent pairs that strongly interact, and that the coal measurably swells. This limited the study to solvents that are strong electron donors [25]. In our particular application of the technique, measurements of the extent of swelling were made manually, *vide infra*, which required at least a few minutes per measurement. This limited the study to systems that did not swell on a timescale faster than a few minutes. The timescale of experiments could be adjusted by variation of either temperature (lower temperatures slowed the process) or particle size (larger particles swelled more slowly). This limited the experimental matrix that could be conveniently studied, but a broad range of conditions was still available, as will be apparent below. It should be noted that the automated techniques for measuring swelling rates [7,8,15,23,24] were considered, but felt to pose certain problems with respect to heat transfer and maintenance of constant packing. The vapor sorption techniques require pre-extraction and corrections for pore filling [3,4,26,27], which made these unattractive for present purposes.

In this paper, discussion is limited to the effects of temperature on the swelling process. The temperature influences not only the kinetics of swelling, but also the nature of the swelling (whether Fickian or non-Fickian).

EXPERIMENTAL

The data were obtained on the coals from the Argonne Premium Coal Sample Program [28]. Since the composition and properties of these coals have been carefully tabulated elsewhere, the information will not be repeated here. To assure uniformity among samples, all were dried for 3 hours at 373 K in vacua. As we have noted before, the effects of drying can be quite significant [19]. Studies of dried coals are nevertheless relevant, both because in practical applications coals are first dried, and because the fundamental phenomena of interest here are not changed in basic nature by the drying procedure (even if the kinetics are affected).

It was learned early in this study that particle size has a significant effect upon the results obtained. One major reason is that if a broad range of particle sizes is employed, packing of fine particles into the interstices between larger particles can cause significantly higher packing of the particles, and

lead to artifacts in the volumetric swelling measurements. Thus efforts were made to always work with relatively well-defined particle size fractions, even though the means of the size fractions varied widely from experiment to experiment, for the reasons noted above. When the results are given below, the size fractions will be indicated.

The swelling experiments were performed as described in an earlier paper [17]. The technique involved immersion of the prepared coal samples in pure, reagent grade solvents. The measurements were performed in constant diameter glass tubes of 3 mm inner diameter and about 5 cm in length. After a 30 to 100 mg sample was placed in the tube, it was centrifuged at 7500 rpm for 3 minutes in a 30 cm diameter horizontal rotor centrifuge, to permit accurate measurement of an initial dry packed height of coal. Solvent, prewarmed or precooled as necessary to the experimental temperature, was then added to the tube, and the contents were vigorously stirred with a thin rod. Such stirring is important to prevent the coal from rapidly swelling and forming a solid plug in the tube. The tube was then placed in a thermostatted water bath, for the desired time, and was agitated as noted during this immersion. The temperature of the water bath was controlled to about 0.1°K.

The coal was then allowed to swell for the desired time, and then was removed from the bath and placed in an ice bath to slow the swelling to a negligible rate. Then the sample was again centrifuged as above, and the height of the column of coal remeasured. The ratio of the swollen height to the initial height is what is reported here as the volumetric swelling ratio. Several different samples were employed to determine the extent of swelling as a function of time, in cases in which the swelling was rapid. It was often necessary during the course of the swelling measurements to change the solvents, as they became visibly extract-laden. This was done by carefully decanting the extract-containing solvents, and replacing with fresh solvents. No attempt was made to pre-extract the coals prior to these measurements, since it was desired that the diffusion rates be studied in what was as close to the virgin coal state as possible, except that the coals were dried.

RESULTS AND DISCUSSION

Effect of Temperature on the Extent of Swelling of Coals

There are two potential effects of temperature on the swelling behavior of coals. Temperature may influence both the ultimate extent of swelling as well as the rate of swelling. Many workers have noted the insensitivity of ultimate swelling ratio on temperature [17, 23, 29]. In the present experiments, we have again confirmed that there is no significant effect of temperature on the extent of swelling, at least in the range from 10 to 60°C. This is understood in terms a near zero enthalpy of swelling near the equilibrium extent of swelling [25]. The near thermoneutrality of the swelling process is what dictates a temperature-independent final equilibrium, which may be easily seen as a consequence of the Gibbs-Helmholtz equation of classical thermodynamics.

It has also been argued that the weak dependence of the extent of equilibrium coal swelling on temperature could be a consequence of a rather special form of the equation describing the partial molar Gibbs free energy of elastic deformation [29]; in this case, the partial molar energy of coal elastic deformation must be temperature independent. The recognized need for inclusion of the combinatorial entropy of mixing raises questions about the validity of this theory, however, since this reintroduces the temperature dependence to the expression governing equilibrium.

It should be noted that there is one report of great sensitivity of the swelling ratio to temperature [1]. The experiments in question were conducted by allowing solvent uptake from a *vapor* phase, as opposed to the *liquid* phase, as in the other studies. In this case, there is always a significant (exothermic) enthalpy of solvent condensation, which dictates that condensation, and swelling, would be less extensive, the higher the temperature.

Solvent Swelling Kinetics

The diffusion of solvents into coals, as governs their swelling, has been noted by virtually all workers to be highly non-Fickian in nature, in many cases. The behavior is often that observed in glassy polymers, and involves "Case II" diffusion, as defined by Alfrey et al. [30]. The Case II situation involves a solvent uptake process which is controlled by the relaxation of the macromolecular network structure, as opposed to diffusion itself. It is characterized by a sharp front separating the swollen and unswollen regions of the coal.

To the extent that solvent swelling is linearly related to mass uptake, it is possible to relate the two

quantities via:

$$M/M_{\infty} = (Q-1)/(Q_{\infty}-1) \quad (1)$$

where M refers to mass uptake of solvent by the coal, Q is the coal's volumetric swelling ratio, and the subscript ∞ refers to the final equilibrium values. The error associated with the neglect of small amounts of empty voidage is generally negligible. Analysis of the nature of the diffusional process has been greatly aided by a simple empirical approach, which relates M/M_{∞} to time [2]:

$$M/M_{\infty} = k t^n \quad (2)$$

where k is a constant related to the rate of swelling, and n is a number that crudely indicates the nature of the diffusion. For nearly spherical particles and for mass uptakes up to about 60% of the equilibrium value, $n = 0.43$ for Fickian diffusion, and $n = 0.85$ for Case II diffusion. Values above $n = 0.85$ are possible, and are termed "super-Case II" [2].

Table 1 gives the results for the Argonne Premium Coal Samples, swollen by pyridine. All results were obtained on particles of 150-212 μm size range, unless noted otherwise. The results show the measured values of the parameter n , as a function of temperature. Generally speaking, the values of n are reasonably constant with temperature, though in two cases, they showed a significant decrease with temperature above 40°C. The values indicate a range of behaviors ranging from clearly Fickian (Illinois No.6) to clearly Case II (or even super-Case II, in Pittsburgh No.8). This range of behaviors is precisely the same as has been recently reported for a suite of British coals [23]. It should be noted that we provide no values for two Premium Sample Coals (Pocahontas and Upper Freeport), because as has been noted earlier, these coals swell to a negligible degree until thermally relaxed at much higher temperatures [21].

Given the values of n from Table 1, it is possible to evaluate activation energies for the swelling process, from:

$$E = -nR \left[d(\ln 1/t_f)/d(1/T) \right] \quad (3)$$

where E is the activation energy, R is the gas constant and t_f refers to the time at a fixed extent of swelling. This definition of activation energy is based upon the rate law (2), and is slightly different from that which we used earlier [17,18]. The values from (3) are more directly comparable with other values recently published [23]. The results for the Argonne Coals are again shown in Table 1. The values range from about 20 to 50 kJ/mol. It may be noted that the coals with the higher rates of swelling (indicated by the time to achieve 50% swelling, t_{50}), generally exhibit lower activation energies for swelling. It is logical to associate a lower energy barrier to swelling with a higher rate. In fact, swelling in the coal with the lowest activation energy, Illinois No. 6, apparently was limited by ordinary Fickian diffusion, though with a reasonably high activation energy of 20 kJ/mol.

Earlier, we reported that low rank coals generally exhibit higher activation energies for swelling than do higher rank coals [18]. The opposite conclusion was more recently presented by another group [23], but they examined a somewhat narrower range of rank. Here, we again see a low rank coal show a high activation energy, but now there is no clear trend with rank. The conclusion is that there is no definite trend of activation energy with rank. The actual rates of swelling were also earlier reported to show no correlation with rank [18, 23]. Again, this is seen to be the case here as well.

There is a strong dependence of activation energy on the nature of the solvent. The results obtained using various solvents to swell the Pittsburgh No. 8 sample are shown in Table 2. It has been earlier concluded that the degree of coal swelling is strongly correlated with the electron donor strength of the swelling solvent [25], or equivalently, the basicity of the solvent [23]. It was also earlier reported that the basicity is an important factor only during initial swelling, prior to initial relaxation of the coal structure [23]. In the case of raw coals it was suggested that the stronger the base, the faster the initial swelling. The results of Table 2 show that there is little correlation of activation energy for swelling of raw coals with basicity alone. Butyl- and hexyl-amines are stronger bases than is pyridine, which is stronger than THF. Recently, this issue was addressed in another similar study with alkyl amines, in which it was shown that activation energy increases with the size of the amine [24], as is seen also in Table 2. The conclusion that both size and electron donor strength need to be considered in predicting activation energies is supported by the present results. The present results, however, suggest that the shape of the molecule has an enormous influence, as the much weaker electron donor THF exhibits an activation energy intermediate between the much larger and stronger bases butylamine and hexylamine. It should be recalled that despite this, THF swells the coal less and much more slowly than either of the two

bases.

We have earlier shown that this Pittsburgh No. 8 coal can be thermally relaxed by heating to 350°C at 8°C/min [20,21]. We explored the swelling kinetics of samples treated in this manner. The results are also shown in Table 2. These results show that the activation energies for swelling are only slightly decreased by the thermal relaxation and that in pyridine, the ultimate degree of swelling is unaffected, but that the rate is slightly increased. In THF, both the ultimate extent and rate of swelling are significantly increased. These pre-pyrolytic effects are a result of relaxation of the structure. The relaxation does not, however, change the activation energy. This appears to suggest that the activation energies for swelling are determined by a relaxation which is distinct from that which is thermally induced, and from its magnitude, might be speculated to be associated with breaking single hydrogen bonding interactions. Hydrogen bonding interactions have long been known to be a key in determining swelling behavior [e.g.,31]. The range of activation energies observed is in the ranges typically reported for hydrogen bonding in coals [e.g., 32,33].

CONCLUSIONS

The swelling kinetics of several raw coals have been examined in various solvents at various temperatures. These data have been examined in terms of apparent activation energies. Both size and shape of the solvent molecules appears to play a role in determining the values, as does the electron donor strength of the solvent. The overall rates of diffusion were naturally lower, the bigger the solvent. There was generally an enormous variability in diffusional/swelling rates, which did not correlate well with coal rank. In cases in which the swelling was relaxation-controlled, the activation energies for diffusion were of the same order of magnitude as hydrogen bonding interactions.

ACKNOWLEDGEMENTS

We gratefully acknowledge the financial support of this work by the U.S. Department of Energy through Contract DE-AC22-91PC91027 and Grant DE-FG22-90PC90308.

REFERENCES

- 1 Ritger, P.L.; Peppas, N.A. *Fuel*, **1987**, *66*, 1379.
- 2 Ritger, P.L.; Peppas, N.A. *Fuel*, **1987**, *66*, 815.
- 3 Peppas, N.A.; Lucht, L.M., *Chem. Eng. Commun.*, **1985**, *37*, 333.
- 4 Barr-Howell, B.D.; Peppas, N. A.; Winslow, D. *Chem. Eng. Comm.*, **1986**, *43*, 301.
- 5 Olivares, J.M.; Peppas, N.A. *Prepr. Pap.- Am. Chem. Soc. Div. Fuel Chem.*, **1990**, *35(2)*, 292.
- 6 Barr-Howell, B.D.; Howell, J.M.; Peppas, N.A. *Thermochim. Acta*, **1987**, *116*, 153.
- 7 Aida, T.; Squires, T.G. *Prepr. Pap.- Am. Chem. Soc. Div. Fuel Chem.*, **1985**, *30(1)*, 95.
- 8 Aida, T.; Fuku, K.; Fujii, M.; Yoshihara, M.; Maeshima, T.; Squires, T.G. *Energy Fuels*, **1991**, *5*, 79.
- 9 Larsen, J.W.; Lee, D. *Fuel*, **1983**, *62*, 1351.
- 10 Hsieh, S.T.; Duda, J.L. *Fuel*, **1987**, *66*, 170.
- 11 Brenner, D.; Hagan, P.S. *Prepr. Pap.- Am. Chem. Soc. Div. Fuel Chem.*, **1985**, *30(1)*, 71, also Brenner, in same volume, p83.
- 12 Maturro, M.G.; Liotta, R.; Isaacs, J.J. *J. Org. Chem.*, **1985**, *50*, 5560.
- 13 Green, T.K.; Kovac, J.; Brenner, D.; Larsen, J.W., *Coal Structure*, R. Meyers, Ed., **1982**, Academic Press, Chapter 6.
- 14 Green, T.K.; Ball, J.E.; Conkright, K. *Energy Fuels*, **1991**, 609.
- 15 Hall, P.J.; Thomas, K.M.; Marsh, H., *Fuel*, **1992**, *72*, 1271.
- 16 Cody, G.D.; Botto, R.E. *Energy Fuels*, **1993**, *7*, 561.
- 17 Otake, Y.; Suuberg, E.M. *Fuel*, **1989**, *68*, 1609.
- 18 Otake, Y.; Suuberg, E.M. *Proc. 1989 Int. Conf. Coal Sci.*, Vol. I, **1989**, I.E.A., p 17.
- 19 Suuberg, E.M.; Otake, Y.; Yun, Y.; Deevi, S.C. *Energy Fuels*, **1993**, *7*, 384.
- 20 Yun, Y.; Suuberg, E.M. *Energy and Fuels*, **1992**, *6*, 328.
- 21 Yun, Y.; Suuberg, E.M. *Fuel*, **1993**, *72*, 1245.
- 22 Cody, G.D.; French, D.C.; Botto, R.E. *Prepr. Pap.- Am. Chem. Soc. Div. Fuel Chem.*, **1994**, *39(1)*, 59.
- 23 Ndaji, F.E.; Thomas, K.M. *Fuel*, **1993**, *72*, 1525 and 1531.
- 24 Ndaji, F.E.; Thomas, K.M. *Fuel*, **1995**, *74*, 842.
- 25 Suuberg, E.M.; Otake, Y.; Langner, M.; Leung, K.T.; Milosavljevic, I. *Energy Fuels*,

- 1994, 8, 1247.
 26 Nelson, J.R.; Mahajan, O.P.; Walker, P.L., Jr. *Fuel*, **1980**, 59, 831.
 27 Nelson, J.R. *Fuel*, **1983**, 62, 112.
 28 Vorres, K. *Energy Fuels*, **1990**, 4, 420.
 29 Cody, G.D.; Eser, S.; Hatcher, P.G.; Davis, A.; Sobkowiak, M.; Shenoy, S.; Painter, P.C. *Energy Fuels*, **1992**, 6, 716.
 30 Alfrey, T.; Gurnee, E.F.; Lloyd, W.G. *J. Poly. Sci.*, **1966**, C2, 249.
 31 Larsen, J.W.; Green, T.K.; Kovac, J. *J. Org. Chem.*, **1985**, 50, 4729.
 32 Glass, A.S.; Larsen, J.W. *Energy Fuels*, **1994**, 8, 284.
 33 Miura, K.; Mae, K.; Takebe, S.; Wakiyasu, H.; Hashimoto, K. *Ener. Fuels*, **1994**, 8, 874.

Table 1- Summary of Swelling Results on Argonne Premium Coal Samples in Pyridine

Coal	Q_{∞}	$T(^{\circ}\text{C})$	$t_{50}(\text{min.})$	n	$k \cdot 10^3$	$E(\text{kJ/mol})$
Beulah-Zap Lignite	2.33	25.8	230.0	0.67	12.7	51.1
		45.8	35.5	0.70	40.2	
		59.5	11.3	0.72	87.8	
Wyodak Subbit.*	2.42	11.9	47.0	0.65	41.5	36.8
		24.2	12.8	0.77	72.8	
		42.1	5.1	0.47	231.4	
Illinois No. 6 hvb*	2.23	11.9	4.5	0.53	206.9	20.1
		24.0	1.7	0.43	378.6	
		44.7	0.7	0.50	588.0	
Blind Canyon hvb*	2.22	11.9	92.0	0.76	16.2	44.9
		24.3	30.0	0.70	47.1	
		42.1	7.3	0.67	129.4	
Lewiston - Stockton hvb	1.94	20.0	41.0	0.67	40.2	37.3
		40.7	9.4	0.77	92.6	
		50.9	5.3	0.70	151.1	
Pitts. No. 8 hvb	2.14	11.7	90.0	1.04	5.0	51.9
		24.1	30.5	0.81	30.1	
		41.0	8.5	0.68	113.4	

* Particle size: 212-300 μm .

Table 2. Swelling of Pittsburgh No. 8 Coal in Various Solvents

Solvent	Q_{∞}	$T(^{\circ}\text{C})$	$t_{50}(\text{min.})$	n	$k \cdot 10^3$	$E(\text{kJ/mol})$
Pyridine (80.9)*	2.14	11.7	90.0	1.04	5.0	51.9
		24.1	30.5	0.81	30.1	
		41.0	8.5	0.68	113.4	
Butylamine (98.8)*	1.93	25.3	16.2	0.82	36.6	22.2
		35.5	10.5	0.90	43.1	
		46.7	8.1	0.85	58.8	
Hexylamine (132.1)*	2.28	25.3	117.0	1.09	2.6	55.0
		35.5	62.0	1.31	2.3	
		46.7	35.2	1.23	6.4	
THF (81.0)*	1.41	24.2	143.0	0.92	5.6	39.3
		34.9	80.0	0.94	8.7	
Pyridine (Heat Treated) ^o	2.18	15.5	35.0	0.79	32.2	48.3
		24.1	15.4	0.94	39.0	
THF (Heat Treated) ^o	1.76	19.1	16.2	0.67	96.1	38.5
		24.2	8.9	0.86	81.1	
		34.9	4.6	ND	ND	
		40.0	3.0	ND	ND	

* Molar volume of solvent, in cc/mol

^o Samples heat treated at 8 $^{\circ}\text{C}/\text{min}$ to 350 $^{\circ}\text{C}$, then quenched

RECENT ADVANCES IN MAGNETIC RESONANCE MICROSCOPY TO THE PHYSICAL
STRUCTURE CHARACTERIZATION OF CARBONACEOUS AND INORGANIC
MATERIALS**

D. M. Gregory, R. E. Gerald, G. D. Cody and R. E. Botto
Chemistry Division
Argonne National Laboratory
9700 South Cass Avenue, Argonne, IL 60439

Abstract

Magnetic resonance microscopy (MRM) techniques have been employed to study the molecular architectures and properties of structural polymers, fossil fuels, microporous carbons and inorganic catalysts.

Keywords: solid state NMR, imaging, microscopy, materials

INTRODUCTION

In recent years, the field of magnetic resonance microscopy (MRM) has been advanced by the introduction of several new experimental techniques for the study of materials [1]. Our research has focused on specific methods that facilitate proton MRM of rigid solids, by utilizing proton multipulse line-narrowing in the presence of high gradient fields [2]. We have also developed new chemical-shift imaging strategies, which have been devised to highlight specific chemistries. We have used these techniques to investigate molecular transport of solvents and gases within polymers, catalysts and coals. Time-sequenced imaging of solvent uptake within macromolecular solids have been used to differentiate between Fickian and anomalous, or Case II, transport processes, analytical solutions to which form the basis of a model yielding information on the nature of transport in these systems, and ultimately, on their molecular architecture [3]. Current research in our laboratory is focussed on MRM to monitor porosities, pore-size distributions and diffusivities of methane and other gases in inorganic catalysts and high surface-area carbons.

In this paper, we highlight three recent developments in our laboratory: Applications to the areas of porosity measurements and the characterization of polymeric materials will be presented.

EXPERIMENTAL

Samples

A porous ceramic catalyst sphere (brand X) approximately 1.6 mm in diameter was prepared by immersing in water for several hours prior to the imaging experiment. The treated sample was then placed in a sealed teflon tube for imaging; the specimen contained 3.2 mg of water or the equivalent of about 10^{20} proton spins. The polymethylsilicone rubber sample was rectangular with initial dimensions of 2 x 2 x 1 mm, and the upper and lower sample surfaces protected from solvent infiltration by glass cover slips.

For chemical-shift imaging experiments, a test phantom was assembled from two concentric tubes: a 5-mm NMR tube was placed inside a 10-mm NMR tube. The inner tube contained acetone ($^1\text{H}\delta_B = 2.1$ ppm) and the annular region contained chloroform ($^1\text{H}\delta_A = 7.3$ ppm). A small amount of relaxation agent added to each solvent reduced the spin-lattice relaxation times by approximately one order of magnitude. The values of τ_{null}^A and τ_{null}^B were determined in a separate experiment by the inversion recovery method and found to be 35 and 50 ms, respectively.

MRM System and Experimentation

The MRM experiments were implemented on a portable, home-built Tecmag system operating at a proton Larmor frequency of 100.2 MHz. The system is capable of operating at frequencies between 50 and 400 MHz. Spectrometer control and data processing were executed by the software program MacNMR operating on a Macintosh Quadra 950 host computer.

The imaging probe having an outside diameter of 70 mm was constructed to fit within the room temperature shim stack of a wide-bore (89-mm) 2.35 T superconducting magnet, and could accommodate samples up to 28-mm in diameter. The design included rf coils for excitation and detection of the nuclear signals, and a set of gradient coils to create orthogonal gradient fields with respect to the three spatial coordinates. To maximize the filling factor of the rf coil and allow for different samples shapes, various coil and resonating structures ranging in diameter from 3-mm to 25-mm were interfaced to the probe. The probe was force-air cooled and was capable of operating with duty cycles in excess of 20% while producing a highly linear magnetic field gradient of up to 58 G/cm over a volume 30 mm in diameter.

MRM experiments were performed on the spherical catalyst specimen using 256 complex data points and a total of 3600 projections (30 θ angles over $\pi/2$ radians \times 120 ϕ angles over 2π radians). A gradient field of 25 G/cm and a sweep width of 60 kHz were employed. A total of 16 scans were collected for each projection using a 90^o-pulse width (4- μ s duration) and a recycle delay time of 1 s, resulting in a total acquisition time of 16 hr.

In order to obtain sufficiently high quality images on the polymethylsilicone rubber specimen, it was necessary to acquire 32 (128 point) transients with a recycle delay of 500 ms for each of 128 phase-encoded gradient positions using a standard imaging spin-echo pulse sequence. This yielded a resolution on the order of 70 μ m, which was obtained over intervals of approximately 30 min. Typically a 64-kHz spectral width was chosen, establishing an echo time of 0.5 ms. Signal-to-noise improvement for the series of phase encoded echos was accomplished by apodization using a biexponential weighting function developed within the Macro subroutine of MacNMR.

RESULTS AND DISCUSSION

Determination of Porosity of Catalysts

In the first application, we have explored the potential of MRM to further the development of advanced formed absorbents and heterogeneous catalyst materials. Formed absorbents and catalyst systems on porous oxide supports are currently in use and are continually being improved in applications involving the production of upgraded hydrocarbon fuels or specialty chemicals. A detailed knowledge of the spatial distribution of the pore network is essential to the evaluation and improvement of catalyst and absorbent performance. MRM, utilizing filler fluids, offers the potential of spatially mapping the porosity of a variety of porous media. With application to spent catalysts, imaging techniques can be utilized to study the chemistry of catalyst coking, and has the ability to detect the spatial distributions of coke and other agglomerates in the pore matrix.

Figure 1 shows sequential 3D surface-rendered images with 20- μ m thick 2D slices displayed of internal portions throughout the catalyst sphere. The MRM experiment required a total of 3600 projections, or about 16 hr. for data acquisition. In this manner, an image resolution of 20 μ m was attained in each of the three spatial dimensions. Some thirty-two 2D image projections of proton spin density (where spin density scales linearly with image brightness) were used to provide estimates of total porosity and spatial distributions of pores throughout the specimen.

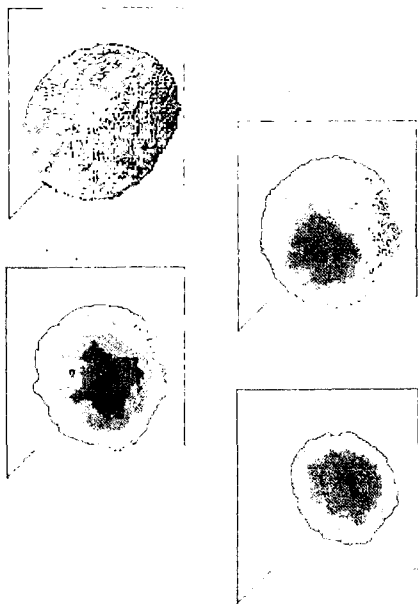


Figure 1. Three-dimensional MRM images of catalyst sphere.

Performing MRM experiments on the catalyst sphere presents the opportunity to discuss the limits of resolution in image reconstruction, on a sample for which the spectral resolution of individual projections is very high ($< 1 \mu\text{m}$) because of its inherently narrow proton linewidth. For example, given our catalyst sample of maximum radius equal to 0.8 mm (a diameter of 1.6 mm), the total number of projections required to obtain an image having a resolution of $20 \mu\text{m}$ is calculated to be 10,953. If lower resolution can be tolerated in the resultant images, the number of projections becomes even more reasonable. In order to achieve a resolution of $40 \mu\text{m}$, for example, the number of projections required is only 3,943. In practice, these numbers can be reduced by a factor of two or three if one employs significant filtering in the reconstruction algorithm. Thus, acquiring 3600 projections for our catalyst specimen is sufficient to achieve the desired resolution provided that appropriate filtering is applied. Finding that an adequate SNR ratio for each projection can be attained in 16 acquisitions employing a 1 s pulse repetition time translates into a total experimental averaging time of about 16 hr.

^{19}F MRM of Solvent Transport In Rubbers

Significant insight into the character of solvent transport has been obtained through time-resolved, ^{19}F NMR imaging of solvent concentration and network dilation changes that occur during solvent uptake within rubbery polymer networks. Complications found in proton NMR imaging experiments, because contributions to the signal intensity can arise from both the protons of the solvent and protons of the mobile polymer backbone, can be averted using fluorinated solvents. In the present study, ^{19}F imaging has been employed to investigate Fickian transport of hexafluorobenzene within a specimen of polymethylsilicone (PMS) rubber.

Sequential 2D ^{19}F images of a specimen of PMS swelling in hexafluorobenzene, observed at early (top), intermediate (middle) and advanced (bottom) solvent diffusion times are shown in Figure 2. Clearly evident is the smooth, exponential, solvent gradients directed into the core of the sample, indicating a Fickian transport mechanism.

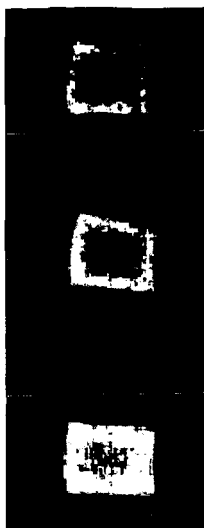


Figure 2. Sequential ^{19}F images of hexafluorobenzene transport in polymethylsilicone.

The measured front velocities from MRM provide a valuable and quantitative constraint for the parameterization of the uptake data. Direct measurement of linear dilation accompanying swelling is a simple means to quantify the overall swelling behavior of rubbery networks. Linear dilation behavior for PMS was consistent with Fickian transport in rubbery networks. Given the uptake data, it was trivial to derive a mass-fixed diffusion coefficient through linear fitting of the experimental data. The generation of a curve for Fickian transport, in the present case, requires solving the two-dimensional diffusion equation and integrating this solution with respect to time. Fitting of the dilation data results in values of $D_R = 1.1 \times 10^{-6} \text{ cm}^2/\text{s}$ for PMS-hexafluorobenzene. These relatively large values of D_R reflect the high degree of inter- and intra-molecular mobility of the network, which explains the rapidity with which the rubbery systems respond to applied stresses that are osmotic in nature.

Chemical-Shift MRM of Binary Systems

In this last section, we present a new method for chemical-shift selective MRM, selective-echo chemical-shift imaging (SECSI), which is easily implemented and can be executed in a short time period ($< 1 \text{ ms}$). The SECSI pulse sequence is designed to select the magnetization from one of two chemical species. Subsequently, this magnetization is used to form a spin-echo in the conventional manner. The magnetization of the second chemical species is initially placed antiparallel to the Zeeman field and is then allowed to decay to zero via T_1 relaxation; therefore, it does not contribute

to the spin-echo. In the simplest case, each chemical species is represented by a single NMR resonance; however, a cluster of closely spaced resonances for each species is also suitable for NMR imaging by the SECSI method. The full Boltzmann magnetization is used for imaging either chemical species; this approach presents an advantage over many other pulse methods. Both chemical species can have any value for T_1 and concentration. Additionally, the method employs only hard pulses of quadrature phase and is easily implemented using standard spectrometer hardware.

The SECSI pulse sequence is a *chemical-shift filter* consisting of two 90° pulses and two delays ($90^\circ_x - \tau_{\text{antiphase}} - 90^\circ_x - \tau_{\text{null}}$) and is executed prior to a standard spin-echo imaging sequence [4]. The RF transmitter is centered on one of the NMR resonances of a two-component system A and B where $\delta_A > \delta_B$. In a reference frame rotating (clockwise) at ω_A (component A on resonance), the magnetization vector for the A spins is stationary, while the magnetization vector for the B spins precesses (counterclockwise) at $\omega_A - \omega_B$. The initial 90°_x pulse tips the magnetization of both components on to the $+y$ axis in the xy -plane. An antiphase period, $\tau_{\text{antiphase}}$, equal to $\pi/(\omega_A - \omega_B)$ is allowed to elapse such that the magnetization vectors from both components become mutually out of phase by 180° . The second pulse, 90°_{-x} , restores the Boltzmann magnetization of component A along the $+z$ axis while inverting the spin population of component B . After an inversion recovery delay, τ_{null}^B , equal to $\ln 2 T_1^B$, the only net z magnetization remaining is that of component A (restored along the $+z$ axis following the second RF pulse). At this point a standard 2D spin-echo imaging pulse sequence is executed, which yields the chemical-shift selective image of component A . The complementary image, the chemical-shift selective image of component B , is obtained by placing component B on resonance and repeating the pulse sequence. The antiphase period remains the same, however, the inversion recovery delay in this case is set to τ_{null}^A , given by $\ln 2 T_1^A$.

The antiphase period, $\tau_{\text{antiphase}}$, defines the duration of the transverse spin evolution within the pulse sequence and, therefore, the time during which T_2^* processes play a role in diminishing the final signal intensity. A general expression for the antiphase period is given by

$$\tau_{\text{antiphase}} = \frac{\pi \times 10^6}{\Delta \gamma_N B_0} \quad [1]$$

where Δ is the separation between the two resonances in parts per million ($\Delta = \delta_A - \delta_B$), γ_N is the gyromagnetic ratio of the nuclear spins ($2.67506 \times 10^8 \text{ rad T}^{-1} \cdot \text{s}^{-1}$ for ^1H), and B_0 is the external magnetic field strength. The antiphase period decreases monotonically for higher field strengths. For systems in which the bandwidths of the resonances are inhomogeneously broadened, the inversion recovery delay following the antiphase period serves a second purpose. Following the second RF pulse, any off-resonance contribution to the magnetization of the species returned to the $+z$ axis will not have been returned completely to the Boltzmann equilibrium position. Therefore, during the inversion recovery delay this off-resonance magnetization recovers towards Boltzmann equilibrium. This added feature of the pulse sequence compensates for effects of the antiphase period, during which the net magnetization may be reduced by the inhomogeneity of the magnetic field, a dispersion of chemical shifts, and spin-spin relaxation.

Figure 3 represents a proton 2D NMR image of the phantom that was acquired by using the conventional spin-echo imaging technique. The central region of this image appears brighter because of the greater concentration of protons in acetone; the proton concentration ratio is 6.54 : 1.00 for acetone vs. chloroform. Although the large difference in proton concentrations provides substantial contrast between the two solutions, one cannot determine from the image alone which regions represent chloroform or acetone *a priori*. The SECSI method was used to selectively image the protons of acetone at ${}^1\text{H}\delta_B = 2.1$ ppm (Fig. 3b) and the protons of chloroform at ${}^1\text{H}\delta_A = 7.3$ ppm (Fig. 3c). In images 3b and 3c there is no ambiguity as to what the bright regions represent, and no inference is necessary to describe the spatial distribution of either chemical species. Furthermore, note the large dynamic range obtained for suppressing the image intensity of the unwanted magnetization.

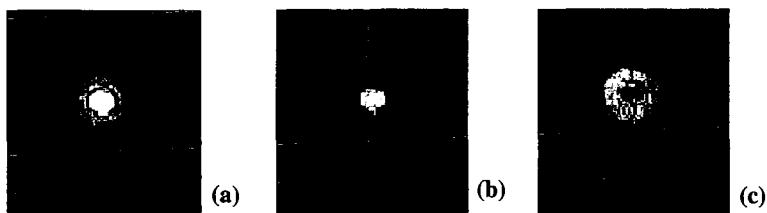


Figure 3. Proton MRM images of acetone-chloroform phantom: (a) conventional 2D spin-echo image; (b) chemical-shift selective image of acetone in the 5 mm NMR tube; (c) chemical-shift selective image of chloroform in the annular region between the 5 and 10 mm NMR tubes.

For systems containing three NMR resonances, representing different chemical species, the SECSI sequence may be applied sequentially to preferentially select one of the chemical species for imaging. The method requires phase cycling to cancel interfering transverse magnetization and can only be executed optimally for certain ratios of the T_1 's. Simultaneous selective excitation and subsequent imaging of two groups of resonances in a complex ${}^{19}\text{F}$ NMR spectrum was effectively demonstrated by Börnert and coworkers [5]. For the ubiquitous cases of water/fat or water/oil systems the SECSI technique offers simplicity, fast execution, and the highest sensitivity.

ACKNOWLEDGMENT

This work was performed under the auspices of the Office of Basic Energy Sciences, Division of Chemical Sciences, U. S. Department of Energy, under Contract No. W-31-109-ENG-38.

REFERENCES

1. "MRI of Materials", R. E. Botto, Ed., *Solid State NMR*, **6**, No. 4 (1996).
2. S. L. Dieckman, P. Rizo, N. Gopalsami, J. P. Heeschen and R. E. Botto, *J. Am. Chem. Soc.*, **114**, 2717 (1992).
3. G. C. Cody and R. E. Botto, *Energy Fuels*, **7**, 561 (1993).
4. S. L. Talagala and I. J. Lowe, *Concepts Magn. Reson.* **3**, 145-159 (1991).
5. P. Börnert, W. Dreher, A. Gössler, G. Klee, R. Peter, and W. Schneider, *J. Magn. Reson.* **81**, 167-172 (1989).

CHANGE IN THE ASSOCIATED MOLECULAR STRUCTURE OF COALS
IN PYRIDINE/CS₂ MIXED SOLVENTS.

H.Kumagai, K.Matuoka, K.Norinaga T.Chiba,
Center for Advanced Research of Energy Technology, Hokkaido
University,
Kita-ku, Sapporo 060, Japan,

M.Sasaki,
Hokkaido National Industrial Research Institute,
Toyohira-ku, Sapporo 062, Japan

Keywords: Swelling, noncovalent interactions, Mixed solvent

ABSTRACT

In order to evaluate noncovalent interactions in coal, change in the associated molecular structure of coals in pyridine/CS₂ mixed solvents have been investigated. For bituminous coal, variation in L-band EPR spectra with mixing ratio of the solvents is in a close correspondence to that in equilibrium swelling ratio and in molecular mobility obtained from ¹H-NMR. The EPR spectra for lignite show similar variation to that for bituminous coal, however, does not correlate with equilibrium swelling ratio and molecular mobility. Since the L-band EPR characteristics appear to reflect the situation of aromatic π - π and charge transfer interactions in coal, these results indicate that swelling in the mixed solvents proceed with the declining of non-covalent interaction, such as aromatic π - π and charge transfer interaction, in coal.

INTRODUCTION

The chemical and physical properties of coal are affected not only with the chemical structure of coal molecules, but also with the associated molecular structure. Coal is believed to be complex macromolecular compounds containing several types of noncovalent interactions, such as hydrogen bonding, van der Waals, charge transfer and aromatic π - π interaction. The type and strength of noncovalent interactions existing in coal have been postulated to govern the associated molecular structure. Since the noncovalent interactions play an important role in the physical and chemical properties of coal, it has become of general interest in recent years.

Larsen and Kovac [1,2] have proposed two components (phase) coal structure model, in which coal consists of two components, i.e., a covalently cross-linked macromolecular network component (MM phase) and a low molecular weight component (M phase) trapped noncovalently inside the network. Based on the two components coal structure model, Marzec and co-worker [3,4] have attempted to elucidate the extraction mechanism of bituminous coal with electron-donor-acceptor interaction between M phase in the coal and solvents. The contribution of noncovalent interactions to cross-linked structure was also suggested from coal swelling and extraction studies [5,6]. While, it was argued that such noncovalent interactions are too weak to form and stabilize the cross-linking structure which affects swelling behaviour of coal [7].

Mixed solvent systems, such as NMP/CS₂ and pyridine/CS₂ have a high potential to get large amount of extracts from many bituminous coals at room temperature [8,9]. Iino and Takanohashi have indicated that no significant reaction between coal and the solvent, which results in an increase of the extraction yields, occur for this extraction [8]. In spite of the extensive studies of swelling and extractability of coal with the mixed solvent systems [10-12], the mechanism of coal extraction and swelling with the mixed solvent systems has not been clarified in detail.

In this paper, in order to evaluate the effects of noncovalent interactions on the associated molecular structure of coals, swelling behaviour of coals in the mixed solvents has been investigated by means of ¹H-NMR relaxation time and L-band EPR spectroscopy. EPR spectroscopy is one of the useful techniques to investigate noncovalent interactions such as aromatic π - π and charge transfer interaction. X-band EPR is, however, not allowed to measure the spectrum of sample in solvents with high permittivity. Thus, we have attempted to build L-band EPR from which favorable results are provided. Measurement L-band EPR for swelling and extraction of coal

may bring deep information about noncovalent interaction in coals.

EXPERIMENTAL SECTION

Coal Samples and Reagents.

Upper Freeport bituminous coal (UF) and Beulah Zap lignite (BZ) were selected from Argonne Premium coal samples and used in this study. Pyridine-d₅ and CS₂ (G.R. grade) for solvent were used without further purification.

Sample Preparation.

Coal sample was dried under a vacuum at 40°C for 24 hours. The dried coal sample was placed in glass sample tube (10mm o.d.). The initial height (h₁) of the coal particle bed was measured by a caliper. The mixed solvent was then poured into the sample tube. The coal suspension was standing for 7 days under nitrogen atmosphere. Swollen coal bed height (h₂) was measured prior to the EPR and NMR measurement. Equilibrium swelling ratio was expressed as the ratio of h₂ and h₁.

¹H-NMR Measurement.

Spin-spin relaxation time (T₂) of the swollen coal sample was measured with JEOL JNM-Mu25 spectrometer (25MHz) employing solid-echo (90°x-τ-90°y) pulse sequence at 20°C under nitrogen atmosphere.

L-band EPR Measurement.

L-band EPR spectra were monitored with a Varian E-109 EPR spectrometer equipped with Micro Device Co.Ltd. MWG-2L L-band microwave bridge and MSC-2LG loop-gap resonator. In order to get the high signal sensitivity, 10mm (o.d.) sample tube was used. The effective portion of sample tube to be irradiated with microwave is 22mm. L-band EPR measurement was carried out at 20°C under nitrogen atmosphere. Spectral intensities of coals in the mixed solvents were corrected by the effects of dielectric characteristics (permittivity) of solvents and density decrease of coal particles due to swelling.

RESULTS AND DISCUSSION

Equilibrium Swelling Ratio

The equilibrium swelling ratio of UF and BZ in the mixed solvents are shown in Figure 1 and 2 as a function of mixing ratio of pyridine and CS₂ (pyridine vol%). The swelling ratio of UF increases with the fraction of pyridine and reaches a maximum value at about 50vol% pyridine. Then, the swelling ratio decreases with the increase in pyridine vol%. For BZ, the swelling ratio increases with increase in pyridine vol%, and show maximum value at about 80-100vol% pyridine. These results suggest that the swelling characteristics, i.e., change in the equilibrium swelling ratio with mixing ratio, is dependent on the chemical and associated structure of coal molecules. Since the swelling of coal in polar solvents is results from declining of noncovalent interactions in coal [13], the difference of the swelling characteristics with mixing ratio of the solvent appear to be reflecting the type and strength of noncovalent interactions existing in the coals.

¹H-NMR Relaxation Time.

The solid-echo signals obtained from coal in the mixed solvents contained two components, namely the relatively slowly relaxing tail of the signals and rapidly decaying signals. The former can be attributed to the hydrogen in mobile molecular structures, and later can be attributed to the hydrogen in rigid-like (immobile) molecular structure. The variations of T₂ values for two components of UF and BZ are plotted as a function of pyridine vol% in Figure 3 and 4, respectively. For UF, T₂ for mobile structures (T_{2m}) increases with increase in pyridine vol% in the mixed solvent and reaches a maximum value at about 50vol% pyridine. T₂ for immobile structures (T_{2im}) remains almost constant value with increase in pyridine vol%. The T_{2m} for BZ increases monotonously with increase in pyridine vol%.

The separation of the solid-echo signals permits hydrogen-weighted mobile and immobile fractions of the molecular structure in coal. The distribution of the mobile and immobile fractions for UF and BZ are shown in Figure 5 and 6. Variations in the fraction of mobile components for both UF and BZ are well correlated with the variation of T_{2m}. The ¹H-NMR relaxation characteristics described above are in a close correspondence with swelling characteristics. The spin-spin relaxation time and the fraction of mobile components

vary in proportion to equilibrium swelling ratio. The enhancement of molecular mobility due to solvent induced swelling may result the ¹H-NMR relaxation characteristics.

L-band EPR spectroscopy.

The intensity of EPR spectra for UF coal decrease with increase in the mixing ratio of pyridine. It is noted that the intensities decrease at the mixing ratio from 0 to 50% and reach a minimum in the vicinity of 50 vol% of pyridine. The EPR characteristics for UF in the mixed solvents reflect the swelling behaviour of coal. For BZ, the characteristics are almost similar to those of UF, but independent of the swelling behaviour.

The EPR spectra for UF and BZ consist two components, one broad (BC) and one narrow (NC) components. Variations in the components with pyridine vol% in the mixed solvents are shown in Figure 7 and 8. It can be clearly seen that the narrow components for both UF and BZ do not change with pyridine vol%, while the broad components show minimum values at pyridine 50vol%. With EPR spectroscopy, not only stable free radical, but also the sifted and transferred electrons can be detected. The swelling in the mixed solvents proceed without significant reaction between coal and the solvents [8]. Therefore, variation in the intensities for BC might be due to disappearance of the sifted and transferred electrons result from declining of noncovalent interactions, such as aromatic π - π and charge transfer interactions.

CONCLUSIONS

1. L-band EPR characteristics are considered to have a close relation to the aromatic π - π and charge transfer interaction in coals.
2. The molecular mobility of coals obtained from ¹H-NMR vary in proportion to swelling behaviours.
3. For UF, L-band EPR characteristics are well correlated with swelling behaviour and molecular mobility, indicating that the associated structure of UF is affected strongly with the aromatic π - π and charge transfer interactions.
4. For BZ, the characteristics are almost similar to those of UF, and independent of the swelling behaviour and molecular mobility. These facts indicate that the interaction is much less effective for the associated structure of BZ than that for UF.

REFERENCE

- (1) Larsen, J.M.; Kovac, J. In *Organic Chemistry of Coal*; Larsen, J.W., Eds.; ACS Symposium Series 71; American Chemical Society: Washington, DC, 1981; 43
- (2) Kovac, J.; Larsen, J.W. *Prepr. Am. Chem. Soc., Div. Fuel Chem.* 1975, 20(2), 122
- (3) Marzec, A.; Juzwa, M.; Betlej, K.; Sobkowiak, M. *Fuel Processing Technology* 1979, 2, 35
- (4) Marzec, A. *Proc. Symposium on Chemistry of Coal Liquefaction and Catalyst*; Hokkaido Univ.: Sapporo, Japan, 1985, 42
- (5) Nishioka, M. *Fuel* 1972, 71, 941
- (6) Fujikawa, M.; Ohsuga, H.; Takanohashi, T.; Iino, M. *Energy Fuels* 1992, 6, 859
- (7) Painter, P. *Energy & Fuels* 1992, 6, 863
- (8) Iino, M.; Takanohashi, T.; Ohsuga, H.; Toda, K. *Fuel* 1988, 67, 1639
- (9) Iino, M.; Takanohashi, T.; Ohsuga, H.; Tsueta, H.; Sanokawa, Y. *Fuel* 1989, 68, 1588
- (10) Ishizuka, T.; Takanohashi, T.; Ito, O.; Iino, M. *Fuel* 1993, 72, 579
- (11) Liu, H.-T.; Ishizuka, T.; Takanohashi, T.; Iino, M. *Energy Fuels* 1993, 7, 1108
- (12) Yun, Y.; Suuberg, E.M. *Fuel* 1993, 72, 1245
- (13) Larsen, J.W.; Green, T.K.; Kovac, J. *J. Org. Chem.* 1985, 50, 4729-4735

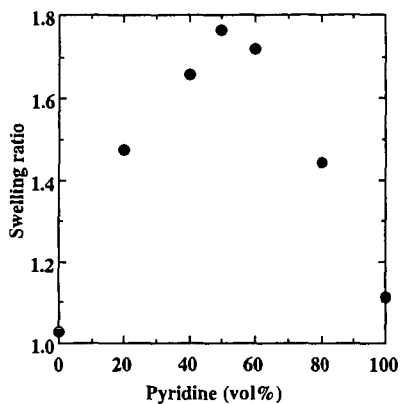


Figure 1. Change in equilibrium swelling ratio for UF with pyridine vol.% in mixed solvent

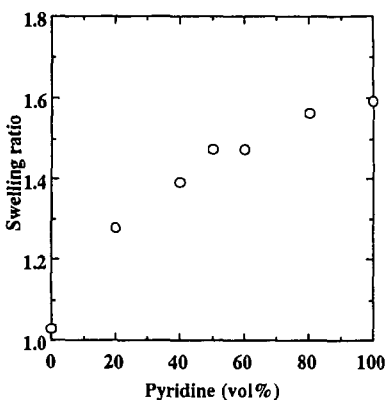


Figure 2. Change in equilibrium swelling ratio for BZ with pyridine vol.% in mixed solvent

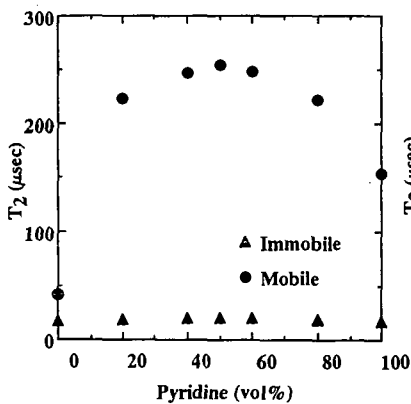


Figure 3. Effects of pyridine vol% in mixed solvent on spin-spin relaxation time, T_2 , for UF

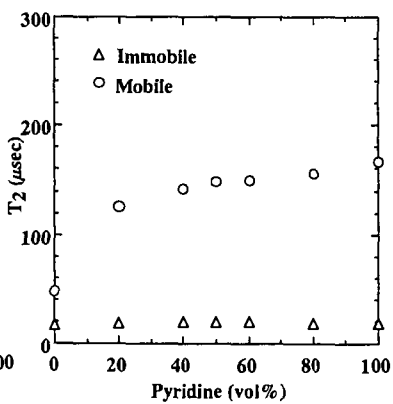


Figure 4. Effects of pyridine vol% in mixed solvent on spin-spin relaxation time, T_2 , for BZ

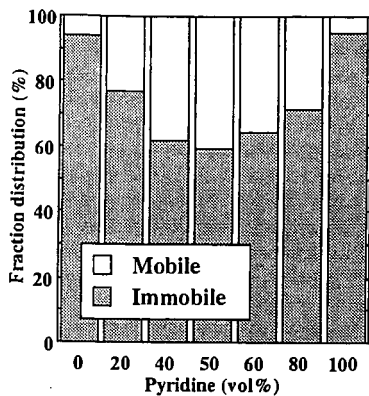


Figure 5. Distribution of mobil and immobile fractions for UF in mixed solvent

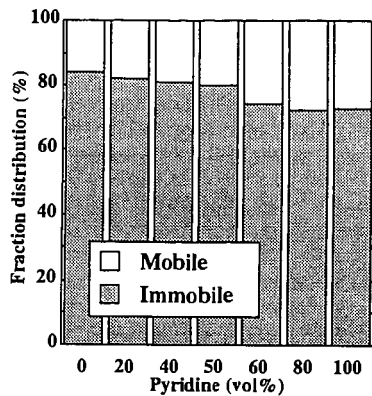


Figure 6. Distribution of mobil and immobile fractions for BZ in mixed solvent

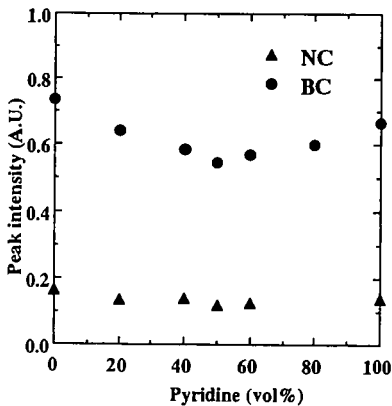


Figure 7. Change in the peak intensity of NC and BC for UF with pyridine vol% in mixed solvent

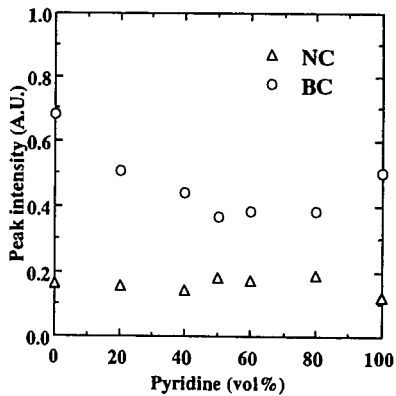


Figure 8. Change in the peak intensity of NC and BC for BZ with pyridine vol% in mixed solvent

INVESTIGATION OF THE POROUS STRUCTURE OF COAL USING ^{129}Xe NMR WITH SELECTIVE PRESATURATION AND SATURATION TRANSFER.

Stasia A. Anderson¹, Patrick G. Hatcher², Ljubisa R. Radovic² and Alan J. Benesi*¹

¹Pennsylvania State University, Department of Chemistry, University Park, PA

²Pennsylvania State University, Department of Materials Science and Engineering
Fuel Science Division, University Park, PA

Keywords: ^{129}Xe NMR, low power presaturation, saturation transfer, coal porosity, microporosity.

ABSTRACT

The technique of selective low power presaturation applied to ^{129}Xe NMR of xenon adsorbed in coal can clearly demonstrate the existence of a distribution of similar adsorption sites for xenon, where the signals from xenon in these sites are not resolved as individual signals. Differences in inter/extra particle exchange in two coals of different rank, available from a saturation transfer technique, are significant. This technique can be used to investigate pore connectivity in microporous materials of unknown pore structure.

INTRODUCTION

Coal Microporosity. Coal microporosity accounts for most of its surface area. The largely amorphous physical structure of many coals, and the small dimensions of micropores (<20 Å), have made accurate assessment of the dimensions, size distribution, and connectivity of microporous networks in coal very difficult. Techniques such as SAXS (Bale et al., 1984; Lin et al., 1978; Larsen et al., 1995), X-ray diffraction (Hirsch, 1954), TEM (Lin et al., 1978; Harris and Yust 1976; 1981), gas adsorption (reviewed by Walker, 1981; Larsen et al., 1995), and others have all contributed to our understanding of coal porosity but, when applied to the characterization of microporosity, continue to have severe limitations.

There is wide acceptance of the following general model, however: "coals contain an interconnected pore network of high surface area, the slit-shaped pores having constricted openings of molecular dimensions...[and] coals contain both open and closed porosity." (Mahajan, 1991). The question of the extent of open or closed porosity is an area of continuing controversy, the major source of which is the large difference in coal surface area determined by adsorption of gases of similar molecular dimensions, or the *molecular sieving effect*. There are several critical reviews on the subject (Marsh, 1987; Mahajan, 1991; Walker and Mahajan, 1993). Molecular sieving effects are open to conflicting interpretations in terms of the pore structure of coal. Larsen et al. (1995) contend that the magnitude of the molecular sieving effect, along with the high fractal dimensionality of coal as determined by SAXS, are inconsistent with an interconnected, bottlenecked micropore network model; and that microporosity in coal exists primarily as isolated 'bubbles' in the solid matrix. This is a controversial conclusion; Larsen's results do not eliminate activated diffusion, as opposed to closed porosity, as a cause of molecular sieving according to Walker and Mahajan (1993). This issue is likely to remain unresolved without additional information that does not depend on gas uptake measurements.

Our approach to characterizing coal microporosity uses ^{129}Xe NMR spectroscopy (reviewed by Dybowski et al., 1991). ^{129}Xe NMR offers a way to derive different and more extensive information about xenon gas in its adsorbed state than would be available from classical adsorption experiments. The ^{129}Xe NMR signal contains information about both adsorption-site environment and dynamics of adsorbed xenon. In order to clarify the terminology used in this paper, we will note here that differences in adsorption sites in coal that affect the ^{129}Xe NMR signal chemical shift are size differences among micropores and possibly mesopores. However, given the heterogeneity of coal, it is possible that variations in pore wall chemistry may also affect the chemical shift. We will use the term adsorption site, meaning porosity of different size and/or chemistry, where appropriate. The results presented in this study can be used to address the question of whether the broad NMR signal from xenon adsorbed in coal arises from a distribution of similar adsorption sites and will demonstrate the differences in intra/extra particle exchange in two different pore networks, which can be interpreted in terms of whether the pores are open or closed, and how porosity changes with coal rank.

Theoretical basis of the NMR experiment. ^{129}Xe NMR spectra in this study detect xenon gas adsorbed on or in contact with the solid surface of coal. ^{129}Xe NMR has been previously applied to coal as a possible tool to determine micropore sizes (Wernett et al., 1990; Tsiao and Botto, 1992). The basic NMR concepts employed in this study are selective saturation and saturation transfer, which have widely varied utility in NMR spectroscopy, as reviewed in Freeman (1988). There are several studies that, while not the same as the experiment described here, utilize similar basic concepts. Selective inversion has been used in ^{129}Xe NMR studies to monitor interstage exchange in a zeolite (Larsen et al., 1993; Jameson et al., 1994), to demonstrate that two xenon

populations are coupled (Ripmeester and Ratcliffe, 1993), and to measure diffusion coefficients in polystyrene (Simpson et al., 1995).

In the presaturation experiment we irradiated only a portion of the frequency range covered by the adsorbed xenon signal, using a low power presaturation pulse followed by a high power 90 degree pulse. We are interested in whether and to what extent the irradiation produces saturation of the signal. If saturated, the xenon atoms do not give an NMR signal when the 90 degree pulse is applied. The key ideas used in conceptualizing this experiment are as follows: NMR signals from ^{129}Xe adsorbed in and outside the coal particle are distinguishable; and the possibility that xenon atoms are to some degree mobile means that a xenon atom that is saturated while in one environment can move to another in a given time frame, carrying the saturation with it. (Spin-lattice relaxation is a competitive process.) Possible outcomes of a presaturation experiment are as follows:

(1) The xenon atoms are in distinct internal adsorption sites and are effectively immobile during the time the pulse is applied. In this case we would expect to see a well defined break or a dip in the outline of the adsorbed gas signal in the area where the low power pulse was applied.

(2) The xenon atoms do have distinct internal adsorption sites, but exchange among them during the presaturation time. Here we would expect to see saturation of the adsorbed gas signal, or overall loss of signal intensity, which may be accompanied by a change in the signal shape.

Note that outcomes (1) and (2) are related in that they are only distinguished by the time frame of site to site motion. For example, if the xenon atoms sample all the sites in 100 ms, then in a 10 ms period they are effectively immobile in their adsorption sites. A 10 ms presaturation pulse, assuming it is sufficiently narrow and delivers enough power to cause saturation, would be able to selectively saturate a portion of the overall adsorbed gas signal. A 100 ms pulse, however, should saturate the entire signal. Variation of the time frame of the experiment can identify the transition from one effect of presaturation to another.

(3) Xenon atoms are exchanging both into and out of the particle during the time the sample is presaturated. In this case, we would expect the intensity of both adsorbed and external surface signals to decrease or completely saturate.

(4) The linewidth is not due to a distribution of sites, but to a short T2 and/or magnetic field inhomogeneity. The signal intensity could be decreased by presaturating the peak maximum, but the shape should remain the same, and presaturating the signal off center should have much less or no effect.

EXPERIMENTAL

Powdered samples of Wyodak subbituminous (subB; 76.3% C) and Sewell medium volatile bituminous (mvb; 88.9% C) coals were obtained from the Penn State/DOE coal sample bank and sieved to 60-100 Tyler mesh particle size. They were dried overnight in 10 mm NMR tubes with rototite valves (Wilmad), heated to 90° C for 2 to 4 hours, then kept under vacuum at room temperature for 24 hours or more. Once dry, the samples were charged with xenon to ~ 1 atm pressure (730-760 torr). Equilibration time was 8-12 hours.

NMR spectra were acquired on a Bruker AMX 360 NMR spectrometer operating at 99.61 MHz. A low power presaturation pulse was applied with the carrier frequency centered on the signal of interest followed by a 90 degree high power pulse and 3 s delay. The low power pulse length was varied as described in the next section. Spectra were run 300 to 1000 scans depending on the individual sample. All sets of spectra for a particular sample were run the same number of scans. Xenon gas at 700 torr was used as an external chemical shift reference.

RESULTS AND DISCUSSION

The ^{129}Xe NMR spectrum of coal and effect of presaturation. The ^{129}Xe NMR spectrum of xenon gas adsorbed on Sewell coal is shown in Figure 1a.

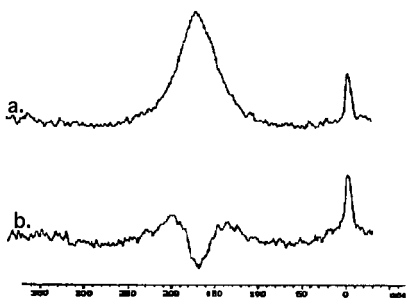


FIGURE 1. ^{129}Xe NMR spectrum of Sewell coal with (a) 80dB presaturation pulse, which has negligible effect and (b) 37 dB presaturation pulse centered at 21870 Hz (approx. 174 ppm).

A presaturation pulse of negligibly low power was applied. The appearance of this spectrum is like that of a ^{129}Xe NMR spectrum of a high rank coal without presaturation. The signal centered at 174 ppm is from xenon adsorbed on the internal surfaces of the coal, and that at 0 ppm is the interparticle or external gas signal. Figure 1b shows the loss of a portion of the signal when a 37 dB presaturation pulse was applied for 0.3 ms at the center of the signal.

Two coals were presaturated on the principal adsorbed xenon signal for increasing lengths of time. The reference spectra for both coal samples are presaturated on the center of the adsorbed gas signal at very low power (80 dB power for 0.1 ms). All subsequent spectra for a given sample were phased relative to the reference.

The Sewell coal was presaturated at 37 dB on the 174 ppm adsorbed xenon signal (21,870 Hz) for increasing times from 0.3 ms to 800 ms. The results are shown in Figure 2. There is a 'hole' in the signal at 0.3 ms accompanied by overall intensity loss. A spectral hole, or the loss of a portion of the adsorbed xenon signal, is evidence that some of the xenon atoms contributing to a broad signal have a resonant frequency close to the applied pulse; some do not, however, hence the residual portions of the signal. This is evidence that the signal is broad due to an overlap of chemical shifts, which in turn indicates that there exist slightly different adsorption sites from which the different xenon chemical shifts arise. At 1 ms the signal is almost saturated. There was no effect on the interparticle gas signal. Upon increasing the pulse length the saturation extends to the remainder of the signal it is focused on, and to the external gas signal. This clearly illustrates the motion of saturated xenon through the solid and out into the interparticle space. At 200 ms, the adsorbed signal in Sewell coal was completely saturated while the interparticle gas signal was less intense. At 400 ms the gas signal intensity decreased noticeably, and at 800 ms it was nearly saturated.

The Wyodak coal was presaturated at 40 dB power at about 150 ppm (20,000 Hz) for increasing times from 1 ms to 40 ms. The results are shown in Figure 3. The spectra show a 'hole' at 1 and 2 ms which is almost saturated at 5 ms. From 1 to 5 ms, the interparticle gas signal at 0 ppm is unchanged. At 10 ms, the adsorbed signal is completely saturated and the interparticle gas signal has some intensity loss. At 30 ms the gas signal is reduced to a little over the noise level, and at 40 ms it is saturated.

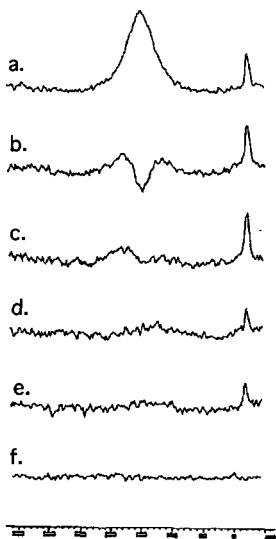


FIGURE 2. Effect of increasing presaturation pulse length on ^{129}Xe NMR spectra of Sewell coal. (a) Reference; (b) 0.3 ms; (c) 1 ms; (d) 200 ms; (e) 400 ms; (f) 800 ms.

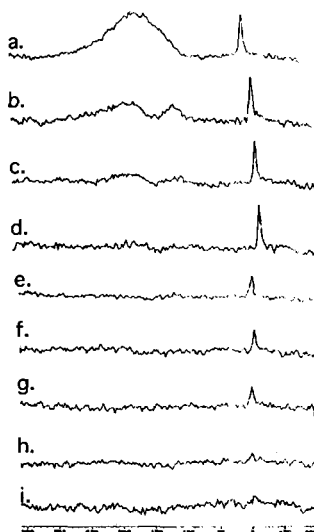


FIGURE 3. Effect of increasing presaturation pulse length on ^{129}Xe NMR spectra of Wyodak coal. (a) Reference; (b) 1 ms; (c) 2 ms; (d) 5 ms; (e) 10 ms; (f) 15 ms; (g) 20 ms; (h) 30 ms; (i) 40 ms.

Implications for the porous structure of the coals. In the Wyodak coal, the adsorbed gas signal survives presaturation longer than the Sewell coal. The longer time for the saturation transfer from the 'hole' effect to saturation of the entire signal is coupled with much shorter time to saturate the external surface signal compared to the Sewell coal. We interpret this as indicating that in the Wyodak coal, it takes a longer time for saturated xenon atoms to exchange among the internal sites and a shorter time for their exchange with gas at the external surface. This indicates that the Wyodak coal has a wider distribution of internal adsorption sites and greater connectivity of the pore network to the outside. The Wyodak coal, at 76.3% C, has meso- as well as microporosity as determined by N₂ and CO₂ adsorption, as is expected based on its rank (Gan et al. 1972). The NMR data in this study is in keeping with the presence of larger pores, in which diffusion of xenon would be faster, acting as feeder pores to the microporosity in this coal.

In the Sewell coal, an apparently shorter time to exchange among the internal sites indicates a narrower distribution of adsorption sites than in the Wyodak coal. It should be noted that the signal itself, without presaturation, is narrower than in the Wyodak coal. This too is an indication of greater site homogeneity. The longer time saturate to the external surface gas signal shows that the access of adsorbed xenon to the external surface in the Sewell coal is far more restricted than in the Wyodak coal. This indicates a significantly different type of pore network in the two coals. The evidence points to a greater number of internal pore network connections than there are openings to the external surface in the Sewell coal. This is consistent with the notion of a highly interconnected microporous system lacking a significant amount of larger porosity.

In both coals the complete saturation of the adsorbed xenon signal, with no portion resistant to saturation after allowing 1-20 ms for xenon to exchange among internal sites with the presaturation pulse applied, demonstrates *interconnection* of porosity. This information could be useful in resolving the continuing controversy on whether coal micropores are primarily open or closed (Larsen et al., 1995; Walker and Mahajan, 1993). There was no isolated adsorbed xenon signal for either coal, an indication that the xenon atoms are moving through an open porous network. If a significant portion of the porosity existed as isolated pockets, movement of xenon through the coal would require passing through regions of both solid matrix and pores. If dissolved in the solid, an NMR signal would be expected either resolved from xenon that is in porosity, or overlapped but detectable as a portion of the signal with a longer lifetime in the saturation transfer experiment. It is very unlikely that xenon can diffuse through the solid matrix at a rate comparable to its passage through pores, and this experiment reveals no indication in either coal that a detectable proportion of the adsorbed xenon is dissolved in solid coal.

REFERENCES

- Bale, H. D., Carlson, M. L., Kalliat, M., Kwak, C.Y, and Schmidt, P.W. in The Chemistry of Low Rank Coals, A.C.S. Washington, D.C. pp. 79-94 (1984).
Dybowski, C. Bansal, N., and Duncan, T. M. *Ann. Rev. Phys. Chem.* **42**, 433 (1991).
Freeman, R. A Handbook of Nuclear Magnetic Resonance, J. Wiley, N.Y. pp. 198-202 (1988).
Gan, H., Nandi, S. P., and Walker, P. L. Jr., *Fuel* **51**, 272 (1972).
Harris, L. A. and Yust, C. S. *Fuel* **55**, 233 (1976).
Harris, L. A. and Yust, C. S. in Coal Structure, A.C.S. Washington, D. C. pp. 321-336 (1981).
Hirsch, P. B. *Proc. Royal Soc., (London)* **A226**, 143 (1954).
Jameson, A. K., Jameson, C. J., and Gerald, R. E. *J. Chem. Phys.* **101**, 1775 (1994).
Lin, J. S., Hendricks, R. W., Harris, L. A., and Yust, C. S. *J. Appl. Cryst.* **11**, 621 (1978).
Larsen, R. G., Shore, J., Schmidt-Rohr, K., Emsley, L., Long, H., Pines, A., Janicke, M. and Chmelka, B. F. *Chem. Phys. Lett.* **214**, 220 (1993).
Larsen, J. W., Hall, P., and Wemett, P. C. *Energy Fuels* **9**, 324 (1995).
Mahajan, O. P., *Carbon* **29**, 742 (1991).
Marsh, H. *Carbon* **25**, 49 (1987).
Ripmeester, J. A. and Ratcliffe, C. I. *An. Chim. Acta* **283**, 1103 (1993).
Simpson, J. H., Wen, W.-Y., Jones, A. A., Inglefield, P. T., and Bendler, J. T. *Appl. Magn. Reson.* **8**, 349 (1995).
Tsiao, C. and Botto, R. E. *Energy Fuels* **5**, 87 (1992).
Walker, P. L. Jr *Phil Trans. Royal Soc. Lond. A* **300**, 65 (1981).
Walker, P. L. Jr., and Mahajan, O. P. *Energy Fuels* **7**, 559 (1993).
Wemett, P. C., Larsen, J. W., Yamada, O., and Yue, H. J., *Energy Fuels* **4**, 412 (1990).

MICROSCOPIC OBSERVATION AND IMAGE ANALYSIS FOR THE EVALUATION OF TOPOLOGICAL FEATURES OF SINGLE COAL PARTICLES IN PYRIDINE

Hong Gao, Satoru Murata, and Masakatsu Nomura
Department of Applied Chemistry, Faculty of Engineering, Osaka University,
2-1 Yamada-oka, Suita, Osaka 565, Japan

Keywords: Single coal particle, Pyridine, Image Analysis.

ABSTRACT

Time dependent solvent swelling behavior of six different rank coal particles in pyridine was observed by the application of a microscopy combined with a video camera: the time-resolved swelling ratios were evaluated quantitatively by an image analysis system. The topological features of the coal particles with three dimensional macromolecular structure in pyridine are classified into four types among six different rank coals. We also found that the solvent-swelling ratios of single coal particles at quasi-equilibrium state are rank dependent.

INTRODUCTION

Coal is a complex and heterogeneous material. This heterogeneity leads to difficulties in accurately characterizing its structure, so that there is no universally accepted model for the chemical structure of coal. However, it appears to have been generally conceived that coal consists of a small chain substituted aromatic and hydroaromatic units linked by covalent bonds and non-covalent bonds like hydrogen bonding and van der Waals interactions, with entanglements of skeletal chain structure to form a three-dimensional network structure [1-4]. Apart from its three-dimensional cross-linked macromolecular structure, coal is viscoelastic and largely does not dissolve in conventional solvent, but swells when exposed to a solvent. The extent of swelling is thought to be controlled by the cross-link density and the magnitude of its interaction with the solvent [5-7]. In general, the density of cross-link is evaluated in terms of volumetric swelling ratio (Q_v), defined simply as the swollen sample volume divided by the unswollen sample volume. In evaluation of coal swelling, three methods of measurement have been adopted: volumetric measurement based on packed bed [8-10]; gravimetric measurements using solvent sorption from the vapor phase [11]; microscopy coupled with image analysis [12] and Malvern laser diffraction particle sizer [12] based on the measurement of particle distribution.

The important problem existing in volumetric techniques, with which the cross-link density of macromolecular level is evaluated with packed bed, is that the topological features of particles and interactions among the particles in solvent are not yet clear. Another problem of volumetric techniques is that the soluble fractions in polar solvent are present in coal. When the solvent like pyridine is introduced into the tube, a significant amount of dissolution occurs, resulting in the reduction of solvent activity. Therefore, it is clear that there is an enthusiastic need for the more reasonable method on the measurement of coal swelling in solvent on the macromolecular level. The methods based on particle size distribution measurement [12] offers a significant advantage over volumetric method, since the ambiguity of the packing of particle beds is removed, and the method employs a coal solid concentration which is sufficiently low for solubilization of the coals not to markedly affect the solvent activity. However, two implicit assumptions were made in this approach. They are particles of all sizes swell to the same average extent and the particles must not fracture or agglomerate during swelling. In practice, because of heterogeneity of coals, the distribution of equilibrium swelling ratios and the fracture exist in some kinds of coal particles, especially for the high-solvent-swelling coal. It is clear that the systematic investigation on the dynamical behavior and characteristics of single coal particle in solvent are in need for further understanding of the change of macrostructure of coal in solvent at the macromolecule level.

EXPERIMENTAL

Coal Samples. In the present study, six kinds of coal sample with different rank used in this study ranging from low rank to anthracite, were Witbank [weak coking coal, 83.1 C% (daf), Canada], Prima [coking coal, 81.0 C% (daf), Indonesia], Goonyella [coking coal, 84.6 C% (daf), Australia], Blue Creek [coking coal, 80.0 C% (daf), USA], K-9 [coking coal, 90.1 C% (daf), Russia], and Honken [anthracite coal, 93.2 C% (daf), Vietnam].

Swelling measurements on six kinds of coals in pyridine were conducted. Pyridine used in this study was of analytical reagent grade.

Experimental Apparatus and Procedure. As shown in Figure 1, the experimental apparatus consists of a microscope coupled with a TV camera system for observing and recording the behavior of the coals in solvent container. An image analysis system was used for quantitative evaluation of time-resolved swelling ratio of the single coal particles.

The microscope (Japan Olympus Co. Ltd.) fitted with a video camera provides input to an image analysis system (Japan Nireco Co. Ltd., LUZEX-3). A 6.3 \times objective was used with the microscope which, with the other optical components used, gave a magnification, at the analyzer monitor, from 20 to 100 \times objective.

Under the conditions of atmospheric pressure and ambient temperature (20 $^{\circ}$ C), pyridine (3 ml) was injected into the cell and then single coal particle was placed into pyridine and the recording was started until to the quasi-equilibrium-state of swelling. The recorded images were directly examined

and analyzed with the image analyzer. The time-resolved swelling ratio of single coal particles were evaluated with an equivalent volume converted from particle projection area under the assumption of spherical coal particle.

RESULTS AND DISCUSSION

As shown in Figure 2, Witbank coal particle (850-1000 μm) swells up to 2.47 times within 28 h. During this period the cracks largely developed, and no change was observed during an additional time exposure both in shape and size. The massive cracks may be caused by any stresses built up from the resultant swelling gradients or uneven swelling of sample. Other cracks may have been due to non-uniform swelling which causes some stresses not being sufficiently relieved. It is also likely that the stresses were caused by heterogeneities in the structure or by differences in the equilibrium swelling of different regions of the specimens. It is clear that transport process of pyridine in the coal macromolecule is greatly enhanced locally by the formation of a large discernible crack for the large specimen. This result suggests the new interface between coal macrostructure and solvent is important for solvent-swelling for high solvent-swollen coals. This phenomenon is consistent with the results of Cody and Botto [13], and Motsegood and Clarkson [28]. It is known that the chemical heterogeneity of coal leads to anisotropic swelling [18]. And coal swelling has been found to be greater in perpendicular direction to the bedding plane than in parallel to it [27]. Cracking at mineral-organic interfaces is also expected due to differential swelling of the organic matrix relative to mineral matter because diffusion of pyridine through areas is different with susceptibility differences, particularly at organic-mineral interfaces and at surface of microfractures.

As shown in Figure 3, the swelling ratio at quasi-equilibrium state of the sample with small size (210-250 μm) is 2.10 which is somewhat smaller than the larger one (2.47). The time required for reaching quasi-equilibrium state is about 10 hours. Moreover, only a few sizable cracks developed during swelling.

The reasons why the smaller sample apparently tended to reduce fracturing of the sample could be interpreted as follows: First, it caused the penetration of the swelling agent into the coal rapid and fairly uniform over the area of the sample so that uneven swelling of the sample was minimized. Second, the smaller sample has limitation of the distance over which liquid concentration gradients could develop perpendicularly to the surface, so any stresses built up from the resultant swelling gradients would be less likely to induce fracture.

For the case of Prima coal, the quasi-equilibrium swelling ratio is 2.34 for the case of smaller coal particle (210-250 μm) and 2.78 for the case of larger particle (850-1000 μm). The times for reaching the equilibrium state were about 5 h for smaller sample (210-250 μm) and 10 h for the larger one (850-1000 μm). During the swelling there is no cracks developed, the shape of the swollen coal particle samples being close to that of the initial specimens. These phenomena were different from the case of Witbank coal.

As described previously, the cracking at mineral-organic interfaces and surface of microfractures is due to differential swelling of the organic matrix relative to mineral matter because the diffusion of pyridine is through areas with susceptibility differences, particularly at organic-mineral interfaces and at surface of microfractures. The difference in solvent-swollen deformation characteristics, therefore, is caused by difference in degree of physical and chemical heterogeneity existing among the coals. The present results suggest that physical and chemical heterogeneity of Witbank coal is much larger than that of Prima coal. On the other hand, it is obvious that energetic interactions between solvent molecules and the coals play an important role in the swelling phenomena. For the coal to expand, the macromolecule chains must be able to reorient. Since the solvent-swollen coal was observed to be substantially more flexible than the dry coal, some bonds among macromolecular chains are apparently broken by solvation. The substantial decrease in modulus which occurs on swelling demonstrates that the bonding is significantly different in the dry and the swollen coal; it indicates that the effective molecule weight between crosslinks in the highly swollen coal is substantially greater than in the original dry coal. This suggests that the elasticity of the swollen sample may have much more of an entropic or rubbery nature than that of the original sample. Therefore, the difference in deformational features between Witbank and Prima is also related to the difference in energetic interactions between solvent molecular and the coal macrostructure. The present results suggest that the interactions of Witbank coal and Prima coal with pyridine are larger than that of other coals or pyridine has sufficient force to destroy the non-covalent bonds existed in Witbank coal and Prima coal.

For the case of Goonyella coal, the quasi-equilibrium swelling ratio was 1.11 for the coal particle of 210-250 μm and 1.16 for the coal particle of 850-1000 μm . The times for reaching the equilibrium state are about 16 h for the smaller sample (210-250 μm) and 20 h for the larger sample (850-1000 μm), respectively. Moreover, during swelling there is a few sizable cracks developed with distortion, and in the initial swollen stage there is a shrinking period for both particle size although the appearance of this stage is much faster in the case of small coal particle than the case of large one. These phenomena are different from the cases of Witbank coal and Prima coal. The shrinking phenomena may be caused by transition from glass to rubbery or change in amount of the coal microporosity, although it is unclear how much the change occurs.

For the cases of Blue Creek coal, K-9 coal and Honken coal, there are almost no swelling and deformation in pyridine.

The detailed discussion on above phenomena will be conducted from the view point of non-covalent interaction existed in different rank coals in the following parts.

The physical properties of solvent-swollen coal are related to its three dimensional macromolecular architecture. The dynamic nature of the macromolecular structure of coal governs the time dependence of its response during the solvent-swollen processes. The extent of swelling is thought to be controlled by the cross-link density and magnitude of interaction between coal and solvent [19-21]. The mechanism of coal swelling in polar basic solvents such as pyridine involves the disruption of hydrogen bonding cross-links of the network [29-31]. Pyridine is often used in solvent swelling

experiments on coal and, because of its basic character [5], is capable of reacting with many of the hydrogen bonds in coal to cause swelling, if these hydrogen bonds are cross-links [22]. Brenner [23] demonstrated that swelling of coals in pyridine involves the transformation of the coal from glassy to a rubbery state. In the differential scanning calorimetric investigation on solvent-swollen coals, Hall and Larsen [30] demonstrated the existence of second-order phase transitions well below room temperature. It has been hypothesized that these phase transitions are glass to rubber transitions. Usual state of coal is glassy at room temperature. When hydrogen bonds are disrupted by pyridine, the effective cross-link density decreases. There is an associated change in the viscoelastic properties of the coal as it becomes more rubbery. The degree to which coal becomes rubbery is a function of the density of hydrogen bonds disrupted and hence the solvent swelling. It is reasonable and sufficient to assume that when swollen with pyridine, the coals behave as if some or all of the hydrogen bonds or other non-covalent bonds have been eliminated. The fact that the diffusion mechanism is a strong function of the number of hydrogen bonds disrupted suggests that this in some way limits the extent to which coals can become rubbery. Solvent sorption into glassy polymers contains contributions from both concentration gradient controlled diffusion and relaxation controlled swelling. It was reported that particle size was a factor with case-II [24] behavior being observed for large particles and Fickian diffusion for small particles. Swelling of coal in pyridine involves the disruption of hydrogen bonds in the coal and the formation of bonds between the solvent and functionalities in the coal. It has also been suggested that solvent will disrupt only those coal-coal hydrogen bonds whose bond strengths are lower than those of the coal-solvent hydrogen bonds [25]. It has also been suggested that pyridine, because of its strong basicity, is capable of breaking nearly all hydrogen bonds in coal [26]. Therefore, when coal containing an appreciable amount of hydrogen bonding is exposed to pyridine, it swells to a limitation that is primarily a function of the covalent cross-link density.

As for the present study, the swelling ratio of single coal particles (850-1000 μm) in pyridine at ambient temperature versus time are 2.47 for Witbank coal, 2.34 for Prima coal, 1.12 for Goonyella coal, 1.04 for Blue Creek coal, 0.983 for K-9 coal and 1.04 for Honken coal, respectively. These results suggested that Witbank and Prima coal contain rather more hydrogen bonds, Goonyella coal has small amount of hydrogen bonds, while few hydrogen bond exists in Blue Creek coal, K-9 coal and Honken coal (As for Blue Creek coal, detailed study on oxygen-containing functionalities seems to be needed).

As to the time required for reaching to quasi-equilibrium state, for the case of 850-1000 μm coal particle size, they are 24 h for Witbank coal, 10 h for Prima coal, 16 h for Goonyella coal, respectively. For the case of 210-250 μm coal particle size, the times required for reaching to equilibrium state is almost same each other (10 h) for three kinds of coal (Witbank, Prima, Goonyella). Therefore, it seems that the diffusion velocity of pyridine molecules in the larger coal particles and relaxation velocity of the coals in pyridine are in the order: Prima > Goonyella > Witbank.

As shown in Figure 4, for the case of large particle size (850-1000 μm), the equilibrium swelling ratios are rank-dependent with decrease of carbon content from 77 to 93 wt % (daf). The pattern is consistent generally with the previous analysis on molecular weight between crosslinks [32,33] and network mobility analysis [34-35]. For the case of particle size of 210-250 μm , the change of swelling ratio with rank is similar to the case of large one.

From the observation on the recorded images, as shown in Figures 5-10, the general features of solvent-swelling behavior of the large coal particles (850-1000 μm) in pyridine seem to be classified into four types: (1) high swelling with massive crack deformation (Witbank); (2) high swelling ratio with non cracks deformation that the shape of swollen coal sample was close to that of the initial specimen (Prima); (3) no-crack shrinkage and distortion with low swelling ratio (Goonyella); and (4) no swelling with no deformation (Blue Creek, K-9, and Honken).

For comparison of the results, it should be noted that measured particles differ in size, shape and in mineral and maceral content. We observed that the distribution of equilibrium solvent swelling ratios exists in some kinds of coals. These results suggest that available data measured by conventional volumetric method may be, at most, an average expression on the equilibrium solvent swelling ratio of the coals. The systematic analysis on the distribution of equilibrium solvent swelling ratios of coals with wide range ranks is in progress in our laboratory.

CONCLUSIONS

Solvent swelling behavior of single coal particles of six different rank coals in pyridine was observed with the application of microscopy combined with video camera and the changes of solvent swelling ratio with time were evaluated quantitatively by an image analysis system. The deformation of the large coal particles seems to be classified into four types: (1) high swelling ratio with massive cracking (Witbank); (2) high swelling ratio with non-cracking and the shape of the swollen sample was close to that of the initial specimen (Prima coal); (3) non cracking shrinkage and distortion with low swelling ratio (Goonyella); and (4) non-swelling and non-deformation (Blue Creek, K-9, and Honken). In the case of coal particle size being 850-1000 μm , the quasi-equilibrium swelling ratios were 2.47 for Witbank coal, 2.34 for Prima coal, 1.12 for Goonyella coal, 1.04 for Blue Creek coal, 0.983 for K-9 coal and 1.04 for Honken coal, respectively. In the case that the coal particle size is 210-250 μm , the quasi-equilibrium swelling ratios are 2.10 for Witbank coal and 2.78 for Prima coal, respectively. On the other hand, it seems that the diffusion velocity of pyridine molecules in the larger coal particles and relaxation velocity of large coal particles in pyridine are in the order: Prima > Goonyella > Witbank.

ACKNOWLEDGMENTS

This work was supported by Grant-in-Aid for Scientific Research No. 07455323 from the Ministry of Education, Science and Culture, Japan.

REFERENCES

- 1 Van Krevelen, D. W., 'Coal', Elsevier, Amsterdam, 1981.

- 2 Lucht, L. M.; Peppas, N. A. *Fuel* 1989, 66, 803.
- 3 M. Vahrman, *Fuel* 1970, 49, 5.
- 4 Spence, J. A.; Vahrman, M. *Fuel* 1970, 49, 395.
- 5 Sanada Y.; Honda, H. *Fuel* 1966, 45, 295.
- 6 Marzec, A.; Kisielow, W. *Fuel* 1983, 62, 971.
- 7 Mastral, A. N.; Izquierdo, M.; Rubio, T., B. *Fuel* 1990, 69, 892.
- 8 Liotta R.; Brons, G.; Isaacs, J. *Fuel* 1983, 62, 781.
- 9 Larsen, J. W.; Green, T. K. *Fuel* 1984, 63, 1538.
- 10 Ndaji, F. E.; Thomas, K. M. *Fuel* 1993, 72, 1525.
- 11 Hsieh, S. T.; Duda, J. L. *Fuel* 1987, 66, 170.
- 12 Turpin, M.; Rand, B.; Ellis, B. *Fuel* 1996, 57, 107.
- 13 Cody, G. D.; Botto, R. E. *Energy Fuels* 1993, 7, 561.
- 14 Lynch, L. J.; Peppas, N. A. *Fuel* 1987, 66, 803.
- 15 Ritger, P. L.; Peppas, N. A. *Fuel* 1987, 66, 1379.
- 16 Barton, W. A.; Lynch, L. J. *Energy Fuels* 1989, 3, 402.
- 17 Barton, W. A.; Lynch, L. J. In 'Proceedings of 1989 International Conference on Coal Science' Tokyo, 1989, pp. 13-16.
- 18 Brenner, D. *Fuel* 1984, 63, 1324-1328.
- 19 Suuberg, E. M.; Otake, Y.; Langner, M. J.; Leung, K. T.; Milosavljevic, I. *Energy Fuels* 1994, 8, 1247-1262.
- 20 Ndaji, F. E.; Thomas, K. M. *Fuel* 1995, 74, 842-845.
- 21 Cody, G. D.; Davis, A.; Hatcher, P. G. *Energy Fuels* 1993, 7, 455
- 22 Marzec, A.; Kisielow, W. *Fuel* 1983, 62, 971.
- 23 Hall, P. J.; Marsh, H.; Thomas, K. M. *Fuel* 1988, 67, 863.
- 24 Nishioka, M.; Larsen, J. W. *Energy Fuels* 1988, 2, 351
- 25 Larsen, J. W.; Green, T. K.; Kovac, J. J. *Org. Chem.* 1985, 50, 4729.
- 26 Brenner, D. *Fuel* 1985, 64, 167.
- 27 Cody, G. D.; Larsen, J. W.; Siskin, M. *Energy Fuels* 1988, 2, 340
- 28 Mosegood, A. G. W.; Clarkson, R. B. *Fuel* 1993, 72, 1235-1237.
- 29 Green, T. K.; Kovac, J.; Brenner, D.; Larsen, J. W., in 'Coal Structure' (Ed. R. A. Meyer), Academic Press, New York, 1982
- 30 Cody, G. D.; Larsen, J. W.; Siskin, M. *Energy Fuels* 1988, 2, 342
- 31 Hall, P. J.; Thomas, K. M.; Marsh, H. *Fuel* 1988, 67, 863
- 32 Lynch, L. J.; Peppas, Nikolaos A. *Fuel* 1987, 66, 803-809.
- 33 Ritger, Philip L.; Peppas, Nikolaos A. *Fuel* 1987, 66, 1379-1388.
- 34 Barton, W. A.; Lynch, L. J. *Energy Fuels* 1989, 3, 402
- 35 Sakurovs, R.; Lynch, L. J.; Barton, W. A., In 'Coal Science II', Symposium Series 461 (Eds Schobert, H. H.; Bartle, K. D.; Lynch, L. J.), American Chemical Society, Washington, DC, 1991, pp. 111-126.

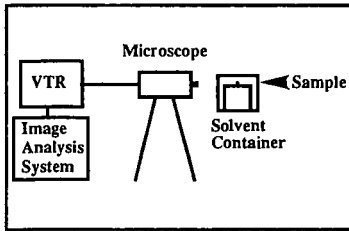


Figure 1. Schematic diagram of the apparatus for the observation and measurement of solvent swelling of single coal particles.

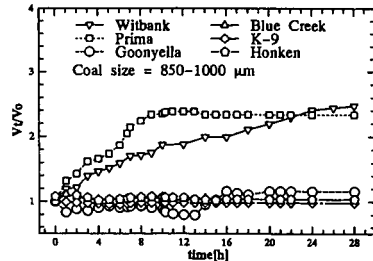


Figure 2. Changes of solvent swelling ratio with time in pyridine at ambient temperature.

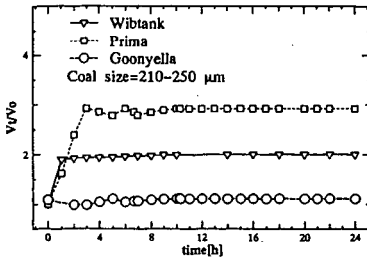


Figure 3. Changes of solvent-swelling ratio with time in pyridine at ambient temperature.

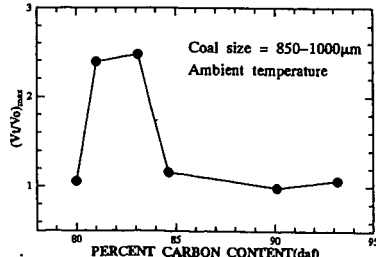


Figure 4. Relationship between maximum solvent swelling ratio in pyridine and carbon content.



Figure 5. Frame photographs of swelling of Witbank coal particle (850-1000 μm) in pyridine at ambient temperature (a: 0 h, b: 1 h, c: 2 h, d: 3 h, e: 4 h, f: 5 h, g: 6 h, h: 7 h, i: 8 h, j: 9 h, k: 10 h, l: 11 h, m: 11.25 h, n: 12 h, o: 13 h, p: 14 h, q: 14.5 h, r: 24 h).

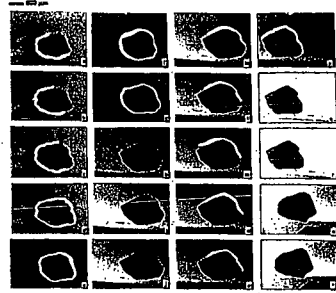


Figure 6. Frame photographs of swelling of Prima coal particle (850-1000 μm) in pyridine at ambient temperature (a: 0 h, b: 1 h, c: 2 h, d: 3 h, e: 4 h, f: 5 h, g: 6 h, h: 7 h, i: 8 h, j: 9 h, k: 10 h, l: 11 h, m: 12 h, n: 13 h, o: 14 h, p: 15 h, q: 16 h, r: 17 h, u: 18 h, v: 20 h, w: 21 h, x: 24 h).

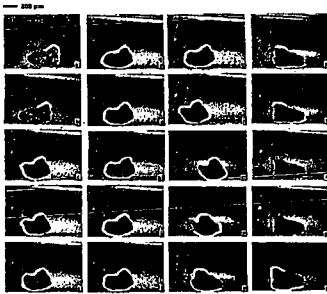


Figure 7. Frame photographs of swelling of Goonyella coal particle (850-1000 μm) in pyridine at ambient temperature (a: 0 h, b: 1 h, c: 2 h, d: 3 h, e: 4 h, f: 5 h, g: 6 h, h: 7 h, i: 8 h, j: 10 h, k: 12 h, l: 14 h, m: 14.25 h, n: 14.5 h, o: 15 h, p: 16 h, q: 18 h, r: 20 h, u: 22 h, v: 24 h).

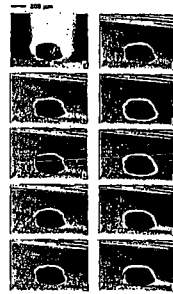


Figure 8. Frame photographs of swelling of Blue Creek coal particle (850-1000 μm) in pyridine at ambient temperature (a: 0 h, b: 1 h, c: 2 h, d: 3 h, e: 4 h, f: 6 h, g: 8 h, h: 10 h, i: 18 h, j: 24 h).



Figure 9. Frame photographs of swelling of K-9 coal particle (850-1000 μm) in pyridine at ambient temperature (a: 0 h, b: 2 h, c: 4 h, d: 6 h, e: 8 h, f: 10 h, g: 12 h, h: 24 h).

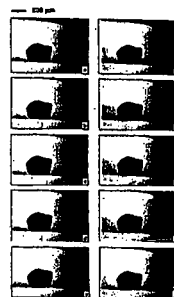


Figure 10. Frame photographs of swelling of Honken coal particle (850-1000 μm) in pyridine at ambient temperature (a: 0 h, b: 2 h, c: 4 h, d: 6 h, e: 8 h, f: 10 h, g: 12 h, h: 16 h, i: 18 h, j: 24 h).

SORPTION MECHANISM OF VARIOUS ORGANIC VAPORS TO ARGONNE PREMIUM COAL SAMPLES

Toshimasa Takanohashi, Kazuhiko Shimizu, and Masashi Iino
Institute for Chemical Reaction Science, Tohoku University
Katahira, Aoba-ku, Sendai 980-77, JAPAN

KEYWORDS: Coal, Sorption, Organic Vapor

ABSTRACT

Sorption of various organic vapors into Argonne Premium coals was systematically investigated to clarify coal-solvent interaction, sorption mechanism, and micropore and cross-linking structure of coals. Especially, the sorption at low vapor pressures was measured under temperature- and pressure-controlled gravimetric sorption system. Methanol was not only quickly sorbed into all ranks of coals used, but also easily desorbed under vacuum at 30 °C. While, pyridine was slowly sorbed into lignite and a significant pyridine was retained after desorption process. Methanol sorption isotherm for all ranks of coals could be explained by the dual-sorption model, i.e., a physical adsorption described by a Langmuir isotherm and a dissolution into bulk of coals described by Henry's law. For Illinois # 6 coal, in relative vapor pressures of 0.01-0.6, the sorption could be treated by the dual-sorption model, regardless of the kinds of organic vapors (methanol, benzene, pyridine, and cyclohexane). The adsorption mechanism by a BET equation did not fit the sorption data. At high relative vapor pressures, an equilibrium sorption could not be obtained, i.e., the sorbed amount was increasing with time, probably due to condensation of organic vapors in the pores and relaxation process of coal macromolecular structure.

INTRODUCTION

When a coal sorbs a solvent, several phenomena occur i.e., coal surface (functional groups)-solvent interaction, adsorption of solvent on the coal surface, coal cross-link-solvent interaction (specific interacting sites), diffusion of solvent into the bulk of coal (cross-link), extraction, swelling, and structural relaxation etc. Although the mechanism of solvent penetration into coal has no well been clarified, the study on the sorption of various organic substances including solvents is considered to be very useful for understanding coal chemistry such as the porosity structure and cross-linking structure of coals.

Hsieh and Duda have reported¹ that organic vapor sorption by coal particles can involve the several complex phenomena including the migration of mobile molecules in the coal and solvent-induced changes in coal structure, and that several analyses which have been used to investigate the structure of synthetic macromolecules were not directly applicable for coals. On the other hand, recently, Green and Selby² proposed that pyridine sorption isotherms can be modeled by a dual-mode sorption mechanism which have been widely used to explain the sorption isotherms of glassy polymers.³ This model is represented by two phenomena, i.e., a physical adsorption described by a Langmuir isotherm and a dissolution described by Henry's law. The linear portion of the pyridine isotherms represents dissolution of pyridine according to the Henry's law, i.e, sorption is linear with pressure. However, pyridine is sometimes troublesome for analysis of the sorption behavior, since pyridine strongly interacts with coals. Pyridine is considered to interact preferentially with the sites such as hydroxyl group in coals, attack the hydrogen-bonds, and disrupt all hydrogen-bonds. Pyridine also can cause the structural changes by diffusion into coal and it makes coals rubbery.^{4,5} Thus, the mechanism of solvent sorption can be dependent upon the chemical properties of solvents, and coal porosity and coal cross-links. The steric hindrance of the pore and the density of coal cross-links may be also an important factor on the vapor sorption.^{6,9}

In the present study, organic vapor sorption experiments were carried out by using Argonne Premium Coal Samples which are suitable for the sorption experiments since they have been stored under oxygen-free condition. The sorption mechanisms of various coal-vapor systems, coal porosity, and cross-linking structure of the coals will be discussed.

EXPERIMENTAL

Sample Preparation.

Argonne Premium Coal Samples were obtained in ampoules of 5 g of -150 μm . The coals were dried at 80 °C for 12 h under vacuum. As a organic solvent vapor, benzene, pyridine, cyclohexane, methanol were used without purification.

Sorption Experiments.

Sorption experiments was carried out in an acrylic box under temperature-control condition, using a quartz spring balance at 30 °C. The sorption was estimated by measuring the extension of a spring by a cathetometer with a telescope. Approximately 50 mg of the coal sample was placed in the quartz bucket, weighed, suspended from the quartz spring, vacuumed overnight at 30 °C. The deaeration treatment of organic solvent was carried out three times through freeze-thaw cycles three times to remove gases in the system. Two experiments were carried out. At a saturate vapor pressure, sorption change with time was measured. After 1 day, the desorption was measured under vacuum. In the other experiment, approximately 0.01 of relative vapor pressure of solvent was set and the sorption was measured until it attains an equilibrium. As the relative pressure was stepwise raised, the equilibrium sorption was measured.

RESULTS AND DISCUSSION

Sorption Behaviors.

For Pocahontas # 3, Illinois # 6, and Beulah Zap coals, the sorption was measured under at a saturate vapor pressure.

<Pocahontas # 3 Coal> Figure 1 shows the result for Pocahontas # 3 coal using methanol, pyridine, benzene, and cyclohexane as an organic vapor. For all vapors, the quantity sorbed was small, due to developed aromatic ring systems in which a vapor is difficult to penetrate the coal. The rate of methanol sorption was the fastest of all and total sorption was also large after 1 day, although pyridine and benzene sorption contain even 1 day, suggesting that the sorption rate of pyridine and benzene was relatively slow. A similar tendency was obtained for Upper Freeport coal. We have reported^{10,11} that the swelling ratios of high-rank raw coals in solvents were small, compared to those of its extraction residues and extract fractions. These results suggests that the diffusion of a solvent in the coals might be retarded by structural factors in the coals, such as stacking among aromatic rings. We have also reported^{8,9} that the size exclusion effect of coal macromolecular structures is an important factor for penetration of aromatic compounds in the coals from a inverse liquid chromatography study. Even in liquid phase, pyridine could not extract all pyridine-extractables in the coals at room temperature, indicating that the penetration of pyridine into the coals was incomplete.¹² We have also found¹² that a carbon disulfide-N-methyl-2-pyrrolidinone mixed solvent gave high extraction rates as well as high extraction yields for some bituminous coals. The kinetics of solvent diffusion into the coals may greatly influence the extraction yield and the swelling ratio of the coals.

<Illinois # 6 Coal> Figure 2 shows the result for Illinois # 6 coal. Generally, the initial rate of sorption was high and the amount sorbed was large, compared to other coals, suggesting that Illinois # 6 coal has porosity and cross-linking structure which a solvent easily diffuses. The sorption of pyridine was the largest of the solvents used, while those of benzene and cyclohexane were small. Polar solvents such as pyridine and methanol was greatly sorbed by Illinois # 6 coal. These results suggest that adsorption on the surface and the diffusion easily occurs through interaction between polar solvents and the coal. Illinois # 6 c is known to contain more functional groups than higher rank coals such as Pocahontas # 3 and Upper Freeport coals.

<Beulah-Zap Coal> Figure 3 shows the result for Beulah-Zap coal. As expected, the sorption by benzene and cyclohexane was very small as well as for Illinois # 6 coal as indicated in Figure 2. Methanol gave a high initial rate of sorption and a high equilibrium sorption. Since Beulah-Zap coal has much more oxygen functional groups than the other coals used, polar solvents would preferentially diffuse through interaction between coal and solvent. Coal is considered¹³ to have two types of interacting sites, i.e., one is free interacting sites which have not interacted with other sites, and the other is interacting sites which interacted already with other sites of coal. The methanol sorption in Figure 3 suggests that methanol may diffuse the coal through disrupting noncovalent bonds such as hydrogen bonds, since it has a high polarity. While, it is noted that the pyridine sorption rate was unexpectedly slow compared to the case of methanol. Pyridine is known to disrupt almost of hydrogen bonds in coals, since pyridine forms a strong hydrogen bond with hydroxyl groups. However, the slow diffusion of pyridine suggests that the disruption is not so much fast as methanol. The difference of pyridine sorption between Illinois # 6 coal and Beulah-Zap coal may be attributed to a difference in the distribution of strength of hydrogen bonds in the both coals.

Dual-Mode Sorption Model.

Figure 4 (a)-(d) shows sorption isotherms for Illinois # 6. In the range of 0.1 – 0.7 of relative vapor pressure, sorption was linear with the pressure for all the cases. The

isotherms was examined to be interpreted by the dual-mode sorption model. The equilibrium isotherm of the model can be expressed by the following equation:

$$C = C_H + C_D = \{C_H \times b \times p / (1 + b + p)\} + k_D \times p \quad (1)$$

where C is the quantity of the sorption, and the first term represents physical adsorption followed by a Langmuir isotherm and the second term represents dissolution into the bulk of coals followed by Henry's law. C_H is the pore saturation constant, b is the pore affinity constant, p is the relative vapor pressure, and k_D is Henry's law dissolution constant. Figure 4 shows that the observed values are consistent with the calculated lines from the model, especially at low pressures, suggesting that the isotherm behaviors can be explained by the dual-mode sorption model. The calculated C_H and C_D lines are also shown in the Figure, respectively. For benzene, cyclohexane and methanol, in the low vapor pressure ranges the physical adsorption (C_H) predominates, while for pyridine there is a large contribution of dissolution even at low pressure ranges. The value of C_H was similar, 0.37, 0.32, and 0.33 (mmol / g-coal) for benzene, cyclohexane, and pyridine, respectively, although their total sorptions are considerably different, as shown in Figure 4.

4. Their adsorption area per molecule, i.e., van der Waals radius, is also similar. These facts indicate that the number of the solvent molecules adsorbed is independent of types of solvents. The Henry's law dissolution constant, k_D , was in the order of cyclohexane < benzene < methanol < pyridine, being consistent with the order of the extraction yield and the swelling ratio for Illinois # 6.

Figure 5 and 6 show the results of Pocahontas # 3 - methanol and Beulah-Zap - methanol systems, respectively. The data could be also analyzed by the dual-mode sorption model and the calculated lines are shown in Figure 5 and 6. It should be noted that for Pocahontas # 3 coal the physical adsorption was predominant for the sorption, indicating that the most of sorption is attributed to the adsorption on the surface. The result also corresponds a very low swelling ratio and extraction yield for Pocahontas # 3 coal in methanol. On the other hand, for Beulah-Zap lignite a significant amount of methanol diffused the coal, as shown in Figure 6. The dissolution constant, k_D , of methanol in Beulah-Zap coal was much higher, while the pore saturation constant, b , was much lower than those in Illinois # 6 coal, reflecting the affinity of methanol to the pore surface and cross-links of both coals.

Thus, measurements of isotherms using various organic vapors are an useful method to elucidate interaction between coal and solvent, coal surface, chemical properties, and cross-linking structure (the distribution of the molecular weight between cross-links) of coals. Further works is continued by changing the experimental parameters such as temperature, types of organic vapors, coal samples (extract and extraction residue).

ACKNOWLEDGMENT

This work has been carried out as one of "Research for the Future" project of the Japan Society for the Promotion of Science (JSPS) through the 148 committee on coal utilization technology of JSPS.

REFERENCES

1. Hsieh, S. T.; Duda, J. L. *Fuel* **1987**, *66*, 170.
2. Green, T. K.; Selby, T. D. *Energy Fuels* **1994**, *8*, 213.
3. Vieth, W. R. *Diffusion in and Through Polymers*, Hanser Publishers: Munich, 1991.
4. Brenner, D. *Fuel* **1985**, *64*, 167.
5. Cody, G. D. J.; Davis, A.; Hatcher, P. G. *Energy Fuels* **1993**, *7*, 455.
6. Larsen, J. W.; Hall, P. J.; Wernett, P. C. *Energy Fuels* **1995**, *9*, 324.
7. Aida, T.; Fuku, K.; Fujii, M.; Yoshihara, M.; Maeshima, T.; Squires, T. G. *Energy Fuels* **1991**, *5*, 79.
8. Morino, M.; Kaneko, H.; Takanohashi, T.; Iino, M. *Energy Fuels*, **1996**, *10*, 1012.
9. Kaneko, H.; Morino, M.; Takanohashi, T.; Iino, M. *Energy Fuels*, **1996**, *10*, 1017.
10. Fujiwara, M.; Ohsuga, H.; Takanohashi, T.; Iino, M. *Energy Fuels* **1992**, *6*, 859.
11. Takanohashi, T.; Iino, M.; Nishioka, M. *Energy Fuels* **1995**, *9*, 788.
12. Iino, M.; Takanohashi, T.; Ohsuga, H.; Toda, K. *Fuel* **1988**, *67*, 1639.
13. Suuberg, E. M.; Otake, Y.; Langner, M. J.; Leung, K. T.; Milosavljevic, I. *Energy Fuels* **1994**, *8*, 1247.

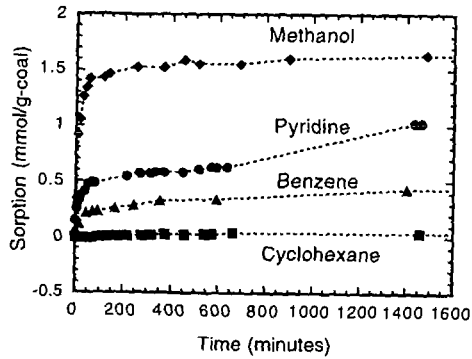


Figure 1 Sorption Behaviors Various Solvent Vapors by Pocahontas #3 Coal at 30 °C

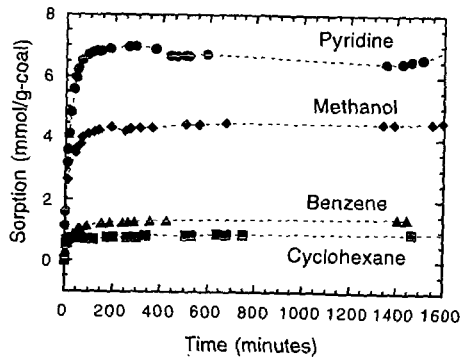


Figure 2 Sorption Behaviors Various Solvent Vapors by Illinois #6 Coal at 30 °C

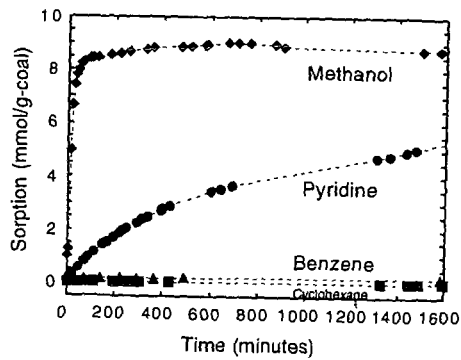


Figure 3 Sorption Behaviors Various Solvent Vapors by Beulah-Zap Coal at 30 °C

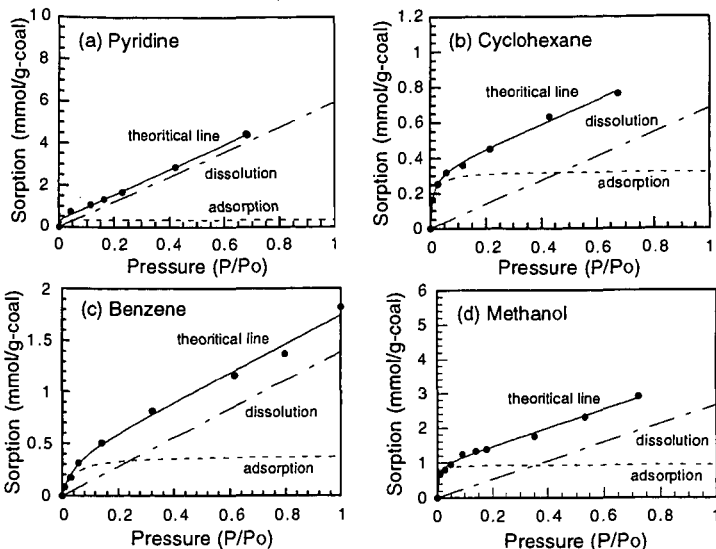


Figure 4 Pyridine Sorption Isotherm of Illinois #6 Coal at 30 °C and the theoretical lines.

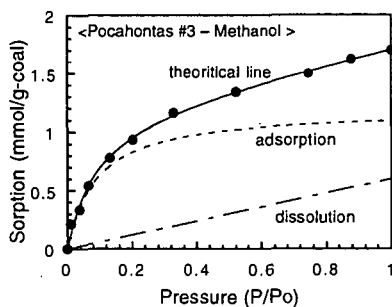


Figure 5 Methanol Sorption Isotherm of Pocahontas #3 Coal at 30 °C and the theoretical lines.

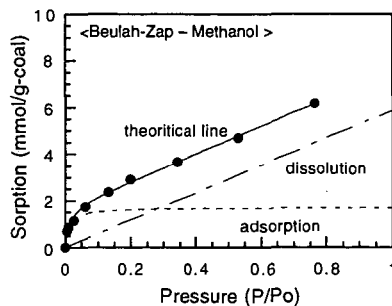


Figure 6 Methanol Sorption Isotherm of Beulah-Zap Coal at 30 °C and the theoretical lines.